University of Melbourne

Doctoral Thesis

# Resonant Leptogenesis and Quark-Lepton Unification with Low-Scale Seesaws

*Author:*
Tomasz P. Dutka

*Supervisors:*
Prof. Raymond R. Volkas
Dr. Matthew J. Dolan

*A thesis submitted in fulfilment of the requirements for the degree of Doctor of Philosophy*

*in the*

Particle Theory Group

*within the*

School of Physics
Faculty of Science

December 2020

ORCID: 0000-0001-9480-7611

# Declaration of Authorship

I, Tomasz P. Dutka, declare that this thesis titled, 'Resonant Leptogenesis and Quark-Lepton Unification with Low-Scale Seesaws' and the work presented in it are my own. I confirm that:

- This work was done wholly or mainly while in candidature for a research degree at this University.
- Where any part of this thesis has previously been submitted for a degree or any other qualification at this University or any other institution, this has been clearly stated.
- Where I have consulted the published work of others, this is always clearly attributed.
- Where I have quoted from the work of others, the source is always given. With the exception of such quotations, this thesis is entirely my own work.
- I have acknowledged all main sources of help.
- Where the thesis is based on work done by myself jointly with others, I have made clear exactly what was done by others and what I have contributed myself.

Signed:

Date: December 2020

UNIVERSITY OF MELBOURNE

# *Abstract*

Faculty of Science
School of Physics

Doctor of Philosophy

**Resonant Leptogenesis and Quark-Lepton Unification with Low-Scale Seesaws**

by Tomasz P. Dutka

The seesaw mechanism, where a hierarchy exists between the moduli of different entries of a mass mixing matrix, is a simple and theoretically attractive explanation for the observed large hierarchy between the neutral- and charged-fermion masses of the Standard Model. The simplest neutrino mass seesaw predicts that, upon diagonalisation, the physical mass states will either all be Majorana or all form pseudo-Dirac pairs. Non-minimal variants of this seesaw often generate a hybrid scenario with the physical mass states being a combination of both Majorana and pseudo-Dirac pairs. Such models often predict unique phenomenology and also allow for much lower mass scales of new physics. This thesis explores the implications such non-minimal variants can have beyond the simple generation of neutrino mass, particularly the possible role they may have in explaining the observed matter-antimatter asymmetry as well as implications for particular models of quark-lepton unification.

Chapter 1 reviews the current experimental evidence for neutrino mass and discusses some possible tree-level origins. The matter-antimatter asymmetry is introduced and the conditions necessary for the dynamical generation of this observed asymmetry are reviewed. The idea of thermal leptogenesis is outlined as a simple mechanism for generating an asymmetry dynamically at an epoch between the the period of reheating and the electroweak phase transition of the early universe. Finally, the idea that quarks and leptons are related by hidden symmetries are discussed with a particular emphasis on the quark-lepton unifying Pati-Salam gauge group.

In Chapter 2 we consider the leptogenesis implications for the Standard Model extended by two gauge-singlet fermions for each generation of charged lepton. We focus on the possibility of resonant scenarios without the need for inter-generational mass degeneracies and therefore do not require a possible flavour symmetry origin. The possible connection

between neutrino parameters measureable in low-energy experiments and the generation of a matter-antimatter asymmetry is explored.

In Chapter 3 we extend the analysis of the previous chapter and highlight how a flavour symmetry can allow for leptogenesis in a much wider region of parameter space for the extended seesaw used in Chapter 2. The benefits of this extended seesaw, compared to the minimal seesaw scenario, when the proposed flavour symmetry is included are discussed and implications for low-energy flavour-violation experiments are explored.

In Chapter 4 different possible Pati-Salam models are discussed with an emphasis on the connection between the scale of Pati-Salam breaking and the scale of heavy neutrino masses. Models allowing for the breaking scale to occur close to the electroweak scale are introduced. The dominant experimental probe of Pati-Salam is discussed and the current limits on the scale of breaking are calculated. Simple extensions of this model are proposed which both break an undesired mass degeneracy in the theory and allow for a significant reduction in the experimental limits on Pati-Salam breaking. A thorough analysis of the possible allowed parameter space in which both of these effects occur is explored and any possible connection to the symmetries of the theory is made.

Chapter 5 briefly concludes.

# Preface

This thesis comprises five main chapters and five appendices. Chapter 1 is an original introduction intended to motivate the work of this thesis and contains a review of the literature. Chapter 2 and Appendices A and B are based on the work in *Dirac-Phase Thermal Leptogenesis in the extended Type-I Seesaw Model* which was done in collaboration with R. Volkas and M. Dolan and predominantly written by the author. Chapter 3 is based on the work in *Low-scale Leptogenesis with Minimal Lepton Flavour Violation* in collaboration with R. Volkas and M. Dolan and written predominantly by the author based on ideas explored in Chapter 2. Chapter 4 and Appendices C to E are based on the work *Lowering the scale of Pati-Salam breaking through seesaws* done in collaboration with R. Volkas and M. Dolan and written predominantly by the author. All calculations, results and analyses presented within this thesis in Chapters 2 to 4 and Appendices A to E are the author's own work unless stated otherwise. Chapter 5 is an original summary of the ideas explored in each chapter.

# List of Publications

- M. J. Dolan, T. P. Dutka and R. R. Volkas, *Dirac-Phase Thermal Leptogenesis in the extended Type-I Seesaw Model*, *JCAP* **1806** (2018) 012, [1802.08373]
- M. J. Dolan, T. P. Dutka and R. R. Volkas, *Low-scale leptogenesis with minimal lepton flavor violation*, *Phys. Rev. D* **99** (2019) 123508, [1812.11964]
- M. J. Dolan, T. P. Dutka and R. R. Volkas, *Lowering the scale of Pati-Salam breaking through seesaw mixing*, [2012.05976]

# *Acknowledgements*

I am indebted firstly to my supervisors Ray and Matt for their patience, ongoing support, guidance and advice. None of this work would have been possible without their signficant contributions throughout my (long) time as a PhD student. I would also like to mention the friends I have made along the way, the discussions we often had (both related and unrelated to physics) helped to keep my spirits high and and help maintain my motivations. In particular I would like to thank my office mates throughout the years: Ahmad Galea, Benjamin Callen, Laurence Spiller, Iason Baldes, Jackson Clarke, Stephen Lonsdale, Timothy Trott, Peter Cox, Rebecca Leane, Johnathan Gargalionis, Leon Friedrich, Isaac Sanderson, Joshua Ellis, Innes Bigaran, Iulia Popa-Mateiu and Nick Leerdam. I would like to thank the rest of the members of CoEPP and the School of Physics at large with a particular thanks to my committee chair Jeff McCallum and others including K. G. Tan, David Jennens, Tony Shao, Lucas Ong, Nicholas Rodd, Pere Rados, Brian Le, Millie McDoland, Alex Millar, Callum Jones, Joel Smith, Abhishek Sharma, Thomas Shiell and Paul Giansiracusa.

Lastly I would like to like to thank my family, particularly Anna and Katarzyna for their continued support. Do moich rodziców, Genowefa i Janusz, bez waszego wsparcia nie udałoby mi się ukończyć tej pracy. Dziękuję, że we mnie uwierzyliście i pomogliscie mi podążać moją własną drogę.

# Contents

# List of Figures

# List of Tables

# Abbreviations

| | |
|---|---|
| **BAU** | **B**aryon **A**symmetry of the **U**niverse |
| **BBN** | **B**ig **B**ang **N**ucleosynthesis |
| **BSM** | **B**eyond the **S**tandard **M**odel |
| **CKM** | **C**abibbo-**K**obayashi-**M**askawa |
| **CMB** | **C**osmic **M**icrowave **B**ackground |
| **C$\nu$B** | **C**osmic ($\boldsymbol{\nu}$)Neutrino **B**ackground |
| **CP** | **C**harge **P**arity |
| **GUT** | **G**rand **U**nified **T**heory |
| **H.c.** | **H**ermitian **c**onjugate |
| **ISS** | **I**nverse **S**ee**S**aw |
| **LFV** | **L**epton **F**lavour **V**iolation |
| **LSS** | **L**inear **S**ee**S**aw |
| **MFV** | **M**imimal **F**lavour **V**iolation |
| **MLFV** | **M**imimal **L**epton **F**lavour **V**iolation |
| **PMNS** | **P**ontecorvo-**M**aki-**N**akagawa-**S**akata |
| **PS** | **P**ati-**S**alam |
| **QCD** | **Q**uantum **C**hromo**D**ynamics |
| **RGE** | **R**enormalisation **G**roup **E**quation |
| **SM** | **S**tandard **M**odel |
| **SN** | **S**terile **N**eutrinos |
| **UV** | **U**ltra**v**iolet |
| **VEV** | **V**acuum **E**xpectation **V**alue |

# Chapter 1

# Introduction

Currently the dynamics within our universe are well described by the combination of the theory of general relativity [4] together with the interactions of matter through fundamental forces described by the "Standard Model" (SM) [5–12]. The experimental successes of the SM (see e.g. [13]) have been firmly established with varying degrees of precision down to distance scales roughly as low as $10^{-20}$ m. The SM is a combined theory of the electroweak and strong interactions[1] described by Lorentz invariance and the gauge group

$$G_{\mathrm{SM}} = SU(3)_c \otimes SU(2)_L \otimes U(1)_Y \tag{1.1}$$

which fixes the properties of the gauge bosons. The matter sector of the theory can be considered more arbitrary as its existence is not predicted by the symmetries of the theory and therefore must be experimentally observed and measured. Table 1.1 summarises the experimentally observed field contents of the SM, grouped by their Lorentz structure, in combination with their transformation properties under $G_{\mathrm{SM}}$ which fixes the interactions for each particle. Eighteen parameters[2] are required in order to accurately model the dynamics of particle interactions which are summarised in Table 1.2. Thirteen of the parameters are due to the fermions of the SM, nine for their masses and four to described the dynamics of quark mixing. With the exception of the lighter quark masses, which are largely unimportant due to their confinement into hadrons, the remaining parameters

[1] Gravity, while the most relevant force in the dynamics of macroscopic objects, is by far the weakest force and as yet has no properly formulated quantum description. Probing distances scales below roughly $10^{-35}$ m will necessarily require a formulation of quantum gravity.

[2] The phase $\theta_{\mathrm{QCD}}$ in the CP-violating term of the QCD Lagrangian can be included which would lead to nineteen parameters however experimental observations suggest that this parameter is zero in the SM (or close to) and for simplicity we neglect it.

| | Field Content | $SU(3)_c \otimes SU(2)_L \otimes U(1)_Y$ |
|---|---|---|
| Scalar | $\phi = \begin{pmatrix} \phi^+ \\ \phi^0 \end{pmatrix}$ | $(\mathbf{1}, \mathbf{2}, \frac{1}{2})$ |
| Fermion | $Q_L^i = \begin{pmatrix} u^i_{r,b,g} \\ d^i_{r,b,g} \end{pmatrix}_L$ | $(\mathbf{3},\ \mathbf{2},\ \frac{1}{6})$ |
| | $(u_{r,b,g})^i_R$ | $(\mathbf{3},\ \mathbf{1},\ \frac{2}{3})$ |
| | $(d_{r,b,g})^i_R$ | $(\mathbf{3},\ \mathbf{1},\ -\frac{1}{3})$ |
| | $\ell_L^i = \begin{pmatrix} \nu^i \\ e^i \end{pmatrix}_L$ | $(\mathbf{1},\ \mathbf{2},\ -\frac{1}{2})$ |
| | $e^i_R$ | $(\mathbf{1},\ \mathbf{1},\ -1)$ |
| Gauge | $G^A$ | $(\mathbf{8},\ \mathbf{1},\ 0)$ |
| | $W^a$ | $(\mathbf{1},\ \mathbf{3},\ 0)$ |
| | $B$ | $(\mathbf{1},\ \mathbf{1},\ 0)$ |

TABLE 1.1: The SM field contents grouped by their Lorentz structure (scalar, fermion and gauge) with their corresponding transformation properties under $G_{\text{SM}}$. The bolded numbers correspond to the dimension of the representation of the given non-Abelian group and the final unbolded number simply represents the hypercharge of the field with the normalisation $Q = T^3_L + Y$. Here $A = 1, \ldots, 8$ are $SU(3)_c$ indices, $a = 1, \ldots, 3$ are $SU(2)_L$ indices and $i = 1, \ldots, 3$ denotes the generational index for the fermions: $e^i = (e, \mu, \tau)^i$, $\nu^i = (\nu_e, \nu_\mu, \nu_\tau)^i$, $d^i = (d, s, b)^i$ and $u^i = (u, c, t)^i$. The fermion fields are subcategorised into quarks (which come in three different 'colours') and leptons which are listed above and below the appropriate horizontal line respectively.

have all been measured to a remarkably high degree of experimental accuracy which leads to highly testable and precise predictions for current and future experiments. In addition to the gauge symmetries, the SM implies several 'accidental' global $U(1)$ symmetries which appear within the Lagrangian but are not imposed. These global symmetries can be identified with baryon number, B, related to quark interactions and three unbroken lepton numbers, $L_{e,\mu,\tau}$, which relate to the leptons. As a consequence of these additional global symmetries the proton is predicted to be absolutely stable in agreement with current experimental observations.

Despite its numerous successes, there is overwhelming evidence suggesting that the SM cannot be a complete description of nature and must be extended. For example: it predicts that the neutrinos are exactly massless, however neutrino oscillations have been observed in conflict with this prediction, it does not contain a viable dark matter candidate for which there is compelling evidence and our present understanding of particle

| | Parameter | Experimental Value | Comment |
|---|---|---|---|
| Scalar | $G_F$ | $1.1663787(6) \times 10^{-5}$ GeV$^{-2}$ | - |
| | $m_h$ | 125.10(14) GeV | - |
| Fermion | $m_e$ | 0.5109989461(31) MeV | Scheme-independent |
| | $m_\mu$ | 105.6583745(24) MeV | —— 〃 —— |
| | $m_\tau$ | 1776.86(12) MeV | —— 〃 —— |
| | $m_u$ | $2.16^{+0.49}_{-0.26}$ MeV | $\overline{\text{MS}}$ scheme at $Q = 2$ GeV |
| | $m_c$ | $1.27^{+11}_{-5}$ GeV | $\overline{\text{MS}}$ scheme running mass |
| | $m_t$ | 172.76(30) GeV | Direct measurement |
| | $m_d$ | $4.67^{+0.48}_{-0.17}$ MeV | $\overline{\text{MS}}$ scheme at $Q = 2$ GeV |
| | $m_s$ | $93^{+11}_{-5}$ MeV | —— 〃 —— |
| | $m_b$ | $4.18^{+0.03}_{-0.02}$ GeV | $\overline{\text{MS}}$ scheme running mass |
| | $\lambda$ | 0.22453(44) | - |
| | $A$ | 0.836(15) | - |
| | $\overline{\rho}$ | $0.122^{+0.018}_{-0.017}$ | - |
| | $\overline{\eta}$ | $0.355^{+0.012}_{-0.011}$ | - |
| Gauge | $\alpha_1$ | 0.0102021(23) | at $Q^2 = m_Z^2$ |
| | $\alpha_2$ | 0.03392266(10) | —— 〃 —— |
| | $\alpha_3$ | 0.1179(10) | —— 〃 —— |

TABLE 1.2: Parameters of the SM at their current experimental precision [14] grouped by their Lorentz structure (scalar, fermion, gauge). The values for the CKM mixing parameters are given in the Wolfenstein parametrisation and numbers in parenthesis after the values are the one-sigma standard deviation uncertainties in the last digit(s).

cosmology overwhelmingly indicates that the SM cannot explain the observed baryon asymmetry. Additional evidence for modifications of the SM, which are not necessarily in conflict experimentally but aesthetically appealing, also exist. For example: the small size of the neutron electric dipole moment may suggest an additional global symmetry, the flavour structure of the SM leads to a large hierarchy in Yukawa couplings (and also leads to the most parameters) in the SM which may suggest additional flavour symmetries, gauge coupling unification is suggested by renormalisation group equation running leading to additional gauge and scalar fields which itself may lead to a potential gauge hierarchy problem requiring additional stabilisation to protect the electroweak scale mass of the SM Higgs. The purpose of this thesis is to pursue some of the above motivating factors specifically for models appearing at low energy scales close to experimental observation. The particular focus of this thesis is on the impact that mass matrix "see-saws" at scales not far from the electroweak scale can have on some Beyond Standard Model (BSM) theories in the context of neutrino mass, baryogenesis via leptogenesis and quark-lepton unification.

## 1.1 Neutrino Physics

As a result of the chiral nature of $SU(2)_L$, the SM Lagrangian does not contain any terms which explicitly give mass to the fermions. As indicated by Table 1.1, all left-handed fermions transform non-trivially under the gauge group $SU(2)_L$ whereas every right-handed state transforms trivially. As a result, bare mass terms for the SM fermions are forbidden by the combined requirements that the Lagrangian remain gauge and Lorentz invariant. Instead masses are generated for the SM fermions through the couplings of each fermion to the SM Higgs scalar $\phi$:

$$-\mathcal{L}^{\text{SM}} \supset (Y_\ell)_{ij}\overline{\ell^i_L}\phi\, e^j_R + (Y_d)_{ij}\overline{Q^i_L}\phi\, d^j_R + (Y_u)_{ij}\overline{Q^i_L}\phi^c\, u^j_R + \text{H.c} \tag{1.2}$$

with $\phi^c = \epsilon\phi^*$. The gauge-invariant, renormalisable self-interaction terms of the doublet $\phi$ produces the potential,

$$V(\phi) = -\frac{\mu^2}{2}\left(\phi^\dagger\phi\right) + \frac{\lambda}{4}\left(\phi^\dagger\phi\right)^2, \tag{1.3}$$

which develops a non-zero classical minimum known as a vacuum expectation value (vev) at the field value $\langle\phi\rangle$. The minimum can always be rotated into the form

$$\langle\phi\rangle = \frac{1}{\sqrt{2}}\begin{pmatrix} 0 \\ v_{EW} \end{pmatrix} \tag{1.4}$$

where $v_{EW} = \mu/\sqrt{\lambda}$. As a result, the ground state of the Lagrangian is no longer invariant under $SU(2)_L \otimes U(1)_Y$ transformations and mass terms for the charged leptons, down- and up-quarks will be given by the singular values of

$$M_E = \frac{v_{EW}}{\sqrt{2}}Y_\ell, \quad M_D = \frac{v_{EW}}{\sqrt{2}}Y_d \quad \text{and} \quad M_U = \frac{v_{EW}}{\sqrt{2}}Y_u \tag{1.5}$$

respectively. Clearly the field content of Table 1.1 predicts the neutrinos, $\nu_L^i$, to be exactly massless as the SM does not formally contain a right-handed Weyl degree of freedom to pair up with the left-handed field in the same way as for the charged-leptons and quarks.

### 1.1.1 Neutrino Oscillations

All fermions come in three generations, or flavours, which couple to the gauge bosons through their kinetic terms

$$-i\mathcal{L}_{\text{gauge}}^{\text{SM}} \supset \overline{(\ell_L)_i}\not{D}\ell_L^i + \overline{(Q_L)_i}\not{D}Q_L^i + \overline{(e_R)_i}\not{D}e_R^i + \overline{(d_R)_i}\not{D}d_R^i + \overline{(u_R)_i}\not{D}u_R^i \tag{1.6}$$

where $\not{D} \equiv D_\mu\gamma^\mu$ is the covariant derivative for the given fermion. Of particular interest are the interactions between the left-handed fermions, corresponding to the first two terms of Eq. (1.6), which when expanded out generates

$$\mathcal{L}_{\text{gauge}}^{\text{SM}} \supset -\frac{g_2}{\sqrt{2}}\left[(\overline{\nu_L})_i\not{W}^+(e_L)^i + (\overline{u_L})_i\not{W}^+(d_L)^i\right] + \text{H.c} \tag{1.7}$$

for the electroweak charged-current interactions. For massless fermions this implies that there are no inter-generational couplings between the gauge bosons and fermions, however for massive particles, time-evolution is determined through the Hamiltonian and therefore all fields must first be rotated such that they have definitive mass. Diagonalisation of $M_{E,D,U}$ proceeds via

$$U_L^x M_X (U_R^x)^\dagger = M_X^{\text{diag}} \tag{1.8}$$

for $X = E, D, U$ where $U_{L/R}^x$ are unitary matrices and $M_X^{\text{diag}}$ is a diagonal matrix with real and positive-definite values to be identified with each particle's mass. The flavour basis therefore relates to the mass basis for the left-handed fermions through

$$(x'_L)_i = \sum_i (U_L)_{ij}(x_L)_j \tag{1.9}$$

where primed parameters correspond to the mass eigenstate. After rotating into the mass basis the relevant charge-current quark interactions of Eq. (1.7) are now given by

$$\mathcal{L}_{\text{gauge}}^{\text{SM}} \supset -\frac{g_2}{\sqrt{2}} (\overline{u'_L})_i \left[ \underbrace{(U_L^u)^\dagger U_L^d}_{V_{\text{CKM}}} \right]_{ij} \not{W}^+ (d'_L)^j + \text{H.c} \tag{1.10}$$

where $V_{\text{CKM}}$ is known as the Cabibbo-Kobayashi–Maskawa (CKM) matrix [15, 16] and is necessarily unitary as it is the product of two unitary matrices. *A priori* there is no reason to expect that the mass matrices $M_{E,D,U}$ are diagonal, unless a flavour symmetry was enforced, which implies that in general $V_{\text{CKM}}$ will be non-diagonal. Therefore for massive particles, inter-generational charged-current interactions will be induced and the strength of these interactions will be determined by the misalignment between the flavour and mass basis. Importantly for the charged-current lepton interactions, as the SM predicts massless neutrinos, there is no misalignment between $\nu'_L$ and $\nu_L$ and therefore $U_L^\nu$ can always be rotated such that the equivalent of $V_{\text{CKM}}$, known as the Pontecorvo-Maki–Nakagawa–Sakata (PMNS) matrix [17, 18] which we label as $U_{\text{PMNS}}$, is equal to the identity matrix. Therefore in the SM, massless neutrinos necessarily predict that the left-handed leptonic charged-current interactions will be flavour diagonal.

Neutrino oscillation experiments proceed by producing neutrinos through charged-current interactions of *known flavour* and then measuring the flavour of the neutrino at a fixed distance away from the point of production. If the given neutrino's flavour composition changes between the point of production and measurement, e.g. a $\nu_e$ neutrino is produced but a $\nu_\mu$ neutrino is measured at the observation point, an oscillation between the different neutrino flavours has occurred. Importantly for massless neutrinos, the charged-current interactions contain no inter-generational mixing and therefore flavour oscillations are forbidden within the SM. The probability to observe the oscillation $\nu_\alpha \to \nu_\beta$ over a distance $L$ can be calculated (see e.g. [19] for a review):

$$P(\nu_\alpha \to \nu_\beta) = \sum_{i,j} \left[ (U_L)_{\beta i} (U_L)^*_{\alpha i} (U_L)^*_{\beta j} (U_L)_{\alpha j} \right] \exp\left( \frac{i \Delta m_{ij}^2 L}{2E} \right) \tag{1.11}$$

where we have written $U_L = U_{\text{PMNS}}$ for brevity, $\Delta m_{ij}^2 = m_i^2 - m_j^2$ and $m_i$ corresponds to a neutrino's would-be mass. In the case of massless neutrinos $(U_L)_{\beta i}(U_L)^*_{\alpha i} = 0$ for $\alpha \neq \beta$ and $\Delta m_{ij}^2 = 0$ for all choices of $i$ and $j$, therefore the predicted probability of oscillation is zero as expected. Therefore observations of neutrino flavour oscillation unambiguously

| | Normal Ordering | Inverted Ordering |
|---|---|---|
| $\Delta m^2_{21}$ | $7.42^{+0.21}_{-0.20} \times 10^{-5}$ eV$^2$ | $7.42^{+0.21}_{-0.20} \times 10^{-5}$ eV$^2$ |
| $\Delta m^2_{3k}$ | $+2.514^{+0.028}_{-0.027} \times 10^{-3}$ eV$^2$ | $-2.497^{+0.028}_{-0.028} \times 10^{-3}$ eV$^2$ |
| $\theta_{12}$ | 0.584(13) | 0.584(13) |
| $\theta_{23}$ | 0.855(24) | 0.860(21) |
| $\theta_{13}$ | 0.1496(21) | 0.1503(21) |
| $\delta_{CP}$ | 3.4(4) | 5.0(6) |

TABLE 1.3: Most recent universal fit data [34] on the neutrino mass squared differences along with the mixing angles of the PMNS matrix (excluding the Majorana phases) assuming either a normal ($k = 2$) or inverted ($k = 1$) hierarchy.

imply that neutrinos in fact have mass as $U_L$ cannot be diagonal and therefore the SM must be extended.

Neutrino oscillations have now been firmly established as a phenomenon occurring in nature, historically observed from atmospheric [20–22] and solar [23–28] sources and further confirmed by terrestrial sources from various long baseline [29, 30] and reactor [31–33] experiments. Due to the relationship between Eq. (1.11) and physical parameters, oscillation measurements allow for measurements of the entries of the PMNS matrix as well as the neutrino mass squared differences, for a given $L$ and $E$. The PMNS matrix is conventionally parametrised by

$$U_{\text{PMNS}} = \begin{pmatrix} 1 & 0 & 0 \\ 0 & c_{23} & s_{23} \\ 0 & -s_{23} & c_{23} \end{pmatrix} \begin{pmatrix} c_{13} & 0 & s_{13}e^{-i\delta_{CP}} \\ 0 & 1 & 0 \\ -s_{13}e^{i\delta_{CP}} & 0 & c_{13} \end{pmatrix} \begin{pmatrix} c_{12} & s_{12} & 0 \\ -s_{12} & c_{12} & 0 \\ 0 & 0 & 1 \end{pmatrix} \begin{pmatrix} e^{i\alpha_1} & 0 & 0 \\ 0 & e^{i\alpha_2} & 0 \\ 0 & 0 & 1 \end{pmatrix} \tag{1.12}$$

where $c[s]_{ij} = \cos[\sin](\theta_{ij})$ and the phases in the final matrix are possible Majorana phases. The most recent universal fit results [34] from all oscillation experiments for the mass squared differences and mixing angles are summarised in Table 1.3. The hierarchy (normal or inverted) refers to the possible hierarchy between the three neutrino mass states which is as yet undetermined: $m_{\nu_1} < m_{\nu_2} < m_{\nu_3}$ or $m_{\nu_3} < m_{\nu_1} < m_{\nu_2}$ in the case of a normal and inverted ordering respectively. Oscillation experiments are not sensitive to the Majorana phases, if they exist, but they can be probed in other experiments, such as neutrinoless double beta decay [35].

The absolute mass scale of the neutrinos is as yet undetermined and oscillation experiments, being only sensitive to the mass squared differences, cannot measure the mass of the lightest neutrino. Cosmological and kinematic probes of the sum of neutrino masses exist which can be used to place an obvious upper bound on the absolute mass scale. Cosmological bounds on the sum of neutrino masses arises from late times (on a cosmological scale) when neutrinos become non-relativistic and their energy density changes from contributing to the total radiation density to the total matter density. This produces measurable effects in CMB data, baryon acoustic oscillations and large scale structure measurements. Most recently [36, 37] the limits on the sum of the masses has been set at roughly

$$\sum_i m_{\nu_i} \leq 0.110 \text{ eV} \tag{1.13}$$

at a 95% confidence level although this limit varies somewhat depending on different model-dependent cosmological assumptions, but is certainly below the eV scale. Kinematic experiments offer a less model-dependent limit, for example from measuring the end point distribution of final-state electrons in beta decay, which similarly offers upper bounds on an 'effective electron neutrino mass' defined as

$$m_{\nu_e} = \sqrt{\sum_i \left|U_{1i}^2\right| m_{\nu_i}^2} \tag{1.14}$$

which has most recently set the bound [38]

$$m_{\nu_e} \leq 1.1 \text{ eV} \tag{1.15}$$

at a 90% confidence level and is expected to be further reduced down to 0.2 eV [39]. As the current neutrino mass limits arise from a combination of observed mass squared differences as well as upper bounds on the sum of the masses, it is still phenomenologically possible for the lightest state to be exactly massless. The existence of neutrino mass (with a non-diagonal $U_{\text{PMNS}}$) also indicates that three of the four accidental global symmetries of the SM Lagrangian $L_e$, $L_\mu$ and $L_\tau$ are broken, which is clearly evident from an oscillation event such as $\nu_e \to \nu_\mu$. However it is still possible for certain linear combinations of the these three global symmetries to remain unbroken, for example the global lepton number $L = L_e + L_\mu + L_\tau$.

In summary, observation of neutrino oscillations necessarily requires a modification of the SM such that neutrino masses can be accommodated. As a result, the number of parameters in the theory must be increased from the eighteen within the SM to more than twenty-four. Furthermore although the absolute mass scale of neutrino mass is as yet unknown, current upper bounds suggest that the neutrino mass scale is extremely small compared to the masses of the other SM fermions listed in Table 1.2. These limits place the neutrino mass *of each generation* close to seven order of magnitude below the lightest charged fermion. This hierarchy is unlike the charged fermion mass hierarchies where each generation of particle masses are sufficiently grouped such that all particles within a given generation are lighter or heavier than all particles of a different generation:

$$\nu_e,\, \nu_\mu,\, \nu_\tau \ll m_e,\, m_d,\, m_u < m_\mu,\, m_s,\, m_c < m_\tau,\, m_b,\, m_t. \tag{1.16}$$

### 1.1.2 Neutrino Mass

There are a large number of ways in which masses for the SM left-handed neutrinos can be generated, most of which require the introduction of additional fields to those listed in Table 1.1. Arguably the simplest extension is to introduce at least two right-handed Weyl fermion states such that neutrino mass is generated through the Higgs vev in complete analogy with the other SM fermions, as in Eq. (1.2):

$$-\mathcal{L}^{\nu\text{-mass}} = (Y_\nu)_{ij}\, \overline{\ell^i_L} \phi\, \nu^j_R + \text{H.c.} \tag{1.17}$$

which leads to

$$m_\nu = \frac{v_{EW}}{\sqrt{2}} Y_\nu. \tag{1.18}$$

While aesthetically this has the advantage of explaining mass generation of all SM fermions through the same mechanism, the very stringent upper bounds on the neutrino mass of each generation requires that the singular values of the matrix $Y_\nu$ are significantly smaller than for all other Yukawa couplings within the SM.

Additionally, from the principles in which the Lagrangian of the SM was constructed, all possible renormalisable and gauge-invariant terms should be included. The would-be right-handed neutrinos, required in order to generate the Dirac mass term of the form $\overline{\nu_L}\, \nu_R$, have the unique property of being gauge singlets and therefore transform trivially under $G_{\text{SM}}$:

$$\nu_R \sim (\mathbf{1}, \mathbf{1}, 0) \tag{1.19}$$

and we will therefore refer to them as sterile neutrinos (SN). An additional Majorana mass term

$$-\mathcal{L}^{\nu\text{-mass}} \supset \frac{1}{2}\overline{(\nu_R^c)^i}(M_R)_{ij}\,\nu_R^j + \text{H.c} \tag{1.20}$$

is both Lorentz and gauge invariant and therefore should be included within the Lagrangian. It is important however to note that the inclusion of this term will completely break the accidental global $L$ symmetry present within the SM. The neutrino mass states are now found by diagonalising the full neutrino mass matrix

$$-\mathcal{L}^{\nu\text{-mass}} = \frac{1}{2}\begin{pmatrix}\overline{\nu_L} & \overline{\nu_R^c}\end{pmatrix}\begin{pmatrix}0_{3\times 3} & m_D^\nu \\ (m_D^\nu)^T & M_R\end{pmatrix}\begin{pmatrix}\nu_L^c \\ \nu_R\end{pmatrix} + \text{H.c} \tag{1.21}$$

where $m_D^\nu = Y_\nu v_{EW}/\sqrt{2}$ and $M_R$ are $3\times n$ and $n\times n$ dimensional matrices respectively, with $n$ corresponding to the number of generations of SNs, and the mass matrix is written in the Majorana basis and is therefore symmetric. Note that the top-left entry of this mass matrix is a $3\times 3$ zero matrix as an explicit Majorana mass term for $\nu_L$ would violate gauge invariance, though it can be generated spontaneously with the introduction of a $SU(2)_L$ triplet scalar with non-zero hypercharge.

Diagonalisation of this $(3+n)\times(3+n)$ dimensional matrix does not in general have a simple analytic solution. However, if large hierarchies between the two matrices $m_D^\nu$ and $M_R$ exist, then perturbative expressions can be derived. The entries of $M_R$ are not generated through any symmetry breaking, as they are in $m_D^\nu$, and therefore there is no reason to expect these two matrices to be similar in size to each other perhaps suggesting that a hierarchy between these two mass blocks is almost expected. For more complicated extensions of the SM beyond the simple introduction of gauge singlet fermions, the Majorana mass terms could be dynamically generated through some mechanism, for example through the breaking of a gauged[3] $U(1)_{B-L}$. Even without considering possible experimental constraints for the size of this new scale in the theory, there is no reason to expect these two scales to be of similar order in general.

[3]The combination $B-L$ is required from anomaly cancellation.

Assuming the hierarchy $M_R \gg m_D^\nu$, which is known as the type-I seesaw scenario [40–44], with one generation of fields for simplicity, leads to

$$m_\nu \simeq -\frac{(m_D^\nu)^2}{M_R} \qquad \text{and} \qquad m_N \simeq M_R \tag{1.22}$$

for the two mass states after diagonalisation at lowest order in the perturbative expansion where $\nu \simeq \nu_L$ and $N \simeq \nu_R^c$ which we show in Appendix D.0.1. Due to the assumed hierarchy between $M_R$ and $m_D^\nu$, the two masses themselves are hierarchical with

$$m_\nu \ll m_N \tag{1.23}$$

and a suppression in the lightest mass state in proportion to the heaviest mass state occurs. Therefore the structure of the matrix $m_D^\nu$ in the multi-generational scenario could be such that the observed flavour structure of the SM is preserved and, in the limit where $M_R \to 0_{3\times 3}$, might predict

$$\nu_e,\, m_e,\, m_d,\, m_u < \nu_\mu,\, m_\mu,\, m_s,\, m_c < \nu_\tau,\, m_\tau,\, m_b,\, m_t. \tag{1.24}$$

Although this hierarchy of masses is only speculative and not enforced in this limit, such a hierarchy might imply additional flavour symmetries within the Yukawa sector which are unobserved due the 'seesaw' induced by the size of $M_R$. This results in the observed smallness of neutrino mass and attractively allows for the Yukawa couplings in the entires of $Y_\nu$ to be significantly larger. Figure 1.1 plots the required size of $M_R$ for different choices of the Yukawa coupling matrix $Y_\nu$ in the one-generational scenario for different choices of the light neutrino mass scale. Requiring order one couplings for $Y_\nu$ requires the Majorana mass term to satisfy $M_R \simeq 10^{13-14}$ GeV, significantly larger than the electroweak scale.

As the Majorana mass term is (in the simplest scenario) a free parameter, two mass scales are now introduced into the extended SM Lagrangian[4]: the electroweak scale $v_{EW}$ and the Majorana mass scale $M_R$. However the hierarchy $M_R \gg v_{EW}$ causes the mass mixing matrix to generate a third scale $m_\nu \sim v_{EW}^2/M_R$ which can explain the required lightness of the active neutrinos albeit requiring ultra-heavy SNs. In the multi-generational mass

[4] A third mass scale is generated by the scale of QCD confinement, however this is not relevant for neutrino mass generated through the seesaw mechanism.

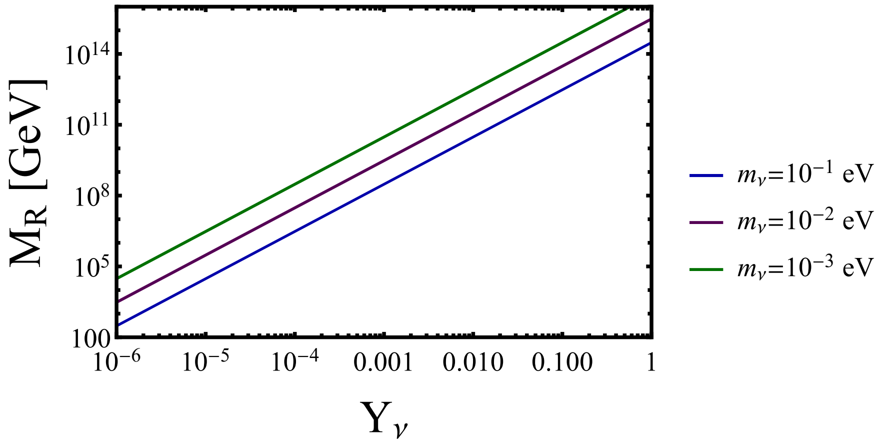


FIGURE 1.1: Plot of the variation in the required size of $M_R$ as a function of different choices of Yukawa coupling $Y_\nu$ in the one-generational type-I seesaw scenario for different choices of the light neutrino mass scale. Requiring an $\mathcal{O}(1)$ coupling requires Majorana mass scales close to the traditional GUT scale.

mixing scenario of Eq. (1.21), the light and heavy mass states are now given by

$$m_\nu \simeq -m_D^\nu M_R^{-1}(m_D^\nu)^T \qquad \text{and} \qquad m_N \simeq M_R \tag{1.25}$$

where $m_\nu$ and $m_N$ are $3 \times 3$ and $n \times n$ dimensional matrices respectively. The derivation of Eq. (1.25) is outlined in Appendix D.0.2. The condition required for the desired seesaw effect due to a hierarchy between $M_R$ and $m_D^\nu$ in a multi-generational scenario is if $\sigma_i(m_D^\nu) < \sigma_1(M_R)$ for all $i$ is satisfied, where $\sigma_i(\dots)$ corresponds to the singular values of the given matrix sorted in ascending order.

For the opposite hierarchy in Eq. (1.21) where $m_D^\nu \gg M_R$ the mass states are simply given by

$$m_\nu \simeq m_D^\nu - \frac{1}{2}M_R \qquad \text{and} \qquad m_N \simeq m_D^\nu + \frac{1}{2}M_R \tag{1.26}$$

and therefore the two neutrino states develop masses at a similar scale with a mass-splitting determined by $M_R$. As in the limit $M_R \to 0$ the neutrino mass simply arises from the Dirac-mass term (similar to the other SM fermions), in this hierarchy the physical neutrino states are known as pseudo-Dirac. Importantly this hierarchy implies that the entries of $Y_\nu$ are required to be orders of magnitude smaller than the other SM Yukawa couplings and will spoil the potential flavour structure observed in the SM. One theoretically attractive feature of this hierarchy stems from the fact that $M_R$ is the only parameter of the Lagrangian which leads to violation of the accidental, global lepton number $L$. Therefore setting $M_R \to 0$ restores this symmetry which is allowed to be small by the principle of technical naturalness [45] which guarantees that quantum corrections will not spoil the small size of $M_R$ assumed at tree-level.

Both hierarchies between $m_D^\nu$ and $M_R$ can therefore be motivated through different theoretical arguments. A large $M_R$, known typically as a "high-scale" seesaw, leads to the required light neutrino masses with Yukawa couplings within the entries of $Y_\nu$ much closer in size to the other Yukawa couplings in the SM. Additionally $M_R$ can quite naturally be associated with the breaking of a gauged $U(1)_{B-L}$ symmetry, which often is required to occur at high scales, motivating the large size assumed. This hierarchy however leads to SN masses significantly larger than what can be currently experimentally probed. Small values of $M_R$ can be attractive from technical naturalness arguments albeit requiring the entries of $Y_\nu$ to be very small. An interesting variation on the two scenarios presented above exists which allows for significantly larger Yukawa couplings compared to those required by the simple seesaw of Eq. (1.21) for a given SN mass and can also motivated by technical naturalness.

If instead two SNs are introduced per generation of $\ell_L$, which for definitiveness will be labelled $\nu_R$ and $S_L$, the most general mass mixing matrix which arises will be given by

$$-\mathcal{L}^{\nu S\text{-mass}} = \frac{1}{2}\begin{pmatrix}\overline{\nu_L} & \overline{\nu_R^c} & \overline{S_L}\end{pmatrix}\begin{pmatrix}0 & m_D^\nu & m_L^\nu \\ (m_D^\nu)^T & \mu_N & M_R \\ (m_L^\nu)^T & (M_R)^T & \mu_S\end{pmatrix}\begin{pmatrix}\nu_L^c \\ \nu_R \\ S_L^c\end{pmatrix} + \text{H.c}, \tag{1.27}$$

where now $\mu_N$ and $\mu_S$ correspond to the allowed Majorana mass terms for $\nu_R$ and $S_L$ respectively and the remaining entries arise from Dirac couplings amongst $\nu_L$, $\nu_R$ and $S_L$. A number of different scenarios are now possible depending on the different hierarchies amongst each block matrix. For brevity we focus on arguably the most interesting and well studied scenario which assumes that the Dirac-mass terms within $M_R$ are much larger than all other masses. Under this assumption, diagonalisation leads to

$$\begin{aligned} m_\nu &\simeq m_D^\nu (M_R^{-1})^T \mu_S\, M_R^{-1} (m_D^\nu)^T - m_D^\nu (M_R^{-1})^T (m_L^\nu)^T - \left[m_D^\nu (M_R^{-1})^T (m_L^\nu)^T\right]^T \\ m_{N_1} &\simeq M_R - \frac{1}{2}\left(\mu_S + \mu_N\right) \\ m_{N_2} &\simeq M_R + \frac{1}{2}\left(\mu_S + \mu_N\right) \end{aligned} \tag{1.28}$$

for the relevant block matrices at lowest order where $\nu \simeq \nu_L$ and $N_{1,2}$ is a pseudo-Dirac pair of neutrinos composed primarily of $\nu_R$ and $S_L$. Note that the Majorana mass term $\mu_N$ is absent from $m_\nu$ at lowest order and that $\mu_S \to 0$ leads to $m_\nu = 0$ at all orders regardless whether $\mu_N$ is non-zero or not. Therefore, $\mu_N$ is often set to zero due to its subdominant contribution to the light neutrino masses. Most commonly, limiting cases of Eq. (1.27) are considered: taking $m_L^\nu \to 0$ is known as the Inverse Seesaw (ISS) where

$$m_\nu \simeq m_D^\nu (M_R^{-1})^T \mu_S \, M_R^{-1} (m_D^\nu)^T \tag{1.29}$$

and $\mu_{N/S} \to 0$ is known as the Linear Seesaw (LSS) with

$$m_\nu \simeq -m_D^\nu (M_R^{-1})^T (m_L^\nu)^T - \left[ m_D^\nu (M_R^{-1})^T (m_L^\nu)^T \right]^T . \tag{1.30}$$

The additional parameters which are now present can lead to a significant reduction in the scale of the SN masses (dictated primarily by the size of $M_R$) as the Lepton Number Violating (LNV) mass terms $\mu_{N/S}$ and $m_L^\nu$ are linearly proportional to the light neutrino mass block. This can be compared to the simpler scenario of Eq. (1.25) where the light neutrino mass block is inversely proportional to the scale of LNV. Now the SN mass scale can be reduced for a fixed Dirac mass $m_D^\nu$ by decreasing the size of the LNV parameters. This scenario is therefore a hybrid of the two possible hierarchies of parameters in the minimal type-I seesaw: the lightest neutrino mass states have masses inversely proportional to the heavy SN masses similar to Eq. (1.25), but additionally the LNV parameters are assumed to be small in a similar way to Eq. (1.26), which is motivated by technical naturalness, albeit at the cost of introducing an additional singlet state per generation of SM fermions. As this scenario allows for large couplings within $Y_\nu$ for much lighter overall SN masses (even TeV scale masses are viable with order one couplings) this is an example of a “low-scale" seesaw with much more optimistic implications for testability in current and future experiments. An important prediction in such a scenario is the pseudo-Dirac nature of the SNs introduced which are expected to have a mass splitting well below the GeV scale.

As gauge singlet fields do not introduce any quantum anomalies, more complicated seesaw scenarios are also possible with additional mixing effects between an even larger array of neutral particles, one of which we will explore in Chapter 4. However, the above two models demonstrate the overall possible relationships between the LNV parameters, the SN masses and the desired light neutrino mass states. The light neutrinos can be inversely proportional to powers of the LNV parameters as in Eq. (1.25) requiring large LNV effects, the light neutrinos can be (pseudo-)Dirac and insensitive to small LNV parameters (requiring extremely small Yukawa coupling if the Dirac mass arises from the SM Higgs) as in Eq. (1.26) or the light neutrinos can be proportional to positive powers of the LNV parameters requiring the LNV to be small as in Eq. (1.28).

The minimal scenario of Eq. (1.21) is known as the type-I seesaw mechanism which induces neutrino mass at tree level, the more exotic scenario of Eq. (1.27) is an extension of the minimal type-I scenario. There exist two additional models which generate neutrino mass at tree level: through the addition of a scalar $SU(2)_L$ triplet field, known as the type-II seesaw [46–50], or through the addition of fermion $SU(2)_L$ triplet fields, known as the type-III seesaw [51]. In both cases sufficiently light neutrino masses are produced in a similar way through a seesaw due to a large hierarchy between two parameters in a mass mixing matrix. Non-minimal extensions to these two neutrino mass models are of course possible through the introduction of additional triplet scalar or fermions however these three models constitute the full set of minimal scenarios that generate a tree-level Majorana neutrino mass. Other neutrino mass mechanisms exist, many of which generate the light neutrino mass at loop level, however in this work we will focus on seesaw induced light masses and particularly focus on extended type-I seesaw scenarios as described above.

## 1.2 The Cosmological Baryon Asymmetry

An explanation for the origin of the baryon and lepton asymmetries required in the early universe is an important area of particle cosmology. While the field content of the SM listed in Table 1.1 is quite large and diverse, the *visible* matter content of the universe is primarily made up of the composite proton and neutron, which themselves contain only up and down quarks as valence particles, and the fundamental electron. The Dirac equation [52, 53] famously predicts that for each fermion which is introduced into a theory an accompanying antifermion must be introduced which has identical properties with the exception of opposite charges. The subsequent discovery of the positron [54] cemented the existence of antimatter which led to rich history of experimental discovery. Arguably the most important consequence of the discovery of antimatter is its role in the early thermal history of the universe.

As matter and antimatter annihilate into radiation, an imbalance in the early universe between their respective number densities would lead to a universe primarily composed of one type after annihilation of the symmetric parts. In contrast a symmetric abundance of the two would lead to, after thermal freeze out, an admixture of the two where likely different patches of the universe would be composed of matter or antimatter. Therefore precise measurements of the matter and antimatter content of the universe leads to important implications on the evolution dynamics of the early universe. This motivates the measurement of the total baryon number density of the universe defined as

$$n_B = n_b - n_{\bar{b}} \tag{1.31}$$

where $n_{b(\bar{b})}$ corresponds to the number densities of baryons(antibaryons) in the universe at the present epoch. A similar quantity could be defined for the total lepton number density however currently this quantity is unmeasured. Although electric charge conservation implies that the total number density for *charged* leptons, $n_{L^{+/-}}$, is required to equal that of the protons, the equivalent *neutral* lepton number density is currently unknown and requires accurate measurements of the cosmic neutrino background (C$\nu$B) which corresponds to the remnant population of light neutrinos which decoupled from the thermal bath[5].

### 1.2.1 Evidence of a baryon asymmetry

The experimentally measured baryon number density is typically expressed by normalising it to the photon number density observed today

$$\eta_B \equiv \frac{n_B}{n_\gamma}. \tag{1.32}$$

This asymmetry has famously been measured from cosmological observations at two distinct epochs of the early universe.

[5]There are however some constraints on the electron-neutrino asymmetry due to its unique role in BBN, which is expected to apply to all three flavours due to efficient neutrino flavour oscillations occurring below $T \simeq 10$ MeV [55, 56]. This asymmetry affects the overall neutron-to-proton ratio which changes the predicted $^4$He abundance and the $^2$H/$^1$H ratio. The current limit [57] on the electron-neutrino asymmetry fixes $-4.5 \times 10^{-3} \leq \eta_{\nu_e} = \frac{n_{\nu_e} - n_{\bar{\nu}_e}}{n_\gamma} \leq 2 \times 10^{-3}$ at a 68% confidence level and therefore it is still unknown whether there is an excess of electron-neutrinos or electron-antineutrinos.

Firstly, when the universe was at a temperature of $T \simeq$ MeV, roughly corresponding to a time scale of seconds after the big bang, protons and neutrinos begin to fuse together to make nuclear elements. Importantly different assumed values of $\eta_B$ at this temperature will lead to different expected yields of various elements. After propagating these predicted nuclear abundances to the current epoch, the currently observed abundances can be used to estimate the required value of $\eta_B$ at the time of big bang nucleosynthesis (BBN). This prediction is dominated by the measured abundances of the lightest elements, e.g. $^2$H, $^3$He and $^4$He, which are most abundant in the universe. The resultant baryon to photon density is conservatively constrained [58] to be between

$$2.5 \times 10^{-10} \leq \eta_B \leq 6 \times 10^{-10}. \tag{1.33}$$

Two key observations stem from this measurement: $\eta_B$ is positive implying that the number density of baryons exceeded that of antibaryons before annihilation and that this value of $\eta_B$ must have existed *before* the epoch of BBN.

A more precise measurement of $\eta_B$ can be obtained from the epoch when electrons and protons combined to form neutral Hydrogen, known as recombination. At this point the universe became transparent to the remaining photons which, after redshifting, make up the cosmic microwave background (CMB) radiation we observe today. A detailed calculation [59] finds that recombination occurs at a temperature of $T_{\text{rec}} = 0.308$ eV, corresponding to a time scale of $t \sim 10^5$ years after the big bang, significantly after BBN. A value of $\eta_B$ can be measured from the small anisotropies present in the temperature map of the CMB. Specifically, peaks and troughs within the power spectrum of the anisotropies are sensitive to the value of $\eta_B$ as before recombination, baryons and photons are coupled due to Thomson scattering. Recent measurements [36] lead to a derived value of

$$\eta_B = (6.097 \pm 0.035) \times 10^{-10} \tag{1.34}$$

which is broadly consistent with previous measurements from different collaborations [60] as well as the value derived from BBN above.

### 1.2.2 Baryogenesis

Experimental measurements have thus firmly established the existence of a non-zero baryon asymmetry within the universe whose origin is required to be explained. In particular, dynamic explanations, where the universe started with $\eta_B = 0$ and through some early universe dynamics a non-zero value was generated, are preferred from both aesthetic and theoretical arguments. Importantly, a period of rapid expansion, known as inflation, was required at very early times [61, 62] in order to provide a solution to the various theoretical problems with the model of big bang cosmology, namely the flatness and horizon problems. This period of rapid expansion would effectively dilute any primordial baryon asymmetry which may be present at earlier times to levels exponentially smaller than that which we currently observe. Therefore at some post-inflationary period, a non-zero baryon asymmetry must have developed dynamically which is referred to as the period of "Baryogenesis". Inflationary models therefore restrict baryogenesis to occur between the periods of reheating ($T_{\text{reh}}$), when the universe re-thermalises after inflation, and the epoch of BBN, from which we have the earliest experimental evidence of a non-zero $\eta_B$ which appears to remain constant up to the present epoch.

Three conditions are famously required in order to dynamically generate a baryon asymmetry and are known as the "Sakharov conditions" [63]. These conditions are:

- Baryon number violation.
- $C$ and $CP$ violation.
- Departure from thermal equilibrium.

The first condition is required in order to produce an overall increase of baryons over antibaryons, or vice versa. Although $B$ appears to be a conserved global symmetry of the SM Lagrangian, non-perturbative effects [64, 65] which will be discussed below occur rapidly at high temperatures allowing for $B$ violation in the early universe even within the SM, though we note that these effects, while not controversial, are yet to be experimentally verified. The second condition is required in order for the interaction rates between baryons and antibaryons to be different, otherwise antibaryons would be produced at the same rate as baryons and therefore $\eta_B$ would remain unchanged. Finally a departure from thermal equilibrium is required in order to generate a difference in the number densities of baryons over antibaryons. In thermal equilibrium the reaction rates of a process will equal its time-reversed rate. This will lead to an equal number of particle and antiparticle microstates which necessarily implies their number densities will be equal through CPT invariance. Often baryogenesis models utilise the expansion of the universe as the catalyst for the departure of thermal equilibrium. If the relevant interaction rates are slower then the expansion rate, sufficient cooling of the final-state products will occur such that the inverse reaction become kinematically suppressed.

In principle the SM itself almost satisfies all three of these requirements. $C$ and $CP$ violation exists within the quark sector and, as mentioned, baryon number violation (although suppressed at zero temperature) can occur rapidly in the early universe. The interactions of the SM quarks, which violate $C$ and $CP$, remain in thermal equilibrium far longer than the non-perturbative $B$ violating processes and therefore the departure from thermal equilibrium can only be achieved if the electroweak phase transition in the early universe is strongly first order, see e.g. [66] for a detailed review. Detailed numerical simulations have shown that a strong first order electroweak phase transition requires a Higgs mass, $m_\phi$, below 80 GeV [67–72]. As the Higgs mass has been measured to be significantly heavier, the SM is unable to dynamically generate a baryon asymmetry alone and additional fields must be introduced. Assuming an unrealistically light Higgs such that all three Sakharov conditions are satisfied by the SM leads to a prediction [73] of $\eta_B \simeq 10^{-20}$ many order of magnitude smaller than what is measured. This indicates that extending the SM to allow for a departure from thermal equilibrium is not sufficient and additional $CPV$ interactions are therefore also required.

#### 1.2.2.1 $B + L$ within the Standard Model

In the SM $B$ and $L$ are anomalously violated by fermion currents of the form [64, 65, 74, 75]

$$\partial_\mu j^\mu_B = \partial_\mu j^\mu_L = \frac{n_G}{64\pi^2}\epsilon^{\mu\nu\rho\sigma}\left(g^2\, W^a_{\mu\nu} W^a_{\mu\nu} + g'^2 B_{\mu\nu} B_{\rho\sigma}\right) \tag{1.35}$$

where $j^\mu_B$ and $j^\mu_L$ are the baryonic and leptonic fermion currents respectively, $n_G$ corresponds to the number of fermion generations, $g$ and $g'$ are the $SU(2)_L$ and $U(1)_Y$ gauge couplings with $W^a_{\mu\nu}$ and $B_{\mu\nu}$ their respective field strength tensors. Clearly the linear combination $B - L$ will be anomaly free whereas the orthogonal combination $B + L$ is anomalously violated. Although naïvely this may suggest that in the SM global $U(1)$

symmetries for $B$ and $L$ cannot exist, a more subtle treatment shows that within perturbation theory these two currents are conserved (see e.g. [76] for a detailed explanation). Non-perturbative field configurations for the non-Abelian $SU(2)_L$ gauge fields however lead to interactions which violate the potential conservation of the two charges [65]. At zero temperature this occurs through tunneling between degenerate vacua, termed "instantons", and the rate of charge nonconservation can be calculated. An exponential suppression by a factor of $\exp(-8\pi^2/g^2) \simeq 10^{-81}$ occurs, with additional factors of Yukawa couplings leading to an even larger suppression. Therefore, at zero temperature $B$ and $L$ can be considered effectively conserved.

At finite temperature however, for a sufficiently hot thermal bath, thermal fluctuations can overcome the potential barrier between the degenerate vacua and classically transition between vacua without the need for tunnelling. These transitions, known as "sphaleron processes", are not exponentially suppressed and therefore can happen more rapidly. $B+L$ violation will therefore occur in the early universe, at sufficiently large temperatures, where the rate of violation depends on the height of the potential barriers as well as the temperature of the thermal bath. Sphaleron induced $B+L$ violation is rapid enough to be in thermal equilibrium in the temperature range [77–81]

$$100 \text{ GeV} \lesssim T_{\text{sph}} \lesssim 10^{12} \text{ GeV} \tag{1.36}$$

and can therefore play an important role in baryogenesis, provided that the remaining two Sakharov conditions are satisfied within this temperature range. Importantly sphaleron processes violate the aforementioned $B+L$ but not $B-L$, therefore if some asymmetry in $B-L$ is generated by some mechanism, the net $B-L$ cannot be increased or decreased. The $B+L$ violation causes a reprocessing such that this asymmetry is shared proportionally between $n_B$ and $n_L$. An analysis of the chemical potentials of processes within the early universe [82] indicates that

$$n_B = \frac{8n_G + 4n_\phi}{22n_G + 13n_\phi} n_{B-L} \qquad \text{and} \qquad n_L = -\frac{14n_G + 9n_\phi}{22n_G + 13n_\phi} n_{B-L} \tag{1.37}$$

where $n_\phi$ counts the number of complex Higgs doublets in the theory and only the SM fermion field content has been assumed to be in thermal equilibrium. Therefore if some mechanism injects a net $n_{B-L}$ into the thermal bath, the net asymmetry stored in $B$

and $L$ individually can be predicted. This can be simplified to

$$n_B = -\frac{8n_G + 4n_\phi}{14n_G + 9n_\phi} n_L = -\frac{28}{51} n_L \tag{1.38}$$

where in the second equality we have set $n_G = 3$ and $n_\phi = 1$ as in the SM. Therefore if baryogenesis occurs in a temperature regime where sphaleron processes are in equilibrium, a net asymmetry should be observed in both the net number of baryons in the universe as well as leptons. Interestingly this allows for baryogenesis to occur from processes which solely violate $L$ as long as the sphaleron rates are sufficiently rapid. If possible, measurements of the neutral lepton asymmetry stored in the C$\nu$B, such that the total lepton asymmetry $n_L$ can be determined, could therefore play a pivotal role in determining whether nonperturbative SM effects are responsible for the measured baryon asymmetry.

### 1.2.3 Baryogenesis through Thermal Leptogenesis

One of the most appealing models of baryogenesis, known as leptogenesis, occurs through the decays of heavy neutrino states which violate $L$ [83]. As previously discussed, provided that the majority of $L$ asymmetry generation occurs within the temperature regime of Eq. (1.36), where electroweak sphaleron processes are in equilibrium, more than half of the generated lepton asymmetry will be reprocessed into a baryon asymmetry. Its appeal is in large part due to the connection formed between the BAU and the seesaw mechanism described in Section 1.1.2.

In the high-scale variant of the type-I seesaw a large Majorana mass term, $M_R$, is responsible for the smallness of the active neutrino masses which necessarily implies the violation of $L$. Additionally due to the large size of $M_R$ assumed, the heavy neutrino mass eigenstates, $m_N$, in Eq. (1.22) ensure that the region in which the $L$ asymmetry is produced is before the critical temperature of the electroweak phase transition, $T_c \simeq 100$ GeV, after which reprocessing of $n_L$ into $n_B$ becomes exponentially suppressed. Additionally, a minimum of two heavy SNs are required to be introduced such that at least two of the active neutrinos gain a non-zero mass, and quite conveniently at least two SNs coupling to $\ell$ are also required in leptogenesis in order to generate a non-zero $n_L$. This therefore satisfies two of the three Sakharov conditions by construction: $B$ violation occurs due to $M_R$ violating $L$ with $M_R \gg T_c$ and the departure of thermal equilibrium

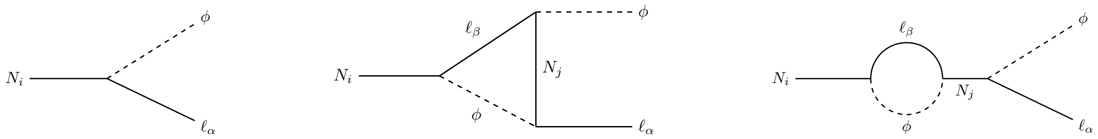


FIGURE 1.2: The tree-level and one-loop diagrams contributing to the L-violating decay chain $N \to \ell\phi$. The interference between the tree and one-loop diagrams is necessary such that a non-zero asymmetry is generated. The middle and right one-loop diagrams are known as the vertex and self-energy contributions respectively.

will occur when the decay rate of the SNs

$$\Gamma_{N_i} \equiv \Gamma_{N_i \to \ell\phi} \simeq \frac{1}{8\pi}\left(Y_\nu^\dagger Y_\nu\right)_{ii} M_{N_i} \tag{1.39}$$

falls below the Hubble expansion rate of the universe where it is sufficient to calculate $\Gamma_{N_i}$ at tree-level in this case. Once the universe cools to temperatures roughly around the masses of the SNs, the inverse decays $\ell\phi \to N_i$ will become Boltzmann suppressed and therefore the process $N_i \to \ell\phi$ will fall out of equilibrium, allowing for a possible net generation of $n_L$. In order for generation of $n_L$ to occur, CPV within the leptonic sector is required, which is simple to incorporate and may even be measured in low-energy oscillation experiments suggesting even more CPV phases may exist in the ultra-violet (UV) theory for the relevant leptons.

Commonly the parameters

$$\epsilon_i^\alpha = \frac{\Gamma(N_i \to \ell_\alpha\phi) - \Gamma(N_i \to (\ell_\alpha)^c\phi^\dagger)}{\sum_\alpha\left[\Gamma(N_i \to \ell_\alpha\phi) - \Gamma(N_i \to (\ell_\alpha)^c\phi^\dagger)\right]} \tag{1.40}$$

are utilised to measure the extent of CPV per SN decay, where $\alpha$ and $i$ represent the CP asymmetry generated from the decays of a SN $N_i$ to the lepton flavour $\alpha$. At tree-level the decay rate and the CP conjugate process are equal and therefore $\Gamma_{N_i}$ must be calculated including loop-level corrections in this case. Figure 1.2 shows the relevant diagrams at lowest order which will generate a non-zero $\epsilon_i^\alpha$. The middle and rightmost Feynman diagrams of Fig. 1.2 are known as the vertex and self-energy diagrams respectively and their relative importance in the calculation of $\epsilon_i^\alpha$ varies depending on the specifics of the model.

A detailed calculation [84, 85] finds

$$\varepsilon_i^\alpha = \frac{m_{N_i}}{64\pi^2\Gamma_{N_i}} \sum_{j\neq i} \Bigg( \underbrace{\mathcal{A}_{ij}^\alpha\, f(x_{ij})}_{\varepsilon_{\mathrm{V}}} + \underbrace{(\mathcal{A}_{ij}^\alpha \sqrt{x_{ij}} + \mathcal{B}_{ij}^\alpha) \frac{m_{N_j}^2\,(1-x_{ij})}{m_{N_j}^2\,(1-x_{ij})^2 + \Gamma_{N_j}^2}}_{\varepsilon_{\mathrm{S}}} \Bigg) \tag{1.41}$$

where $x_{ij} = (m_{N_j}/m_{N_i})^2$ and the loop function $f(x_{ij})$ is defined in Section 2.4.

$\mathcal{A}_{ij}^\alpha$ and $\mathcal{B}_{ij}^\alpha$ are expressions which are fourth order in the Yukawa couplings[6] within $Y_\nu$ which we suppress here for brevity but write in full in later chapters. The right hand side of Eq. (1.41) is the leading order contribution to $\epsilon_i^\alpha$. Higher-order diagrams will lead to additional terms albeit suppressed with additional powers of the Yukawa couplings. The labels $\epsilon_V$ and $\epsilon_S$ in Eq. (1.41) identify the contribution to $\epsilon_i^\alpha$ arising from the vertex and self-energy diagrams of Fig. 1.2 respectively.

Importantly, the self-energy contribution within Eq. (1.41) grows significantly in the limit where

$$m_{N_j}\,(1-x_{ij}) \to \Gamma_{N_j} \tag{1.42}$$

whereas the vertex contribution does not. This will occur when the mass splittings between $m_{N_i}$ and $m_{N_j}$ become comparable to their decay widths. In this limit $\epsilon_S$ dominates over $\epsilon_V$ by several orders of magnitude and the amount of CP asymmetry generated per SN decay grows significantly. Leptogenesis models can therefore be categorised by the mass spectrum between the heavy SNs, $m_{N_i}$ which we sort from smallest to largest mass.

Scenarios where $m_{N_j} \gg m_{N_1}$, for $j \neq 1$, are known as "hierarchical" leptogenesis scenarios. Here $\epsilon_S$ and $\epsilon_V$ have similar contributions[7] to $\epsilon_i^\alpha$ and due to the hierarchical spectrum, the heavier SNs will fall out of equilibrium in the early universe well before the lightest SN. Therefore any asymmetry generation due to the decays of $N_j$ will, in general[8], be effectively washed out from the inverse decays of $N_1$ which remain in thermal equilibrium. Therefore the final lepton, and therefore baryon, asymmetry can be

[6] From the full expressions for $\mathcal{A}$ and $\mathcal{B}$ written in Eq. (3.43), note that $\mathcal{A}_{ii}^\alpha = \mathcal{B}_{ii}^\alpha = 0$, confirming that at least two massive SN are required in order to generate a non-zero asymmetry, and that $\mathcal{A}_{ij}^\alpha = \mathcal{B}_{ij}^\alpha = 0$ if all CPV phases are switched off.

[7] A simple argument to justify this is that in the limit where $m_{N_j} \gg m_{N_1}$, $m_{N_j}$ can be integrated out from the diagrams of Fig. 1.2 leading to an effective four-point interaction and therefore the two one-loop diagrams will become identical.

[8] See e.g. [86] for an example where the heavier SNs are important for asymmetry generation in a hierarchical sceneario.

predicted purely from tracking the decays of $N_1$ at the temperature in which it falls out of equilibrium.

Scenarios where $m_{N_j} \simeq m_{N_1}$, for some $j$, are known as "degenerate" or "resonant" scenarios of leptogenesis. As discussed, the self-energy contribution to $\epsilon_i^\alpha$ can be resonantly enhanced and therefore sufficiently large asymmetry generation can occur for a larger region of parameter space. This comes at the cost of a highly degenerate mass spectrum of SNs which ideally should be motivated and also requires tracking the asymmetry generated in the decays of multiple different SNs which fall out of equilibrium at almost identical temperatures.

The final lepton asymmetry is determined by solving Boltzmann equations of the form

$$\begin{aligned} \frac{dn_{N_i}}{dz} &= -D\left(n_{N_i} - n_{N_i}^{\text{eq}}\right) \\ \frac{dn_L}{dz} &= \epsilon D\left(n_{N_i} - n_{N_i}^{\text{eq}}\right) - Wn_L \end{aligned} \tag{1.43}$$

where $z = m_{N_i}/T$, $D$ is a function of source terms, such as the two-body decay of $N_i$, which leads to asymmetry generation and $W$ is a function of the washout processes in the theory, for example the inverse decay, which removes the net asymmetry. Typically the densities are normalised such that a co-moving volume contains one heavy neutrino in ultra-relativistic thermal equilibrium such that $n_{N_i}^{\text{eq}}(T \gg m_N) = 1$. For simplicity only the dominant $1 \leftrightarrow 2$ decay and inverse decays are included plus the resonant part of the some[9] $2 \leftrightarrow 2$ processes which cannot be ignored to prevent overcounting [87]. A number of additional processes will contribute to the evolution of $n_{N_i}$ and $n_L$: $\Delta L = 1$ scattering terms which involve additional SM fields, the non-resonant parts of the $2 \leftrightarrow 2$ scattering terms already included and additional $2 \leftrightarrow 2$ processes which involve other SM fields. A more complete set of equations including expressions for $D$, $W$ and the additional scattering terms can be found in Chapter 2 and Appendix A. Additionally, depending on the temperature regime in which the asymmetry generation is occurring, tracking the total lepton asymmetry, $n_L$, compared to the asymmetry in each lepton flavour, $n_{L_\alpha}$, can incorrectly predict the final asymmetry [88]. This is particularly important in low scale models where the lightest SNs fall out of equilibrium below $T \lesssim 10^9$ GeV and will be further discussed in Section 2.1.

[9]Specifically the ($\Delta L = 0$ and $\Delta L = 2$) $2 \leftrightarrow 2$ diagrams which involve only $N_i$, $\ell_\alpha$ and $\phi$.

#### 1.2.3.1 Constraining Thermal Leptogenesis

Leptogenesis is clearly an attractive explanation for the measured BAU with a compelling connection to the experimentally measured light neutrino masses. Unfortunately the simplest variant of leptogenesis, that is a high-scale type-I seesaw with CPV couplings, is notoriously difficult to test experimentally. Due to the relationship between $m_\nu$ and $m_N$ in Eq. (1.22), requiring sizeable Yukawa couplings for testability leads to SN masses significantly larger than what can be probed by current terrestrial experiments. Additionally, to confirm any connection to leptogenesis, a detection of a SN is not sufficient. Precise measurements between CP conjugate processes are required in order to confirm, then measure, CPV in its relevant interactions.

However, a number of indirect constraints can be placed on the high-scale type-I seesaw if successful generation of the BAU is required. For a hierarchical spectrum of SN masses, such that the asymmetry is generated from the decay of the lightest SN and any potential resonance effects are avoided, a lower bound can be placed on the masses of the SNs. Decreasing the masses of the SNs implies a reduction in the Yukawa couplings, for a fixed $m_\nu$, which leads to a reduction in the relevant decay rates and therefore in the final baryon asymmetry generated. At some SN mass scale the smallness of the required Yukawa couplings from neutrino mass imply that the generated asymmetry from SN decay will fall below what is experimentally measured. This lower bound, known as the Davidson-Ibarra bound [89], is given by

$$m_{N_1} \gtrsim 10^9 \text{ GeV} \tag{1.44}$$

which was found from analytic arguments and confirmed numerically [90, 91]. This relied on a few simplifying assumptions; in particular only the lightest SN decay was considered and flavour effects ignored, and therefore can vary slightly when these assumptions are lifted. Nonetheless this suggests that leptogenesis requires experimentally unreachable masses.

However, a number of theoretical implications can be derived for such large SNs masses which might be in tension with this lower bound. In particular a possible upper bound, known as the Visanni bound [92, 93], can be placed on the SN neutrino mass of order $10^7$ GeV by requiring that radiative corrections to the Higgs mass parameter $\mu^2$, driven by the high seesaw scale, does not exceed 1 TeV[2]. A clear tension exists due to the lack of overlap, which can be resolved in a number of ways, for example by invoking supersymmetry to stabilise the Higgs mass. Supergravity however famously predicts the existence of gravitinos which are long-lived, and their decay products can spoil predictions of BBN. Requiring successful BBN in supersymmetric models leads to an additional, upper bound on the reheating temperature of $T_{\text{reh}} \sim 10^9$ GeV [94–96] and the tension remains as the Davidson-Ibarra bound now suggests that asymmetry generation occurs before reheating. Additionally, a recent study also finds that high scale thermal leptogenesis would have a catastrophic destabilising effect on the Higgs potential during reheating if it couples to the inflaton [97].

An exciting prospect for testing high-scale leptogenesis is through the potential gravitational wave signatures, although this requires the SN masses to arise from some high-scale symmetry breaking. Future space-borne missions can probe the entire parameter space of [98] and may begin to give a definitive answer whether high-scale leptogenesis is a viable baryogenesis mechanism.

Although the above does not rule out type-I seesaw high-scale leptogenesis, it strongly motivates the study of alternative scenarios, particularly those which allow for leptogenesis to occur at much lower scales such that possible issues at large cosmological temperatures are avoided and the Vissani bound is respected. The simplest way of lowering the scale of leptogenesis is by utilising the resonant enhancement in asymmetry generation which occurs for a degenerate spectrum of SNs. Alternatively leptogenesis could occur with SN masses *below* the critical temperature of the electroweak phase transition [99–101] if the SN population never reaches thermal equilibrium or through a modification of the scalar sector such that the tight connection between the heavy and light neutrino masses predicted in the type-I scenario is relaxed [102–104]. Particularly in the case of low-scale models, experimental discovery of any particles involved can be more optimistic, and identifying the regions of parameter space in these models which lead to viable asymmetry generation is important.

Leptogenesis as a baryogenesis mechanism relies on the reprocessing of $n_L$ into $n_B$ from electroweak sphalerons. As such the lepton asymmetry of the universe is strongly predicted by Eq. (1.38) to be of similar order to $n_B$ and, importantly, predicts an excess of antileptons. Charge conservation enforces that the lepton asymmetry stored in charged leptons is equal, in size *and* sign, to that of the protons and therefore leptogenesis models almost fundamentally predict a large antilepton asymmetry stored in the C$\nu$B. A future measurement[10] of the net neutral lepton asymmetry will therefore serve as the strongest evidence for or against leptogenesis as a baryogensis mechanism.

## 1.3 Quark-Lepton Symmetries

At the level of the SM, quarks and leptons are unrelated to each other. Obvious parallels exist between these two fermion types, namely: the experimentally discovered left- and right-handed quark and lepton states transform the same way under $SU(2)_L$ of $G_{\rm SM}$ and there are three identical generations of both particle types. There are of course a number of key difference between them: quarks are coloured and leptons are not, leptons carry integer charge whereas quarks have fractional charge, quark and lepton masses differ and the electrically-neutral right-handed lepton state is potentially absent unlike in the quark sector.

Nonetheless the idea that quarks and leptons can be related by some symmetry is one which precedes the SM itself. Before the development of the quark model of the strong interactions a similarity between the electric charges of the three baryons ($p$, $n$, $\Lambda^0$) and the three discovered leptons ($\nu_e$, $e^-$, $\mu^-$), when ordered from lightest to heaviest, was noticed. From this a baryon-lepton symmetry was proposed [109] and their electric charges could be predicted by a formula if ($p$, $n$) and ($\nu_e$, $e^-$) were assigned to transform as doublets under a new isospin group while $\Lambda^0$ and $\mu^-$ were iso-singlets. After the introduction of the quark model this proposed symmetry was modified to a quark-lepton symmetry with two triplet multiplets ($u$, $d$, $s$) and ($\nu_e$, $e^-$, $\mu^-$) which similarly led to a formula for the electric charges of each fermion with an additional reflection symmetry proposed between these two quark and lepton multiplets. After the discovery of the muon neutrino [110], $\nu_\mu$, the previously formulated quark-lepton symmetry was obviously no longer viable, but the idea of a reflection symmetry persisted, which motivated the successful theoretical prediction of the existence of a heavier up quark [111] which we know today as the charm quark. The subsequent discovery of the third generation of quarks and leptons only strengthens this apparent similarity between the two.

[10] Currently the C$\nu$B is completely unmeasured but a number of detection techniques have been proposed [105–108].

The aesthetic similarities between the quarks and leptons strongly suggest some extension to the SM in which a quark-lepton symmetry exists in the fundamental Lagrangian. Additionally, a significant fraction of the parameters within the SM in Table 1.2 arises from the large number of Yukawa couplings present. If additional symmetries are present between the SM fermions, such as a quark-lepton symmetry, this could lead to a theoretically attractive decrease in the number of free Yukawa couplings. As this would generically imply mass equality between certain[11] quarks and leptons at some higher scale, this may ultimately lead to an understanding of the large hierarchies of masses observed at low scales.

A number of different quark-lepton symmetries or unifications are possible, most often through a continuous symmetry. The many different grand unified theories (GUTs) are well motivated and studied candidates. Here the fermion content of the SM is embedded into larger multiplets of a gauge group which contains the SM gauge groups as a subgroup. Minimally, the fifteen chiral fermions of a given generation of the SM fit into two representations, the $\overline{\mathbf{5}}$ and $\mathbf{10}$, of $SU(5)$ [112]:

$$\begin{aligned} \overline{\mathbf{5}} &\to (\overline{\mathbf{3}}, \mathbf{1}, \frac{1}{3}) \oplus (\mathbf{1}, \mathbf{2}, -\frac{1}{2}) \equiv (d_R)^c \oplus \ell_L \\ \mathbf{10} &\to (\mathbf{3}, \mathbf{2}, \frac{1}{6}) \oplus (\overline{\mathbf{3}}, \mathbf{1}, -\frac{2}{3}) \oplus (\mathbf{1}, \mathbf{1}, 1) \equiv Q_L \oplus (u_R)^c \oplus (e_R)^c \end{aligned} \tag{1.45}$$

which contains $G_{\rm SM}$ as a maximal subgroup. Although unable to explain neutrino mass without the introduction of a singlet, quarks and leptons are now partially unified which at the very least explains why quarks and leptons have the same number of generations at the low scale and their unequal electric charges. With the addition of a singlet to the SM field content, for the purpose of neutrino mass, additional possibilities of unification become possible. The now sixteen chiral fermions can be unified into just *one* multiplet of $SO(10)$ [113, 114], the spinorial $\mathbf{16}$ dimensional representation. Although many GUT theories are possible beyond the two presented, they all commonly require large scales of symmetry breaking when moving from the scale where quarks and leptons are unified to the SM. A consequence of many quark-lepton unifying models is the existence of new exotic bosons, both scalar and vector, which couple quarks and leptons together. As a consequence quarks can convert into leptons leading to unobserved processes such as proton decay. Requiring sufficiently slow proton decay rates requires the scales of

[11] Depending on the specific quark-lepton symmetry assumed different mass equalities may be predicted.

quark-lepton unification breaking to be even larger than the seesaw scale described in Section 1.1.2 in the case of the two aforementioned GUTs.

Although in general quark-lepton symmetries are expected to be broken at extremely high scales simply due to the need to suppress baryon number violating interactions, some scenarios can be constructed with low scales of quark-lepton unification breaking. The Pati-Salam (PS) [115, 116] gauge group, which embeds the SM into

$$G_{\mathrm{PS}} = SU(4)_{\mathrm{c}} \otimes SU(2)_{\mathrm{L}} \otimes SU(2)_{\mathrm{R}}, \tag{1.46}$$

is one such variant. The breaking of $SU(4)_c \to SU(3)_c \otimes U(1)_X$ is required and the SM fermions, plus a right-handed neutrino, are embedded in the **4** dimensional representation of $SU(4)$ which breaks as per

$$\mathbf{4} \to \mathbf{1}_{-1} \oplus \mathbf{3}_{1/3}. \tag{1.47}$$

$X$ can be identified with $B - L$ and lepton number can be thought of as a "fourth colour", explaining the observed pattern that quarks, with fractional charge, are coloured whereas leptons, with integer charge, are not. Here, the proton can remain absolutely stable due to the combination of the gauged $B - L$ and an accidental symmetry of the Yukawa Lagrangian and therefore gauge-mediated proton decay is forbidden, allowing for much lower phenomenological scales of PS breaking. Importantly two mass relations are predicted in the minimal model,

$$m_\nu^{\mathrm{Dirac}} = m_u \qquad \text{and} \qquad m_d = m_e, \tag{1.48}$$

which must be broken. It naturally generates a seesaw mechanism through the scalar content required for PS breaking which leads to high-scale and low-scale breaking variants depending on the neutrino mass generation mechanism, which will be discussed in detail in Chapter 4. If the neutrino mass mixing matrix is of the form of the minimal type-I seesaw, as in Eq. (1.21), PS breaking is constrained to occur at a minimum of $v_{PS} \gtrsim 10^{12}$ GeV, well outside of experimental reach. If instead the matter content is modified such that a low-scale seesaw is generated, as in Eq. (1.27), the breaking scale is not fixed by the smallness of the active neutrino masses and can therefore be at a sufficiently low scale such that it can be constrained experimentally. The PS gauge group also happens to be a maximal subgroup of $SO(10)$ and therefore quark-lepton unification may be a part of a chain of breakings from a large GUT down to $SU(3) \otimes U(1)_{\text{EM}}$.

The gauge and scalar leptoquarks within the theory, while not strongly constrained by proton decay, still mediate processes which are experimentally testable allowing for the possibility of discovering a quark-lepton symmetry in current and future experiments. A recent resurgence in the popularity of low-scale PS has occurred due to a number of discrepant measurements related to semi-leptonic decays of various hadrons. In particular a set of anomalies has been measured involving the charged-current transition $b \to c\tau\nu$ [117–119] and the neutral-current transition $b \to s\mu\mu$ [120, 121] which can be explained quite naturally in a low-scale PS model, or PS-like models, through its gauge and various possible scalar leptoquarks. If these anomalies are confirmed in the future, this may be the first hint of a quark-lepton symmetry which is broken at scales not far from the electroweak scale, of which the PS gauge symmetry is one of the most promising candidates.

An alternative way of achieving quark-lepton unification at low scales may be through a discrete symmetry between quarks and leptons, similar to that which was historically proposed between baryons and leptons, where $G_{\text{SM}}$ is embedded into

$$G_{q\ell} = SU(3)_q \otimes SU(3)_\ell \otimes SU(2)_L \otimes U(1)_X, \tag{1.49}$$

where $SU(3)_q$ corresponds to ordinary colour and $SU(3)_\ell$ is a leptonic equivalent [122–124]. Three copies of leptons per generation are predicted similar to the quarks but the breaking of $SU(3)_\ell$, and not $SU(3)_q$, at some scale above the electroweak scale results in the extra leptonic states having masses significantly heavier than their quark counterparts. Here a discrete symmetry relates the quarks and leptons and similar to the case of the continuous PS symmetry, the $SU(3)_\ell$ breaking can be brought low through a low-scale seesaw.

The aesthetic similarities between quarks and leptons is therefore a promising indication of a theory beyond the SM which contains additional symmetries broken at larger scales compared to electroweak symmetry breaking. The large number of ways in which quarks and leptons can be related to each other, both at high scales and low scales, leads to unique phenomenology for each model which, particularly for low-scale variants, can lead to exciting experimentally testable predictions.

## 1.4 Thesis Outline

In this chapter we have presented a brief overview of the SM and presented evidence for two areas in which the SM is unable to explain experimentally observed and measured phenomena: neutrino oscillations and the measured BAU. Additionally we have discussed a third area, quark-lepton symmetries, which also motivates an extension of the SM albeit from theoretical arguments and aesthetics as opposed to unambiguous experimental observation. An obvious connection exists between neutrino mass and the areas of leptogenesis and quark-lepton symmetries. The simplest explanation of neutrino mass leads to a super heavy SN state whose decays naturally lead to an $L$ asymmetry which SM processes can reprocesses into a $B$ asymmetry, connecting the BAU with neutrino mass. Neutrino mass and quark-lepton symmetries are also obviously quite naturally related due to the disparate masses between the quarks and leptons, particularly in the case of the neutrinos, which quark-lepton symmetries often predict to be degenerate. We will focus our attention on the Pati-Salam quark-lepton unifying gauge group where the scalars required to break the PS symmetry also generate masses for SNs at the same scale.

The purpose of this thesis is to explore these two connections, particularly the implications that low-scale neutrino mass seesaws can have for leptogenesis and some phenomenological implications they have in the case of PS. As a working definition we will define a low-scale seesaw as one in which the heaviest SN masses are close to the electroweak scale (no heavier than 1000 TeV). This typically requires small LNV parameters within a seesaw in order to generate a viable active neutrino mass spectrum.

In Chapter 2 we study the leptogenesis implications of assuming an inverse or linear seesaw for neutrino mass with the lightest SN masses fixed at the TeV scale. In particular we focus on a resonant scenario where the only mass splittings between the SNs arise from the small LNV parameters within the mass mixing matrix and therefore avoid degeneracies between the SN masses of different generations. Due to the exciting connection between low-scale leptogenesis and low-energy CP violation, which we discuss shortly, we analyse the implications for leptogenesis driven solely by the Dirac phase within the PMNS matrix which, at the time when the analysis was performed, was favoured to be maximally violating at one standard deviation for the normal neutrino mass ordering we assumed.

Chapter 3 builds on the work of Chapter 2 by demonstrating that the parameter space of viable leptogenesis can be extended if additional resonance effects, beyond that generated by the small LNV parameters, are included. In order to motivate the additional small mass splittings between SNs, we adopt a continuous flavour symmetry implied by the SM which enforces exactly degenerate SN masses at some higher scale. The breaking of this flavour symmetry generates small deviations from this exact degeneracy and can widen the parameter space of leptogenesis for the low-scale seesaws assumed. Importantly we highlight that a flavour-alignment issue, which strongly suppresses asymmetry generation for the minimal type-I seesaw extended by the same flavour symmetry, is absent in ISS and LSS models and therefore are the simplest viable leptogenesis models with the assumed flavour symmetry.

In Chapter 4 we analyse the seesaw implications of requiring a phenomenologically viable spectrum of neutral and charged fermion masses for all three generations when a PS gauge symmetry is assumed. In particular we establish that if mass matrix seesaws occur in both the neutral *and* charged fermion sectors, a substantial reduction in the experimental limits on PS breaking can occur due to a chiral-suppression in the relevant meson decays. We will quantify which fermion embeddings of exotic fields within PS lead to the desired mixing effects and analyse the regions of parameter space required in each viable model.

Lastly, in Chapter 5 we conclude with a summary of the results of each chapter.

# Chapter 2

# Low-scale Resonant Leptogenesis from Low-energy CP Violation

CP violation is a necessary ingredient for any baryogenesis model, otherwise the B-violating interactions introduced will produce an equal amount of baryons and antibaryons. In thermal leptogenesis, as described in Section 1.2.3, the CP asymmetry arises from the complex phases in the Yukawa interactions between the heavy SNs and the SM leptons. This therefore requires the two processes $\Gamma_{N\to \ell\phi}$ and $\Gamma_{N\to \ell^c\phi^\dagger}$ to occur at different rates at the time of asymmetry generation. Two distinct sources of CP violation occur in leptogenesis: from low-energy CP violating phases observable in neutrino oscillation or double beta decay experiments, or from high-scale CP violating phases related to the SNs themselves. The low-scale CP violating phases appear within the PMNS matrix whereas the high-scale phases can be grouped into an "R-matrix" in the Casas-Ibarra parametrisation of the Yukawa coupling matrix, which we will define below. In this chapter we simultaneously explore the viability of a low-scale inverse (ISS), linear (LSS) or a combined (ISS+LSS) seesaw as a leptogenesis candidate as well as determine whether leptogenesis in these models can viably arise when the CP violation occurs solely due to low-energy phases. Specifically we analyse the feasibility of leptogenesis arising from the CPV Dirac phase within the PMNS matrix, which is the only low-scale CPV phase guaranteed to be measured in the near future. At the time when this analysis was performed [1], the Dirac-phase had its best fit value close to the maximum violating value of $3\pi/2$ for a normal ordering between the three light neutrino masses [125], which we assumed in our analysis for simplicity. Since then the best fit value has shifted closer to the

CP conserving value of $\pi$ [34] although this may continue to fluctuate and a maximally violating value for $\delta_{CP}$ is still well within three standard deviations of the best fit value. Once the experimental limits on $\delta_{CP}$ begin to significantly narrow, it will become clearer whether the Dirac phase is at least partially responsible for asymmetry generation[1]. If the Dirac phase was eventually measured to be CP conserving, low-energy CP violating leptogenesis would remain a viable possibility through the Majorana phases which are currently unconstrained. For simplicity however, we set them to zero in this particular analysis.

This chapter is organised as follows. Section 2.1 briefly discusses the viability of leptogenesis ocurring from PMNS phases at different temperatures. Sections 2.2 and 2.3 explain how neutrino masses arise in this low-scale model and demonstrates how to guarantee the correct light, active neutrino physics. Section 2.4 describes the relevant leptogenesis calculations. Section 2.5 details the constraints used and estimates the possibility of future experiments in constraining such models. Finally, Section 2.6 presents numerical results obtained in the analysis and discusses implications of these results. In Appendices A and B we present the decay and scattering formulas used, and discuss the $\delta_{CP}$ dependence of the asymmetry in more detail.

## 2.1 Viability of low-energy CP violation in leptogenesis

Depending on the temperature regime in which leptogenesis occurs, different SM processes are in or out of thermal equilibrium. This affects the validity of certain approximations used in the calculations of the generated baryon asymmetry. If leptogenesis occurs at high scales,

$$T_{\text{lepto}} \gtrsim 10^{12}\ \text{GeV}, \tag{2.1}$$

the Yukawa interactions of the charged leptons are far out of equilibrium and it is justifiable to simply track the total lepton asymmetry generated in each SN decay, as opposed to tracking the net lepton asymmetry generated into each specific lepton flavour. The heavy SN will decay into the three lepton flavours, $L_e$, $L_\mu$ and $L_\tau$ in proportion to its couplings and as no other processes are in equilibrium, the ratio of lepton flavour asymmetries will remain fixed. A basis could therefore be chosen such that the SN decays

[1]However we note that the best fit value in the case of an inverted ordering still favours a maximal CP violating value.

into only one flavour of leptons, $L_z = aL_e + bL_\mu + cL_\tau$, which is not spoiled by any other interactions within the thermal bath and the other two orthogonal flavour combinations have zero net asymmetry generated[2]. As a consequence of this, the low-energy CP violating phases of the PMNS matrix can play no role in the production of an asymmetry in type-I seesaw hierarchical leptogenesis. In regions where tracking of individual lepton flavour asymmetries is not required, the CP asymmetry parameter depends only on the matrix $Y_\nu^\dagger Y_\nu$, which does not depend on $U_{\mathrm{PMNS}}$. This is clear to see from Eq. (2.24) in Section 2.3.3.

At lower temperatures, the Yukawa interactions of the charged leptons begin to come into thermal equilibrium, with the tau lepton Yukawa interaction coming into equilibrium below $10^{12}$ GeV and the muon Yukawa interaction coming into equilibrium at roughly $10^9$ GeV. As a result of this, the additional thermal interactions will cause a decoherence effect and tracking of individual lepton flavour asymmetries becomes important. It is in this regime where low-energy CP violating phases of the PMNS contribute to a non-zero value of $\epsilon_i$ in type-I leptogenesis. As between $10^{9-12}$ GeV only the tau lepton Yukawa comes into thermal equilibrium, two lepton flavours must be tracked in this regime: the asymmetry in $n_{L_\tau}$ and the asymmetry in $n_{L_{\mu+e}}$. Below $10^9$ GeV two lepton flavours have Yukawa interactions in thermal equilibrium and as such all three lepton flavours must be tracked even though the electron Yukawa is still far from equilibrium.

Therefore high-scale leptogenesis models are, in general, unable to produce an asymmetry from the low-energy PMNS phases, further removing possible chances of connecting it to terrestrial experiments. Leptogenesis models with asymmetry generation at much lower temperatures however can viably generate an asymmetry through these potentially measurable low-energy phases. This possibility was first noted over a decade ago [88, 126–128] in the case of type-I seesaw hierarchical leptogenesis. However, due to the Davidson-Ibarra bound discussed in Section 1.2.3.1, the PMNS phases can only contribute to asymmetry generation in a very small window of SN masses, as larger masses will cause the relevant Yukawa interactions to fall out of equilibrium[3]. This effect is quite interesting

[2] This statement assumes a hierarchical spectrum of SN masses where the asymmetry generated in the decays of the heavier SNs is sufficiently washed out such that their contribution to the final asymmetry is negligible. If multiple different physical SN decays need to be tracked at the epoch of leptogenesis their individual couplings to the lepton flavours may break this potential flavour basis choice and would likely require tracking of all three flavours. Nonetheless low-energy CPV phases will still not contribute.

[3] See [129] for a scenario where the Davidson-Ibarra bound can be lowered through a cancellation between tree- and loop-level neutrino mass contributions widening the potential parameters space for low-energy CPV leptogenesis in the type-I seesaw.

to explore in low-scale models, however, as a measurement of CP non-conservation in the PMNS phases coupled with a discovery of the Majorana nature of the massive neutrinos could conceivably lead to strong circumstantial evidence for, but not definitively prove, a thermal leptogenesis mechanism.

## 2.2 Neutrino masses in the Inverse and Linear Seesaws

For completeness, we briefly derive the resultant light neutrino mass block in the ISS and LSS models after diagonalisation. A neutrino mass matrix of the form

$$M_{\text{type-I}} = \begin{pmatrix} 0 & m_D^\nu \\ (m_D^\nu)^T & M_R \end{pmatrix} \tag{2.2}$$

has its lightest neutrino mass block given by

$$m_\nu \simeq -m_D^\nu M_R^{-1} (m_D^\nu)^T \tag{2.3}$$

which we perturbatively show in Appendix D.0.2. The general ISS+LSS mass mixing matrix

$$M_{\text{ISS+LSS}} = \begin{pmatrix} 0 & m_D^\nu & m_L \\ (m_D^\nu)^T & \mu_N & M_R \\ m_L^T & M_R^T & \mu_S \end{pmatrix} \tag{2.4}$$

can be repartitioned into a type-I-like matrix:

$$M_{\text{ISS+LSS}} = \begin{pmatrix} 0 & \mathcal{M}_\mathcal{D} \\ (\mathcal{M}_\mathcal{D})^T & \mathcal{M}_\mathcal{R} \end{pmatrix} \tag{2.5}$$

where

$$\mathcal{M}_\mathcal{D} = (m_D^\nu, m_L) \quad \text{and} \quad \mathcal{M}_\mathcal{R} = \begin{pmatrix} \mu_N & M_R \\ M_R^T & \mu_S \end{pmatrix}. \tag{2.6}$$

By assumption, the singular values of $M_R$ are larger than all the singular values of $\mu_{N/S}$, $m_L$ and $m_D^\nu$ which implies that the singular values of $\mathcal{M}_\mathcal{R}$ are all larger than the singular values of $\mathcal{M_D}$[4]. Therefore the result in Eq. (2.2) applies leading to

$$m_\nu \simeq -\mathcal{M_D}(\mathcal{M_R})^{-1}\mathcal{M_D}^T. \tag{2.7}$$

This can be expanded with the definitions of $\mathcal{M_D}$ and $\mathcal{M_R}$ to give

$$m_\nu \simeq m_D^\nu (M_R^{-1})^T \mu_S \, M_R^{-1} (m_D^\nu)^T - m_D^\nu (M_R^{-1})^T (m_L^\nu)^T - \left[m_D^\nu (M_R^{-1})^T (m_L^\nu)^T\right]^T. \tag{2.8}$$

At lowest order, the two heavy SN mass states are trivially given by diagonalising $\mathcal{M_R}$ itself which leads to

$$m_{N_{1/2}} \simeq M_R \pm \frac{1}{2}\left(\mu_N + \mu_S\right). \tag{2.9}$$

Note that the Majorana mass term $\mu_N$ does not affect the light neutrino masses at lowest order[5] and therefore is of negligible importance to the analysis below and justifies setting it to zero for simplicity, as is commonly done. In this limit the mixing between the light and heavy states is given very simply by

$$\zeta = \mathcal{M_D}\mathcal{M_R}^{-1} \simeq \left(m_L M_R^{-1},\, m_D^\nu (M_R^T)^{-1}\right) \tag{2.10}$$

and the combinatoin $\zeta^*\zeta^T$ will measure the degree of unitarity violation within the observed PMNS matrix.

## 2.3 Model

The full Lagrangian, with the addition of three extra SM gauge singlet fermions alongside the three right-handed neutrinos, is given by,

$$\begin{aligned} -\mathcal{L}_{BSM} = \lambda_D \overline{l_L}\, \phi^c N_R + \lambda_L \overline{l_L}\, \phi^c \left(S_L\right)^c + M_R \overline{(N_R)^c} \left(S_L\right)^c \\ + \frac{1}{2}\mu_S \, \overline{S_L} \left(S_L\right)^c + \frac{1}{2}\mu_N \, \overline{(N_R)^c} N_R + \text{H.c.} \end{aligned} \tag{2.11}$$

[4]This is certainly true when $\|\mu_{N/S}\| \ll \|m_D^\nu,\, m_L\|$ however care must be taken if $\mu_N$ or $\mu_S$ contain entries close in size (but still smaller) to the singular values of $M_R$. For large enough values within $\mu_{N/S}$, some singular values of $\mathcal{M_R}$ could become suppressed compared to $m_D^\nu$ and $m_L$ potentially breaking the assumed hierarchy between the singular values of $\mathcal{M_R}$ and $\mathcal{M_D}$.

[5]As mentioned previously, higher order terms in $m_\nu$ which contain $\mu_N$ will always contain at least one factor of $\mu_S$ and therefore in the limit $\mu_S \to 0_{3\times 3}$, assuming the above hierarchy of block matrix singular values, the entries of $\mu_N$ do not contribute to $m_\nu$ regardless of their size.

After the SM Higgs doublet $\phi$ gains a vacuum expectation value, $v_{EW}$, and breaks $SU(2)_L \otimes U(1)_Y \to U(1)_{\text{EM}}$, the neutral lepton mass matrix arising from Eq. (2.11) has the general form, in the $[(\nu_L)^c,\, N_R,\, (S_L)^c]^T$ basis[6],

$$M_\nu = \begin{pmatrix} 0 & m_D^\nu & m_L \\ (m_D^\nu)^T & 0 & M_R \\ m_L^T & M_R^T & \mu \end{pmatrix}, \tag{2.12}$$

where $\mu$ is in general a complex, symmetric $3\times3$ matrix and $m_D^\nu = \lambda_D v_{EW}$, $m_L = \lambda_L v_{EW}$ and $M_R$ are in general complex $3 \times 3$ mass matrices. The full mass matrix of Eq. (2.12) has a number of limiting cases, according to assumptions on the allowed couplings and their strengths.

### 2.3.1 Inverse seesaw (ISS)

The ISS mechanism arises from Eq. (2.12) in the parameter regime where $\sigma_i(\mu,\, m_D^\nu) \ll \sigma_1(M_R)$ and $m_L \to 0_{3\times3}$, leading to the neutrino mass matrix

$$M_\nu = \begin{pmatrix} 0 & m_D^\nu & 0 \\ (m_D^\nu)^T & 0 & M_R \\ 0 & M_R^T & \mu \end{pmatrix}. \tag{2.13}$$

Upon block diagonalisation of Eq. (2.13), one can calculate the light neutrino mass matrix to first order,

$$m_\nu = m_D^\nu \left(M_R^T\right)^{-1} \mu\, M_R^{-1}\, (m_D^\nu)^T. \tag{2.14}$$

The heavy Majorana neutrinos will be primarily admixtures of the $N_R$ and $(S_L)^c$ states with mass matrices of the form (above the critical temperature and again to first order),

$$M_N = M_R \pm \frac{1}{2}\mu. \tag{2.15}$$

By contrast with the type-I seesaw model, there is now a double suppression of the light neutrino states in Eq. (2.14) due to the smallness of $\left(m_D^\nu M_R^{-1}\right)^2$ as well as the smallness of the parameter $\mu$ as discussed above. In the limit of $\mu \to 0_{3\times3}$ the light neutrinos

[6]For brevity in the remainder of this chapter we will write $\mu_S = \mu$ and set $\mu_N = 0$ as justified in Section 2.2.

become massless and the heavy sterile states form heavy Dirac singlets in a way that is independent of any other parameter in the theory restoring lepton number conservation.

The scale required in order to achieve the necessary active neutrino masses can be estimated[7] [130]

$$\left(\frac{m_\nu}{0.1\text{ eV}}\right) = \left(\frac{m_D^\nu}{100\text{ GeV}}\right)^2 \left(\frac{\mu}{1\text{ keV}}\right) \left(\frac{M_R}{10^4\text{ GeV}}\right)^{-2}, \tag{2.16}$$

where now the mass scale of the heavy SNs has been brought down to a relatively low, potentially experimentally testable level and with electroweak scale couplings.

### 2.3.2 Linear Seesaw (LSS)

The limit $\mu \to 0_{3\times3}$ of Eq. (2.12) is known as the linear see-saw (LSS), with a mass matrix of the form

$$M_\nu = \begin{pmatrix} 0 & m_D^\nu & m_L \\ (m_D^\nu)^T & 0 & M_R \\ m_L^T & M_R^T & 0 \end{pmatrix}. \tag{2.17}$$

After block diagonalisation, assuming a similar hierarchy: $\sigma_i(m_D^\nu, m_L) \ll \sigma_1(M_R)$, the effective light neutrino mass matrix is now given by,

$$m_\nu = -\left[m_D^\nu \left(m_L M_R^{-1}\right)^T + \left(m_L M_R^{-1}\right)\left(m_D^\nu\right)^T\right]. \tag{2.18}$$

The heavy SNs have mass matrix (above the critical temperature)

$$M_N = M_R. \tag{2.19}$$

Similar to above, the correct active neutrino masses are possible with low-scale heavy SNs,

$$\left(\frac{m_\nu}{0.1\text{ eV}}\right) = \left(\frac{m_D^\nu}{100\text{ GeV}}\right) \left(\frac{m_L}{10\text{ eV}}\right) \left(\frac{M_R}{10^4\text{ GeV}}\right)^{-1}. \tag{2.20}$$

Massless light neutrinos are recovered in the limit of vanishing $m_L$, and, in complete analogy with the ISS parameter $\mu$, this is the parameter in the LSS that can be chosen to explicitly break lepton number and therefore can be set small from the point of view of technical naturalness.

[7] In the one generation approximation.

### 2.3.3 Casas-Ibarra parametrisation

The Casas-Ibarra parametrisation of the Dirac mass matrix $m_D^\nu$ [131] can be generalised in order to satisfy the light neutrino constraints for this extended type-I scenario. In the conventional type-I scenario, the effective light neutrino mass matrix is given by [132]

$$m_\nu \simeq -m_D^\nu M_R^{-1} (m_D^\nu)^T \tag{2.21}$$

in the limit $m_D^\nu \ll M_R$, and with the effective mass term being $\bar{\nu}_L m_\nu (\nu_L)^c + \text{H.c.}$ This $3 \times 3$ block is approximately diagonalised by the unitary PMNS matrix $U_{\text{PMNS}}$,

$$U_{\text{PMNS}}^\dagger \, m_\nu \, U_{\text{PMNS}}^* = m_n \equiv \text{diag}(m_1, m_2, m_3), \tag{2.22}$$

$m_{1,2,3}$ are the light neutrino masses, and

$$U_{\text{PMNS}} = \begin{pmatrix} c_{12}c_{13} & s_{12}c_{13} & s_{13}e^{-i\delta_{CP}} \\ -s_{12}c_{23} - c_{12}s_{23}s_{13}e^{i\delta_{CP}} & c_{12}c_{23} - s_{12}s_{23}s_{13}e^{i\delta_{CP}} & s_{23}c_{13} \\ s_{12}s_{23} - c_{12}c_{23}s_{13}e^{i\delta_{CP}} & -c_{12}s_{23} - s_{12}c_{23}s_{13}e^{i\delta_{CP}} & c_{23}c_{13} \end{pmatrix} \times \text{diag}(e^{i\alpha_1},\, e^{i\alpha_2},\, 1) \tag{2.23}$$

where we have specifically assumed a basis for the charged-lepton mass matrix which is diagonal. For the remainder of this chapter, the low energy Majorana CP-violating phases $\alpha_1$ and $\alpha_2$ will be set to zero as our aim is to see if leptogenesis may be successfully driven solely by $\delta_{CP}$, we also suppress the PMNS subscript on $U_{\text{PMNS}}$ as there is not chance of confusion.

Equations (2.21) and (2.22) can be solved for the Dirac mass matrix $m_D^\nu$ to obtain the Casas-Ibarra parametrisation,

$$m_D^\nu = i U \, m_n^{1/2} \, R \, M_R^{1/2}, \tag{2.24}$$

where the matrix $R$ must be orthogonal: $RR^T = \mathbb{1}_{3\times 3}$ but not necessarily real. Thus, inputting $U$ and two out of the three masses in $m_n$ from experiment, this equation specifies the required neutrino Dirac mass matrix for given choices of the unknown absolute neutrino mass scale for the light neutrino sector, and the matrices $M_R$ and $R$.[8]

### 2.3.4 Extended Casas-Ibarra parametrisations

We now derive equivalent Casas-Ibarra-type parametrisations in different extended type-I seesaw models for $m_D^\nu$ in order to ensure agreement with neutrino oscillation experimental results.

#### 2.3.4.1 Inverse Seesaw

In the case of the ISS, combining Eqs. (2.14) and (2.22) gives

$$\left(m_n^{-1/2}\, U^\dagger\, m_D^\nu\, \left(M_R^T\right)^{-1}\, \mu^{1/2}\right)\left(\mu^{1/2}\, M_R^{-1}\, (m_D^\nu)^T\, U^*\, m_n^{-1/2}\right) = \mathbb{1}_{3\times 3}. \tag{2.25}$$

Since $\mu$ is symmetric, we define an $R$ matrix and rearrange for $m_D^\nu$ to obtain

$$m_D^\nu = U\, m_n^{1/2}\, R\, \mu^{-1/2}\, M_R^T\,. \tag{2.26}$$

In general $R$ is a complex orthogonal matrix. However, in order to maintain $\delta_{CP}$ as the only source of CP-violation, we restrict $R$ to being real orthogonal, parametrised by

$$R = \begin{pmatrix} c_y c_z & -s_x c_z s_y - c_x s_z & s_x s_z - c_x s_y c_z \\ c_y s_z & c_x c_z - s_x s_y s_z & -c_z s_x - c_x s_y s_z \\ s_y & s_x c_y & c_x c_y \end{pmatrix} \tag{2.27}$$

where $c_x = \cos x$ and $s_x = \sin x$ and so on for $x, y, z \in \mathbb{R}$.

#### 2.3.4.2 Linear Seesaw

For completeness the parametrisation required for the linear seesaw is also presented.[9]

---

[8]Note that the generated Dirac mass matrix will only be guaranteed to recover the correct mass differences among the light neutrinos if it continues to satisfy the approximation used for the block diagonalisation of the original mass matrix, namely $\sigma_i(m_D^\nu) \ll \sigma_1(M_R)$ in the case of the type-I seesaw, and any other approximation used in extended or different seesaw models.

[9]The pure linear seesaw will not be considered further (in this chapter) as above the critical temperature, relevant for thermal leptogenesis, the SNs will have degenerate masses and the generated asymmetry is highly suppressed which we discuss in Chapter 3.

Combining Eqs. (2.18) and (2.22) leads to

$$-m_n^{-1/2}\,U^\dagger\left[m_D^\nu\left(m_L M_R^{-1}\right)^T\right]U^*\,m_n^{-1/2}+m_n^{-1/2}\,U^\dagger\left[\left(m_L M_R^{-1}\right)(m_D^\nu)^T\right]U^*\,m_n^{-1/2}=\mathbb{1}_{3\times 3}. \tag{2.28}$$

Defining

$$R=-m_n^{-1/2}\,U^\dagger\left[m_D^\nu\left(m_L M_R^{-1}\right)^T\right]U^*\,m_n^{-1/2} \tag{2.29}$$

implies that the $R$ matrix must now satisfy $R+R^T=\mathbb{1}_{3\times 3}$. Rearranging Eq. (2.29) gives the parametrisation for $m_D^\nu$,

$$m_D^\nu=-U\,m_n^{1/2}\,R\,m_n^{1/2}\,U^T\,\left(m_L^T\right)^{-1}M_R^T\,. \tag{2.30}$$

### 2.3.5 Inverse + Linear Seesaws (ISS + LSS)

In the case where terms from both the linear and inverse seesaws are present, the effective light neutrino mass matrix at first order is a linear combination of Eqs. (2.14) and (2.18),

$$m_\nu=m_D^\nu\,\left(M_R^T\right)^{-1}\mu\,M_R^{-1}\,(m_D^\nu)^T-\left[\left(m_D^\nu\left(m_L M_R^{-1}\right)^T+\left(m_L M_R^{-1}\right)(m_D^\nu)^T\right]. \tag{2.31}$$

Combining with Eq. (2.22) leads to

$$m_n^{-1/2}\,U^\dagger\left[m_D^\nu\,\left(M_R^T\right)^{-1}\mu\,M_R^{-1}\,(m_D^\nu)^T-m_D^\nu\left(m_L M_R^{-1}\right)^T-\left(m_L M_R^{-1}\right)(m_D^\nu)^T\right]U^*\,m_n^{-1/2}$$
$$=\mathbb{1}_{3\times 3}. \tag{2.32}$$

It is convenient to define a new matrix

$$\begin{aligned} A\;&=\frac{1}{2}\,m_D^\nu\left(M_R^T\right)^{-1}\mu\,M_R^{-1}\,(m_D^\nu)^T-m_D^\nu\left(m_L M_R^{-1}\right)^T,\\ A^T\;&=\frac{1}{2}\,m_D^\nu\left(M_R^T\right)^{-1}\mu\,M_R^{-1}\,(m_D^\nu)^T-\left(m_L M_R^{-1}\right)(m_D^\nu)^T. \end{aligned} \tag{2.33}$$

Rewriting Eq. (2.32) in terms of this new A matrix gives

$$m_n^{-1/2}\,U^\dagger\left[A+A^T\right]U^*\,m_n^{-1/2}=\mathbb{1}_{3\times 3}. \tag{2.34}$$

We thus define

$$R=m_n^{-1/2}\,U^\dagger\,A\,U^*\,m_n^{-1/2}\,, \tag{2.35}$$

where $R$ now satisfies $R + R^T = \mathbb{1}_{3\times 3}$. Combining Eqs. (2.32) to (2.35) leads to the non-linear matrix equation

$$U\, m_n^{1/2}\, R\, m_n^{1/2}\, U^T = \frac{1}{2}\, m_D^\nu \left(M_R^T\right)^{-1} \mu\, M_R^{-1} \left(m_D^\nu\right)^T - m_D^\nu \left(m_L M_R^{-1}\right)^T \tag{2.36}$$

which will satisfy the light neutrino bounds when solved for $m_D^\nu$.

The choice of $R$ above is not a unique parametrisation of $m_D^\nu$ for the neutrino mass matrix. It is, however, convenient. Due to the non-linearity of Eq. (2.36) it is difficult to find an analytic solution for $m_D^\nu$. We therefore solve this equation numerically to obtain our results in Section 2.6, using an $R$-matrix of the form

$$R = \begin{pmatrix} \frac{1}{2} & r_1 & r_2 \\ -r_1 & \frac{1}{2} & r_3 \\ -r_2 & -r_3 & \frac{1}{2} \end{pmatrix} \tag{2.37}$$

where $r_i \in \mathbb{R}$ in order to make $\delta_{CP}$ the sole source of CP-violation.

## 2.4 Leptogenesis

In order to assess the viability of low-scale, Dirac-phase leptogenesis it is necessary to change basis such that the SN mass sub-matrix is diagonal and real in order to consider the decays of physical SNs to the standard leptons and Higgs boson. At this time in the early universe, above the electroweak phase transition critical temperature $T_c$, the SM leptons are massless and the SNs decay either to a charged lepton and a charged scalar of the opposite sign, or a neutral lepton and a neutral scalar. Taking Eq. (2.12), performing a block diagonalisation of the lower right $2\times 2$ block such that the SNs are in their mass basis, and rotating the Yukawa couplings to the SM leptons, transforms the mass matrix to the form [133]

$$M_\nu \to M_\nu' \simeq \begin{pmatrix} 0 & \frac{v_{EW}}{\sqrt{2}} y_D' & \frac{v_{EW}}{\sqrt{2}} y_L' \\ \frac{v_{EW}}{\sqrt{2}} \left(y_D'\right)^T & M_R - \frac{1}{2}\mu & 0 \\ \frac{v_{EW}}{\sqrt{2}} \left(y_L'\right)^T & 0 & M_R + \frac{1}{2}\mu \end{pmatrix}, \tag{2.38}$$

where $y_D'$ and $y_L'$ correspond to the rotated $3\times 3$ Yukawa matrices coupling the heavy, sterile fermions to the SM leptons. For this $3+6$ generation case, the rotation will be performed numerically. In the one generation, it case can be expressed analytically (to lowest order) as [134]

$$\begin{aligned} y'_D &\simeq \frac{i}{v_{EW}}\left[\left(1+\frac{\mu}{4M_R}\right)m_D^\nu - m_L\right] \\ y'_L &\simeq \frac{1}{v_{EW}}\left[\left(1-\frac{\mu}{4M_R}\right)m_D^\nu + m_L\right]. \end{aligned} \tag{2.39}$$

The rotated couplings are a linear combination of the unrotated couplings. Note that the coupling $m_L$ does not influence the heavy SN masses at this temperature.

Thermal leptogenesis proceeds because, once the temperature of the universe drops below the mass regime of the heavy SNs [in our case $\mathcal{O}(\text{TeV})$], the inverse decays producing SNs will fall out of thermal equilibrium and a net lepton asymmetry will be generated by forward decays due to the non-zero Dirac phase, $\delta_{CP}$, in the PMNS matrix.

Because of the low-temperature regime in which the lepton asymmetry will be generated, where the individual lepton flavours are distinguishable, it is necessary to adopt flavour-dependent Boltzmann equations, which is nicely consistent with our requirement that the low-energy CP-violating phases contribute to leptogenesis. As can be seen in Eq. (2.38), and given that the parameter $\mu$ can be small in a technically-natural way, a small mass splitting exists amongst the SNs and therefore the lepton asymmetry generated may be enhanced due to a resonance effect [84, 85]. It is therefore necessary to account for this potential resonant enhancement in the calculation of the generated lepton asymmetry.

The CP asymmetry generated due to the decays of an SN, $N_{iR}$, to a specific lepton flavour $\alpha$ is defined as

$$\varepsilon_i^\alpha = \frac{\Gamma\left(N_{iR}\to l_\alpha\Phi\right) - \Gamma\left(N_{iR}\to (l_\alpha)^c\,\Phi^\dagger\right)}{\sum\limits_\alpha\left[\Gamma\left(N_{iR}\to l_\alpha\Phi\right) + \Gamma\left(N_{iR}\to (l_\alpha)^c\,\Phi^\dagger\right)\right]}. \tag{2.40}$$

For later use we also define the individual branching ratios of each SN into a specific lepton flavour as

$$B_i^\alpha = \frac{\Gamma\left(N_{iR}\to l_\alpha\Phi\right) + \Gamma\left(N_{iR}\to l_\alpha^c\Phi^\dagger\right)}{\sum\limits_\alpha\left[\Gamma\left(N_{iR}\to (l_\alpha)^c\,\Phi\right) + \Gamma\left(N_{iR}\to (l_\alpha)^c\,\Phi^\dagger\right)\right]}. \tag{2.41}$$

The CP asymmetry parameter $\varepsilon_i^\alpha$ has been calculated previously for the general case, incorporating both the hierarchical as well as degenerate scenarios as limiting cases, and including potential resonance effects [135]:

$$\varepsilon_i^\alpha = \frac{1}{8\pi\,(h^\dagger h)_{ii}} \sum_{j\neq i} \Bigg( \underbrace{\mathcal{A}_{ij}^\alpha\, f(x_{ij})}_{\varepsilon_{\rm V}} + \underbrace{(\mathcal{A}_{ij}^\alpha \sqrt{x_{ij}} + \mathcal{B}_{ij}^\alpha) \frac{(1-x_{ij})}{(1-x_{ij})^2 + \frac{1}{64\pi^2}\,(h^\dagger h)_{jj}^2}}_{\varepsilon_{\rm S}} \Bigg) + \mathcal{O}(h^6) \tag{2.42}$$

where $\mathcal{A}_{ij}^\alpha = \mathfrak{Im}\left\{\left(h^\dagger h\right)_{ij} h_{\alpha i}^* h_{\alpha j}\right\}$, $\mathcal{B}_{ij}^\alpha = \mathfrak{Im}\left\{\left(h^\dagger h\right)_{ji} h_{\alpha i}^* h_{\alpha j}\right\}$, $x_{ij} = \left(\frac{m_{N_j}}{m_{N_i}}\right)^2$ and $h = (y_D',\, y_L')$. The loop function of the vertex diagram contribution $f(x_{ij})$, is given by [83]

$$f(x_{ij}) = \sqrt{x_{ij}} \left[1 - (1 + x_{ij}) \ln\left(\frac{1+x_{ij}}{x_{ij}}\right)\right]. \tag{2.43}$$

Eq. (2.42) includes a resonant enhancement in the CP asymmetry of a SN decay if and only if

$$1 - x_{ij} \simeq \frac{1}{8\pi} \left(h^\dagger h\right)_{jj}. \tag{2.44}$$

### 2.4.1 Boltzmann equations

The flavour-dependent Boltzmann equations valid for the low-scale regime of interest for the extended type-I seesaw considered are given by [85]:

$$\begin{aligned} \frac{d\eta_{N_i}}{dz} &= \frac{z}{H(z=1)} \Bigg[ \left(1 - \frac{\eta_{N_i}}{\eta_{N_i}^{eq}}\right) \sum_{\beta=e,\mu,\tau} \left(\Gamma^{D\,(i\beta)} + \Gamma^{S\,(i\beta)}_{\rm Yuk} + \Gamma^{S\,(i\beta)}_{\rm Gauge}\right) \\ &\quad - \frac{2}{3} \sum_{\beta=e,\mu,\tau} \eta_l^\beta\, \varepsilon_i^\beta \left(\widehat{\Gamma}^{D\,(i\beta)} + \widehat{\Gamma}^{S\,(i\beta)}_{\rm Yuk} + \widehat{\Gamma}^{S\,(i\beta)}_{\rm Gauge}\right)\Bigg], \end{aligned} \tag{2.45}$$

$$\begin{aligned} \frac{d\eta_\alpha}{dz} &= \frac{z}{H(z=1)} \Bigg\{ \sum_{i=1}^{6} \varepsilon_i^\alpha \left(\frac{\eta_{N_i}}{\eta_{N_i}^{eq}} - 1\right) \sum_{\beta=e,\mu,\tau} \left(\Gamma^{D\,(i\beta)} + \Gamma^{S\,(i\beta)}_{\rm Yuk} + \Gamma^{S\,(i\beta)}_{\rm Gauge}\right) \\ &\quad - \frac{2}{3}\eta_\alpha \Bigg[ \sum_{i=1}^{6} B_i^\alpha \left(\widetilde{\Gamma}^{D\,(i\alpha)} + \widetilde{\Gamma}^{S\,(i\alpha)}_{\rm Yuk} + \widetilde{\Gamma}^{S\,(i\alpha)}_{\rm Gauge} + \Gamma^{W\,(i\alpha)}_{\rm Yuk} + \Gamma^{W\,(i\alpha)}_{\rm Gauge}\right) \\ &\qquad + \sum_{\beta=e,\mu,\tau} \left(\Gamma^{\Delta L=2\,(\alpha\beta)}_{\rm Yuk} + \Gamma^{\Delta L=0\,(\alpha\beta)}_{\rm Yuk}\right)\Bigg] \\ &\quad - \frac{2}{3} \sum_{\beta=e,\mu,\tau} \eta_\beta \Bigg[ \sum_{i=1}^{6} \varepsilon_i^\alpha\, \varepsilon_i^\beta \left(\Gamma^{W\,(i\beta)}_{\rm Yuk} + \Gamma^{W\,(i\beta)}_{\rm Gauge}\right) \\ &\qquad + \Gamma^{\Delta L=2\,(\beta\alpha)}_{\rm Yuk} - \Gamma^{\Delta L=0\,(\beta\alpha)}_{\rm Yuk}\Bigg]\Bigg\}, \end{aligned} \tag{2.46}$$

where the functions $\Gamma^X_{\cdots}$ represent various decay and scattering cross sections normalised to photon density. They are explicitly rewritten in Appendix A. An alternative approach is to use flavour-covariant rate equations relevant for resonant scenarios which incorporate quantum decoherence effects [136, 137], in Chapter 3 we roughly estimate that the decoherence effects do not alter the results of our analysis significantly.

The Boltzmann equations in Eqs. (2.45) and (2.46) involve the rescaled variable,

$$z = \frac{m_{N_1}}{T} \tag{2.47}$$

and the number density of each particle species has been normalised to the photon density

$$\eta_a(z) \;=\; \frac{n_a(z)}{n_\gamma(z)} \tag{2.48}$$

with

$$n_\gamma(z) \;=\; \frac{2\,T^3}{\pi^2} \;=\; \frac{2\,m_{N_1}^3}{\pi^2}\,\frac{1}{z^3}. \tag{2.49}$$

The term $H(T)$ corresponds to the Hubble parameter

$$H(T) = \sqrt{\frac{4\pi^3}{45}}\,g_\star^{1/2}\frac{T^2}{M_{\text{Planck}}} \implies H(z) = \sqrt{\frac{4\pi^3}{45}}\,g_\star^{1/2}\frac{m_{N_1}^2}{z^2 M_{\text{Planck}}}, \tag{2.50}$$

where $M_{\text{Planck}} = 1.2 \times 10^{19}$ GeV and $g_\star = g_{SM} = 106.75$ is the number of relativistic degrees of freedom of the SM at the temperature relevant to leptogenesis at $z \gtrsim 1$.

The Boltzmann equations above utilise all $\Delta L = 0, 1, 2$ scattering terms.[10] As shown in Ref. [134], the $\Delta L = 2$ contributions can be of particular importance in this low-scale realisation, where lepton number is approximately conserved, for reducing the total effective washout.

### 2.4.2 Baryon asymmetry

As the SN decays generate the majority of the asymmetry at around the TeV scale, we adopt the approximation that the critical temperature is a hard cutoff for reprocessing the lepton asymmetry into a baryon asymmetry. In other words, we will not be considering the temperature dependence of the sphaleron rate as the temperature passes across the

[10] In flavoured leptogenesis it is necessary to include $\Delta L = 0$ lepton-flavour-violating but lepton-number-conserving interactions.

electroweak phase transition, with [138]

$$T_c = (246\text{ GeV})\left(\frac{1}{2} + \frac{3g^2}{16\lambda} + \frac{g'^2}{16\lambda} + \frac{h_t}{4\lambda}\right)^{-1/2}, \tag{2.51}$$

where $h_t$ is the top-quark Yukawa coupling, $\lambda$ is the Higgs quartic coupling, and $g$ and $g'$ are the $U(1)_Y$ and $SU(2)$ gauge couplings. Therefore the lepton asymmetry will simply be read off at the critical temperature, which is when $z = z_c$ with

$$z_c = \frac{m_{N_1}}{T_c}. \tag{2.52}$$

This asymmetry is reprocessed by sphaleron effects into a baryon asymmetry, and in the case of three families and one Higgs doublet we have

$$\eta_B = -\frac{28}{51}\frac{1}{27}\sum_{\alpha=e,\mu,\tau}\eta_\alpha. \tag{2.53}$$

The factor of 28/51 arises from the fraction of lepton asymmetry reprocessed into a baryon asymmetry by the electroweak sphalerons [82], while 1/27 is the dilution factor from photon production until the recombination epoch [139].

As a consistency check, the asymmetries calculated through numerical solution of the Boltzmann equations were compared with an approximate analytic solution which is valid in the large washout regime, $K_\alpha^{\text{eff}} \geq 5$, where

$$K_{\text{eff}}^\alpha = \kappa^\alpha \sum_i K_i B_i^\alpha, \tag{2.54}$$

and

$$\kappa^\alpha = 2\sum_{i,j(j\neq i)} \frac{\mathrm{Re}\left[(\mathrm{h})_{\mathrm{i}\alpha}(\mathrm{h})^*_{\mathrm{j}\alpha}\left(\mathrm{hh}^\dagger\right)_{\mathrm{ij}}\right] + \mathrm{Im}\left[\left((\mathrm{h})_{\mathrm{i}\alpha}(\mathrm{h})^*_{\mathrm{j}\alpha}\right)^2\right]}{\mathrm{Re}\left[(\mathrm{h}^\dagger\mathrm{h})_{\alpha\alpha}\left\{(\mathrm{hh}^\dagger)_{\mathrm{ii}} + (\mathrm{hh}^\dagger)_{\mathrm{jj}}\right\}\right]}\left(1 - 2i\frac{m_i - m_j}{\Gamma_i + \Gamma_j}\right)^{-1}. \tag{2.55}$$

These low-scale models easily satisfy the $K_{\text{eff}}^\alpha \geq 5$ condition [139, 140]. The approximate asymmetry is then estimated as

$$\eta_B^{\text{approx.}} = -\frac{28}{51}\frac{1}{27}\frac{3}{2}\sum_{\alpha,i}\frac{\varepsilon_i^\alpha}{K_{\text{eff}}^\alpha \mathrm{Min}[\mathrm{z_c}, 1.25\ln(25\mathrm{K}_{\text{eff}}^\alpha)]}. \tag{2.56}$$

| Example parameters (ISS+LSS) | $\lvert\eta_B\rvert$ | $\lvert\eta_B^{\text{approx.}}\rvert$ |
|---|---|---|
| $m_L = 7.42 \times 10^{-5}$ [GeV]<br>$\mu = 7.27 \times 10^{-14}$ [GeV]<br>$r_1 = 0.092, \quad r_2 = 0.163, \quad r_3 = 0.741$ | $3.03 \times 10^{-12}$ | $5.11 \times 10^{-12}$ |
| $m_L = 2.69 \times 10^{-3}$ [GeV]<br>$\mu = 6.59 \times 10^{-10}$ [GeV]<br>$r_1 = 0.013, \quad r_2 = 0.014, \quad r_3 = 0.800$ | $2.39 \times 10^{-14}$ | $6.70 \times 10^{-14}$ |
| $m_L = 9.72 \times 10^{-5}$ [GeV]<br>$\mu = 3.44 \times 10^{-6}$ [GeV]<br>$r_1 = 0.129, \quad r_2 = 0.134, \quad r_3 = 0.202$ | $1.29 \times 10^{-10}$ | $2.94 \times 10^{-10}$ |
| $m_L = 7.71 \times 10^{-4}$ [GeV]<br>$\mu = 1.49 \times 10^{-17}$ [GeV]<br>$r_1 = 0.084, \quad r_2 = 0.359, \quad r_3 = 0.026$ | $7.17 \times 10^{-17}$ | $1.98 \times 10^{-16}$ |

Table 2.1: Comparison between the numerically computed asymmetry $|\eta_B|$ and the analytic approximation $|\eta_B^{\text{approx.}}|$ from Eq. (2.56) for example points of parameter space in the ISS+LSS regime.

A relatively close agreement was found between the numerical results and the analytic approximations in both the pure ISS and the ISS+LSS scenario demonstrated in Table 2.1.

## 2.5 Constraints

In this section we detail the constraints we impose upon our model. Firstly, we place a perturbativity constraint on the Yukawa couplings generated using the Casas-Ibarra formalism, $|h_{ij}|^2 \leq 4\pi$. An alternative perturbative unitarity constraint often used is $\frac{\Gamma_i}{m_i} < \frac{1}{2}$ which results in a similar effect on the parameter space. We also require that the light, active neutrino masses satisfies the oscillation limits taken from Ref. [125] and listed in Table 2.2. We consider only the normal hierarchy for the light neutrinos as the inverted hierarchy is disfavoured in the inverse seesaw model [141]. We rejected points that did not satisfy the current mass difference squared best fit values to within $1\sigma$. For definiteness, the lightest neutrino mass was fixed to 0.1 eV and the Dirac phase $\delta_{CP}$ fixed to $3\pi/2$. The values of the three mixing angles were fixed to their best fit points.

| Parameter | Value |
|---|---|
| $\sin^2\theta_{12}$ | 0.306 |
| $\sin^2\theta_{23}$ | 0.441 |
| $\sin^2\theta_{13}$ | 0.02166 |
| $\Delta m^2_{21}/(10^{-5}\text{ eV}^2)$ | $7.5^{+0.19}_{-0.17}$ |
| $\Delta m^2_{31}/(10^{-3}\text{ eV}^2)$ | $2.524^{+0.039}_{-0.040}$ |
| $m_1/\text{eV}$ | 0.1 |
| $\delta_{CP}$ | $3\pi/2$ |

Table 2.2: List of experimental results relevant to the PMNS matrix and the light neutrino mass splittings fixed by active neutrino oscillation experiments at the time of the analysis. The light neutrino mass differences were allowed to vary within $1\sigma$ of their current best fit values [125].

### 2.5.1 Unitarity

The inclusion of heavy SN states in the theory results in a violation of unitarity of the PMNS matrix due to the mixing between the active and sterile states. Unlike for the vanilla type-I case, the unitarity violation required in the leptonic sector can be potentially used as a discovery signal. To estimate the level of unitarity violation present we define the matrix

$$V = \begin{pmatrix} V_{3\times3} & V_{3\times6} \\ V_{6\times3} & V_{6\times6} \end{pmatrix} \tag{2.57}$$

which diagonalises the *full* $9\times9$ neutrino matrix of Eq. (2.12) through

$$V^T M_\nu V = M_\nu^{\text{diag}}\,. \tag{2.58}$$

The matrix $V$ has an exact representation derived using [142–144],

$$V = \begin{pmatrix} \left(\mathbb{1}_{3\times3}+\zeta^*\zeta^T\right)^{-1/2} & \zeta^*\left(\mathbb{1}_{6\times6}+\zeta^T\zeta^*\right)^{-1/2} \\ -\zeta^T\left(\mathbb{1}_{3\times3}+\zeta^*\zeta^T\right)^{-1/2} & \left(\mathbb{1}_{6\times6}+\zeta^T\zeta^*\right)^{-1/2} \end{pmatrix} \begin{pmatrix} U & 0 \\ 0 & V' \end{pmatrix} \tag{2.59}$$

where $U$ is the usual PMNS matrix which would exactly diagonalise the light neutrino block in the absence of the heavy SNs. $V'$ is the unitary matrix diagonalising the heavy neutrino mass sub-matrix,

$$(V')^T \begin{pmatrix} 0 & M_R \\ M_R^T & \mu \end{pmatrix} V' = \begin{pmatrix} M^- & 0 \\ 0 & M^+ \end{pmatrix} \tag{2.60}$$

and $M^{\pm} = M_R \pm \mu$ above the critical temperature. While $V'$ will be numerically computed, it can be approximated in the case where $M_R$ and $\mu$ are diagonal to lowest order by

$$V' = \frac{\sqrt{2}}{2}\begin{pmatrix} \mathbb{1}_3 & -i\mathbb{1}_3 \\ \mathbb{1}_3 & i\mathbb{1}_3 \end{pmatrix} + \mathcal{O}(\mu M_R^{-1}). \tag{2.61}$$

$\zeta$ is a $3\times 6$ matrix

$$\zeta = \left(m_L M_R^{-1},\, m_D^{\nu}(M_R^T)^{-1}\right) \equiv (F_1, F_2)\,, \tag{2.62}$$

which satisfies[11] $||\zeta|| < 1$ by construction, the matrices $F_i$ are often used instead of $\zeta$ in the literature [145, 146].

Each component of $V$ in Eq. (2.59) can be expressed in terms of $\zeta$, or $F$ if expanding at lowest order,

$$V_{3\times 3} = \left(1_{3\times 3} + \zeta^*\zeta^T\right)^{-1/2} U \simeq \left(1_{3\times 3} - \frac{1}{2}F_i^* F_i^T\right) U = \left(1_{3\times 3} - \eta\right) U^* \tag{2.63}$$

where $\eta$ expresses the "deviation from unitarity",

$$\eta \equiv \mathbb{1}_{3\times 3} - \left(\mathbb{1}_{3\times 3} + \zeta^*\zeta^T\right)^{-1/2} \simeq \frac{1}{2}\left(F_1^* F_1^T + F_2^* F_2^T\right). \tag{2.64}$$

The remaining components of $V$ can be similarly expressed,

$$V_{3\times 6} = \zeta^*\left(\mathbb{1}_{6\times 6} + \zeta^T\zeta^*\right)^{-1/2} V' \simeq \left(F_1^*, F_2^*\right) V', \tag{2.65}$$

$$V_{6\times 3} = -\zeta^T\left(\mathbb{1}_{3\times 3} + \zeta^*\zeta^T\right)^{-1/2} U \simeq -\begin{pmatrix} F_1^T \\ F_2^T \end{pmatrix} U^*, \tag{2.66}$$

$$V_{6\times 6} = \left(\mathbb{1}_{6\times 6} + \zeta^T\zeta^*\right)^{-1/2} V' \simeq \left(\mathbb{1}_{6\times 6} - \frac{1}{2}\begin{pmatrix} F_1^T F_1^* & F_1^T F_2^* \\ F_2^T F_1^* & F_2^T F_2^* \end{pmatrix}\right) V'. \tag{2.67}$$

The deviation from unitarity allowed by experimental observation from universality tests of weak interactions, rare leptonic decays, the invisible width of Z-boson and neutrino oscillation data is expressed through maximum allowed values for the entries in the

[11] In the inverse and linear approximations.

matrix $\eta$ [147],

$$|\eta_{ij}| < \begin{pmatrix} 1.3\times 10^{-3} & 1.2\times 10^{-5} & 1.4\times 10^{-3} \\ 1.2\times 10^{-5} & 2.2\times 10^{-4} & 6.0\times 10^{-4} \\ 1.4\times 10^{-3} & 6.0\times 10^{-4} & 2.8\times 10^{-3} \end{pmatrix} . \tag{2.68}$$

### 2.5.2 Charged Lepton Flavour Violation (cLFV)

#### 2.5.2.1 $\mu \to e\gamma$

The current 90% C.L. upper bound on the branching ratio of $\mu \to e\gamma$ from the MEG collaboration is [148]

$$\mathrm{BR}(\mu \to e\gamma) < 4.2 \times 10^{-13} . \tag{2.69}$$

The branching ratio for this process in the presence of additional sterile neutrinos is given by [141, 149]

$$\mathrm{BR}(\mu \to e\gamma) = \frac{\alpha_w^3 s_w^2}{256\pi^2}\frac{m_\mu^5}{M_W^4}\frac{1}{\Gamma_\mu}\left|\sum_{i=1}^{9} V_{\mu i}^\star V_{ei}\, G(y_i)\right|^2 , \tag{2.70}$$

where the loop function is given by

$$G(x) = -\frac{2x^3+5x^2-x}{4(1-x)^3} - \frac{3x^3}{2(1-x)^4}\ln x \tag{2.71}$$

and $y_i = m_i^2/M_W^2$, $\alpha_w = g_w^2/4\pi$, $s_w^2 = 1-(M_W/M_Z)^2$, $m_i$ refers to both the active and sterile neutrinos and the matrix $V$ is defined above in Eq. (2.57).

The design sensitivity of the proposed MEGII detector [150] is expected to increase the 90% C.L. bound of Eq. (2.69) to

$$\mathrm{BR}(\mu \to e\gamma) < 5 \times 10^{-14} . \tag{2.72}$$

#### 2.5.2.2 $\mu \to e$ conversion

The current strongest limit on the branching ratio for $\mu \to e$ coherent conversion on nuclei is from experiments involving gold [151],

$$\mathrm{BR}(\mu\,\mathrm{Au} \to e\,\mathrm{Au}) < 7.0 \times 10^{-13}. \tag{2.73}$$

The expected sensitivity of the future experiments COMET and Mu2e is estimated at $\mathrm{BR}(\mu^-\mathrm{N} \to \mathrm{e}^-\mathrm{N}) \lesssim 10^{-17}$ [152], providing a potentially competitive cLFV limit to $\mathrm{BR}(\mu \to \mathrm{e}\gamma)$.

It was shown in Ref. [153] that in ISS models the long range, photonic contribution dominates in coherent conversion[12] and so there is a tight relationship between the expected branching ratios of $\mu \to e$ conversion and $\mu \to e\gamma$. When the photonic contribution dominates, $\mu \to e$ conversion can expressed in terms of the $\mathrm{BR}(\mu \to e\gamma)$ as [155]

$$\mathrm{BR}(\mu^- \mathrm{N} \to \mathrm{e}^- \mathrm{N}) \sim \frac{\mathrm{B(A,Z)}}{428}\,\mathrm{BR}(\mu \to \mathrm{e}\gamma), \tag{2.74}$$

where B(A,Z) corresponds to a rate dependence on the mass number $A$ and atomic number $Z$ for nucleus $N$. In this limit it is thus possible to use $\mu \to e$ conversion to constrain $\mu \to e\gamma$ (or vice versa). Both Mu2E and COMET will initially make use of an aluminium target for which $B(A,Z) \sim 1.1$, implying

$$\mathrm{BR}(\mu^- \mathrm{N} \to \mathrm{e}^- \mathrm{N}) \sim 2.6 \times 10^{-3}\,\mathrm{BR}(\mu \to \mathrm{e}\gamma). \tag{2.75}$$

The first run of COMET in 2018 has an expected sensitivity of

$$\mathrm{BR}(\mu^- \mathrm{N} \to \mathrm{e}^- \mathrm{N}) \sim 3 \times\ 10^{-15}. \tag{2.76}$$

Comparing this to Eq. (2.75) constrains $\mathrm{BR}(\mu \to e\gamma) \lesssim 1.15 \times 10^{-12}$, a less competitive limit to the current limit directly measured [Eq. (2.69)]. However, the lifetime sensitivity of the COMET experiment is expected to be $\mathcal{O}(10^{-17})$, implying a constraint of $\mathrm{BR}(\mu \to e\gamma) \lesssim 3.84 \times 10^{-15}$. This would be an order of magnitude more sensitive in constraining models of heavy sterile neutrinos compared to the expectation in Eq. (2.72).

### 2.5.3 Neutrinoless Double Beta Decay

A Majorana mass contribution for neutrinos implies the possibility of neutrinoless double beta decay. In our model, all the SN states are much heavier than the momentum transfer involved in double beta decay $m_{N_i} \gg 100\,\mathrm{MeV}$. Accordingly the light neutrino

[12] For singlet fermion masses in these ISS models much lower than 1 TeV the photonic contribution can become sub-dominant to other diagrams making this approximation invalid [154].

propagator can be approximated by [156]

$$\frac{1}{p^2 - m_{N_i}^2} = -\frac{1}{m_{N_i}^2} + \mathcal{O}\left(\frac{p^2}{m_{N_i}^4}\right). \tag{2.77}$$

The dominant contribution will come from the active, light neutrinos, and the allowed region of the lightest neutrino masses will remain the same as in the SM.[13]. Reference [159] also demonstrates that, in our mass-range of interest, contributions to the electron electric dipole moment are not significant enough to have measurable effects.

## 2.6 Numerical Results

We consider the 3+3 scenario in which three right-handed neutrinos $\nu_R$ and three singlets $S_L$ are added to the SM. The minimal scenario allowed by experiment is actually a $2+2$ theory, since one of the active neutrinos is allowed to be massless. However as we are considering SNs with similar TeV-scale masses, a degenerate spectrum of active neutrino masses is assumed due to the degenerate spectrum of sterile neutrinos considered.

Following [160] we fix both the lepton number violating parameters,[14] $m_L$ and $\mu$ to be diagonal such that $m_D^\nu$ is the only source of flavour violation in the theory for simplicity, in Chapter 3 we discuss how this might be motivated through additional flavour symmetries suggested by the SM. For simplicity all plots below in the three-generational scenarios have $\mu$ and $m_L$ proportional to the identity matrix such that each matrix block depends on only one parameter: $\mu = \mu_p \mathbb{1}_{3\times3}$ and $m_L = (m_L)_p \mathbb{1}_{3\times3}$, the conclusions drawn also apply when these matrices are diagonal, but not proportional to the identity, provided that at least one of the values along the diagonal is of similar size. In our scans over $\mu_p$ and $(m_L)_p$ below we will drop the subscript, it should be clear in the multi-generational scenario when we are referring to the $3\times3$ matrix (proportional to the identity matrix) and the coefficient of this matrix (which is what is scanned over). These parameters are randomly scanned with the ranges,

$$\mu_p \sim \mathcal{O}(10^{-8} - 1)\,\text{GeV} \tag{2.78}$$

[13]A possible caveat to this is when one-loop corrections and higher order terms become non-negligible. SNs as heavy as 5 GeV can dominate in certain limits [157] or if very large complex entries in the R-matrix are considered [158].

[14]The Majorana mass term $\mu$ can be taken to be diagonal without loss of generality, as can $\mu$ and $m_L$, but not $\mu$, $m_L$, $M_R$ simultaneously.

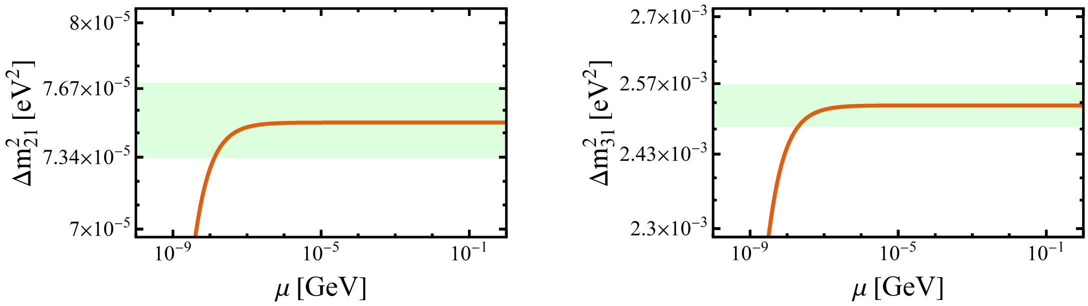


FIGURE 2.1: Log-Log scale plots of the light neutrino mass splittings (orange curves) as a function of the Majorana parameter $\mu$ in the ISS, for normal ordering and parameter choices as described in the text. The coloured bands correspond to the current $1\sigma$ experimental limits on the allowed mass splittings between the light neutrino mass eigenstates. For regions below $\mu \lesssim 10^{-8}$ GeV, the generated Dirac matrix $m_D^\nu$ grows too large and the block diagonalisation assumptions in Eq. (2.14) break down.

for the pure ISS and,

$$\begin{aligned} \mu_p &\sim \mathcal{O}(10^{-17} - 1)\,\mathrm{GeV} \\ (m_L)_p &\sim \mathcal{O}(10^{-9} - 1)\,\mathrm{GeV} \end{aligned} \tag{2.79}$$

in the ISS+LSS scenario. The reasons for these choices are shown in Figs. 2.1 and 2.2. Figure 2.1 shows the light neutrino mass splittings as a function of $\mu$ in the inverse seesaw model. Once $\mu < 10^{-8}$ GeV the Dirac mass matrix $m_D^\nu$ generated using the Casas-Ibarra method becomes too large and the block-diagonalisation assumptions used in Eq. (2.14) break down. Figure 2.2 shows the light neutrino mass splittings in the ISS+LSS scenario. The top panels demonstrate that $m_L$ should be greater than $10^{-9}$ GeV. The bottom panels show the neutrino mass splitting dependence on $\mu$, where we only select points that satisfy $m_L > 10^{-9}$ GeV. Clearly in this case we can achieve much lower values of $\mu$ than in the ISS model.

Similarly, the matrix $M_R$ which will fix the overall mass scale of the SNs is taken to be diagonal with values given by

$$\left(\frac{M_R^{\mathrm{deg}}}{1\,\mathrm{TeV}}\right) = \begin{pmatrix} 1 & 0 & 0 \\ 0 & 1 & 0 \\ 0 & 0 & 1 \end{pmatrix}$$

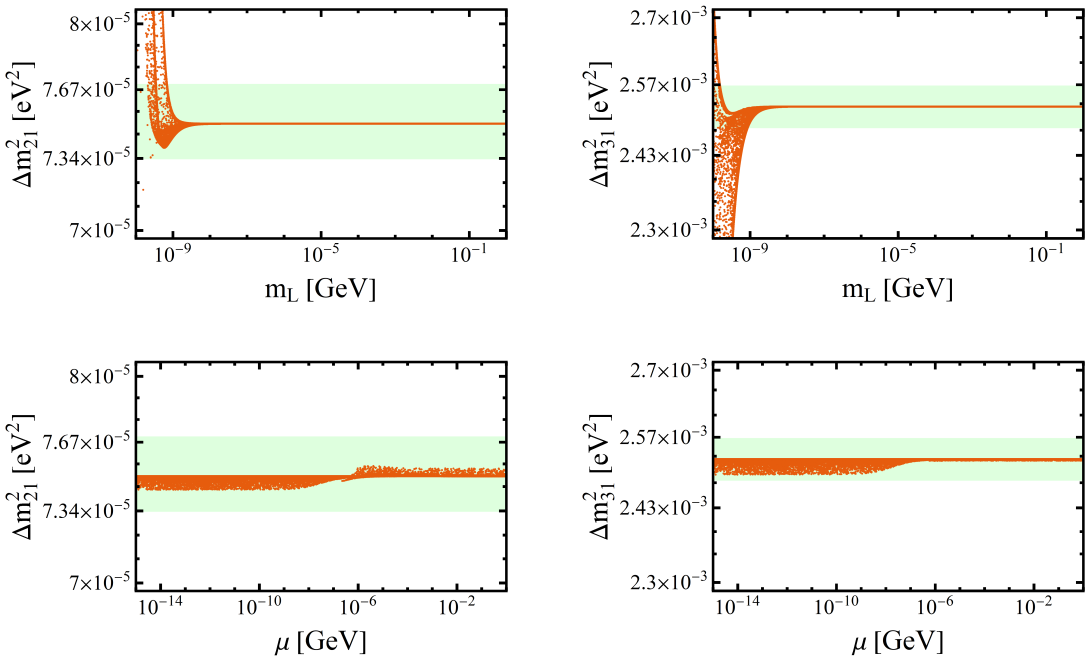


FIGURE 2.2: **Top panels:** Log-Log scale plots of the light neutrino mass splittings as a function of the linear parameter $m_L$ in the ISS+LSS, for normal ordering and parameter choices as described in the text. The coloured bands correspond to the current $1\sigma$ experimental limits on the allowed mass splittings. For regions $m_L \lesssim 10^{-9}$ GeV, the generated Dirac matrix $m_D^\nu$ grows too large and the block diagonalisation assumptions in Eq. (2.14) break down. **Bottom panels:** Log-Log scale plots of the light neutrino mass splittings as a function of $\mu$ *when* $m_L > 10^{-9}$ GeV. Note that much smaller values of $\mu$ are allowed if $m_L$ is turned on compared to the pure ISS scenario.

$$\left(\frac{M_R^{\text{hier}}}{1\,\text{TeV}}\right) = \begin{pmatrix} 1 & 0 & 0 \\ 0 & 5 & 0 \\ 0 & 0 & 5 \end{pmatrix} \tag{2.80}$$

in the degenerate and hierarchical cases, respectively, as justified below.

As stated earlier, the Casas-Ibarra $R$ matrix is kept real in order to explore leptogenesis purely driven by the Dirac phase. It was varied according to

$$x,\, y,\, z \sim [0, 2\pi] \tag{2.81}$$

in the case of the pure ISS, where $x, y$ and $z$ are the elements of the $R$ matrix as defined in Eq. (2.27). In the case of the ISS+LSS, it was varied according to

$$r_{1,2,3} \sim \mathcal{O}(10^{-2} - 1) \tag{2.82}$$

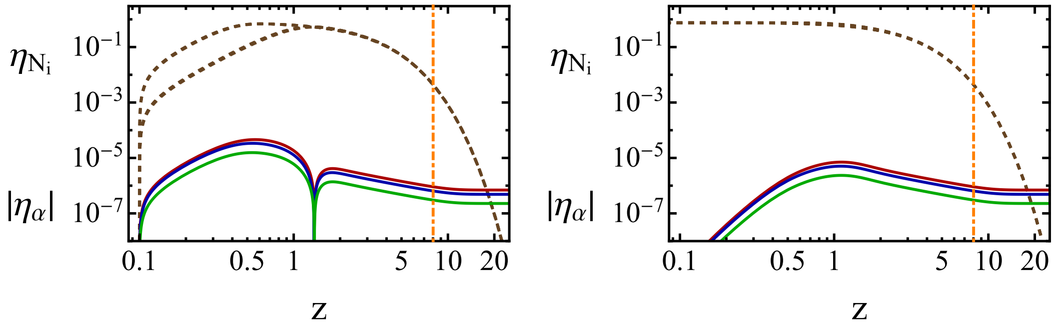


FIGURE 2.3: Solutions of the Boltzmann equations for the same set of parameters solved with $\eta_{N_i}(z_{in}) = 0$ (**Left Panel**) and $\eta_{N_i}(z_{in}) = \eta^{\rm eq}_{N_i}$ (**Right Panel**). The brown, dotted lines correspond to the population of the six SNs $\eta_{N_i}$ and the coloured, full lines to $|\eta_\alpha|$. The orange, dot-dashed line is the critical temperature, $z_c \simeq 8.02$ at which the lepton asymmetry is read off $\eta_\alpha(z_c)$. In both cases the same asymmetry is generated, $\eta_B = -\frac{28}{1377}\sum_\alpha \eta_\alpha = 7.229 \times 10^{-10}$ which is expected for strong washout thermal leptogenesis. Any asymmetry generated while thermally populating the sterile neutrinos is quickly washed out once a thermal population is reached. The parameters chosen in this example are: $m_L = 1.84 \times 10^{-4}$ [GeV], $\mu = 6.148 \times 10^{-8}$ [GeV], $\mathrm{r}_1 = 3.869 \times 10^{-2}$, $\mathrm{r}_2 = 4.676 \times 10^{-2}$, $\mathrm{r}_3 = 6.989 \times 10^{-2}$.

with the $R$ matrix satisfying Eq. (2.37).

In solving the Boltzmann equations we considered the initial conditions $\eta_\alpha(z_{in}) = 0$ for the lepton asymmetry and $\eta_{N_i}(z_{in}) = \eta^{\rm eq}_{N_i}$ for the SN population. Due to the strong washout nature of this low-scale theory there is an insensitivity to any primordial lepton asymmetry (which gets washed out immediately). Likewise the theory is insensitive to the initial abundance of SNs in the thermal bath. Due to the relatively low-scale masses of the SN, it should however be expected that a thermal abundance of them should be produced at temperatures well before an asymmetry is generated, thus motivating the initial conditions used. The insensitivity to the initial abundance and initial asymmetry is illustrated in Fig. 2.3. These show the solutions of the Boltzmann equations for the same set of parameters as a function of $z$, using different initial conditions. In the left panel we take $\eta_{N_i}(z_{in}) = 0$ and in the right we take $\eta_{N_i}(z_{in}) = \eta^{\rm eq}_{N_i}$. The upper, dotted lines show the population abundances of the sterile neutrinos, and the lower, solid lines the active neutrino asymmetries. The vertical dot-dashed line shows the value, $z_c$ from Eq. (2.52), at which we read off the lepton asymmetry. The plots show that this is independent of the initial conditions used. The parameters used are detailed in the figure caption.

### 2.6.1 Hierarchical Limit

The hierarchical limit is taken to be the point at which the heavier sterile neutrinos' contribution to the final asymmetry is frozen out; the decays of these heavier SNs occur in a region in which the lighter SNs remain in thermal equilibrium and whose interactions wash out the generated asymmetry. In order to quantify the point at which the heavy SN contributions freeze out, a scan was performed over the masses of the heavier SNs whilst leaving all other parameters fixed.[15] The hierarchical limit is chosen by hand at a point in which the final baryon asymmetry is largely insensitive to the heavier SN masses. Based on the scan of a few hundred sample parameters it was found that this decoupling was generally comfortably achieved by $m_{\text{heavy}}/m_{\text{light}} \sim 5$. Sample plots are shown in Fig. 2.4 in order to illustrate this behaviour and justify the choice made in this section. These figures all show that the value of $\eta_B$ has stabilised once $m_{\text{heavy}}/m_{\text{light}} \sim 3$, so that 5 is a conservative choice.

### 2.6.2 Inverse Seesaw Case

Before considering the full 3+3 generation case, firstly we estimate the washout associated within the pure ISS scenario by considering the one generation $1+1$ limit.[16] In this case the associated mass matrix becomes,

$$M_{\text{inv},1g} = \begin{pmatrix} 0 & m_D^\nu & 0 \\ m_D^\nu & 0 & M_R \\ 0 & M_R & \mu \end{pmatrix}. \tag{2.83}$$

Employing Eq. (2.38) to rotate into the mass basis for the heavy sterile neutrinos (to first order)

$$M'_{\text{inv},1g} \simeq \begin{pmatrix} 0 & i\,m_D^\nu\left(1+\frac{\mu}{4M_R}\right) & m_D^\nu\left(1-\frac{\mu}{4M_R}\right) \\ i\,m_D^\nu\left(1+\frac{\mu}{4M_R}\right) & M_R-\frac{\mu}{2} & 0 \\ m_D^\nu\left(1-\frac{\mu}{4M_R}\right) & 0 & M_R+\frac{\mu}{2} \end{pmatrix} \tag{2.84}$$

[15] The active neutrinos are still taken to have a quasi-degenerate mass spectrum since, due to the strong washout nature of the theory, the hierarchical limit as defined above is achieved before a very large mass hierarchy is formed amongst the heavy SNs.

[16] As mentioned previously, we need at least two $\nu_R$ states in order to satisfy neutrino oscillation data, but it is convenient to examine this unrealistic but simple case in order to illustrate how $\mu$ influences the washout.

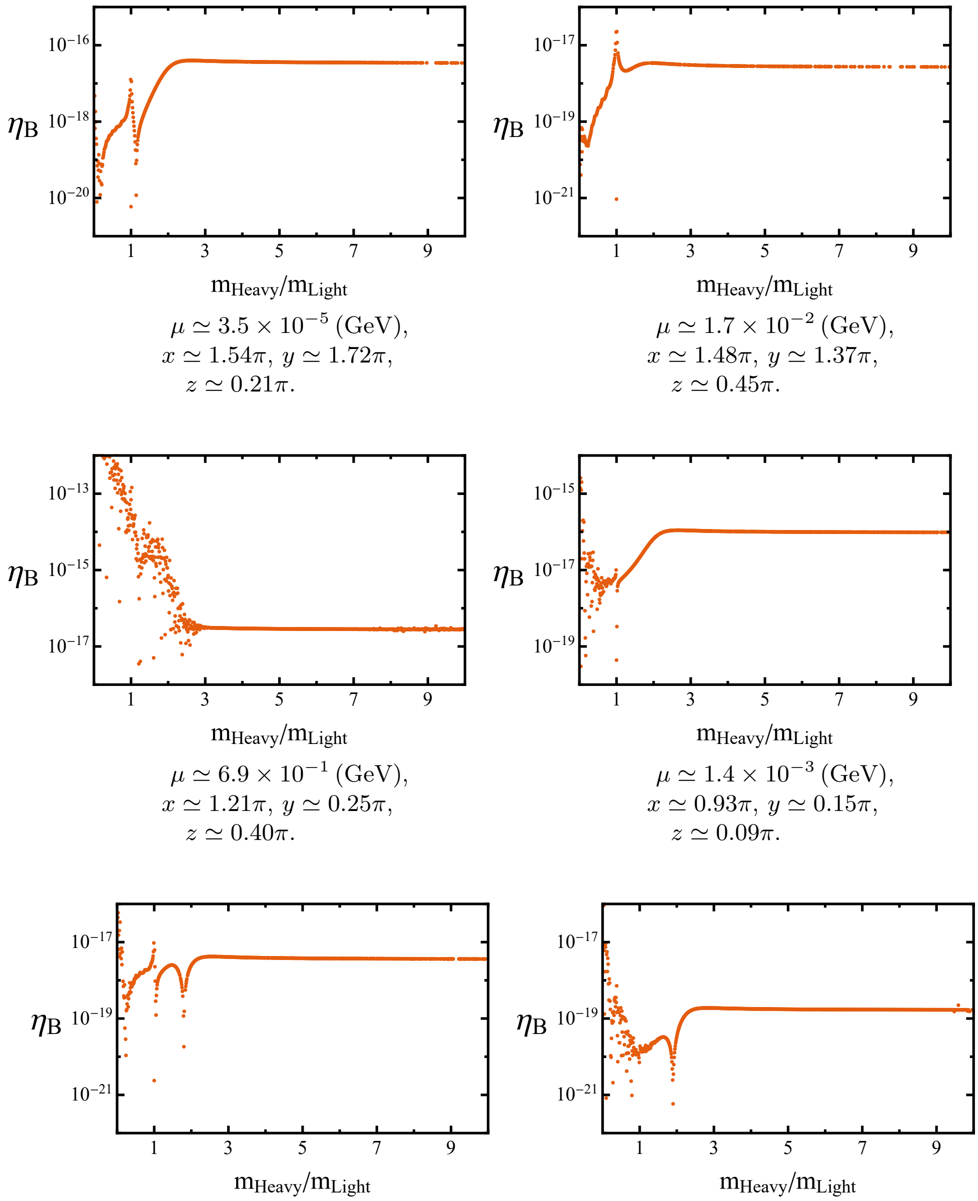


$\mu \simeq 3.5 \times 10^{-5}$ (GeV),
$x \simeq 1.54\pi$, $y \simeq 1.72\pi$,
$z \simeq 0.21\pi$.

$\mu \simeq 1.7 \times 10^{-2}$ (GeV),
$x \simeq 1.48\pi$, $y \simeq 1.37\pi$,
$z \simeq 0.45\pi$.

$\mu \simeq 6.9 \times 10^{-1}$ (GeV),
$x \simeq 1.21\pi$, $y \simeq 0.25\pi$,
$z \simeq 0.40\pi$.

$\mu \simeq 1.4 \times 10^{-3}$ (GeV),
$x \simeq 0.93\pi$, $y \simeq 0.15\pi$,
$z \simeq 0.09\pi$.

$\mu \simeq 2.9 \times 10^{-4}$ (GeV),
$x \simeq 0.74\pi$, $y \simeq 0.29\pi$,
$z \simeq 0.91\pi$.

$\mu \simeq 3.8 \times 10^{-3}$ (GeV),
$x \simeq 1.52\pi$, $y \simeq 1.62\pi$,
$z \simeq 0.68\pi$.

FIGURE 2.4: Log-Log plots of final baryon asymmetry generated as a function of ratio of heavy SN masses to light SN masses (which remains fixed at 1 TeV) for some sample points. For computational convenience, only the ISS scenario is plotted and therefore none of the points generate the correct asymmetry (as discussed in the text). However, the plots serve to illustrate the freeze out of the asymmetry as some of the sterile neutrino masses get heavier. By $m_{\text{Heavy}}/m_{\text{Light}} \sim 5$, the asymmetry is almost completely insensitive to the heavy masses.

and substituting the Dirac mass term, which in the one generation case is exactly

$$m_D^\nu = \frac{m_n^{1/2} M_R}{\sqrt{\mu}}\,, \tag{2.85}$$

leads to an estimate of the naïve washout parameter as

$$(K^{1gen}_{\text{naïve}})_{N_i} \simeq \frac{\Gamma_{N_i}}{H(T=M_{N_i})} \simeq \frac{\sqrt{45} M_p M_R m_n}{16\pi^{5/2} v_{EW}^2 g_*^{1/2} \mu} \left| 1 \pm \frac{\mu}{4M_R} \right|^2 . \tag{2.86}$$

While $K_{\text{naïve}}$ is the usual parameter within hierarchical, type-I seesaw leptogenesis which determines the efficacy of asymmetry generation, with $K_{\text{naïve}} < 1$ known as the weak washout regime and $K_{\text{naïve}} > 1$ the strong, in seesaw models with small LNV effects this washout estimate leads to unphysical behaviour. For small values of $\mu$ in Eq. (2.86) the washout grows without bounds. However, in the limit $\mu \to 0$ there is no LNV within the theory, so no asymmetry generation can occur in this limit and neither can any washout of the asymmetry. Therefore the true washout should tend to zero in the same limit. An 'effective' washout can be defined, however, by including the on-shell part of the dominant $\Delta L = 2$ scattering terms[17] on top of the usual inverse decay terms when calculating the washout [134]. This leads to an effective washout estimate given by

$$(K^{1gen}_{\text{eff}})_{N_i} \simeq (K^{1gen}_{\text{naïve}})_{N_i} \underbrace{\frac{\delta^2}{1 + \frac{\Gamma_N}{m_{N_1}}\delta + \delta^2}}_{\kappa} \tag{2.87}$$

with $\delta \simeq \mu/\Gamma_N$. Due to the additional scaling factor, $\kappa$, the correct behaviour is now observed in each limit. For small values of $\mu$, $\delta \ll 1$, and $(K^{1gen}_{\text{eff}})_{N_i} \simeq (K^{1gen}_{\text{naïve}})_{N_i}\delta^2$ which now correctly goes to zero whereas for $\delta > 1$, $(K^{1gen}_{\text{eff}})_{N_i} \simeq (K^{1gen}_{\text{naïve}})_{N_i}$, and the effective and naïve washouts coincide. Interestingly while in the limit $\mu \to 0$ no lepton asymmetry can be created or destroyed, the thermal population of $N_i$ is controlled by the Yukawa coupling $h$ which is non-zero in this limit. Therefore leptogenesis via small LNV effects, such as the ISS scenario we are considering, has the thermal population of $N_i$ controlled by the naïve washout whereas the washout of the lepton asymmetry is controlled by $(K^{1gen}_{\text{eff}})_{N_i}$. This is in contrast with the vanilla, type-I seesaw where the

[17]The $2 \leftrightarrow 2$ process, $\phi\ell \leftrightarrow \phi^\dagger \ell^c$, is the most important process to include which has a contribution from a minimum of two of $N_i$ due to the pseudo-Dirac nature of the heavy SNs. A majority of their contributions cancel but the interference between the two does not [134].

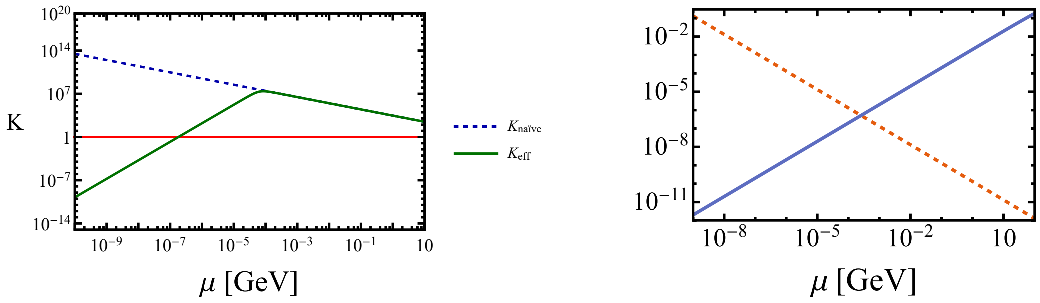


FIGURE 2.5: **Left panel:** Log-Log plot of the naïve and effective washout as a function of $\mu$. As $\mu$ is decreased, the Yukawa coupling must increase in order to account for the correct active neutrino masses thereby increasing the total washout, however when all relevant $\Delta L = 2$ LNV washout processes are included, which decrease for smaller $\mu$, the *effective* washout tends to zero as $\mu \to 0$. **Right panel:** Log-Log plot of the mass splitting, $(1 - x_{ij})$ in blue (solid) against $\frac{1}{8\pi}\left(h^\dagger h\right)_{jj}$ in orange (dashed) as a function of $\mu$. For the one generation case, $\mu \sim 10^{-3.5}$ GeV satisfies the resonance condition.

production of the heavy SNs and the washout of the asymmetry are both controlled by $(K^{1gen}_{\text{naïve}})_{N_i}$.

In the left panel of Fig. 2.5, the washout parameters are plotted against $\mu$, with $M_R$ fixed to 1 TeV and $m_n = 0.1$ eV. For the region applicable to the inverse seesaw, $\mu < M_R$, where the SNs are pseudo-Dirac, the theory is squarely in the strong-washout regime as $(K^{1gen}_{\text{naïve}})_{N_i} > 1$. However, there are both regions of strong and weak effective washout with $(K^{1gen}_{\text{eff}})_{N_i} \propto \mu^3$. Therefore this suggests that the asymmetry should be independent of the initial conditions assumed for the population of $N_i$ due to the strong washout nature of the thermal production of $N_i$ controlled by $(K^{1gen}_{\text{naïve}})_{N_i}$ and that large values of $\mu$ lead to a washout of the asymmetry close to the naïve value. The right panel of Fig. 2.5 shows the mass splitting between the two sterile neutrinos

$$1 - x_{ij} = 1 - \left(\frac{m_{N_j}}{m_{N_i}}\right)^2 = 1 - \frac{\left(M_R \pm \frac{1}{2}\mu\right)^2}{\left(M_R \mp \frac{1}{2}\mu\right)^2} \simeq \pm 2\frac{\mu}{M_R} \tag{2.88}$$

as a function of $\frac{1}{8\pi}\left(h^\dagger h\right)_{jj}$, the two parameters relevant for the resonance condition of Eq. (2.44). Resonance can be achieved in the theory, allowing for the potential generation of a net asymmetry, even in this regime of strong washout. It is important to note that in the pure ISS, the parameter which determines the strength of the washout also determines the mass splitting between the heavy sterile neutrinos; in other words, it also affects the potential resonance contributions. The resonance condition is satisfied where the two lines in the right-hand panel cross, at $\mu \sim 10^{-3.5}$ GeV which is in agreement with equating Eq. (2.88) to the decay width using Eq. (2.85). We observe that the region of resonance corresponds to a high value of the washout parameter: $(K_{\rm eff}^{1gen})_{N_i} \sim 10^{6-7}$. The results presented in Fig. 2.5 are estimates of the strength of the washout in the theory as well as the size of a possible resonant enhancement. Moving to a three-generational scenario will lead to similar behaviour with regions of strong and weak effective washout as well as a region of resonance. In Section 3.4.1 of Chapter 3 we will compare the above rough estimates on $(K_{\rm eff}^{1gen})_{N_i}$ to a numerical computation of the effective washout with all $\Delta L = 2$ scattering terms included for the full three-generational scenario and find similar conclusions to the shape of the left figure of Fig. 2.5.

For TeV scale sterile neutrinos, Eq. (2.86) can be used to estimate the required Majorana mass $\mu$ in order to move to the weak washout regime, $K_{N_i} < 1$:

$$\mu \sim 4 \text{ TeV}, \tag{2.89}$$

which is completely outside the region of applicability of the ISS.[18]

Moving on to the full 3+3 scenario, Fig. 2.6 plots the generated baryon asymmetry from numerically solving the Boltzmann equations as a function of $\mu$/GeV for the degenerate case. All points generate the correct active neutrino mass differences; points in purple at low $\mu$ are excluded by unitarity violation. As we are specifically considering the scenario of Dirac-phase leptogenesis, all points generate a baryon asymmetry of the correct sign for $\delta_{CP} \sim 3\pi/2$, though obviously the magnitude is too small by many orders of magnitude. The thickness of the green band in Fig. 2.6 and for most figures that follow is due to a scan over the Casas-Ibarra matrix $R$.

The reason for such a small amounts of asymmetry generated is that, in scenarios of TeV-scale ISS, the generated asymmetry is heavily washed out. Figure 2.7 demonstrates that a resonant enhancement occurs in the theory,[19] in line with expectations from the one generation scenario. The resonant enhancement can clearly be seen in the left-hand plot at $\mu \sim 10^{-3} - 10^{-4}$ GeV as expected from the one-generational toy scenario presented

[18] We note that Ref. [161] proposed a weak-washout scenario by setting the SN mass scale to 1 GeV and relying on zero initial abundance of neutrinos close to the sphaleron decoupling point in order to successfully satisfy the out-of-equilibrium condition for asymmetry generation.

[19] As the asymmetry is purely generated by the Dirac phase $\delta_{CP}$, for this scenario $\sum_\alpha \epsilon_i^\alpha = 0$ and as such only one of the 18 CP-asymmetry parameters is plotted, in this case $\epsilon_1^1$. Each CP-asymmetry parameter $\epsilon_i^\alpha$ has similar behaviour due to the degenerate limit considered.

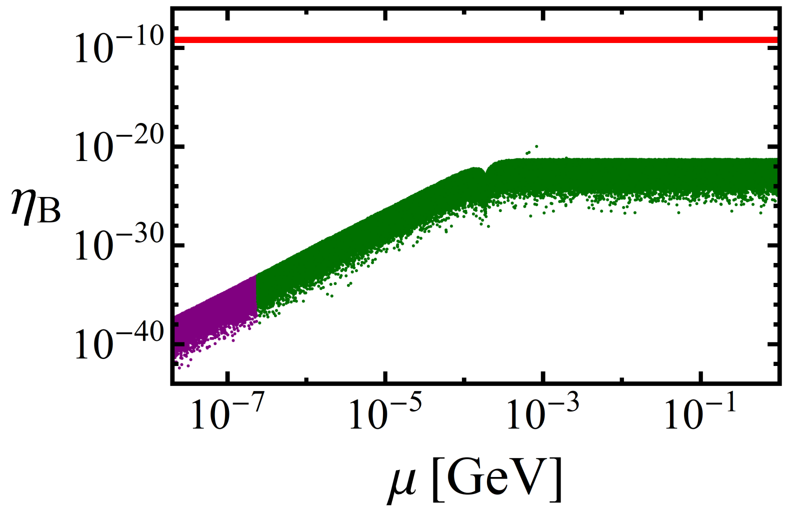


FIGURE 2.6: The generated baryon asymmetry as a function of the lepton number violating parameter $\mu$ for the degenerate case. The points in purple, which correspond to larger values in at least one of the entries of $m_D^\nu$, are excluded by unitarity violation limits for the PMNS matrix. In red is the required BAU, $\eta_B \simeq 6.21 \times 10^{-10}$. For the pure ISS scenario, the washout is extremely strong, even in regions of resonance and therefore a sizeable asymmetry cannot be generated in the case of CPV via the Dirac phase. The thickness of the green band is due to a scan over the Casas-Ibarra matrix $R$.

above. The right-hand plot demonstrates where the resonance condition is satisfied where $\Delta_N/\Gamma_N = (1 - x_{ij})/\frac{1}{8\pi}\left(h^\dagger h\right)_{jj}$ and $1 - x_{ij}$ is defined in Eq. (2.88).

However, while the net CP asymmetry generated per sterile neutrino decay may increase, this is accompanied by an increased rate of washout, ultimately preventing the generation of a sufficiently large final baryon asymmetry. This behaviour is obviously unaffected by the hierarchy among the SN masses and therefore will be the same for the hierarchical case. Regions of weak effective washout, where $\|\mu\| < 10^{-5}$ GeV, generate much smaller values of $\epsilon_i^\alpha$ and therefore do not generate sufficient levels of asymmetry. We find therefore find that both regions of strong and weak effective washout are unable to generate sufficient asymmetry in the ISS scenario and confirm numerically that the final asymmetry is insensitive to the assumed initial population of the heavy SNs in both regions as $(K_{\text{naïve}}^{1gen})_{N_i} > 1$. The strength of the washout could potentially be lowered in some pure ISS scenarios by resorting to special textures of $m_D^\nu$, $\mu$ or $M_R$. As an example if a mass splitting is introduced by hand in the matrix $M_R$ (in the degenerate scenario) an additional resonant contribution will exist independent of $\mu$ without generating an increased washout along with it. Such textures would require additional symmetries in the theory such as a flavour symmetry in order to justify their existence and we will

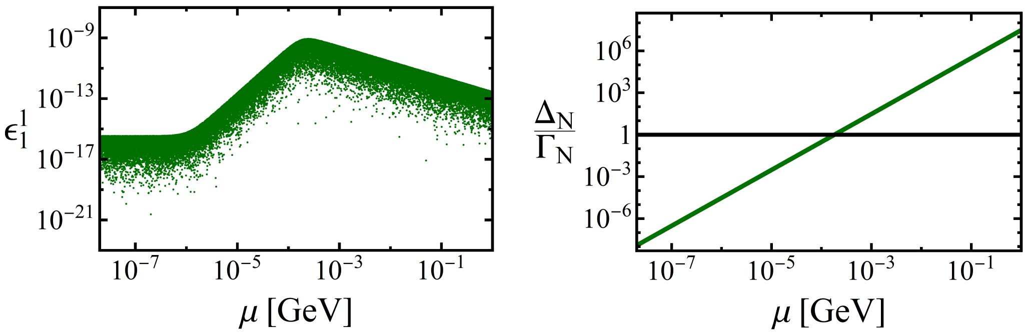


FIGURE 2.7: Estimating the resonance contribution in 3+3 low-scale ISS models. **Left panel:** Plot of the CP-asymmetry parameter $\epsilon_i^\alpha$ (in this case $\alpha = 1$ and $i = 1$) as a function of $\mu$ (in GeV). A clear resonance peak appears in the regime: $\mu \sim 10^{-3} - 10^{-4}$. The thickness of the green band is due to a scan over the Casas-Ibarra matrix $R$. **Right panel:** Plot of $\Delta_{N_i}/\Gamma_{N_i}$ against the same parameter where $\Delta_N/\Gamma_N = (1 - x_{ij})/\frac{1}{8\pi}\left(h_\nu^\dagger h_\nu\right)_{jj}$ where $1 - x_{ij}$ is defined in Eq. (2.88). The horizontal lines corresponds to where the resonance condition is satisfied. Unlike in traditional resonant models, the mass splitting between the heavy sterile states cannot be adjusted independently of the required Yukawa couplings, because both depend on $\mu$. Nevertheless, a region satisfying the resonance condition of Eq. (2.44) is possible.

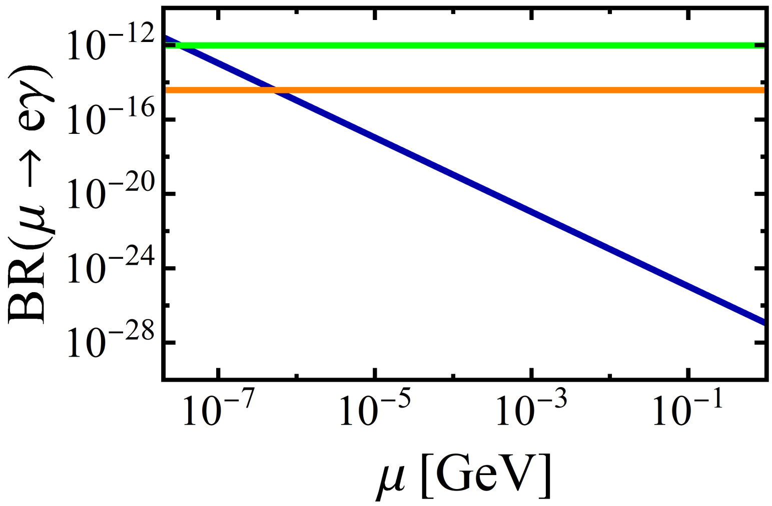


FIGURE 2.8: A plot of the branching ratio of $\mu \to e\gamma$ in the low-scale ISS model as a function of $\mu$ (blue line). The green line is the current upper limit, while the orange line is the combined future limit expected from MEGII and the $\mu \to e$ conversion experiments, in particular COMET. While currently unconstrained, future cLFV experiments will begin to probe the parameter space of these low-scale models. Due to the minimal flavour-violating assumption taken, the size of the LFV is tied to the size of $m_D^\nu$.

explore this possibility further in Chapter 3.

Finally, though unable to account for baryogenesis, the discovery potential of the ISS through cLFV is estimated in Fig. 2.8, which plots BR($\mu \to e\gamma$).[20] The current limits

[20] As discussed above, in regimes where the photon diagram dominates, $\mu \to e\gamma$ and $\mu - e$ conversion are complementary.

placed on cLFV processes involving electrons does not constrain the ISS model. The parameter space which MEGII, COMET and Mu2E is predicted to probe is already constrained from unitarity violation experiments. Due to the minimal flavour-violating scenario considered, the cLFV effects are generated through the Casas-Ibarra parametrisation of $m_D^\nu$ (rather than imposing large cLFV effects through non-diagonal entries in $M_R$ or $\mu$) which will therefore have the largest contributions in regions of small entries in $\mu$ for fixed choices in $M_R$.

### 2.6.3 Inverse + Linear Seesaw Case

As in Section 2.6.2, we first consider a one-generation example to estimate how inclusion of the LSS term influences the strength of the washout relevant for thermal leptogenesis. As the LSS contribution to the light neutrino mass in Eq. (2.18) depends on an inverse power of $M_R$ compared to two inverse powers in the case of the ISS term of Eq. (2.14), its contribution typically dominates in the light neutrino mass generation through $m_D^\nu$. The washout efficiency of the ISS+LSS scenario can therefore be estimated by considering the pure $1+1$ LSS case,

$$M_{\text{lin,1g}} = \begin{pmatrix} 0 & m_D^\nu & m_L \\ m_D^\nu & 0 & M_R \\ m_L & M_R & 0 \end{pmatrix}. \tag{2.90}$$

In this limiting case, the (non-unique) matrix rotation into the mass basis of the heavy sterile neutrinos above the critical temperature can be performed exactly and takes the form

$$M_{\text{lin}} = U_{\text{lin}}^T M_{\text{lin}} U_{\text{lin}} = \begin{pmatrix} 0 & \left(\frac{1}{2}-\frac{i}{2}\right)(m_D^\nu + i m_L) & \left(\frac{1}{2}+\frac{i}{2}\right)(m_D^\nu - i m_L) \\ \left(\frac{1}{2}-\frac{i}{2}\right)(m_D^\nu + i m_L) & M_R & 0 \\ \left(\frac{1}{2}+\frac{i}{2}\right)(m_D^\nu - i m_L) & 0 & M_R \end{pmatrix}, \tag{2.91}$$

with

$$U_{\text{lin}} = \begin{pmatrix} 1 & 0 & 0 \\ 0 & \left(\frac{1}{2}-\frac{i}{2}\right) & \left(\frac{1}{2}+\frac{i}{2}\right) \\ 0 & \left(\frac{1}{2}+\frac{i}{2}\right) & \left(\frac{1}{2}-\frac{i}{2}\right) \end{pmatrix}. \tag{2.92}$$

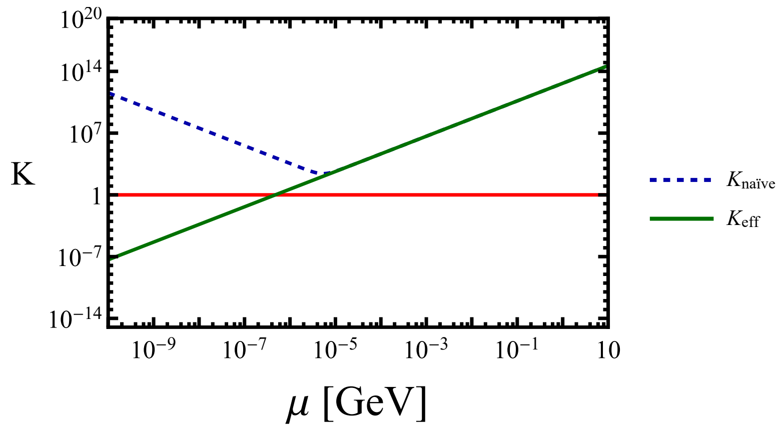


FIGURE 2.9: Log-Log plot of the washout parameters as a function of $m_L$ in the one generation LSS. The naïve washout is minimised in this case for $m_L \sim 4.5 \times 10^{-4}$ [GeV] with $K_{N_i} \sim 100$, which is much lower than in the pure ISS case.

The neutrino oscillation data is recovered with a Dirac mass matrix of the form

$$m_D^{\nu} = -\frac{m_n M_R}{2m_L} \tag{2.93}$$

which can be used to estimate the strength of the naïve washout through the parameter,

$$K_{N_i}^{1gen} = \frac{\Gamma_{N_1}}{H(T = M_{N_i})} = \frac{\sqrt{45}M_p}{16\pi^{5/2}v_{EW}^2 g_*^{1/2} M_R} \left| \left(\frac{1}{2} \mp \frac{i}{2}\right) \left(\frac{2m_n M_R}{m_L} \pm i m_L\right) \right|^2 \tag{2.94}$$

where an effective washout can be defined, with $\delta \simeq m_L/m_D^{\nu}$ [162], similarly to the ISS section above with identical behaviour such that for large values of $m_L$ the effective and naïve washouts coincide and for small values of $m_L$ the effective washout tends to zero.

Figure 2.9 plots the naïve and effective washout parameters in the pure one-generation LSS as a function of $m_L$. Similarly to the case of the pure ISS, for $\mathcal{O}$(TeV) scale sterile neutrinos, the washout remains strong. However, as a result of the mixing between $\nu_R$ and $S_L$, lower values of the washout exist. More importantly, the parameter determining the strength of the washout, $m_L$, does not impact the mass of the heavy sterile neutrinos (above the critical temperature), by contrast with the case of the ISS. Therefore when both $\mu$ and $m_L$ are turned on, $m_L$ will largely be responsible in determining the neutrino masses and couplings (and therefore largely responsible in determining the washout of asymmetry as $\mu$ will generally be sub-dominant), whereas only $\mu$ introduces a mass splitting between the heavy sterile neutrinos above the critical temperature. Therefore when both parameters are switched on, resonant Dirac-phase leptogenesis is possible at

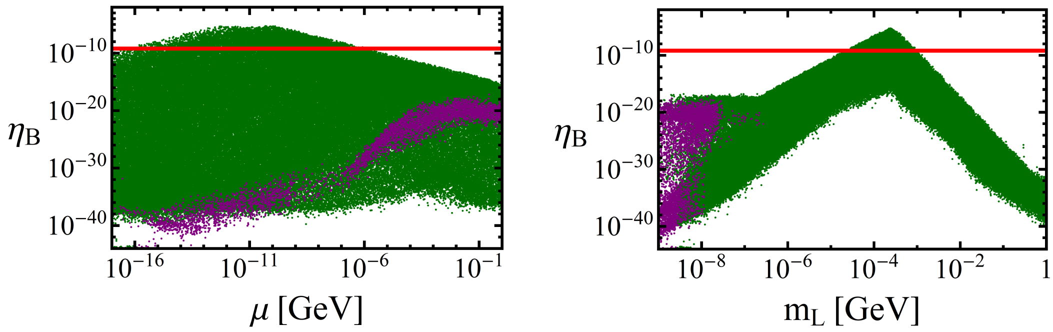


FIGURE 2.10: The generated baryon asymmetry for the degenerate case as a function of the Majorana mass $\mu$ (**Left Panel**) and the lepton number violating parameter $m_L$ (**Right Panel**). The points in purple, which correspond to large values of $m_D$, are excluded from unitarity violation limits on the PMNS matrix. In red is the required BAU, $\eta_B \sim 6.21 \times 10^{-10}$. Generation of the correct asymmetry is possible in regions close to where the naïve washout is minimised (but still in the strong regime) and requires $10^{-5} \lesssim m_L/\text{GeV} \lesssim 10^{-3}$ along with $10^{-16} \lesssim \mu/\text{GeV} \lesssim 10^{-6}$ where resonance occurs due to the small mass splitting.

relatively low values of strong washout.

#### 2.6.3.1 Degenerate Limit

Figure 2.10 plots the baryon asymmetry generated as functions of $\mu$ and $m_L$ for the degenerate case where all $M_R$ masses equal 1 TeV, as per Section 2.6. Similarly to the pure ISS case, all points generate an asymmetry of the correct sign for $\delta_{CP} = 3\pi/2$. The points in purple are ruled out by non-unitarity of the PMNS matrix and are characterised by low values of $m_L$, as can be seen in the right-hand plot. In order to generate the correct asymmetry for these TeV scale sterile neutrinos via the Dirac phase, two ingredients are necessary: the LSS term, $m_L$, needs to be close to the region in which the naïve washout is minimised, $10^{-5} \lesssim m_L/\text{GeV} \lesssim 10^{-3}$, and the ISS term, $\mu$, is required to be in the broad range $10^{-16} \lesssim \mu/\text{GeV} \lesssim 10^{-6}$ in order for the mass splittings amongst the heavy sterile neutrinos to provide a resonant contribution to the asymmetry generation.

Figure 2.11 plots the CP-asymmetry parameter $\epsilon_i^\alpha$ as a function of $\mu$ for fixed bands of $m_L$. While a clear resonance exists as $\mu$ is lowered for all snapshots, it is only for regions close to where the naïve washout is minimised that the resonance enhancement is able to generate a sufficient asymmetry[21]. This serves to illustrate that for $\mathcal{O}$(TeV)

[21] For the hierarchy $\mu > m_L$ the neutrino mass matrix will be approximately given by the ISS mass term and therefore the leptogenesis implications are unchanged from the section above. For small values of $m_L$, (with $\mu$ smaller) the effective washout may be small enough to be weak however there will be less LNV within the theory and we therefore find that this leads to insufficient asymmetry generation.

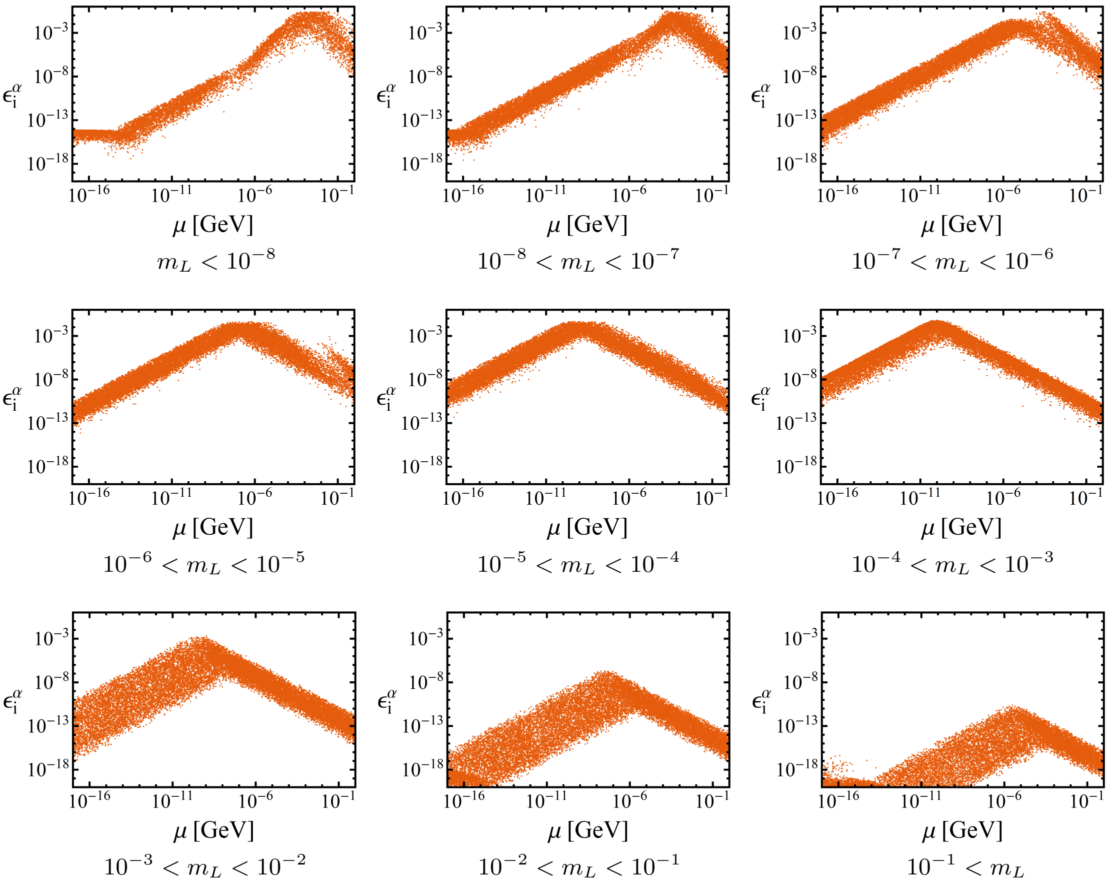


FIGURE 2.11: Log-Log plots of CP asymmetry parameter $\epsilon_i^\alpha$ as a function of $\mu$ for fixed values of $m_L$ described above. In each case a resonant enhancement can occur for a given range of $\mu$ which controls the mass splittings amongst the SNs.

scale extended type-I seesaw models, both the LSS and ISS contributions are required in order for thermal leptogenesis to be possible, potentially providing a unique experimental signature of pseudo-Dirac sterile fermions with leptonic decay channels.

Figure 2.12 plots the average washout parameter in the three generation case, which closely resembles the pure LSS one-generation plot of Fig. 2.9. From Fig. 2.12, it is evident that contributions to the washout (and therefore the couplings $h$) from $\mu$ are sub-dominant compared to $m_L$, justifying the assumption that $m_L$ is almost solely responsible for determining the strength of the washout, even at low values.

In the case of Dirac-phase leptogenesis, a region of parameter space exists for both $m_L$ and $\mu$ for the well-motivated choice $\delta_{CP} = 3\pi/2$. Figure 2.13 plots BR$(\mu \to e\gamma)$ as a function of $m_L$. Similarly to the pure ISS case, current and near-future cLFV experiments will not probe regions where Dirac-phase leptogenesis occurs.

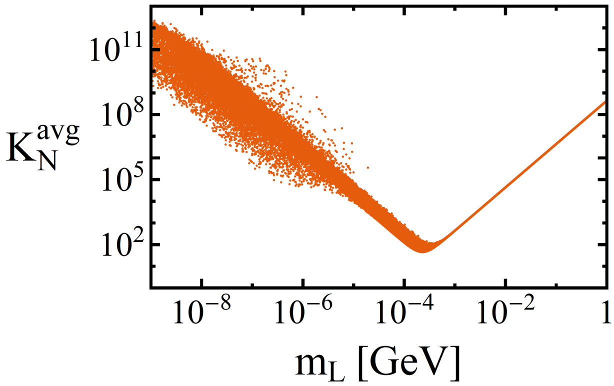


FIGURE 2.12: Log-log plot of the average naïve washout parameter $K_N^{\rm avg} = \frac{1}{6}\sum_i K_{N_i}$ in the three-generation case as a function of $m_L/\text{GeV}$. Comparison of this with the one-generation case of the pure LSS as in Fig. 2.9 justifies the claim that the ISS term is sub-dominant to the LSS in the generation of $m_D^\nu$.

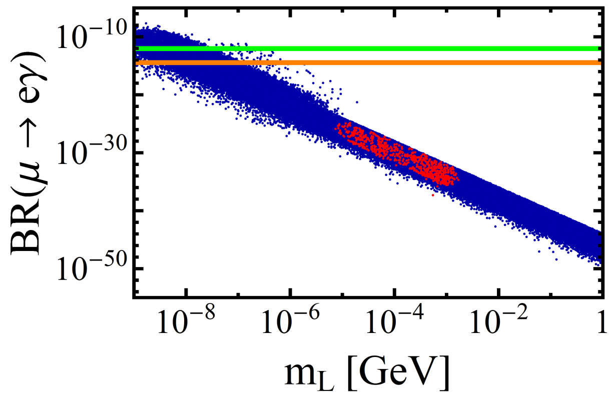


FIGURE 2.13: A plot of contribution to $\mu \to e\gamma$ in the low-scale ISS+LSS model for the degenerate case. The horizontal green line is the current experimental upper limit and the orange line is the combined future limit expected from MEGII and the $\mu \to e$ conversion experiments, in particular COMET, assuming the penguin diagram contribution dominates. Regions of small $m_L$ in the ISS+LSS model are currently constrained. The points in red generate a baryon asymmetry in the required region, $4 \times 10^{-10} < \eta_B < 8 \times 10^{-10}$. This region is currently unconstrained and will remain so in the future. The points in blue give rise to asymmetry values that are too small.

#### 2.6.3.2 Hierarchical Limit

In the hierarchical case, in which the heavier SNs are set to 5 TeV as justified in Fig. 2.4, Dirac-phase leptogenesis is also possible, as illustrated in Fig. 2.14. The asymmetry is produced via the same mechanism as in the degenerate case: the relevant area of parameter space is where $m_L$ minimises the strength of the naïve washout, and the resonant enhancement is due to mass splittings driven by a small $\mu$. Unsurprisingly, this occurs in a smaller region of $\mu$ and $m_L$ than before, $5 \times 10^{-3} \lesssim m_L/\text{GeV} \lesssim 5 \times 10^{-2}$ and $10^{-12} \lesssim \mu/\text{GeV} \lesssim 10^{-6}$, compared to the degenerate case, making the hierarchical case

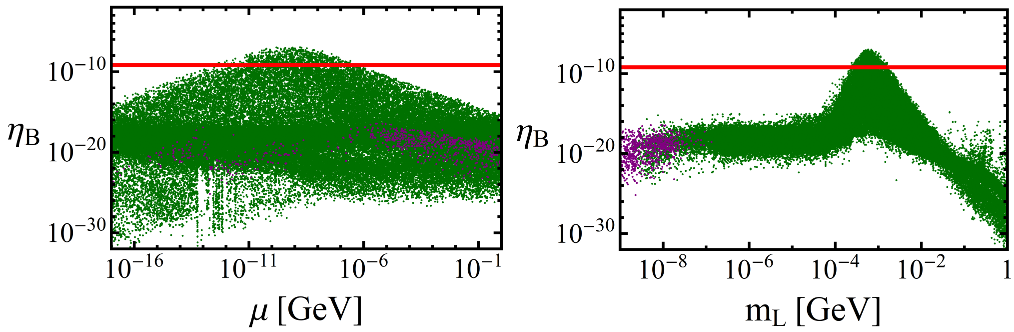


FIGURE 2.14: The generated baryon asymmetry as a function of the Majorana mass $\mu$ (**Left Panel**) and the lepton number violating parameter $m_L$ (**Right Panel**) in the hierarchical case. The hierarchical case behaves similarly to the degenerate case with slightly more constrained allowed couplings, $5 \times 10^{-3} \lesssim m_L/\text{GeV} \lesssim 5 \times 10^{-2}$ along with $10^{-12} \lesssim \mu/\text{GeV} \lesssim 10^{-6}$ compared to the degenerate case. The points in purple are excluded by unitarity violation limits on the PMNS matrix.

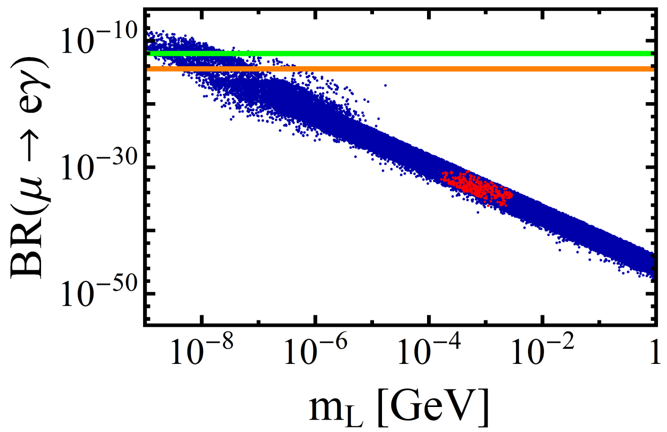


FIGURE 2.15: A plot of contribution to $\mu \to e\gamma$ in the low-scale hierarchical ISS+LSS model. In green is the current limit from MEG and in orange is the combined future limit from MEGII and the $\mu \to e$ conversion experiments, in particular COMET, assuming the penguin diagram contribution dominates. Regions of small $m_L$ in the ISS+LSS model are currently probed and constrained by MEG and future experiments will serve to slightly improve the sensitivity on $m_L$. The points in red generate a baryon asymmetry in the region $4 \times 10^{-10} < \eta_B < 8 \times 10^{-10}$. This parameter region is unconstrained by current experiments and beyond the reach of future cLFV experiments. The points in blue give rise to asymmetry values that are too small.

more constrained. This result is similar to that found for the type-I Dirac-phase case in Ref. [128].

The constraints from current and future cLFV are of similar strength as in the degenerate situation: low scale, viable Dirac-phase leptogenesis cannot be constrained by unitarity violation or cLFV processes as demonstrated in Fig. 2.15. Singlet neutrinos may be produced at particle colliders however the classic signal of same-sign dileptons [163] is suppressed due to the pseudo-Dirac nature of the SNs. Trilepton production has been studied in [144] where constraints have been derived on the mixing between the active and sterile states $|B_{lN}|^2$. However, in our model the region of successful Dirac-phase leptogenesis has $|B_{lN}|^2 \sim 10^{-12}$, far too small to be constrained at the LHC.

## 2.7 Summary

In this chapter we have studied the thermal leptogenesis implications of the low-scale 3+3 inverse-seesaw (ISS) and extended inverse-seesaw (ISS+LSS) models when the mass splittings between the SNs are only given by LNV parameters. Both scenarios provide a framework for TeV-scale sterile neutrinos, with much larger Yukawa couplings required in order to account for current active neutrino oscillation data, in contrast to the vanilla type-I seesaw mechanism. The implications of purely Dirac-phase leptogenesis were considered, as values of $\delta_{CP} \in (0, 2\pi) \setminus \{\pi\}$ will necessarily contribute to the asymmetry generation in any low-scale seesaw model, and $\delta_{CP}$ remains the only phase that can be measured by neutrino oscillation experiments.

In the pure ISS scenario, the washout is too strong for asymmetry generation even when incorporating resonance effects where no special textures are assumed in the theory beyond diagonal couplings. In the ISS+LSS scenario, successful leptogenesis can be achieved due to the mass splitting between the sterile neutrinos providing a resonant enhancement of the asymmetry, a regime which is naturally motivated in the model if the LNV parameters are taken to be small from technical-naturalness arguments. Degenerate and hierarchical cases were considered, and in both situations predictions for the entries of the matrices $m_L$ and $\mu$ are made in order to achieve successful Dirac-phase leptogenesis. Unsurprisingly, the hierarchical case appears slightly more constrained than the degenerate case. However the hierarchical case demonstrates that in the ISS+LSS scenario resonant thermal leptogenesis is possible without the need for inter-generational mass degeneracies between the six SNs.

The discovery potential of these models from precision tests was considered, particularly through probes of unitarity violation in the PMNS matrix and charged-lepton flavour-violating processes such as BR($\mu \to e\gamma$) and $\mu \to e$ conversion. It was found that regions of successful Dirac-phase leptogenesis do not coincide with the current or future reach of such cLFV experiments or unitarity tests. Collider tests were also briefly considered, but the active-sterile mixing in regions of successful Dirac-phase leptogenesis is too low for near-future discovery. It is worth noting, however, that an extension to a left-right symmetric model or similar, well-motivated by the neutrino mass basis choice we have employed, would increase the experimental signatures of such a scenario.

Crucially the above analysis insisted that the mass splittings between the masses of the heavy SNs was purely from the LNV parameters within $\mu$. In the next section we will explore the possibility of sufficient lepton asymmetry generation in the ISS or LSS models with additional resonance effects included within the matrix $M_R$. In order to motivate these small mass degeneracies we will assume the SM is extended by a flavour symmetry and show how the ISS and LSS models are also the minimal choices as leptogenesis candidates in type-I-like seesaw models.

# Chapter 3

# Low-scale Resonant Leptogenesis with a Minimal Lepton Flavour Violating Hypothesis

## 3.1 Introduction

The previous chapter argued that in the specific case of the LSS, above the electroweak phase transition, the heavy SNs are degenerate in mass and therefore self-energy diagrams vanish, leaving only the highly-suppressed vertex contributions to produce the CP asymmetry [164]. In the case of the ISS, a mass splitting is generated at high temperatures allowing for a resonant enhancement in the self-energy contribution for a specific choice of $\mu_S$. However, decreasing the mass splitting also increases the efficiency of washout (as there is less L violation and therefore less B violation) and we find that asymmetry generation cannot occur, assuming the mass splittings are generated by small LNV parameters [1, 165–167] for the ISS at the TeV scale. BSM theories often generate either an ISS or LSS, but not both terms simultaneously if the scalar sector of the theory does not allow the required couplings.

In this chapter we explore the idea that in addition to the intra-family SN degeneracies naturally present in such theories, there is also the possibility of a quasi-degeneracy between SNs from different families, a flavour degeneracy in other words. To that end we explore a scenario in which an $SU(3)^2 \otimes SO(3)^2$ flavour symmetry, to be defined below, is utilised in the lepton sector. Due to the $SO(3)$ symmetry, mass terms for the heavy SNs are proportional to the identity matrix and lead to a flavour degeneracy amongst the SN states in both the ISS and LSS scenarios similar to the degenerate spectrum scenario considered in Chapter 2. However, radiative effects induce $SO(3)$-breaking terms which in turn break these degeneracies, enabling a resonant enhancement in the asymmetry generation for both the LSS and ISS scenarios.

We work in the framework of an extended version of the Minimal Lepton Flavour Violation (MLFV) [168, 169] scenario, which is itself an extension of the well-established idea of Minimal Flavour Violation (MFV) within the quark sector [170–172]. The MFV scheme is an *ansatz* designed to address the very stringent bounds placed on new physics from various rare hadronic decays and neutral meson oscillations. It is motivated by the idea that taking the Yukawa sector couplings to zero recovers five separate[1] flavour space rotations which leave the Lagrangian invariant. Therefore an MFV (or MLFV) *ansatz* is based on the core principle that these are "good" flavour symmetries which are broken solely by the SM Yukawa fields.

Under this *ansatz*, Yukawa couplings are said to arise from dynamical fields typically known as 'spurions' which transform under the flavour symmetries such that the Lagrangian is flavour invariant. These spurion fields are taken to have non-zero vevs which spontaneously break the flavour symmetries and thereby induce the masses and flavour mixing we observe. As a result, in its most minimal realisation, any flavour changing process can be predicted from the well-measured Cabibbo-Kobayashi-Maskawa (CKM) mixing matrix and the fermion masses.

Due to the multiple distinct ways in which neutrino masses can be incorporated into the SM there is no unique way of defining an MLFV *ansatz*, in contrast with MFV in the quark sector. The potential connection between an MLFV *ansatz* and resonant leptogenesis[2] has been identified previously [174–176] in the type-I seesaw context. Since then it has been discovered that, due to developments within flavoured leptogenesis, there is a significant reduction in the allowed parameter space[3] [136, 177, 178] specific to MLFV leptogenesis which we explain in Section 3.3. Additionally, in order to produce large

[1] In the absence of neutrino mass. If neutrino mass is included more rotations are present.

[2] See [173] for an example of an MLFV *ansatz* which incorporates leptogensis without resonance effects.

[3] Recently it was found that flavour effects can still be relevant at much higher temperatures than thought previously, potentially reducing the allowed parameters space even further [129].

leptonic flavour violation whilst suppressing neutrino masses in such models, a separation between the scale of lepton-number violation (LNV) and lepton-flavour violation (LFV) should exist which is not present in the type-I seesaw alone [175, 179]. Neither of these issues are present for MLFV in the ISS and LSS, allowing the possibility of MLFV-induced resonant leptogenesis in these scenarios. We assume an *ansatz* such that the heavy sterile Majorana neutrinos introduced have exactly degenerate masses in the Lagrangian, motivated by the flavour symmetry of the theory. Radiative effects will break this down to a quasi-degeneracy between the SNs, leading to small mass splittings, from which a resonant enhancement in the asymmetry generated per decay of SN will occur. For some choices of parameters which we will identify, this enhancement is able generate the necessary baryon asymmetry observed in the universe. We will explore the viability of leptogenesis both from PMNS phases (specifically only the Dirac phase for the same reasons as in Chapter 2) alone [1, 2, 126–128] as well as from CPV parameters related to the heavy SNs.

This chapter is organised as follows. Section 3.2 reviews the basic idea behind the MFV and MLFV *ansätze* including justification from hadronic observables for the MFV hypothesis. Section 3.3 describes our technique for calculation of the baryon asymmetry in the ISS and LSS models with MLFV, while Sec. 3.4 provides a description of our choice of scans and a discussion of the results. Here we also briefly assess the discovery potential of these models at current and future cLFV experiments. We conclude in Sec. 3.5.

## 3.2 Model

### 3.2.1 MFV in the quark sector

The Minimal Flavour Violation *ansatz* [170–172] recognises that, in the massless limit of absent Yukawa couplings, the quark sector of the three-family SM is invariant under a product of $U(3)$ flavour groups, where an individual $U(3)$ acts in flavour space on a given type of SM multiplet: $q_L$, $u_R$ and $d_R$. Utilising $U(3) = SU(3) \otimes U(1)$, the quark-sector flavour group may be expressed as

$$\mathcal{G}^Q = \underbrace{U(1)_B \otimes U(1)_{A^u} \otimes U(1)_{A^d}}_{\mathcal{G}^Q_{\rm A}} \otimes \underbrace{SU(3)_{q_L} \otimes SU(3)_{u_R} \otimes SU(3)_{d_R}}_{\mathcal{G}^Q_{\rm NA}} . \tag{3.1}$$

| | $U(1)_B$ | $U(1)_{A^u}$ | $U(1)_{A^d}$ | $SU(3)_{q_L}$ | $SU(3)_{u_R}$ | $SU(3)_{d_R}$ |
|---|---|---|---|---|---|---|
| $q_L$ | $1/3$ | $1$ | $1$ | $\mathbf{3}$ | $\mathbf{1}$ | $\mathbf{1}$ |
| $u_R$ | $1/3$ | $-1$ | $0$ | $\mathbf{1}$ | $\mathbf{3}$ | $\mathbf{1}$ |
| $d_R$ | $1/3$ | $0$ | $-1$ | $\mathbf{1}$ | $\mathbf{1}$ | $\mathbf{3}$ |

TABLE 3.1: Representations of the SM quark fields under the Abelian and non-Abelian parts of $\mathcal{G}^Q$ which leave the kinetic terms of the SM Lagrangian invariant.

The Abelian transformations are flavour-blind and we have the freedom to rotate and identify them with baryon number and two axial rotations [180]. The non-Abelian transformations do act in flavour space; they govern interactions between the different flavours and hence are responsible for the flavour violation in the theory. Table 3.1 defines the representations of the SM quark fields under the flavour symmetries and specifies a basis for the Abelian generators.

The Yukawa terms in the SM are not invariant under these flavour transformations, but can be made invariant if the Yukawa matrices are 'promoted' to be spurionic fields.[4] Unique transformations under the flavour symmetries are assigned to the spurions in order to make the would-be flavour-breaking terms invariant. This is a hypothesis motivated by the lack of experimental evidence for new flavour-violating physics; it should be treated as the low-energy limit of an unspecified higher-scale, renormalisable theory. The necessary transformations under the non-Abelian symmetries are summarised in Table 3.2.

Quark masses are generated in this framework when the spurionic fields acquire nonzero vevs alongside the SM Higgs doublet. These background values relate to the physically measurable quark masses and mixings where we have the freedom to choose a basis such that

$$\langle \mathcal{Y}_u \rangle = \frac{\sqrt{2}}{v_{EW}} V_{\text{CKM}}^\dagger \hat{m}_u \qquad \text{and} \qquad \langle \mathcal{Y}_d \rangle = \frac{\sqrt{2}}{v_{EW}} \hat{m}_d \tag{3.2}$$

where

$$\hat{m}_u = \text{diag}(m_u,\, m_c,\, m_t) \qquad \text{and} \qquad \hat{m}_d = \text{diag}(m_d,\, m_s,\, m_b), \tag{3.3}$$

[4]In this chapter, promoting a Yukawa coupling to be a dynamical field will be represented by $Y_i \to \mathcal{Y}_i$.

| | $SU(3)_{q_L}$ | $SU(3)_{u_R}$ | $SU(3)_{d_R}$ |
|---|---|---|---|
| $\mathcal{Y}_u$ | $\mathbf{3}$ | $\overline{\mathbf{3}}$ | $\mathbf{1}$ |
| $\mathcal{Y}_d$ | $\mathbf{3}$ | $\mathbf{1}$ | $\overline{\mathbf{3}}$ |

TABLE 3.2: Representation assignments for Yukawa spurions such that the Yukawa terms in the MFV effective theory respect the flavour symmetry which exists in their absence.

$V_{\rm CKM}$ is the quark mixing matrix measured by experiment and here, by the usual convention, we have chosen the vevs of the spurion fields such that the down-type matrix is diagonal and the up-type is not.

The MFV *ansatz* is based on two assumptions about the high-scale, renormalisable theory:

- The flavour symmetry present in the SM quark kinetic terms is a 'good' symmetry which the high-scale sector respects. The only sources of flavour symmetry breaking within the theory at the high scale are from the vevs of the Yukawa coupling spurions.[5] The dynamics by which these vevs are generated lie in the unspecified high-scale theory.
- The SM is an effective theory for which all renormalisable and non-renormalisable operators must respect both the gauge *and* flavour symmetries of the theory. All operators which are not formally invariant under the flavour symmetry are made so by insertions of the appropriate combinations of Yukawa fields.

A number of consequences follow from this *ansatz*.

SM effective field theory operators which describe flavour changing processes require insertions of spurion combinations in order to become flavour invariant. For example, the four-fermion operator $(\overline{Q_L}\gamma_\mu Q_L)(\overline{Q_L}\gamma^\mu Q_L)$ is forced to be flavour preserving by the flavour symmetry. In order to get a related $\Delta F = 1$ operator, a spurion insertion must be made: $\mathcal{O}_{q1} = (\overline{Q_L}\mathcal{Y}_u\mathcal{Y}_u^\dagger\gamma_\mu Q_L)(\overline{Q_L}\gamma^\mu Q_L)$ is flavour invariant due to the insertion of $\mathcal{Y}_u\mathcal{Y}_u^\dagger$, but gives rise to flavour-changing processes when the spurions acquire vevs. Due to the hierarchy of the couplings within $\mathcal{Y}_u$ there is an in-built suppression of flavour-changing

[5]Therefore under this *ansatz* flavour violation is completely dictated by the flavour structure of the Yukawa terms in the Lagrangian; any new physics introduced into the theory should not contribute to flavour-changing processes.

| Hadronic Process | Bound on $\Lambda_{\mathrm{NP}}$ |
|---|---|
| $K^0 - \overline{K^0}$ | $9 \times 10^3$ TeV |
| $B_{\mathrm{d}} - \overline{B_{\mathrm{d}}}$ | $4 \times 10^2$ TeV |
| $B_{\mathrm{s}} - \overline{B_{\mathrm{s}}}$ | $7 \times 10^1$ TeV |

TABLE 3.3: Approximate lower bounds on the scale $\Lambda_{\mathrm{NP}}$ of new physics from precision measurements of neutral meson oscillations assuming dimension six and $\mathcal{O}(1)$ Wilson coefficients [181]. The bounds are stronger when first-generation quarks are involved.

processes for the first two generations of quarks. A list of relevant spurion insertions for operators involving fermions at dimension six can be found in [172].

Of particular importance when adapted to resonant leptogenesis, which will be discussed in more detail later, all terms in the lowest-order MFV Lagrangian will receive corrections to their couplings from spurion terms which transform in the same way as the basic spurion under the flavour symmetry. For example, in

$$\overline{Q_L}\left(\mathcal{Y}_d + \epsilon_1 \mathcal{Y}_d \mathcal{Y}_d^\dagger \mathcal{Y}_d + \ldots\right) d_R H, \tag{3.4}$$

the higher-order term $\mathcal{Y}_d \mathcal{Y}_d^\dagger \mathcal{Y}_d$ transforms in the same way as $\mathcal{Y}_d$ and therefore under the *ansatz* has to be included. As Yukawa spurion vevs are small in magnitude these corrections are generally not significant.

### 3.2.2 MFV vs Experiment

The motivation behind adopting the MFV *ansatz* is due to the strong limits placed on the mass scale of new physics from flavour-violating hadronic processes involving the first generation, as illustrated in Table 3.3. If new physics appears at scales lower than these bounds it would indicate that either flavour violation arises solely, or dominantly, due to the SM CKM matrix indicating an MFV-like theory, or that it could couple dominantly to the heavier generations which have less stringent bounds.

A key advantage of the former assumption is that strict relations between different flavour changing processes arise due to precise measurements of the CKM parameters. Therefore MFV-like theories have a degree of predictivity which can aid experimental searches. In the case of an exact MFV *ansatz*, relations amongst different flavour transitions, e.g.

| Hadronic Process | Measured value or upper limit | MFV prediction |
|---|---|---|
| $\mathcal{A}_{CP}(\ B \to X_s\gamma\ )$ | $0.0144^{+0.0139}_{-0.0139}$ | $< 0.02$ |
| $\mathcal{B}(\ K_L \to \pi^0\nu\overline{\nu}\ )$ | $< 2.6 \times 10^{-10}$ | $< 2.9 \times 10^{-10}$ |
| $\mathcal{B}(B \to X_s\tau^+\tau^-)$ | - | $[0.2, 3.7] \times 10^{-7}$ |
| $\mathcal{B}(\ B \ \to\ X_d\gamma\ )$ | $(1.41^{+0.57}_{-0.57}) \times 10^{-5}$ | $[1.0, 4.0] \times 10^{-5}$ |
| $\mathcal{B}(B_d \ \to\ \mu^+\mu^-)$ | $(0.39^{+0.16}_{-0.14} \times 10^{-9})_{\text{CMS/LHCb}}$ $< (0.21 \times 10^{-9})_{\text{ATLAS}}$ | $< 0.38 \times 10^{-9}$ |

Table 3.4: Predictions for some rare hadronic observables under the MFV ansatz [182–184], based on other precisely measured processes, compared with their current experimental limits [185–189].

$b \to s, b \to d$ and $s \to d$, can be used to make predictions of unmeasured (or poorly measured) observables [182–184], some of which are summarised in Table 3.4. They can be compared to their corresponding experimental measurement or limit [185–189] showing strong correlation.

Most channels have measurements (or upper limits) in agreement with MFV predictions, however a discrepancy exists for $B_d \to \mu^+\mu^-$ between the CMS/LHCb [186] and ATLAS [189] collaborations. CMS/LHCb measure the rate for this process at the limit of the MFV prediction, whereas ATLAS place an upper-bound consistent with MFV. More precise measurements are required and could potentially suggest a deviation from an exact MFV theory. Certainly, however, we have strong evidence that flavour violation is dominantly generated by the Yukawa couplings.

### 3.2.3 MLFV

While the MFV *ansatz* for the quark sector can be uniquely implemented (with strong agreement with measurement) there is an issue when extending this concept to leptons. Currently we do not know the origin of LFV observed experimentally and most importantly whether the light neutrinos are predominantly Dirac or Majorana. One may expand the MFV *ansatz* to the lepton sector, which is termed MLFV, but a dependence exists on the specific SM extension adopted for neutrino mass generation as well as an additional freedom in choosing which couplings are flavour violating [190] which we will explain below. The simplest approach is to extend the SM by three right-handed neutrinos $N_R$ in the usual way where lepton number violation occurs through gauge-invariant

Majorana neutrino mass terms,

$$\mathcal{L}_{\text{SEESAW}} = \mathcal{L}_{\text{SS}}^{\text{K}} - \mathcal{L}_{\text{SS}}^{\text{M}}, \tag{3.5}$$

where $\mathcal{L}_{\text{SS}}^{\text{K}}$ is the usual kinetic term and

$$\mathcal{L}_{\text{SS}}^{\text{M}} = \epsilon_e \bar{\ell}_L Y_e e_R H + \epsilon_D \bar{\ell}_L Y_D^\nu N_R \tilde{H} + \frac{1}{2}\mu_N \overline{N_R^c} Y_N N_R + \text{ h.c.} \tag{3.6}$$

The *numbers* $\epsilon_{e,D}$ and $\mu_N$ are to be distinguished from the *matrices* (in flavour space) $Y_{e,N}$ and $Y_D^\nu$ which will ultimately act as sources for the breaking of the Abelian and non-Abelian flavour symmetries respectively (once promoted to spurions having non-zero vevs).

Similar to the quarks and MFV, the gauge sector of the leptons obey a flavour-transformation invariance which can be defined analogously to Eq. (3.1):

$$\mathcal{G}^L = \underbrace{U(1)_L \otimes U(1)_{A^e} \otimes U(1)_{A^N}}_{\mathcal{G}_{\text{A}}^L} \otimes \underbrace{SU(3)_{\ell_L} \otimes SU(3)_{e_R} \otimes SU(3)_{N_R}}_{\mathcal{G}_{\text{NA}}^L}. \tag{3.7}$$

In the absence of $\mathcal{L}_{\text{SS}}^{\text{M}}$, the Lagrangian is invariant under the following $SU(3)$ rotations

$$\ell_L \to \mathcal{U}_{\ell_L} \ell_L \qquad e_R \to \mathcal{U}_{e_R} e_R \qquad N_R \to \mathcal{U}_{N_R} N_R \tag{3.8}$$

implying the following representations for the fields:

$$\ell_L \sim (\mathbf{3}, \mathbf{1}, \mathbf{1}) \qquad e_R \sim (\mathbf{1}, \mathbf{3}, \mathbf{1}) \qquad N_R \sim (\mathbf{1}, \mathbf{1}, \mathbf{3}). \tag{3.9}$$

Once again, flavour invariance can be recovered (once $\mathcal{L}_{\text{SS}}^{\text{M}}$ is reintroduced) by promoting the relevant couplings to spurions with fixed transformation properties under the flavour symmetries,

$$\mathcal{Y}_e \to \mathcal{U}_{\ell_L} \mathcal{Y}_e \mathcal{U}_{e_R}^\dagger \qquad \mathcal{Y}_D^\nu \to \mathcal{U}_{\ell_L} \mathcal{Y}_D^\nu \mathcal{U}_{N_R}^\dagger \qquad \mathcal{Y}_N \to \mathcal{U}_{N_R}^* \mathcal{Y}_N \mathcal{U}_{N_R}^\dagger \tag{3.10}$$

implying the following representations for the fields

$$\mathcal{Y}_e \sim (\mathbf{3}, \bar{\mathbf{3}}, \mathbf{1}) \qquad \mathcal{Y}_D^\nu \sim (\mathbf{3}, \mathbf{1}, \bar{\mathbf{3}}) \qquad \mathcal{Y}_N \sim (\mathbf{1}, \mathbf{1}, \bar{\mathbf{6}}). \tag{3.11}$$

Lepton masses and mixings appear once these spurionic fields acquire non-zero vevs along with the SM Higgs. We are free to choose a basis such that

$$\langle \mathcal{Y}_e \rangle = \frac{\sqrt{2}}{v_{EW}} \hat{m}_\ell, \qquad \langle \mathcal{Y}_D^\nu \rangle \langle \mathcal{Y}_N^{-1} \rangle \langle (\mathcal{Y}_D^\nu)^T \rangle = \frac{2\mu_N}{v_{EW}^2} U_{\rm PMNS}\, \hat{m}_\nu\, U_{\rm PMNS}^T \tag{3.12}$$

where

$$\hat{m}_\ell = \text{diag}(m_e,\, m_\mu,\, m_\tau), \qquad \hat{m}_\nu = \text{diag}(m_{\nu_1},\, m_{\nu_2},\, m_{\nu_3}). \tag{3.13}$$

It is clear from Eq. (3.12) that it is not possible to assign unique background values to the spurions $\mathcal{Y}_D^\nu$ and $\mathcal{Y}_N$ in terms of physically measurable parameters. Rather, it is the combination in the seesaw formula that is fixed by the physical observables. As a consequence each individual spurion cannot be uniquely written in terms of physical masses and mixings. In the quark sector, under the MFV *ansatz*, higher-dimensional operators which control rare processes are made flavour invariant from the necessary combination of spurion fields. As their background values are only dependent on quark sector masses and mixings, this prevents any sources of new physics from contributing in a way not aligned with the SM flavour violation. For the lepton sector, however, rare flavour-violating processes will not in general be made invariant by the exact combination $\mathcal{Y}_D^\nu \mathcal{Y}_N^{-1} \mathcal{Y}_D^\nu$, but through different combinations of these two spurions (see [169] for a list of examples). Therefore specific flavour-changing processes cannot be uniquely written in terms of physically measurable parameters in the same way they can be for MFV.

Predictivity can be recovered if only one of the spurion fields is assumed to have non-trivial flavour transformations, and therefore the other will not act as a source of flavour-symmetry breaking. Usually, it is assumed that the Majorana mass term does not act as a source of lepton-flavour breaking and, and as in the quark sector, only the Yukawa couplings are responsible. If it is assumed that the Majorana mass term is lepton-flavour blind, then $Y_N$ must necessarily be equal to the identity matrix (in flavour space). Under this assumption the non-Abelian flavour symmetry of the theory[6] reduces to

$$\mathcal{G}_{\rm NA}^L = SU(3)_{\ell_L} \otimes SU(3)_{e_R} \otimes SO(3)_{N_R} \otimes CP. \tag{3.14}$$

[6] A alternative approach is to assume $\mathcal{G}_{\rm NA}^L = SU(3)_{V=(\ell_L+N_R)} \otimes SU(3)_{e_R}$ and then via Schur's Lemma one of the flavour space matrices must be unitary which can be rotated to the identity matrix with a field redefinition. Under this assumption no degeneracy is implied amongst the right-handed neutrinos and CP invariance is not necessary. [191]

The lepton-flavour symmetry is broken by $\mathcal{Y}_D^\nu$ and $\mathcal{Y}_e$ which can now be written uniquely in terms of lepton masses and mixings

$$\langle\mathcal{Y}_e\rangle = \frac{\sqrt{2}}{v_{EW}}\hat{m}_\ell, \qquad \langle\mathcal{Y}_D^\nu\rangle\langle(\mathcal{Y}_D^\nu)^T\rangle = \frac{2\mu_N}{v_{EW}^2}U_{\rm PMNS}\,\hat{m}_\nu\,U_{\rm PMNS}^T, \qquad \langle\mathcal{Y}_N\rangle = \mathbb{1}_{3\times 3}. \tag{3.15}$$

The measured masses and mixings in the lepton sector fix the combination $\mathcal{Y}_D^\nu(\mathcal{Y}_D^\nu)^T$ in this setup and not the spurion $\mathcal{Y}_D^\nu$ itself. However, often the combination $\mathcal{Y}_D^\nu(\mathcal{Y}_D^\nu)^\dagger$ (which transforms as a **(8,1,1)** under $\mathcal{G}^L$) is required to be inserted for many operators. Without the imposition of CP invariance, additional and yet unmeasured phases will appear in the predictions for flavour-changing processes. However, in general we expect CP violation (CPV) to be present in the lepton sector.

Allowing for leptonic CPV, as necessary for leptogenesis, a slightly less minimal *ansatz* is required, namely

$$\mathcal{G}_{\rm NA}^L = SU(3)_{\ell_L}\otimes SU(3)_{e_R}\otimes SO(3)_{N_R}. \tag{3.16}$$

Lifting the assumption of CP invariance introduces new non-SM phases, as well as allowing non-trivial phases in the Pontecorvo-Maki-Nakagawa-Sakata (PMNS) mixing matrix. While they spoil the absolute predictivity of the theory, they generally lead to only small deviations in cLFV observables [174–176]. This is not in conflict with experiment (as it might be in the quark sector) as currently no cLFV processes have been measured. Additionally, although not definitive, there is an interesting possibility for CPV in neutrino oscillations [192] motivating the less-minimal definition of the MLFV principle, where phases are allowed and their effect on measurable processes are taken into account.

As already emphasised, MFV and MLFV should be understood as hypotheses motivated by experiment and do not provide a complete UV description of the flavour sector. Attempts have been made in moving from this *ansatz* to a renormalisable model. In particular in the case of the simplest type-I MLFV *ansatz*, the spurion scalar potentials have been studied [193–195] with suggestive conclusions. For hierarchical masses amongst the charged leptons, *large* mixing angles appear when Majorana neutrinos are considered, whereas in the quark sector *small* mixing angles are predicted. It has been suggested that the disparity in the mixing between the lepton and quark sector is therefore due to the Majorana properties of the right-handed neutrinos. These results suggest that UV completions of the MFV and MLFV *ansätze* could ultimately explain the origin of the flavour structure of the SM.

### 3.2.4 MLFV and the inverse and linear seesaw models

It was noted in [168, 175, 179] that in order to generate measurable LFV effects whilst explaining the smallness of the active neutrino masses, a decoupling between the LFV scale and LNV scale is required such that $\Lambda_{\rm LFV} \ll \Lambda_{\rm LN}$. This observation, coupled with any future measurement of cLFV, motivates the incorporation of such a scale separation into the MLFV hypothesis. Note that LNV arises from the breaking of Abelian symmetries in Eq. (3.7), whereas LFV arises from the breaking of the non-Abelian symmetries.

Scale separation, however, does not occur in the minimal version of the type-I and type-III seesaw mechanisms where only one new scale is introduced such that $\Lambda_{\rm LFV} = \Lambda_{\rm LNV} = \mu_N$. Under an MLFV *ansatz* the flavour spurions decouple when the LNV scale is taken to infinity [179], preventing significant LFV. In contrast it was argued that the type-II seesaw does exhibit such a behaviour as $\Lambda_{\rm LNV} \sim M_\Delta^2/\mu_\Delta$ while $\Lambda_{\rm LFV} \sim M_\Delta$, where $M_\Delta$ is the mass of the triplet and $\mu_\Delta$ is the dimensionful cubic coupling constant between the triplet and the SM Higgs doublet. This therefore defines the only minimal seesaw model for which an MLFV *ansatz* may lead to significant LFV.

The simplest[7] fermionic completions which achieves a natural scale separation are the ISS and LSS mechanisms (and a combination of the two) where small LNV parameters are introduced in order to ensure an approximate $U(1)_L$ symmetry. As discussed in Chapters 1 and 2, additional sterile neutrino degrees of freedom $S_L$ are introduced alongside the right-handed neutrinos $N_R$,

$$\mathcal{L}_{\rm ESS} = \mathcal{L}^{\rm K}_{\rm ESS} - \mathcal{L}^{\rm M}_{\rm ESS}, \tag{3.17}$$

$$\begin{aligned}\mathcal{L}^{\rm M}_{\rm ESS} = \epsilon_e \overline{\ell_L} \mathcal{Y}_e H e_R + \epsilon_D \overline{\ell_L} \mathcal{Y}^{\nu}_D \phi^c N_R + \epsilon_L \overline{\ell_L} \mathcal{Y}_L \phi^c \left(S_L\right)^c + m_R \overline{(N_R)^c}\, \mathcal{Y}_R \left(S_L\right)^c \\ + \frac{1}{2}\mu_S\, \overline{S_L}\, \mathcal{Y}_{\mu_S} \left(S_L\right)^c + \frac{1}{2}\mu_N\, \overline{(N_R)^c}\, \mathcal{Y}_{\mu_N} N_R + \text{h.c},\end{aligned} \tag{3.18}$$

where it is conventional to choose $L(\ell_L) = L(N_R) = 1$ and $L(S_L) = -1$.

[7] In [175] it was suggested the two scales could be made distinct by embedding the minimal type-I seesaw mechanism into an extended theory such as the MSSM, where $\Lambda_{\rm LFV} = m_{\tilde{\ell}} \sim \mathcal{O}(\text{TeV})$ is proportional to the soft-SUSY breaking terms.

As in the case of type-I MLFV, $\mathcal{Y}_i$ correspond to dimensionless $3\times 3$ matrices in flavour space associated with the breaking of $\mathcal{G}^L_{\rm NA}$. We impose an $SO(3)$ rather than $SU(3)$ flavour invariance for the heavy singlets to ensure that only the Yukawa interactions with the Higgs doublet act as sources of flavour-symmetry breaking. Therefore all bare mass terms related to the heavy singlets are proportional to the identity matrix. The flavour symmetry of the theory is defined analogously to Eq. (3.7),

$$\mathscr{G}^{\rm L} = \underbrace{U(1)_L \otimes U(1)_{A^e} \otimes U(1)_{A^N} \otimes U(1)_{A^S}}_{\mathscr{G}^{\rm L}_{\rm A}} \otimes \underbrace{SU(3)_{\ell_L} \otimes SU(3)_{e_R} \otimes SO(3)_{N_R} \otimes SO(3)_{S_L}}_{\mathscr{G}^{\rm L}_{\rm NA}}. \tag{3.19}$$

The mass matrix has the form

$$M_\nu = \begin{pmatrix} 0 & \frac{1}{\sqrt{2}}\epsilon_D \mathcal{Y}^\nu_D v_{EW} & \frac{1}{\sqrt{2}}\epsilon_L \mathcal{Y}_L v_{EW} \\ \frac{1}{\sqrt{2}}\epsilon_D (\mathcal{Y}^\nu_D)^T v_{EW} & \mu_N \mathcal{Y}_{\mu_N} & m_R \mathcal{Y}_R \\ \frac{1}{\sqrt{2}}\epsilon_L \mathcal{Y}^T_L v_{EW} & m_R \mathcal{Y}_R & \mu_S \mathcal{Y}_{\mu_S} \end{pmatrix} \tag{3.20}$$

where for the ISS ($\epsilon_L = 0$)

$$\Lambda_{\rm LNV} \sim \frac{m_R^2}{\mu} \qquad \text{and} \qquad \Lambda_{\rm LFV} \sim m_R \tag{3.21}$$

and for the LSS ($\mu_N$, $\mu_S = 0$)

$$\Lambda_{\rm LNV} \sim \frac{m_R}{\sqrt{\epsilon_L}} \qquad \text{and} \qquad \Lambda_{\rm LFV} \sim m_R. \tag{3.22}$$

The imposition of small lepton number violation means that $\mu_S$, $\mu_N$ and $\epsilon_L$ are small. This provides the desired separation of scales.

As with the quark sector and the example of the minimal type-I seesaw model, the kinetic terms in Eq. (3.17) are invariant under the following flavour rotations

$$\ell_L \to \mathcal{U}_{\ell_L}\ell_L \qquad e_R \to \mathcal{U}_{e_R} e_R \qquad N_R \to \mathcal{O}_{N_R} N_R \qquad S_L \to \mathcal{O}_{S_L} S_L \tag{3.23}$$

where $\mathcal{U}_i$ are $3\times 3$ special unitary matrices, $\mathcal{O}_i$ are $3\times 3$ real-orthogonal matrices and for example $\ell_L = (e_L, \mu_L, \tau_L)$. The leptons therefore transform as fundamentals under their respective non-Abelian rotations

$$\ell_L \sim (\mathbf{3},\mathbf{1},\mathbf{1},\mathbf{1}) \qquad e_R \sim (\mathbf{1},\mathbf{3},\mathbf{1},\mathbf{1}) \qquad N_R \sim (\mathbf{1},\mathbf{1},\mathbf{3},\mathbf{1}) \qquad S_L \sim (\mathbf{1},\mathbf{1},\mathbf{1},\mathbf{3}). \tag{3.24}$$

It follows that Eq. (3.18) can be made invariant by promoting the relevant couplings to dynamical spurions with the flavour transformation properties,

$$\mathcal{Y}_e \to \mathcal{U}_{\ell_L} \mathcal{Y}_e \mathcal{U}_{e_R}^{\dagger} \qquad \mathcal{Y}_D^{\nu} \;\; \to \;\; \mathcal{U}_{\ell_L} \mathcal{Y}_D^{\nu}\, \mathcal{O}_{N_R}^T \qquad \mathcal{Y}_L \to \mathcal{U}_{\ell_L} \mathcal{Y}_L\, \mathcal{O}_{S_L}^T \tag{3.25}$$

implying that

$$\mathcal{Y}_e \sim (\mathbf{3},\overline{\mathbf{3}},\mathbf{1},\mathbf{1}) \qquad \mathcal{Y}_D^{\nu} \;\; \sim \;\; (\mathbf{3},\mathbf{1},\mathbf{3},\mathbf{1}) \qquad \mathcal{Y}_L \sim (\mathbf{3},\mathbf{1},\mathbf{1},\mathbf{3}). \tag{3.26}$$

Lepton masses and mixings result as usual from non-zero vevs for the spurion fields where, similarly to Eq. (3.12), a basis can be chosen such that

$$\langle \mathcal{Y}_e \rangle = \frac{\sqrt{2}}{v_{EW}} \hat{m}_\ell \qquad\qquad \langle \mathcal{Y}_D^{\nu} \rangle \langle (\mathcal{Y}_D^{\nu})^T \rangle = \frac{2\, m_R^2}{v_{EW}^2 \mu_S} U_{\rm PMNS}\, \hat{m}_\nu\, U_{\rm PMNS}^T \tag{3.27}$$

in the case of the inverse seesaw and

$$\langle \mathcal{Y}_e \rangle = \frac{\sqrt{2}}{v_{EW}} \hat{m}_\ell \qquad \langle \mathcal{Y}_D^{\nu} \rangle \langle \mathcal{Y}_L^T \rangle + \langle Y_L \rangle \langle (\mathcal{Y}_D^{\nu})^T \rangle = \frac{2\, m_R}{v_{EW}^2 \epsilon_L} U_{\rm PMNS}\, \hat{m}_\nu\, U_{\rm PMNS}^T \tag{3.28}$$

in the case of the linear seesaw.

## 3.3 Leptogenesis

The leading-order flavour degeneracy amongst the heavy SNs is built into the *ansatz*, with higher order spurion effects breaking the degeneracy. This allows for a resonant enhancement in asymmetry generation.

The case of the simplest MLFV scenario has been explored in detail [174–176, 196]. Recent developments related to flavoured leptogenesis [136, 177, 178] have, however, highlighted the importance of a term not previously included, such that the flavoured

CP-asymmetry is proportional to

$$\epsilon_i^\alpha \propto 2\sum_{j\neq i}\mathfrak{Im}\left\{(\mathcal{Y}_D^\nu)_{\alpha i}(\mathcal{Y}_D^\nu)_{\alpha j}\right\}\mathfrak{Re}\left\{((\mathcal{Y}_D^\nu)^\dagger\mathcal{Y}_D^\nu)_{ij}\right\}+\mathcal{O}((\mathcal{Y}_D^\nu)^6). \tag{3.29}$$

Equation (3.29) requires the existence of real, off-diagonal entries in $(\mathcal{Y}_D^\nu)^\dagger\mathcal{Y}_D^\nu$ in order for non-zero asymmetry generation to appear at lowest order in the couplings. It turns out that this presents a problem, as we now review, and provides an independent motivation for the ISS and LSS extended seesaw schemes in the MLFV and leptogenesis context.

In the case of the MLFV *ansatz* implemented in the type-I seesaw scenario, the radiative corrections to the SN Majorana masses are incorporated through

$$\tilde{\mu}_N = \mu_N\mathbb{1}_{3\times 3}+\delta\mu_N, \tag{3.30}$$

where $\mu_N$ is defined in Eq. (3.6) and the $SO(3)$ breaking source $\delta\mu_N$ arises from all spurion insertions that transform such that the combination $\overline{N_R^c}\,\delta\mu_N\,N_R$ is flavour invariant. For the remainder of this chapter, Majorana masses with tildes will denote that corrections have been included whereas without will denote the $SO(3)$ conserving bare mass. At lowest order they are

$$\begin{aligned}\delta\mu_N &= \mu_N\left[n_1\left((\mathcal{Y}_D^\nu)^\dagger\mathcal{Y}_D^\nu+(\mathcal{Y}_D^\nu)^T(\mathcal{Y}_D^\nu)^*\right)\right]\\ &= 2\,\mu_N\,n_1\,\mathfrak{Re}\left\{(\mathcal{Y}_D^\nu)^\dagger\mathcal{Y}_D^\nu\right\}\end{aligned} \tag{3.31}$$

where $n_1$ is a Wilson coefficient which at the effective level is a free parameter. The two terms appearing in Eq. (3.31) can be checked to transform in the appropriate way by applying the rotations defined in Eqs. (3.24) and (3.25) to the terms of Eq. (3.31). For the MLFV *ansatz* these terms must be included, but we remain agnostic as to how they are generated.

In order to calculate the CP-asymmetry one must first rotate the SN into their mass basis (above the critical temperature). The unitary matrix responsible for diagonalising the heavy SNs in this case is real (and therefore orthogonal):

$$\begin{pmatrix} 0 & m_D^\nu \\ (m_D^\nu)^T & \mu_N \mathbb{1}_{3\times 3} + \delta\mu_N \end{pmatrix} \longrightarrow$$
$$\begin{pmatrix} 0 & m_D^\nu \mathcal{O} \\ \mathcal{O}^T (m_D^\nu)^T & \mathcal{O}^T(\mu_N \mathbb{1}_3 + \delta\mu_N)\mathcal{O} \end{pmatrix} = \begin{pmatrix} 0 & m_D^\nu \mathcal{O} \\ \mathcal{O}^T (m_D^\nu)^T & \hat{\tilde{\mu}}_N \end{pmatrix}. \tag{3.32}$$

where $\hat{\tilde{\mu}}_N = \text{diag}(\mu_N + \delta_1,\, \mu_N + \delta_2,\, \mu_N + \delta_3)$. Due to the degeneracy required in $\mathcal{Y}_N$ and the allowed flavour invariant terms of Eq. (3.31) the rotation matrix $\mathcal{O}$ is exactly the matrix which diagonalizes $\mathfrak{Re}\left\{(\mathcal{Y}_D^\nu)^\dagger \mathcal{Y}_D^\nu\right\}$. Therefore the CP asymmetry for flavoured leptogenesis shifts to

$$\mathfrak{Re}\left\{(\mathcal{Y}_D^\nu)^\dagger \mathcal{Y}_D^\nu\right\} \to \mathfrak{Re}\left\{\mathcal{O}^T(\mathcal{Y}_D^\nu)^\dagger \mathcal{Y}_D^\nu \mathcal{O}\right\} = \mathcal{O}^T\, \mathfrak{Re}\left\{(\mathcal{Y}_D^\nu)^\dagger \mathcal{Y}_D^\nu\right\}\mathcal{O} = \text{diag}(\dots) \tag{3.33}$$

which has no off-diagonal terms and thus the CP asymmetry vanishes exactly. A non-zero asymmetry could potentially be recovered by including higher-order terms of $\mathcal{O}((\mathcal{Y}_D^\nu)^6)$ of appropriate form. However, due to the suppression from the additional powers of couplings in the assumed perturbative regime, a substantial asymmetry will be difficult to generate even if resonance effects are present.

Alternatively, the consideration of higher-order corrections to the Majorana mass which are not all aligned in flavour space will cause non-zero real entries in the relevant term of Eq. (3.29). Higher-order terms which transform in the same way as in Eq. (3.31) can be constructed from the charged-lepton spurion, as per

$$\begin{aligned}\delta\mu_N = \mu_N \Big[ & c_1 \left((\mathcal{Y}_D^\nu)^\dagger \mathcal{Y}_D^\nu + (\mathcal{Y}_D^\nu)^T (\mathcal{Y}_D^\nu)^*\right) + \dots \\ & + c_i \left((\mathcal{Y}_D^\nu)^\dagger \mathcal{Y}_e \mathcal{Y}_e^\dagger \mathcal{Y}_D^\nu + (\mathcal{Y}_D^\nu)^T \mathcal{Y}_e^* \mathcal{Y}_e^T (\mathcal{Y}_D^\nu)^*\right) + \dots \Big]\end{aligned} \tag{3.34}$$

where, for clarity, only the terms not flavour aligned have been written explicitly (the additional terms in Eq. (3.34) will be fully written out later on). Due to the inclusion of $\mathcal{Y}_e$, $\delta\mu_N$ cannot be diagonalised by the same orthogonal matrix $\mathcal{O}$, since $\mathcal{Y}_e \mathcal{Y}_e^\dagger \not\propto \mathfrak{Re}\left\{(\mathcal{Y}_D^\nu)^\dagger \mathcal{Y}_D^\nu\right\}$. Changing to the mass basis now allows off-diagonal real terms and therefore the generation of a non-zero asymmetry. The necessary off-diagonal entries, however, are generated by the misalignment between the two spurions, and thus they will be suppressed compared to if they had been generated at leading order.

Due to the extra fields introduced, the above flavour alignment problem does not occur in general for the extended seesaw models. Consider the full ISS + LSS scenario where the equivalent radiative corrections to the relevant Majorana masses are included,

$$\begin{pmatrix} 0 & m_D^\nu & m_L \\ (m_D^\nu)^T & \mu_N \mathbb{1}_{3\times3} + \delta\mu_N & m_R \mathbb{1}_{3\times3} \\ m_L^T & m_R \mathbb{1}_{3\times3} & \mu_S \mathbb{1}_{3\times3} + \delta\mu_S \end{pmatrix} \to \begin{pmatrix} 0 & m_D^\nu \mathcal{O} & m_L \mathcal{V} \\ \mathcal{O}^T (m_D^\nu)^T & \hat{\hat{\mu}}_N & m_R \mathcal{V}\mathcal{O}^T \\ \mathcal{V}^T m_L^T & m_R \mathcal{V}^T \mathcal{O} & \hat{\hat{\mu}}_S \end{pmatrix}. \tag{3.35}$$

Here $\hat{\hat{\mu}}_{\mathrm{i}} = \mathrm{diag}(\dots)$ and the rotation matrices $\mathcal{O}$ and $\mathcal{V}$ diagonalise $\delta\mu_N$ and $\delta\mu_S$ respectively. The spoiling of the flavour alignment should be clear: in the process of diagonalising the Majorana mass terms $\mu_i$, the Dirac mass between the two heavy SNs $m_R \mathbb{1}_{3\times3}$ has been rotated as well. Diagonalising the lower right $2 \times 2$ block will now no longer rotate the Dirac mass matrices $m_D^\nu$ and $m_L$ by the same orthogonal rotation that diagonalises $(\mathcal{Y}_D^\nu)^\dagger \mathcal{Y}_D^\nu$. The same alignment effect can occur only for very specific choices between the entries of Eq. (3.35) and is not a general feature. We will provide an illustrative example below.

### 3.3.1 Baryon Asymmetry

Based off the calculations of the preceding chapter, in this section we briefly review the procedure and formalism we employ for estimating the efficiency of asymmetry generation. Due to the introduction of additional sources of mass splittings between the SNs compared to Chapter 2 as well as the MLFV *ansatz* assumed, there are some slight differences between the leptogenesis analyses of Chapter 2 and Chapter 3.

As is conventional, we work in the heavy sterile neutrino mass basis above the critical temperature, i.e. the bottom-right sub-matrix of Eq. (3.20) is real, positive and diagonal. The block diagonalisation of the lower right $2 \times 2$ block defines the required rotation matrix:

$$M_\nu \to U_{\mathrm{rot}}^T \, M_\nu \, U_{\mathrm{rot}} \equiv M_\nu' = \begin{pmatrix} m_\nu^{\text{1-loop}} & m_D' & m_L' \\ (m_D')^T & \hat{M}_+ & 0 \\ (m_L')^T & 0 & \hat{M}_- \end{pmatrix}, \tag{3.36}$$

where primed parameters indicate rotated matrices and $\hat{M}_i = \text{diag}(\dots)$. We have included the one-loop contribution to the active neutrino masses which may significantly contribute in some regions of parameter space, for the analysis of Chapter 2 this one-loop contribution is negligible and therefore was not included. In the most general case, a simple analytic expression for the rotated matrices $m_i'$ is not possible. However, in our setup, where an $SO(3)^2$ flavour symmetry is employed (and before radiative effects are included) the entries of the bottom-right $2\times 2$ sub-block are all commuting. Under this simplification the rotation can be generalised from the simple one-generation case, giving

$$U_{\text{rot}} = \begin{pmatrix} \mathbb{1}_3 & 0 & 0 \\ 0 & \cos\left[\frac{\pi}{4}+\frac{1}{2}\arctan(\frac{\mu_S-\mu_N}{2m_R})\right]\mathbb{1}_{3\times 3} & -i\sin\left[\frac{\pi}{4}+\frac{1}{2}\arctan(\frac{\mu_S-\mu_N}{2m_R})\right]\mathbb{1}_{3\times 3} \\ 0 & \sin\left[\frac{\pi}{4}+\frac{1}{2}\arctan(\frac{\mu_S-\mu_N}{2m_R})\right]\mathbb{1}_{3\times 3} & i\cos\left[\frac{\pi}{4}+\frac{1}{2}\arctan(\frac{\mu_S-\mu_N}{2m_R})\right]\mathbb{1}_{3\times 3} \end{pmatrix} \tag{3.37}$$

leading to

$$\begin{aligned}
m_D' &= \cos\left[\frac{1}{4}\left(\pi + 2\,\text{arccot}\left[\frac{2m_R}{\mu_S-\mu_N}\right]\right)\right] m_D^\nu + \sin\left[\frac{1}{4}\left(\pi + 2\,\text{arccot}\left[\frac{2m_R}{\mu_S-\mu_N}\right]\right)\right] m_L \\
&\simeq \left(\frac{1}{\sqrt{2}} - \frac{1}{4\sqrt{2}}\left(\frac{\mu_S-\mu_N}{2m_R}\right)\right) m_D^\nu + \left(\frac{1}{\sqrt{2}} + \frac{1}{4\sqrt{2}}\left(\frac{\mu_S-\mu_N}{2m_R}\right)\right) m_L \\
m_L' &= -i\sin\left[\frac{1}{4}\left(\pi + 2\,\text{arccot}\left(\frac{2m_R}{\mu_S-\mu_N}\right)\right)\right] m_D^\nu \\
&\qquad + i\cos\left[\frac{1}{4}\left(\pi + 2\,\text{arccot}\left(\frac{2m_R}{\mu_S-\mu_N}\right)\right)\right] m_L \\
&\simeq -i\left(\frac{1}{\sqrt{2}} + \frac{1}{4\sqrt{2}}\left(\frac{\mu_S-\mu_N}{2m_R}\right)\right) m_D^\nu + i\left(\frac{1}{\sqrt{2}} - \frac{1}{4\sqrt{2}}\left(\frac{\mu_S-\mu_N}{2m_R}\right)\right) m_L \\
\hat{M}_+ &= \left(m_R\sqrt{1+\frac{(\mu_S-\mu_N)^2}{4\,m_R^2}} + \frac{\mu_S}{2} + \frac{\mu_N}{2}\right)\mathbb{1}_{3\times 3} \\
&\simeq \left(m_R + \frac{\mu_S}{2} + \frac{\mu_N}{2}\right)\mathbb{1}_{3\times 3} \\
\hat{M}_- &= \left(m_R\sqrt{1+\frac{(\mu_S-\mu_N)^2}{4\,m_R^2}} - \frac{\mu_S}{2} - \frac{\mu_N}{2}\right)\mathbb{1}_{3\times 3} \\
&\simeq \left(m_R - \frac{\mu_S}{2} - \frac{\mu_N}{2}\right)\mathbb{1}_{3\times 3}
\end{aligned} \tag{3.38}$$

where in every second line we have expanded up to $\mathcal{O}(\frac{\mu_S-\mu_N}{m_R})$. Once the spurionic radiative corrections are included in the Majorana self-energies, the $\mathcal{O}(3)^2$ invariance is lifted and the matrices no longer commute. In the regime where these corrections are small these expressions will remain approximately valid. However, once the corrections are included, we perform the rotations numerically during our scan.

The combination

$$h^\dagger h \simeq \frac{2}{v_{EW}^2} \begin{pmatrix} {m'_D}^\dagger m'_D & {m'_D}^\dagger m'_L \\ {m'_L}^\dagger m'_D & {m'_L}^\dagger m'_L \end{pmatrix} \tag{3.39}$$

where $h = \frac{\sqrt{2}}{v_{EW}} (m'_D, m'_L)$, is now the relevant combination for flavoured leptogenesis. The entries in the diagonal blocks of $h^\dagger h$ control the CP asymmetry generated by the interference between two different generations of heavy SNs with same sign mass splitting:

$$\Delta m_{i,j}^{\mathrm{SS}} = (\hat{M}_\pm)_{ii} - (\hat{M}_\pm)_{jj}. \tag{3.40}$$

The off-diagonal blocks control the CP asymmetry generated by the interference between two different heavy SNs of opposite mass splitting (same generation or otherwise):

$$\Delta m_{i,j}^{\mathrm{OS}} = (\hat{M}_\pm)_{ii} - (\hat{M}_\mp)_{jj}. \tag{3.41}$$

Clearly, in the absence of radiative effects where we have $\mu_N$, $\mu_S \propto \mathbb{1}_{3\times3}$ only $\Delta m_{i,j}^{\mathrm{OS}} \neq 0$, with $\Delta m_{i,j}^{\mathrm{SS}} = 0$. Once the corrections are included, however, the $SO(3)^2$ invariance is broken allowing for both $\Delta m_{i,j}^{\mathrm{OS}} \neq 0$ and $\Delta m_{i,j}^{\mathrm{SS}} \neq 0$. From Eqs. (3.38) and (3.39) it can be seen that for example if $m_D^\nu = m_L$[8] along with $\mu_N = \mu_S$ then $m'_D \neq 0$ but $m'_L = 0$. No real, off-diagonal entries would exist and the same alignment problem of the type-I seesaw would occur. This is not a general feature in the extended MLFV seesaw (as it is in the minimal type-I MLFV seesaw) and would require an additional symmetry to justify the necessary relations between the couplings and masses such that this flavour alignment would occur.

Similar to Chapter 2 we consider a low-scale scenario in which the sterile masses are set to $\mathcal{O}(\mathrm{TeV})$. This implies a low-temperature regime of lepton asymmetry generation where individual lepton flavours are in equilibrium with the thermal bath and distinguishable. We employ the same flavour-dependent Boltzmann equations [85, 88] from Chapter 2. For completeness we redefine the CP asymmetry generated from the decays of an SN,

[8] This would imply that $\delta\mu_N = \delta\mu_S$ and therefore $\mathcal{O} = \mathcal{V}$.

$N_i$, to a specific lepton: flavour $\ell_\alpha$,

$$\varepsilon^i_\alpha = \frac{\Gamma\left(N_i \to l_\alpha \Phi\right) - \Gamma\left(N_i \to \left(l_\alpha\right)^c \Phi^\dagger\right)}{\sum\limits_\alpha \left[\Gamma\left(N_i \to l_\alpha \Phi\right) + \Gamma\left(N_i \to \left(l_\alpha\right)^c \Phi^\dagger\right)\right]}. \tag{3.42}$$

This parameter is once again given by

$$\varepsilon_i^\alpha = \frac{1}{8\pi\left(h^\dagger h\right)_{ii}} \sum_{j\neq i} \Bigg( \underbrace{\mathcal{A}^\alpha_{ij}\, f(x_{ij})}_{\varepsilon_{\rm V}} + \underbrace{(\mathcal{A}^\alpha_{ij}\sqrt{x_{ij}} + \mathcal{B}^\alpha_{ij}) \frac{(1-x_{ij})}{(1-x_{ij})^2 + \frac{1}{64\pi^2}\left(h^\dagger h\right)^2_{jj}}}_{\varepsilon_{\rm S}} \Bigg) + \mathcal{O}(h^6) \tag{3.43}$$

where $\mathcal{A}^\alpha_{ij} = \mathfrak{Im}\left\{\left(h^\dagger h\right)_{ij} h^*_{\alpha i}\, h_{\alpha j}\right\}$, $\mathcal{B}^\alpha_{ij} = \mathfrak{Im}\left\{\left(h^\dagger h\right)_{ji} h^*_{\alpha i}\, h_{\alpha j}\right\}$, $x_{ij} = \left(\frac{m_{N_j}}{m_{N_i}}\right)^2$ and the loop function for the vertex-diagram contribution $f(x_{ij})$, is given by [83]

$$f(x_{ij}) = \sqrt{x_{ij}}\left[1 - (1+x_{ij})\ln\left(\frac{1+x_{ij}}{x_{ij}}\right)\right]. \tag{3.44}$$

As before we have indicated the contribution from the vertex $\varepsilon_{\rm V}$ and self-energy $\varepsilon_{\rm S}$ graphs of Fig. 1.2. A resonant enhancement in the CP asymmetry will occur when

$$1 - x_{ij} \to \frac{1}{8\pi}\left(h^\dagger h\right)_{jj} \tag{3.45}$$

which leads to the simplified condition

$$m_{N_i} - m_{N_j} \to \frac{\Gamma_{i,j}}{2} \tag{3.46}$$

where $\Gamma_i \simeq \frac{m_i}{8\pi}\sum_l h^*_{li} h_{li}$ is the decay width of $N_i$ and we assume $m_{N_i} - m_{N_j} \ll m_{N_{i,j}}$ in order to move from Eq. (3.45) to Eq. (3.46).

We choose the regulator of $\varepsilon^i_\alpha$ to be of the form $m_i\Gamma_j$, which as discussed in [136] has consistent behaviour for models with approximate lepton-number conservation. For other choices of regulators typically assumed in leptogenesis analyses, pathological behaviour occurs for approximate lepton-number conserving scenarios. For example choosing a regulator of the form $(m_i\Gamma_i - m_j\Gamma_j)$ diverges in the scenario $m_i \to m_j$ combined with $\Gamma_i \to \Gamma_j$ which occurs in the ISS and LSS when the LNV parameters are taken to zero.

Specifically for the LSS scenario, it is important to note that the second term in Eq. (3.43), due to the one-loop *self-energy* correction $\varepsilon_S$, identically goes to zero when $m_{N_i} \to m_{N_j}$.

By contrast, the first term arises from the one-loop vertex correction $\varepsilon_V$. In the limit $m_{N_i} \to m_{N_j}$ the asymmetry it generates is non-zero. However, $A^{\alpha}_{ij} = -A^{\alpha}_{ji}$ and therefore

$$\varepsilon^{\alpha}_i = -\frac{\left(h^\dagger h\right)_{ii}}{\left(h^\dagger h\right)_{jj}}\varepsilon^{\alpha}_j \tag{3.47}$$

for $m_{N_i} = m_{N_j}$. Therefore the asymmetry produced by the decay of $N_i$ to flavour $\alpha$ is almost equal and opposite to that of $N_j$ and in the limit $\left(h^\dagger h\right)_{ii} \to \left(h^\dagger h\right)_{jj}$ the asymmetry will vanish identically once the decays of all SNs are included. If the two SNs have different decay widths a non-zero asymmetry is possible, albeit highly suppressed.

We again work under the condition that, due to the strong washout nature of the temperature regime we favour [1], asymmetry generation occurs predominately well before the electroweak phase transition crossover and so we need not consider the changing sphaleron rate as the temperature approaches and crosses its critical value. The baryon asymmetry is then expressed as a fraction of the lepton asymmetry generated through

$$\eta_B = -\frac{28}{51}\frac{1}{27}\sum_{\alpha=e,\mu,\tau}\eta_\alpha \tag{3.48}$$

where the factor of 28/51 arises from the fraction of lepton asymmetry reprocessed into a baryon asymmetry by electroweak sphalerons [82], while the dilution factor 1/27 arises from photon production until the recombination epoch [139].

## 3.4 Numerical Results

In full analogy to the type-I scenario, all appropriate flavour invariant operators must be included. This leads to corrections to the Majorana mass terms from spurion combinations transforming the appropriate way such that when coupled with the heavy SN fields, the term is flavour invariant at the high scale. Now in the case of the extended seesaw both Majorana masses receive corrections, as per

$$\begin{aligned}\tilde{\mu}_N = \mu_N\Big(\mathcal{Y}_{\mu_N} &+ n_1\left((\mathcal{Y}^\nu_D)^\dagger\mathcal{Y}^\nu_D + ((\mathcal{Y}^\nu_D)^\dagger\mathcal{Y}^\nu_D)^T\right) \\ &+ n_2^{(1)}\left((\mathcal{Y}^\nu_D)^\dagger\mathcal{Y}^\nu_D(\mathcal{Y}^\nu_D)^\dagger\mathcal{Y}^\nu_D + ((\mathcal{Y}^\nu_D)^\dagger\mathcal{Y}^\nu_D(\mathcal{Y}^\nu_D)^\dagger\mathcal{Y}^\nu_D)^T\right) + \dots\Big)\end{aligned}$$

$$\tilde{\mu}_S = \mu_S\Big(\mathcal{Y}_{\mu_S} + s_1\left(\mathcal{Y}_L^\dagger\mathcal{Y}_L + (\mathcal{Y}_L^\dagger\mathcal{Y}_L)^T\right) + s_2^{(1)}\left(\mathcal{Y}_L^\dagger\mathcal{Y}_L\mathcal{Y}_L^\dagger\mathcal{Y}_L + (\mathcal{Y}_L^\dagger\mathcal{Y}_L\mathcal{Y}_L^\dagger\mathcal{Y}_L)^T\right) + \dots\Big). \tag{3.49}$$

As can be checked explicitly by applying the transformations defined in Eq. (3.25), the combinations of spurions above are flavour invariant when coupled to $\overline{N_R^c}N_R$ and $\overline{S_L}S_L^c$. All terms at next-to-leading order in the flavout-invariant spurion insertions will be explicitly written below.

The coefficients $n_i$ and $s_i$ are dimensionless Wilson coefficients which are treated as free parameters in the absence of an explicit high-scale, renormalisable theory. They are conventionally either taken to be $\mathcal{O}(1)$ numbers [168, 169, 174, 197], or arising from radiative effects [175, 176] so that $n_1 \simeq s_1 \simeq \frac{1}{16\pi^2}$ and $s_2^{(i)} \sim (s_1)^2$ etc. Note that in the ISS regime where $\mathcal{Y}_L = 0$, only the Majorana mass $\mu_N$ receives radiative corrections from flavour effects in our setup, whereas in the LSS regime where $\mathcal{Y}_{\mu_N} = \mathcal{Y}_{\mu_S} = 0$ both Majorana masses receive corrections.

We consider the general scenario similar to Chapter 2 where one copy of $N_R$ and $S_L$ is added for each generation of active neutrino. The tree-level light neutrino mass matrix can be expressed in powers of the LNV parameters [143] which in complete generality (without assuming MLFV) can be expanded out

$$\begin{aligned} m_\nu^{\rm tree} = \; & m_D^\nu\left(M_R^T\right)^{-1}\mu_S M_R^{-1}(m_D^\nu)^T + m_D^\nu\left(M_R^T\right)^{-1}\mu_S M_R^{-1}\mu_N\left(M_R^T\right)^{-1}\mu_S M_R^{-1}(m_D^\nu)^T \\ & - m_L M_R^{-1}(m_D^\nu)^T - m_L M_R^{-1}\mu_N\left(M_R^T\right)^{-1}\mu_S M_R^{-1}(m_D^\nu)^T \\ & - m_D^\nu\left(M_R^T\right)^{-1}m_L^T - m_D^\nu\left(M_R^T\right)^{-1}\mu_S M_R^{-1}\mu_N\left(M_R^T\right)^{-1}m_L^T \\ & + m_L M_R^{-1}\mu_N(M_R^T)^{-1}m_L^T + m_L M_R^{-1}\mu_N(M_R^T)^{-1}\mu_S M_R^{-1}\mu_N(M_R^T)^{-1}m_L^T \\ & + \dots \end{aligned} \tag{3.50}$$

where for completeness we have written all leading and next-to-leading terms valid for $||\mu_S||, ||\mu_N||, ||m_L|| \ll ||M_R||$. The above equation is valid for the general case of non-commuting sub-matrices, but for our MLFV setup $M_R = m_R\mathbb{1}_{3\times3}$, $m_L$ is diagonal and $\mu_S \propto \mu_N \propto \mathbb{1}_{3\times3}$.

In the limiting case of the ISS, only the first line of Eq. (3.50) contributes at leading order to the active neutrino masses. As discussed previously, $m_\nu^{\rm tree}$ vanishes in the limit $\mu_S \to 0$ even if $\mu_N \neq 0$. For $\mu_S \neq 0$ the contribution from terms involving $\mu_N$ are highly suppressed compared to terms without factors of $\mu_N$ even for relatively large values in the entries of $\mu_N$.

At one-loop order however, additional terms are generated for the active neutrino masses which can be important [143],

$$m_\nu^{\text{1-loop}} \simeq \frac{f(m_R)}{m_W^2}\left(m_D^\nu\,\mu_N\,(m_D^\nu)^T + m_L\,\mu_S\,m_L^T + m_R\,m_L\,(m_D^\nu)^T + m_R\,m_D^\nu\,m_L^T\right) \quad (3.51)$$

where

$$f(x) = \frac{\alpha_W}{16\pi}\left(\frac{m_H^2}{x^2 - m_H^2}\ln\left[\frac{x^2}{m_H^2}\right] + \frac{3m_Z^2}{x^2 - m_Z^2}\ln\left[\frac{x^2}{m_Z^2}\right]\right) \quad (3.52)$$

is a one-loop function and Eq. (3.51) is only valid for $M_R = m_R\mathbb{1}_{3\times3}$. Different terms in Eq. (3.51) can contribute significantly for different hierarchies amongst $\mu_N$, $\mu_S$ and $m_L$ which are free parameters in our scan.

Combining the tree-level and one-loop contributions at leading order leads to a general light-neutrino mass matrix in our MLFV *ansatz* of the form

$$\begin{aligned} m_\nu = {} & \left.\frac{1}{m_R^2}\left(m_D^\nu\,\mu_N\,(m_D^\nu)^T + m_L\,\mu_S\,m_L^T\right) - \frac{1}{m_R}\left(m_L\,(m_D^\nu)^T + m_D^\nu\,m_L^T\right)\right\}\text{tree} \\ & \left.\begin{aligned} & + \frac{1}{m_R^2}\left(f(m_R)\frac{m_R^2}{m_W^2}\right)\left(m_D^\nu\,\mu_N\,(m_D^\nu)^T + m_L\,\mu_S\,m_L^T\right) \\ & \qquad + \frac{1}{m_R}\left(f(m_R)\frac{m_R^2}{m_W^2}\right)\left(m_L\,(m_D^\nu)^T + m_D^\nu\,m_L^T\right) \end{aligned}\right\}\text{one-loop} \end{aligned} \quad (3.54)$$

where for both the ISS and LSS we fix $m_R = 1$ TeV. For the ISS specifically, the LNV parameters are randomly (and independently) scanned over the ranges

$$\begin{aligned} \mu_S &\sim \mathcal{O}(10^{-15} - 10^{2})\mathbb{1}_{3\times3}\ \text{GeV} \\ \mu_N &\sim \mathcal{O}(10^{-15} - 10^{4})\mathbb{1}_{3\times3}\ \text{GeV} \end{aligned} \quad (3.55)$$

where we allow for larger values of $\mu_N$ over $\mu_S$ as its contribution to the active neutrino mass is suppressed by a loop factor. For the LSS we vary

$$(m_L)_{ii} \sim \mathcal{O}(10^{-9} - 10^{1})\ \text{GeV} \quad (3.56)$$

where, in order to reduce the number of degrees of freedom, we take it to be diagonal but not proportional to the identity matrix in order for its inclusion to break the flavour symmetry. We fix the diagonal entries of $m_L$ to satisfy $\min(m_L) > \frac{1}{5}\max(m_L)$ such that significant hierarchies between entries of $m_L$ do not occur. In this way the entries of $m_D^\nu$ will act as the most significant sources of flavour symmetry breaking in analogy with MFV and minimal MLFV.

We fit active-neutrino data by fixing the Dirac mass matrix $m_D^\nu$ with an approximate[9] Casas-Ibarra parameterisation [131] which for the ISS is

$$m_D^\nu = m_R \, U_{\text{PMNS}} \, \hat{m}_\nu^{1/2} \, R \, \mu_{\text{eff}}^{-1/2}, \tag{3.57}$$

where we define an effective mass

$$\mu_{\text{eff}} = f(m_R) \left( \frac{m_R}{m_W} \right)^2 \mu_N + \mu_S. \tag{3.58}$$

which is slightly different to the Casas-Ibarra parameterisation of Chapter 2 given in Eq. (2.26) due to the inclusion of non-zero entries in $\mu_N$. For the LSS,

$$m_D^\nu = -m_R \, U \hat{m}_\nu^{1/2} \, C \, \hat{m}_\nu^{1/2} \, U_{\text{PMNS}}^T \, (m_L^{\text{eff}})^{T-1} \tag{3.59}$$

with an equivalently defined effective mass

$$m_L^{\text{eff}} = \left( f(m_R) \left( \frac{m_R}{m_W} \right)^2 - 1 \right) m_L. \tag{3.60}$$

The matrix $R$ is a complex-orthogonal matrix $R\,R^T = \mathbb{1}_{3\times 3}$ which can be parameterised with three complex mixing angles $\theta_i = \theta_i^{\text{r}} + i\theta_i^{\text{c}}$ where

$$R(\theta_1, \theta_2, \theta_3) = R_{12}(\theta_1) \, R_{13}(\theta_2) \, R_{23}(\theta_3),$$

[9] The parameterisation is only approximate as we ignore the corrections to the mass terms e.g. $\tilde{\mu}_i = \mu_i + \delta\mu_i$ generated through spurion insertions when solving for $m_D^\nu$. This approximation is valid in the regime where $\delta\mu_i < \mu_i$. We additionally check that once these corrections are included the active-neutrino mass differences are not spoiled.

$$R_{12}(\theta_1) = \begin{pmatrix} \mathrm{c}_{\theta_1} & -\mathrm{s}_{\theta_1} & 0 \\ \mathrm{s}_{\theta_1} & \mathrm{c}_{\theta_1} & 0 \\ 0 & 0 & 1 \end{pmatrix}, \; R_{13}(\theta_2) = \begin{pmatrix} \mathrm{c}_{\theta_2} & 0 & -\mathrm{s}_{\theta_2} \\ 0 & 1 & 0 \\ \mathrm{s}_{\theta_2} & 0 & \mathrm{c}_{\theta_2} \end{pmatrix}, \; R_{23}(\theta_3) = \begin{pmatrix} 1 & 0 & 0 \\ 0 & \mathrm{c}_{\theta_3} & -\mathrm{s}_{\theta_3} \\ 0 & \mathrm{s}_{\theta_3} & \mathrm{c}_{\theta_3} \end{pmatrix}. \tag{3.61}$$

In order to reduce the number of free parameters we fix the real components of the mixing angles to

$$\theta_1^{\mathrm{r}} = \frac{\pi}{5},\; \theta_2^{\mathrm{r}} = \frac{5\pi}{6},\; \theta_3^{\mathrm{r}} = \frac{4\pi}{7} \tag{3.62}$$

where there is no signficance to the values chosen. From the results of Chapter 2, the asymmetry is not sensitive to the values of the real angles [1] and therefore should apply for any choice of their values. We fix $\theta_1^{\mathrm{c}} = \theta_3^{\mathrm{c}} = 0$ for simplicity and scan over

$$\theta_2^{\mathrm{c}} \quad \sim \quad \mathcal{O}(10^{-3} - 10^{1}). \tag{3.63}$$

By contrast to the complex-orthogonal $R$, the matrix $C$ instead satisfies $C + C^T = \mathbb{1}_{3\times3}$ and therefore must be a combination of a skew-symmetric matrix and a matrix proportional to the identity of the specific form,

$$C = \begin{pmatrix} \frac{1}{2} & a_1 & a_2 \\ -a_1 & \frac{1}{2} & a_3 \\ -a_2 & -a_3 & \frac{1}{2} \end{pmatrix} \tag{3.64}$$

with $a_i = a_i^{\mathrm{r}} + i a_i^{\mathrm{c}}$ where we choose to fix

$$a_1^{\mathrm{r}} = \frac{1}{10},\; a_2^{\mathrm{r}} = \frac{2}{10},\; a_3^{\mathrm{r}} = \frac{1}{2},\; a_1^{\mathrm{c}} = a_3^{\mathrm{c}} = 0 \tag{3.65}$$

and scan over

$$a_2^{\mathrm{c}} \sim \mathcal{O}(10^{-3} - 10^{1}). \tag{3.66}$$

The active-neutrino masses

$$\hat{m}_\nu = \mathrm{diag}(m_{\nu_1}, m_{\nu_2}, m_{\nu_3}) = U_{\mathrm{PMNS}}^{\dagger}(m_\nu^{\mathrm{tree}} + m_\nu^{\text{1-loop}})U_{\mathrm{PMNS}}^{*} \tag{3.67}$$

are inputs for Eqs. (3.57) and (3.59) where for simplicity we assume normal ordering which is currently favoured over inverted ordering [192], implying

$$\begin{aligned} m_{\nu_2} &= \sqrt{m_{\nu_1}^2 + \Delta m_{21}^2} \\ m_{\nu_3} &= \sqrt{m_{\nu_1}^2 + \Delta m_{21}^2 + \Delta m_{31}^2} \end{aligned} \tag{3.68}$$

and unless stated otherwise we fix the lightest neutrino mass $m_{\nu_1}$ to 0.01 eV. Other active neutrino parameters are fixed to their current best fit values [192] and listed in Table 1.3 but the Dirac phase has been fixed to be maximally CP-violating.

We work in the perturbative regime of the Yukawa couplings generated by the Casas-Ibarra parameterisations such that $|\mathcal{Y}_{ij}|^2 \lesssim 4\pi$, which prevents very large choices for the complex parameters. We fix the unknown Wilson coefficients $s_i$ and $n_i$ to $\frac{1}{16\pi^2}$ for definiteness unless stated otherwise.

To check our numerical solutions to the Boltzmann equations, we compare the results to a known approximate analytic expression of the baryon asymmetry that is valid in the strong washout regime ($K_{\text{eff}}^\alpha \geq 5$) [139, 140], where

$$\begin{gathered} K_{\text{eff}}^\alpha = \kappa^\alpha \textstyle\sum_i K_i B_i^\alpha, \\ \kappa^\alpha = 2\sum_{i,j} \frac{\left(\mathbf{h}_{\alpha i}^* \mathbf{h}_{\alpha j} + \mathbf{h}_{\alpha i}^{\mathbf{c}*} \mathbf{h}_{\alpha j}^{\mathbf{c}}\right)\left[\left(\mathbf{h}^\dagger \mathbf{h}\right)_{ij} + \left(\mathbf{h}^{\mathbf{c}\dagger} \mathbf{h}^{\mathbf{c}}\right)_{ij}\right] + \left(\mathbf{h}_{\alpha i}^* \mathbf{h}_{\alpha j} - \mathbf{h}_{\alpha i}^{\mathbf{c}*} \mathbf{h}_{\alpha j}^{\mathbf{c}}\right)^2}{\left[\left(\mathbf{h}\mathbf{h}^\dagger\right)_{\alpha\alpha} + \left(\mathbf{h}^{\mathbf{c}} \mathbf{h}^{\mathbf{c}\dagger}\right)_{\alpha\alpha}\right]\left[\left(\mathbf{h}^\dagger \mathbf{h}\right)_{ii} + \left(\mathbf{h}^{\mathbf{c}\dagger} \mathbf{h}^{\mathbf{c}}\right)_{ii} + \left(\mathbf{h}^\dagger \mathbf{h}\right)_{jj} + \left(\mathbf{h}^{\mathbf{c}\dagger} \mathbf{h}^{\mathbf{c}}\right)_{jj}\right]} \left(1 - 2i\frac{m_{N_i} - m_{N_j}}{\Gamma_i + \Gamma_j}\right)^{-1}, \\ B_i^\alpha = \frac{\Gamma(N_i \to l_\alpha \Phi) + \Gamma\left(N_i \to l_\alpha^c \Phi^\dagger\right)}{\sum_\alpha \left[\Gamma(N_i \to (l_\alpha)^c \Phi) + \Gamma\left(N_i \to (l_\alpha)^c \Phi^\dagger\right)\right]}, \end{gathered} \tag{3.69}$$

with $m_{N_i} = (\hat{M}_\pm)_{ii}$ and $K_i = \Gamma_{N_i}/H(m_N)$ being the naïve washout solely from inverse decays. The inclusion of the scale factor $\kappa^\alpha$ accounts for the numerically significant $2 \leftrightarrow 2$ scattering processes relevant for models with small lepton number violation. The Yukawa couplings $\mathbf{h}$ and $\mathbf{h}^{\mathbf{c}}$ appearing in bold are resummed Yukawa couplings first defined in [84]. They are required to properly account for unstable particle mixing effects amongst the heavy sterile neutrinos. As a consequence of the resummed Yukawa couplings, the scaling parameter $\kappa^\alpha$ is real-valued.

| Example parameters | $\lvert\eta_B\rvert$ | $\lvert\eta_B^{\text{approx.}}\rvert$ |
|---|---|---|
| $m_L \simeq \text{diag}(1.5,\, 2.6,\, 1.2) \times 10^{-3}\,\text{GeV}$<br>$\mu_S = \mu_N = 0$<br>$a_1 = \frac{1}{10}, \quad a_2 \simeq \frac{2}{10} + 0.00028i, \quad a_3 = \frac{5}{10}$ | $1.37 \times 10^{-10}$ | $7.23 \times 10^{-10}$ |
| $m_L \simeq \text{diag}(0.70,\, 1.33,\, 1.26) \times 10^{-5}\,\text{GeV}$<br>$\mu_S = \mu_N = 0$<br>$a_1 = \frac{1}{10}, \quad a_2 \simeq \frac{2}{10} + 2.06i, \quad a_3 = \frac{5}{10}$ | $1.98 \times 10^{-11}$ | $2.31 \times 10^{-11}$ |
| $m_L = 0$<br>$\mu_S \simeq 9 \times 10^{-11}\,\text{GeV}, \;\; \mu_{\text{N}} \simeq 225\,\text{GeV}$<br>$\theta_1 = \frac{\pi}{5}, \quad \theta_2 \simeq \frac{5\pi}{6} + 0.094i, \quad \theta_3 = \frac{4\pi}{7}$ | $2.57 \times 10^{-11}$ | $1.21 \times 10^{-11}$ |
| $m_L = 0$<br>$\mu_S \simeq 1\,\text{GeV}, \;\; \mu_{\text{N}} \simeq 414\,\text{GeV}$<br>$\theta_1 = \frac{\pi}{5}, \quad \theta_2 \simeq \frac{5\pi}{6} + 0.16i, \quad \theta_3 = \frac{4\pi}{7}$ | $1.71 \times 10^{-10}$ | $5.75 \times 10^{-11}$ |

TABLE 3.5: Comparison between the numerically computed asymmetry $|\eta_B|$ and the analytic approximation $|\eta_B^{\text{approx.}}|$ from Eq. (3.70) for example points of the LSS (top two) and ISS (bottom two). All points include all relevant radiative corrections as defined in Eq. (3.49) where for these example parameters we have set all Wilson coefficients at lowest order to $1/16\pi^2$.

The asymmetry is then well approximated by

$$\eta_B^{\text{approx.}} \simeq -\frac{28}{51}\frac{1}{27}\frac{3}{2}\sum_{\alpha,i}\frac{\varepsilon_i^\alpha}{K_{\text{eff}}^\alpha \min[\text{z}_\text{c}, 1.25\ln(25\text{K}_{\text{eff}}^\alpha)]} \tag{3.70}$$

where $z_c = m_N/T_c$ is related to the critical temperature of the electroweak phase transition. The numerical versus analytic approximation comparison illustrated in Table 3.5 provides strong evidence that our numerical routines are accurate.

Finally, the small mass differences between the heavy sterile states generating the resonant enhancement could also lead to coherent oscillations between the SNs. The dynamics of the coherent oscillations will alter the evolution of the lepton asymmetry and could potentially significantly impact the net asymmetry generated for some region of parameter space. To properly account for their effects would require a flavour-covariant set of transport equations, as opposed to the semi-classical Boltzmann equations we employ. We will therefore estimate the impact of coherent sterile neutrino oscillations on the final baryon asymmetry by employing an analytic estimate derived specifically for resonant scenarios of leptogenesis [136],

$$\eta_B^{\rm osc} \simeq -\frac{28}{51}\frac{1}{27}\frac{3}{2}\sum_{\alpha,i\neq j}\frac{1}{z_c}\frac{1}{K_{\ell\ell}}(\mathcal{A}^\alpha_{ij}\sqrt{x_{ij}}+\mathcal{B}^\alpha_{ij})\frac{2(m_i^2-m_j^2)m_N\Gamma_N}{(m_i^2-m_j^2)^2+\frac{4m_N^2\Gamma_N^2\det\left[\mathfrak{Re}\left\{\mathbf{h}^\dagger\mathbf{h}\right\}\right]}{(h^\dagger h)_{ii}(h^\dagger h)_{jj}}}, \quad (3.71)$$

where $K_{\ell\ell} = (m_N(hh^\dagger)_{\ell\ell})/(8\pi H(z=1))$ and $\Gamma_N$ is the average of the sterile neutrino decay widths. Equation 3.71 has a similar behaviour to the asymmetry due to standard mixing effects given in Eqs. (3.43) and (3.48). In particular, the appearance of $(\mathcal{A}^\alpha_{ij}\sqrt{x_{ij}}+\mathcal{B}^\alpha_{ij})$ in both expressions implies that the sign of the asymmetries generated by both of these processes are the same. Therefore for the resonant scenario the effect of including oscillations will only increase the overall asymmetry. The masses of the heavy SNs being larger than the electroweak-phase transition temperature, in combination with the strong washout nature of the parameter space we consider, prevents a 'freeze-in' scenario due to oscillations, as in traditional ARS leptogenesis [99]. Therefore the asymmetry generated from coherent oscillations should be independent of the initial conditions of the heavy SNs.

### 3.4.1 Inverse seesaw (ISS)

For the ISS ($\mathcal{Y}_L = 0$,) the only LNV parameters present are the two small Majorana masses

$$M_\nu = \begin{pmatrix} m_\nu^{\text{1-loop}} & m_D^\nu & 0 \\ (m_D^\nu)^T & \mu_N & M_R \\ 0 & M_R^T & \mu_S \end{pmatrix}. \quad (3.72)$$

From Eq. (3.49) only $\mu_N$ receives radiative corrections from $SO(3)_{N_R}$ breaking terms proportional to the Yukawa spurion $\mathcal{Y}_D^\nu$.

We separately consider three scenarios for the ISS: first where no corrections are introduced, second where corrections are introduced at the next lowest order, labelled $\mathcal{N}_1$ and, third, corrections up to next-to-leading order, labelled $\mathcal{N}_2$:

$$\tilde{\mu}_N = \mu_N\left(\mathbb{1}_{3\times 3}+\mathcal{N}_1+\mathcal{N}_2\right) \quad (3.73)$$

where

$$\begin{aligned}
\mathcal{N}_1 &= n_1 \left( (\mathcal{Y}_D^\nu)^\dagger \mathcal{Y}_D^\nu + ((\mathcal{Y}_D^\nu)^\dagger \mathcal{Y}_D^\nu)^T \right), \\
\mathcal{N}_2 &= n_2^{(1)} \left( (\mathcal{Y}_D^\nu)^\dagger \mathcal{Y}_D^\nu (\mathcal{Y}_D^\nu)^\dagger \mathcal{Y}_D^\nu + ((\mathcal{Y}_D^\nu)^\dagger \mathcal{Y}_D^\nu (\mathcal{Y}_D^\nu)^\dagger \mathcal{Y}_D^\nu)^T \right) + n_2^{(2)} \left( (\mathcal{Y}_D^\nu)^\dagger \mathcal{Y}_D^\nu ((\mathcal{Y}_D^\nu)^\dagger \mathcal{Y}_D^\nu)^T \right) \\
&\quad + n_2^{(3)} \left( ((\mathcal{Y}_D^\nu)^\dagger \mathcal{Y}_D^\nu)^T (\mathcal{Y}_D^\nu)^\dagger \mathcal{Y}_D^\nu \right) + n_2^{(4)} \left( (\mathcal{Y}_D^\nu)^\dagger \mathcal{Y}_e \mathcal{Y}_e^\dagger \mathcal{Y}_D^\nu + ((\mathcal{Y}_D^\nu)^\dagger \mathcal{Y}_e \mathcal{Y}_e^\dagger \mathcal{Y}_D^\nu)^T \right)
\end{aligned} \tag{3.74}$$

and we fix $n_2^{(i)} = (n_1)^2$ for computational convenience. Due to the perturbative regime in which we operate, it will always be the case that $||\mathcal{N}_i|| \ll 1$. All terms are formally flavour invariant and serve to break the flavour degeneracy amongst the heavy SNs when these spurions acquire non-zero vevs.

For the ISS as $m_L = 0_{3\times3}$ the combination in Eq. (3.39) simplifies to

$$h^\dagger h \simeq \frac{2}{v_{EW}^2} \begin{pmatrix} \left( \frac{1}{\sqrt{2}} - \frac{1}{4\sqrt{2}} \left( \frac{\mu_S - \mu_N}{2m_R} \right) \right)^2 (m_D^\nu)^\dagger m_D^\nu & -i \left( \frac{1}{2} - \frac{1}{32} \left( \frac{\mu_S - \mu_N}{2m_R} \right)^2 \right) (m_D^\nu)^\dagger m_D^\nu \\ i \left( \frac{1}{2} - \frac{1}{32} \left( \frac{\mu_S - \mu_N}{2m_R} \right)^2 \right) (m_D^\nu)^\dagger m_D^\nu & \left( \frac{1}{\sqrt{2}} + \frac{1}{4\sqrt{2}} \left( \frac{\mu_S - \mu_N}{2m_R} \right) \right)^2 (m_D^\nu) m_D^\nu \end{pmatrix} \tag{3.75}$$

where we are now dealing with unprimed matrices. Due to the fact that $M_R \propto \mu_S \propto \mathbb{1}_{3\times3}$, in the case where only $\mathcal{N}_1$ is included the corrected Majorana mass $\mu_N$ can be diagonalised without affecting the other entries in the $2\times2$ sub-block, with

$$\begin{pmatrix} 0 & m_D^\nu & 0 \\ (m_D^\nu)^T & \mu_N \mathbb{1}_{3\times3} + \delta\mu_N & m_R \mathbb{1}_{3\times3} \\ 0 & m_R \mathbb{1}_{3\times3} & \mu_S \mathbb{1}_{3\times3} \end{pmatrix} \to \begin{pmatrix} 0 & m_D^\nu \mathcal{O} & 0 \\ \mathcal{O}^T (m_D^\nu)^T & \hat{\tilde{\mu}}_N & m_R \mathbb{1}_{3\times3} \\ 0 & m_R \mathbb{1}_{3\times3} & \mu_S \end{pmatrix} \tag{3.76}$$

under the rotation $N_R \to \mathcal{O} N_R$ and $S_L \to \mathcal{O} S_L$. Similarly to the minimal type-I scenario, if only $\mathcal{N}_1$ is included then $\mathfrak{Re}\left\{ (m_D^\nu)^\dagger m_D^\nu \right\} \propto \mathcal{N}_1 = \delta\mu_N$ and the combinations of $(m_D^\nu)^\dagger m_D^\nu$ appearing in Eq. (3.75) will have no real off-diagonal components. We emphasize that this only occurs for the ISS because $m_L = 0_{3\times3}$. Differently to the type-I scenario however the off-diagonal blocks of Eq. (3.75) have an additional complex phase such that the imaginary components[10] of $\mathcal{O}^T (m_D^\nu)^\dagger m_D^\nu \mathcal{O}$ become real off-diagonal entries in $h^\dagger h$. This therefore allows for non-zero generation of lepton asymmetry unlike the type-I scenario.

[10] This is because $\mathcal{O}^T \, \mathfrak{Re}\left\{ (\mathcal{Y}_D^\nu)^\dagger \mathcal{Y}_D^\nu \right\} \mathcal{O} = \mathrm{diag}(\dots)$ due to the form of the corrections but $\mathcal{O}^T \, \mathfrak{Im}\left\{ (\mathcal{Y}_D^\nu)^\dagger \mathcal{Y}_D^\nu \right\} \mathcal{O} \neq \mathrm{diag}(\dots)$ and therefore off-diagonal imaginary components are generated which become real due to the additional phase in Eq. (3.75).

As only the off-diagonal blocks of $h^\dagger h$ contain the necessary terms, only diagrams between two SNs of different mass splittings, i.e. from $\Delta m_{i,j}^{\rm OS}$, will contribute to asymmetry. The real components of the $(1,1)$ and $(2,2)$ blocks are diagonal, on the other hand, meaning that SNs with the same sign mass splitting $\Delta m_{i,j}^{\rm SS}$ will not contribute to $\varepsilon_\alpha^i$. Once $\mathcal{N}_2$ is included however, the flavour mis-alignment between $\delta\mu_N$ and $(m_D^\nu)^\dagger m_D^\nu$ will generate real off-diagonal components in $(m_D^\nu)^\dagger m_D^\nu$ and therefore all four blocks of Eq. (3.75) will contribute to $\varepsilon_\alpha^i$.

In Fig. 3.1 we plot the baryon asymmetry numerically calculated as a function of both $\mu_N$ and $\mu_S$. All three scenarios are simultaneously plotted. Both in the case where radiative effects are ignored as well as when only $\mathcal{N}_1$ is included, similar behaviour occurs. The inclusion of $\mathcal{N}_1$ breaks the mass degeneracy between all six SNs, as opposed to without its inclusion where two groups of identical mass SNs form. However, as discussed above, due to flavour alignment only diagrams involving opposite mass split SNs contribute to the asymmetry. Therefore the mass difference is generated exclusively from

$$\Delta m_{i,j}^{\rm OS} = \left(m_{N_\pm}\right)_i - \left(m_{N_\mp}\right)_j \simeq \mu_N + \mu_S \tag{3.77}$$

with

$$m_{N_\pm} \simeq m_R \pm \frac{1}{2}\mu_N \pm \frac{1}{2}\mu_S. \tag{3.78}$$

While the spurion corrections are present we have $\mu_N \gg \mathcal{N}_1$ and therefore they are not the dominant source for the mass splittings in this situation. In this regime resonant leptogenesis is not feasible [1, 162, 167]. The inclusion of $\mathcal{N}_2$ generates non-zero, off-diagonal entries in the $(1,1)$ and $(2,2)$ entries of Eq. (3.75) such that new contributions turn on arising from the mass splitting

$$\Delta m_{i,j}^{\rm SS} = \left(m_{N_\pm}\right)_i - \left(m_{N_\pm}\right)_j \simeq \mu_N \left((\mathcal{Y}_D^\nu)^\dagger \mathcal{Y}_D^\nu\right)_{ii}. \tag{3.79}$$

We emphasis that even when only $\mathcal{N}_1$ is included, the mass degeneracy between the same sign mass split SNs is still broken $\Delta m_{i,j}^{\rm SS} \neq 0$. No resonant enhancement occurs between two such SNs in this case not because of a mass degeneracy between them (as is the case when no corrections are included) but because of the flavour alignment issue described above.

Figure 3.2 plots the asymmetry when $\mathcal{N}_2$ is included and a clear resonant enhancement

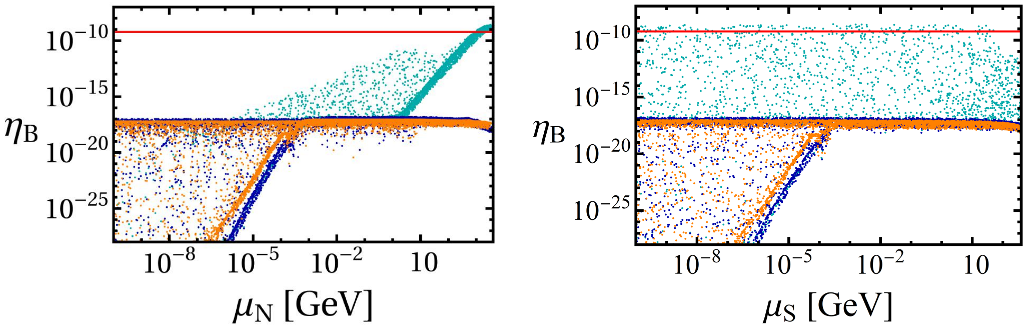


FIGURE 3.1: Plot of the asymmetry generated in the ISS for the individual cases where no radiative corrections are considered (orange), where only $\mathcal{N}_1$ is considered (blue) and when both $\mathcal{N}_1$ and $\mathcal{N}_2$ are included (cyan). This was varied with $\mu_N$ **(left figure)** and $\mu_S$ **(right figure)**. A resonant enhancement in the asymmetry occurs only if the next-to-leading order contributions are included. The red horizontal line indicates the asymmetry required to fit observations.

occurs for large values of $\mu_N$. While the mass splitting is proportional to the decay width, it is also scaled by the Majorana mass $\mu_N$. For small LNV the mass splitting will be much less than the decay width but for large values

$$\mu_N \left( (\mathcal{Y}_D^\nu)^\dagger \mathcal{Y}_D^\nu \right)_{ii} \to \frac{m_{N_i}}{8\pi} \left( (\mathcal{Y}_D^\nu)^\dagger \mathcal{Y}_D^\nu \right)_{ii} \simeq \Gamma_i \tag{3.80}$$

forcing a resonant enhancement to occur. In Fig. 3.2 we distinguish between two different hierarchical cases for the Majorana masses: $\mu_N > \mu_S$ in purple and $\mu_S > \mu_N$ in green. The asymmetry in the resonant regime is independent of $\mu_S$ as in our setup this mass does not receive any radiative corrections. If a stricter setup was considered such that it did receive corrections (if, for example, we took an $SO(3)_{N_R} \otimes SO(3)_{S_L} \to SO(3)_{N_R+S_L}$ flavour symmetry) $\mu_S$ would require equivalently large masses in order to be placed in the required resonant regime. However, such large values of $\mu_S$ are outside the regime of validity required for the ISS and would spoil the guarantee of the parametrisation in Eq. (3.57) to generate the required active neutrino masses. This follows as unlike $\mu_N$, $\mu_S$ does not have a loop suppressed contribution to the active neutrino masses. Therefore we find that $\mu_S$ cannot contribute to the resonance required for MLFV-ISS.

Additionally, the effects of coherent oscillations are estimated (in orange) in the bottom plot of Fig. 3.2, where $\mathcal{N}_2$ is included specifically for the regime $\mu_N > \mu_S$ required for successful resonant leptogenesis. Here we find, for the resonant region of parameter space, that the effects of coherent oscillations are roughly three orders of magnitude smaller than that of standard thermal decay. For similar reasons as presented above for

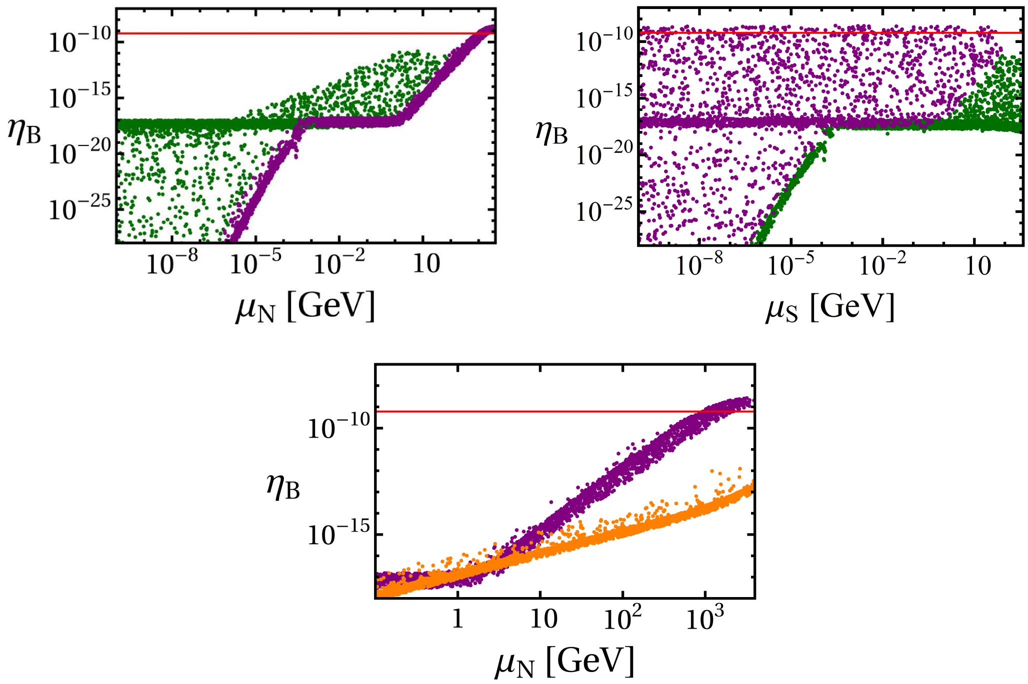


FIGURE 3.2: Plot of the asymmetry generated in the ISS when both $\mathcal{N}_1$ and $\mathcal{N}_2$ are included, as a function of $\mu_N$ **(top-left figure)** and $\mu_S$ **(top-right figure)**. Points in purple correspond to the regime where $\mu_N > \mu_S$, while points in green to $\mu_S > \mu_N$. A resonant enhancement of sufficient size is generated for *large* values of $\mu_N$ as long as the hierarchy $\mu_N > \mu_S$ is satisfied. In order to match active neutrino data, $\mu_S$ which generates a tree-level contribution must be less than $\sim$ 100 GeV, whereas $\mu_N$, which generates it at loop level, is allowed to be larger. The **bottom** figure compares the asymmetry generated from standard decay to oscillations (in orange) in the relevant regime $\mu_N > \mu_S$. While for some region of parameter space the two processes are of similar order, in the resonant regime the asymmetry due to oscillations is roughly three orders of magnitude smaller and is therefore a sub-dominant effect.

resonant leptogenesis, without the inclusion of the second order spurion corrections $\mathcal{N}_2$, the asymmetry generated by coherent oscillations is highly suppressed due to the same flavour related cancellation effects. This is evident as the Yukawa structure of Eq. (3.71) is the same as Eq. (3.43) and therefore the same arguments apply.

Summarising, we find two criteria for successful MLFV-ISS resonant leptogenesis: (1) large values of the Majorana mass $\mu_N$ such that the mass splittings between SNs of different generations moves on resonance in a region of relatively low strong washout, and (2) the inclusion of spurion effects up to lext-to-leading order in order to break flavour alignment and prevent only opposite mass splitting SNs, that is pairs of SNs with mass differences generated by the LNV parameters $\mu_N$ and $\mu_S$, from contributing to the asymmetry. This is illustrated in Fig. 3.3 where the decay width and the mass splittings are plotted with the spurion corrections included. For large values of $\mu_N$ the

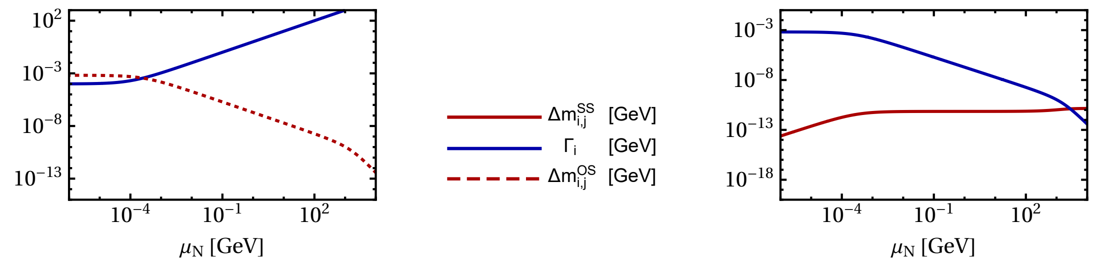


FIGURE 3.3: Plot of the decay width $\Gamma_i \simeq \frac{m_i}{8\pi}\sum_l h^*_{li}h_{li}$ (blue) along with the mass splitting $\Delta m_{i,j}$ (red) as a function of $\mu_N$ for $\mu_S = 10^{-4}$ GeV and all radiative effects included. Here the mass splitting among opposite splitting SNs $\Delta m^{\rm OS}_{i,j}$ **(left)** is compared to those with same sign splitting $\Delta m^{\rm SS}_{i,j}$ **(right)** as defined in Eqs. (3.40) and (3.41). While in both plots a region of resonance occurs, in the case on the left it occurs in a region of extremely strong washout c.f. Fig. 3.5. The inclusion of radiative effects allows for a resonance to occur between SNs with same-sign mass splittings in a region of minimised washout such that asymmetry generation can occur. In this region heavy SNs of opposite sign mass splitting grow in mass difference and their contribution becomes irrelevant.

opposite mass splitting SNs move further away from resonance whilst the same sign mass splitting SNs move onto resonance. This effect occurs both with $\mathcal{N}_1$ and $\mathcal{N}_2$ but, as discussed above, if only $\mathcal{N}_1$ is included then same sign mass splitting SNs combinations do not generate any flavoured asymmetry.

These conclusions were drawn for fixed values of certain parameters. Most importantly the Wilson coefficients were fixed such that $c_1 = 1/16\pi^2$, which we chose under the assumption that the high-scale dynamics arise from radiative effects. Increasing the size of the Wilson coefficients will increase the overall size of $\mathcal{N}_2$ from Eq. (3.74), allowing for smaller values of $\mu_N$ by one or two orders of magnitude. Similarly, we fixed the lightest neutrino mass $m_{\nu_1}$ in our scans. Smaller values of the lightest neutrino mass will increase the hierarchy within $(m^\nu_D)^\dagger m^\nu_D$, which impacts the level of resonance through Eq. (3.57). To illustrate this behaviour, in Fig. 3.4 the asymmetry is plotted as a function of these two parameters where we have fixed all other parameters to a benchmark point within the resonant region. From this figure we conclude that there is a preference for smaller values of neutrino mass $m_{\nu_1} \ll 0.1$ eV and if larger values of the Wilson coefficients were allowed, a larger region of parameter space would go on resonance.

Asymmetry generation is sufficient for large Majorana masses not simply because of the enhancement in the mass splitting. Due to the relationship between the Yukawa couplings required to satisfy active neutrino mixing data and the input parameters from Eq. (3.57), larger values of the Majorana masses (for fixed sterile Dirac mass $m_R$) results in a overall

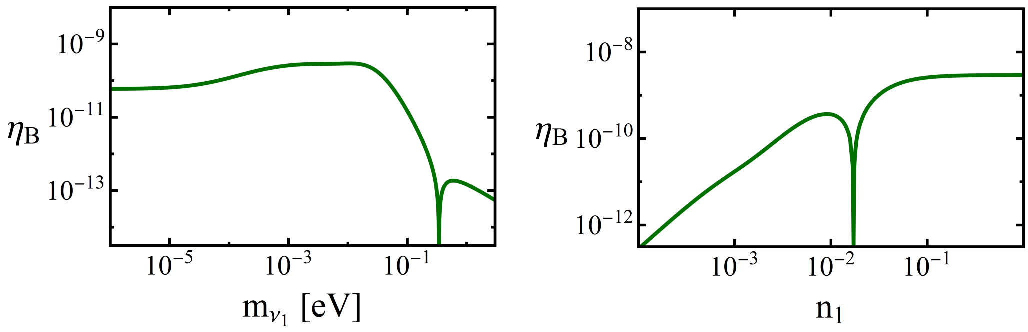


FIGURE 3.4: Variation in the baryon asymmetry as a function of the lightest active neutrino mass $m_{\nu_1}$ **(left)** and varying the Wilson coefficient $n_1$ **(right)** for the case where all radiative spurion effects are included. In this scan we fixed $\theta_2^c = 0.7$, $\mu_S \simeq 10^{-1}$ GeV and $\mu_N \simeq 900$ GeV and in the left plot set $n_1 = 1/16\pi^2$ and $m_{\nu_1} = 0.01$ eV in the right plot. As the lightest neutrino mass is reduced (becomes hierarchical) the asymmetry freezes out. There is a slight preference for light neutrino masses of $\mathcal{O}(10^{-3} - 10^{-2})$ eV. Larger values for $m_{\nu_1}$ lead to a degeneracy amongst the light neutrino masses and decreases the mass splitting generated by the inclusion of $\mathcal{N}_i$ decreasing the resonant enhancement. Increasing the size of the Wilson coefficient allows the mass splitting to be closer to resonance allowing for one or two orders of magnitude increased asymmetry.

decrease in the size of the Yukawa couplings required to generate the same light neutrino masses. This leads to less efficient washout of any generated asymmetry. Figure 3.5 plots the washout as a function of the effective Majorana mass $\mu_{\text{eff}}$ which for the hierarchy $\mu_N > \mu_S$ simplifies to $\mu_{\text{eff}} \simeq \mu_N$. Both the naïve washout $K_\alpha \propto \Gamma_i m_i/\text{H}(m_i)$ and the effective washout $K_\alpha^{\text{eff}}$ defined in Eq. (3.69) (and relevant for scenarios with *small* LN violating parameters [134, 139, 140] due to the sensitivity to $2 \leftrightarrow 2$ scatterings) are plotted together.

While the naïve washout overestimates the efficiency of washout, it is clear that for large values of the LNV parameters palatable values of washout (albeit still very much in the strong washout regime) of $\mathcal{O}(10^3)$ or below are possible and therefore resonant leptogenesis is roughly feasible in this specific region albeit only in a narrow window. Small values of $\mu_N$ may allow the effective washout to become weak however, as discussed in Chapter 2, asymmetry generation is suppressed in this region compared to the region with strong effective washout. The numerically computed effective washout in Fig. 3.5 has consistent behaviour with the one-generational analytic estimate from Chapter 2 in Eq. (2.87) and Fig. 2.5.

Figures. 3.6 and 3.7 plot the CP-asymmetry parameter to a specific lepton flavour[11] $\alpha$

[11] Due to the anarchic nature of our scenario there is no preference for a specific lepton flavour.

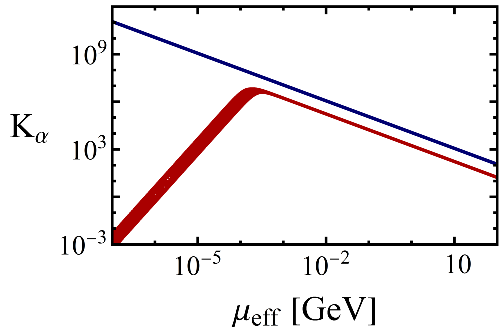


FIGURE 3.5: Plot of the washout as a function of $\mu_{\text{eff}}$. In blue the naïve washout is plotted while in red the effective washout which is defined in Eq. (3.69) relevant for situations with approximate lepton number conservation. As can be seen, naïvely the washout is overestimated. For the hierarchy $\mu_N > \mu_S$, relevant for leptogenesis, $\mu_{\text{eff}} \simeq \mu_N$ and therefore the washout in the theory is dictated by the size of $\mu_N$. In regions of large $\mu_N$ the effective washout is low enough (but still within the strong regime) for resonant leptogenesis to be feasible. For small values of $\mu_N$ the effective washout may be weak, however asymmetry generation is suppressed in this region as discussed in Chapter 2.

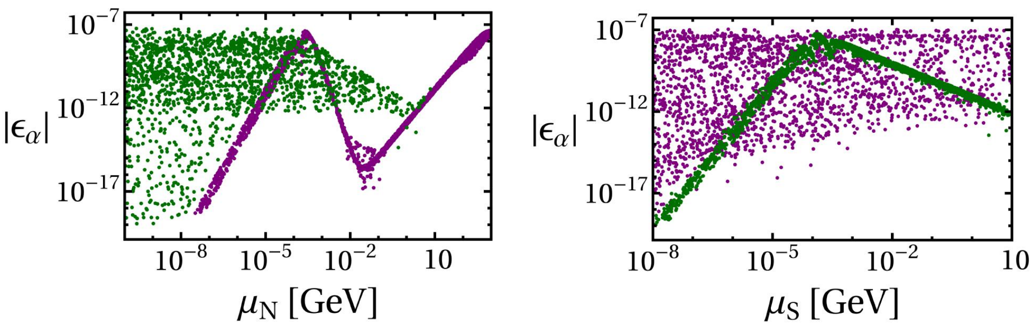


FIGURE 3.6: Plot of the CP asymmetry into a specific flavour $\epsilon_\alpha = \sum_i \epsilon_\alpha^i$ generated in the ISS when both $\mathcal{N}_1$ and $\mathcal{N}_2$ are included, as a function of $\mu_N$ **(left figure)** and $\mu_S$ **(right figure)**. Points in purple correspond to the regime where $\mu_N > \mu_S$, while points in green to $\mu_S > \mu_N$. At around $10^{-4}$ GeV a natural resonance occurs generated by $\Delta m_{i,j}^{\text{OS}}$ in agreement with [1]. Once radiative effects are included an additional resonance occurs for large values of $\mu_N$ and in the regime $\mu_N > \mu_S$.

as a function of the Majorana masses. A 'natural' resonance occurs in the region of $\mu_i \simeq 10^{-4}$ GeV induced by $\Delta m_{i,j}^{\text{OS}}$ independent of the radiative spurion contributions, in agreement with [1] and the results of the preceding chapter. However, this region is accompanied by a much larger effective washout and cannot accommodate sufficient asymmetry generation. In contrast only when both $\mathcal{N}_1$ and $\mathcal{N}_2$ are included does a clear second resonance peak form for large values of $\mu_N$. Larger values of $\mu_N$ would cause $\mu_{\text{eff}} \gg M_R$ and the approximations involved in deriving Eq. (3.50) and (3.57) would break down.

Finally in Fig. 3.8 the asymmetry is varied against the complex angle $\theta_2^c$ for all three

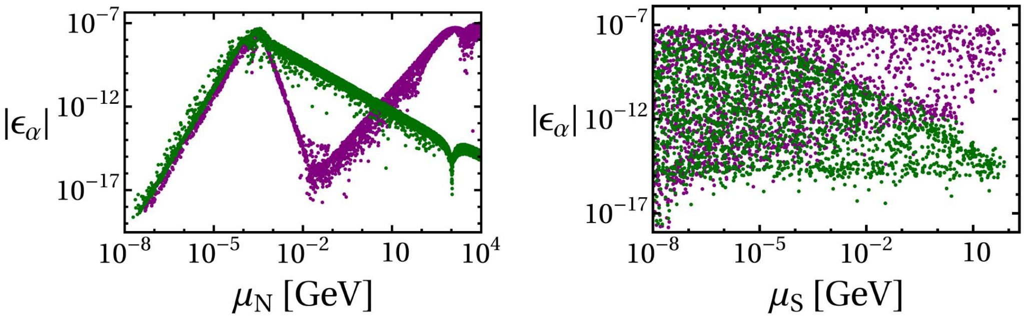


FIGURE 3.7: Plot of the CP asymmetry into a specific flavour $\epsilon_\alpha = \sum_i \epsilon_\alpha^i$ generated in the ISS with no radiative effects included (green) and with $\mathcal{N}_1$ and $\mathcal{N}_2$ included (purple). This is varied with $\mu_N$ **(left figure)** and $\mu_S$ **(right figure)**. A resonant enhancement in the asymmetry occurs only if the next-to-leading order contributions are included.

scenarios for a fixed benchmark point on resonance. In the case where no radiative effects are included, there is a slight dependence on the size of $\theta_2^c$ which can vary the asymmetry generated by one or two orders of magnitude. For small values of $\theta_2^c$ the asymmetry is generated by the CP-violating phase $\delta_{CP}$ within the low-energy mixing matrix. Similar behaviour occurs when $\mathcal{N}_2$ is included, with an overall preference for the range $0.1 < \theta_2^c < 1$. In the case where only $\mathcal{N}_1$ is included, we confirm its strong dependence on the angle $\theta_2^c$ similarly to the type-I scenario [174]. However, we note that in our case the asymmetry is not zero exactly unless $\theta_2^c = 0$. Asymmetry generation can only occur for non-zero values of $\theta_2^c$ independent of any low-energy CP violating phases as phases from $U_{\mathrm{PMNS}}$ cancel in the term $(m_D^\nu)^\dagger m_D^\nu$ in combination with the flavour alignment described above. Leptogenesis is viable both through the Dirac phase as well as high scale CPV but we note that within MLFV-ISS the region in which it is possible is very narrow.

### 3.4.2 $\ell_i \to \ell_j\gamma$ and MLFV-ISS

Here we briefly discuss the consequences of MLFV-ISS on low-energy cLFV processes, specifically the impact that the introduction of CPV has on predictions for $\ell_i \to \ell_j\gamma$. We also assess whether a future measurement of the region important for resonant leptogenesis will be possible. Similar to the MFV hypothesis of the quark sector, models of MLFV predict relationships between the rates for different charged lepton flavour decays.

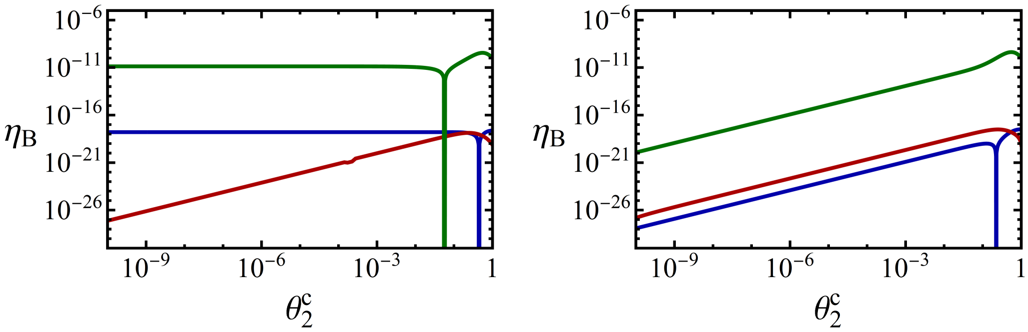


FIGURE 3.8: Plot of the baryon asymmetry as a function of the complex angle $\theta_2^c$ for $\delta_{CP} = 3\pi/2$ **(left)** and $\delta_{CP} = 0$ **(right)**. Here we have fixed $\mu_N \simeq 950$ GeV and $\mu_S \simeq 10$ GeV to be on resonance. In blue no radiative effects are included, in red only to leading order and in green next-to-leading order effects are included. The behaviour of the asymmetry as a function of the complex angle is clear. At small values it freezes out to that provided by the Dirac phase $\delta_{CP}$ however if only the leading radiative effects are included (red), the asymmetry tends to zero with decreasing $\theta_2^c$ even for non-zero $\delta_{CP}$. This effect is similar to what occurs in the type-I MLFV scenario [174, 176, 198]. Asymmetry generation is possible both with low-energy phases as well as complex entries of the $R$ matrix where we loosely find the criterion $0.1 \lesssim \theta_2^c \lesssim 1$ for sufficient asymmetry generation when $\delta_{CP} = 0$.

In the SM effective field theory framework the process $\ell_i \to \ell_j\gamma$ arises from dimension six effective operators that contain $\left(\bar{\ell}\,\Gamma\, e_R\right)$ [168, 169, 197] where family indices have been suppressed. These operators are not invariant under the flavour symmetry defined for MLFV in Eq. (3.19). Insertion of spurion combinations transforming as $\mathbf{(3,\, \bar{3},\, 1,\, 1)}$ make these terms formally invariant. At lowest order this is simply the spurion $\mathcal{Y}_e$. However, as we work in a basis where this matrix is diagonal, it does not contribute to flavour-violating processes. The lowest order spurion combination that makes the relevant operators flavour invariant and contains non-diagonal entries is $\Delta\mathcal{Y}_e$, where

$$\Delta = \mathcal{Y}_D^\nu(\mathcal{Y}_D^\nu)^\dagger. \tag{3.81}$$

The combination transforms as $\left(\Delta\mathcal{Y}_e\right) \to \mathcal{U}_{\ell_L}\left(\Delta\mathcal{Y}_e\right)\mathcal{U}_{e_R}^\dagger$ as required.

A simple expression for the branching ratio is obtained [168] in the limit $m_{\ell_j} \ll m_{\ell_i}$,

$$B_{\ell_i\to\ell_j\gamma} = 384\pi^2 e^2 \frac{v_{EW}^4}{4\Lambda_{\mathrm{LFV}}^4}\left|\Delta_{ij}\right|^2\left|C\right|^2 \tag{3.82}$$

where $C$ accounts for a combination of Wilson coefficients of the relevant operators. As is conventional when considering cLFV in MLFV, we set $|C|^2 = 1$. Note that in a specific UV-complete model based on MLFV, these parameters will be fixed by the high-scale dynamics and may have a different magnitude.

In Eq. (3.81) the only parameter which carries family indices is the spurion combination $\Delta_{ij}$. Therefore useful predictive parameters for MLFV are ratios of branching ratios for different lepton flavour decays,

$$R_{(i,j)[k,l]} \equiv \frac{B_{\ell_i \to \ell_j \gamma}}{B_{\ell_k \to \ell_l \gamma}} = \frac{|\Delta_{ij}|^2}{|\Delta_{kl}|^2}. \tag{3.83}$$

In these ratios, the unknown scale of LFV ($\Lambda_{\mathrm{LFV}}$) cancels out. While it can be identified with $M_R$ in the ISS model, it is also possible that it could arise as the result of some unknown dynamics not directly related to the seesaw mechanism.

Many detailed explorations of cLFV in MLFV have been made for the minimal type-I seesaw scenario [168, 169, 175, 197, 199], the results of which should also hold in the ISS. Here we briefly consider the impact of the complex angle $\theta_2^c$ and the Dirac phase $\delta_{CP}$ on the predictions for specific ratios of cLFV observables. In particular we compare the CP-conserving scenario (assumed in the simplest version of MLFV) with the CP-violating scenario and the size of deviation their inclusion introduces. As we have demonstrated that leptogenesis is viable with both the low-energy phase $\delta_{CP}$ and with the inclusion of the CP-violating angle $\theta_2^c$, we analyse the two limiting cases where CPV arises solely from one of these angles.

Figure 3.9 plots three ratios of cLFV observables as a function of the lightest neutrino mass $m_{\nu_1}$ for $\theta_2^c = 0$ while varying $\delta_{CP}$. The red and orange lines correspond to the CP-conserving scenarios $\delta_{CP} = \{0, 2\pi\}$ or $\pi$, which allows for full reconstruction of $\mathcal{Y}_D^\nu$ from low energy observables. The blue shaded region corresponds to all other values of $\delta_{CP}$ where the green line specifically corresponds to the maximally CP-violating cases $\delta_{CP} = \pi/2$ or $3\pi/2$. The inclusion of CP-violating phases does not spoil the generic MLFV prediction that $R_{(\mu,e)[\tau,\mu]} \ll 1$ and $R_{(\tau,e)[\tau,\mu]} \ll 1$ in both the hierarchical and degenerate scenarios for the light neutrinos. A more potentially measurable effect occurs for the ratio $R_{(\mu,e)[\tau,e]}$, specifically for a hierarchical spectrum of light neutrinos. The CP-conserving case predicts either $R_{(\mu,e)[\tau,e]} > 1$ or $R_{(\mu,e)[\tau,e]} < 1$ depending on the choice of $\delta_{CP}$, while the maximally CP-violating scenario predicts $R_{(\mu,e)[\tau,e]} \simeq 1$.

Similar plots are presented in Fig. 3.10 where we plot the ratios as a function of the lightest neutrino mass $m_{\nu_1}$ for $\delta_{CP} = 0$ and varying $\theta_2^c$. Once again a hierarchical

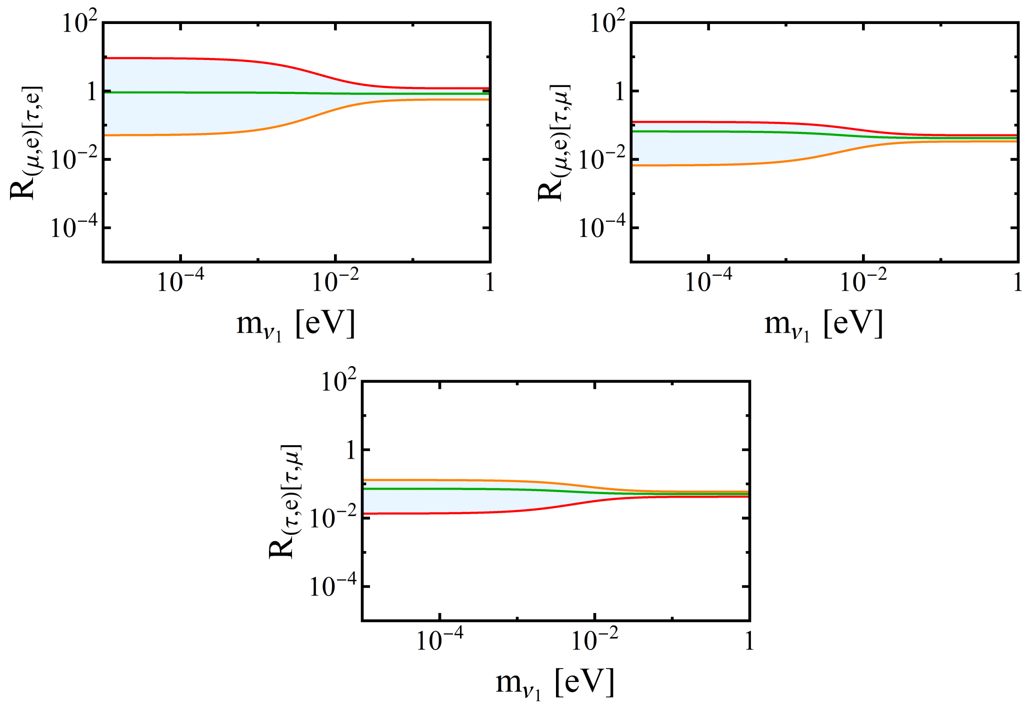


FIGURE 3.9: Plot of the ratios $R_{(i,j)[k,l]}$ for various combinations of flavour initial and final states as a function of the lightest neutrino mass $m_{\nu_1}$. Here the complex angle $\theta_2^c$ has been switched off but the low-energy phase $\delta_{CP}$ is varied. Lines in red and orange correspond to the CP-conserving cases $\delta_{CP} = \{0, 2\pi\}$ and $\delta_{CP} = \pi$ respectively. In green is the maximally violating case of $\delta_{CP} = \pi/2$ or $\delta_{CP} = 3\pi/2$. The shaded blue region corresponds to $\delta_{CP} = (0, 2\pi)\backslash\{\pi/2, \pi, 3\pi/2\}$. All results are in full agreement with [169] for the CP-conserving cases.

spectrum of light neutrinos is required in order for CP-violating phases to have their most significant effect. The inclusion of $\theta_2^c$ does not spoil the generic predictions from the CP-conserving cases presented in Fig. 3.9, however it is clear in the case of $R_{(\mu,e)[\tau,e]}$ and $R_{(\tau,e)[\tau,\mu]}$ that the inclusion of CP-violation (CP-conservation) moves the ratios closer (further) from one. Therefore future measurement of this ratio could constrain scenarios of MLFV that include CP violation.

Finally in Fig. 3.11 the branching ratio $\mathrm{BR}(\mu \to e\gamma)$ is plotted as a function of the LNV parameter $\mu_N$. Here the cases where no CPV is present is distinguished from the cases where CPV arises from the low-energy observable $\delta_{CP}$ and from the complex angle $\theta_2^c$. The LFV scale has been fixed to $\Lambda_{\rm LFV} = M_R = 1$ TeV and the LNV parameter $\mu_S$ has been fixed to the values described in the figure caption. The horizontal dotted (solid) red line corresponds to the current (future) sensitivity of MEG (MEG-II) [148, 150] for this decay process. Currently, MLFV-ISS has been excluded for very low values of $\mu_N$ and $\mu_S$ for which the scales of LNV $\Lambda_{\rm LNV} = m_R^2/\mu_{\rm eff}$ and LFV $\Lambda_{\rm LFV} = m_R$ are most

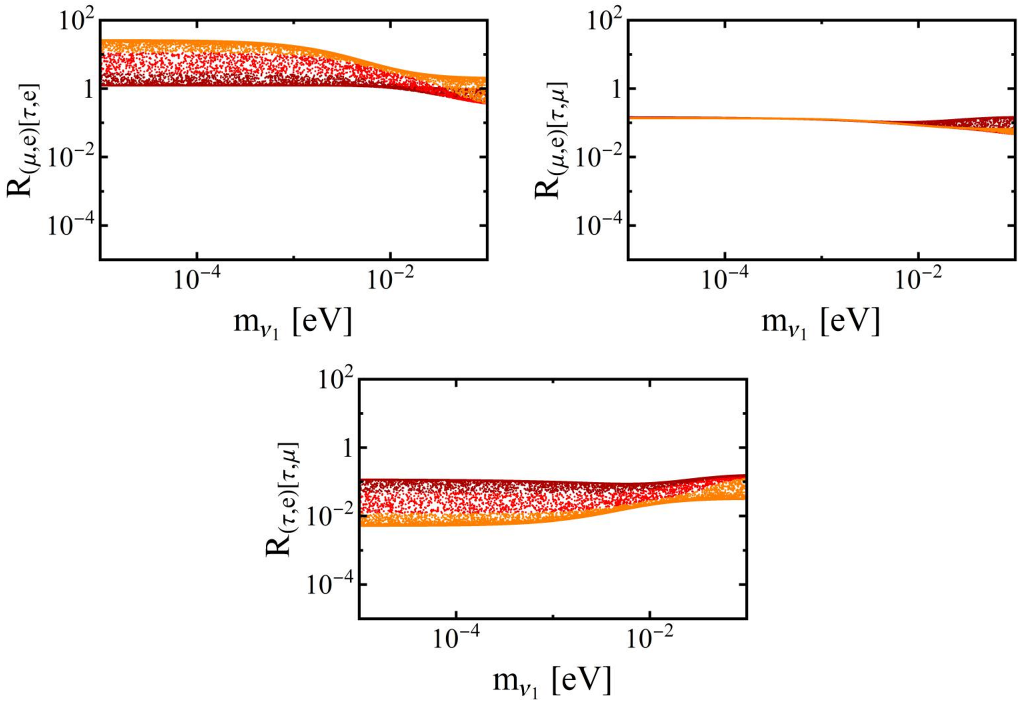


FIGURE 3.10: Plot of the ratios $R_{(i,j)[k,l]}$ for various combinations of flavour initial and final states as a function of the lightest neutrino mass $m_{\nu_1}$. Here the low-energy phase $\delta_{CP}$ has been switched off but the complex angle $\theta_2^c$ is varied. We find the same generic predictions as in the CP-conserving case of $R_{(\mu,e)[\tau,e]} > 1$ **(top-left)** $R_{(\mu,e)[\tau,\mu]} < 1$ **(top-right)** and $R_{(\tau,e)[\tau,\mu]} < 1$ **(bottom)**. For the ratios $R_{(\mu,e)[\tau,e]}$ and $R_{(\tau,e)[\tau,\mu]}$ the introduction of CP-violation brings the ratios closer to one and this difference is most apparent with a hierarchical spectrum of light neutrinos. In orange $\theta_2^c < 0.1$, in red $0.1 < \theta_2^c < 0.3$ and in burgundy $\theta_2^c > 0.3$.

disparate.

Successful MLFV-ISS resonant leptogenesis, however, requires very large values of $\mu_N$ in order for sufficiently reduced washout to occur in combination with a resonant enhancement of the asymmetry. This corresponds to a reduction in the hierarchy between the LNV and LFV scale, suppressing the overall size of this cLFV decay. Therefore, while some overall predictions can be made within MLFV-ISS on the relative strength of various combinations of cLFV observables, a measurement of cLFV in near future experiments will be in conflict with the viable parameter space for MLFV-ISS leptogenesis in the absence of some additional mechanism to reduce the overall washout in this region.

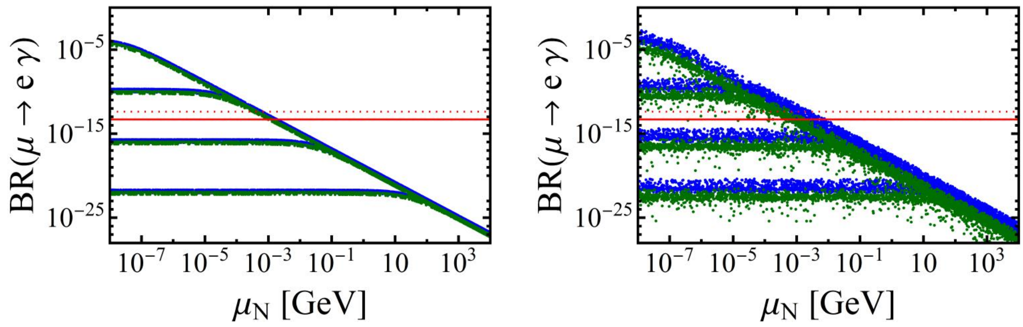


FIGURE 3.11: Plot of the branching ratio $\mathrm{BR}(\mu \to e\gamma)$ for $\theta_2^c = 0$ **(left)** and $0.1 < \theta_2^c < 1$ **(right)** as a function of $\mu_N$. Points in blue correspond to the choice $\delta_{CP} = 0$ whereas points in green correspond to $\delta_{CP} = 3\pi/2$. In these plots the other LNV parameter $\mu_S$ has been fixed to the values $10^{-8}$, $10^{-5}$, $10^{-2}$ and 10 GeV. The ratio plateaus whenever $\mu_N < \mu_S$. The red dotted (solid) line corresponds to the current (future) sensitivity of MEG and MEG-II [148, 150], respectively, for this decay mode. Clearly, small values of the LNV parameters are experimentally accessible, while large values (necessary for MLFV-ISS resonant leptogenesis) correspond to a suppressed signal. The inclusion of low-scale CPV through the Dirac phase has no effect on the prediction, while CPV from $\theta_2^c$ can alter the prediction by approximately an order of magnitude.

### 3.4.3 Linear Seesaw (LSS)

For the LSS ($\mathcal{Y}_{\mu_S} = \mathcal{Y}_{\mu_N} = 0$) the LNV parameter arises from the $(1,3)$ and $(3,1)$ entry of the full neutrino mass matrix,

$$M_\nu = \begin{pmatrix} m_\nu^{\text{1-loop}} & m_D^\nu & m_L \\ (m_D^\nu)^T & 0 & M_R \\ m_L^T & M_R^T & 0 \end{pmatrix} . \tag{3.84}$$

From Eq. (3.49) as long as $\mathcal{Y}_L \not\propto \mathbb{1}_{3\times 3}$ there is a radiative contribution to both the $(2,2)$ and $(3,3)$ entry which will break the $SO(3)^2$ invariance, leading to

$$\begin{aligned} \tilde{\mu}_N &= \mu_N \left(\mathcal{N}_1 + \mathcal{N}_2\right) \\ \tilde{\mu}_S &= \mu_S \left(\mathcal{S}_1 + \mathcal{S}_2\right), \end{aligned} \tag{3.85}$$

where

$$\begin{aligned} \mathcal{N}_1 &= n_1 \left( (\mathcal{Y}_D^\nu)^\dagger \mathcal{Y}_D^\nu + ((\mathcal{Y}_D^\nu)^\dagger \mathcal{Y}_D^\nu)^T \right), \\ \mathcal{N}_2 &= n_2^{(1)} \left( (\mathcal{Y}_D^\nu)^\dagger \mathcal{Y}_D^\nu (\mathcal{Y}_D^\nu)^\dagger \mathcal{Y}_D^\nu + ((\mathcal{Y}_D^\nu)^\dagger \mathcal{Y}_D^\nu (\mathcal{Y}_D^\nu)^\dagger \mathcal{Y}_D^\nu)^T \right) + n_2^{(2)} \left( (\mathcal{Y}_D^\nu)^\dagger \mathcal{Y}_D^\nu ((\mathcal{Y}_D^\nu)^\dagger \mathcal{Y}_D^\nu)^T \right) \\ &\quad + n_2^{(3)} \left( ((\mathcal{Y}_D^\nu)^\dagger \mathcal{Y}_D^\nu)^T (\mathcal{Y}_D^\nu)^\dagger \mathcal{Y}_D^\nu \right) + n_2^{(4)} \left( (\mathcal{Y}_D^\nu)^\dagger \mathcal{Y}_e \mathcal{Y}_e^\dagger \mathcal{Y}_D^\nu + ((\mathcal{Y}_D^\nu)^\dagger \mathcal{Y}_e \mathcal{Y}_e^\dagger \mathcal{Y}_D^\nu)^T \right) \end{aligned}$$

$$
\begin{aligned}
\mathcal{S}_1 &= s_1\left(\mathcal{Y}_L^\dagger\mathcal{Y}_L + (\mathcal{Y}_L^\dagger\mathcal{Y}_L)^T\right), \\
\mathcal{S}_2 &= s_2^{(1)}\left(\mathcal{Y}_L^\dagger\mathcal{Y}_L\mathcal{Y}_L^\dagger\mathcal{Y}_L + (\mathcal{Y}_L^\dagger\mathcal{Y}_L\mathcal{Y}_L^\dagger\mathcal{Y}_L)^T\right) + s_2^{(2)}\left(\mathcal{Y}_L^\dagger\mathcal{Y}_L(\mathcal{Y}_L^\dagger\mathcal{Y}_L)^T\right) \\
&\quad + s_2^{(3)}\left((\mathcal{Y}_L^\dagger\mathcal{Y}_L)^T\mathcal{Y}_L^\dagger\mathcal{Y}_L\right) + s_2^{(4)}\left(\mathcal{Y}_L^\dagger\mathcal{Y}_e\mathcal{Y}_e^\dagger\mathcal{Y}_L + (\mathcal{Y}_L^\dagger\mathcal{Y}_e\mathcal{Y}_e^\dagger\mathcal{Y}_L)^T\right).
\end{aligned} \tag{3.86}
$$

As before, we consider separately the cases where no corrections are included, corrections are included at leading order and corrections are included at next-to-leading order.

For the ISS scenario the corrections to the Majorana mass $\tilde{\mu}_N$ were proportional to the non-zero bare mass $\mu_N$ itself and scaled as $\mu_N$. For the LSS, by contrast, we operate in a regime where an explicit Majorana mass term in the Lagrangian is forbidden. However, flavour-invariant combinations such as $(\mathcal{Y}_D^\nu)^\dagger\mathcal{Y}_D^\nu$ and $\mathcal{Y}_L^\dagger\mathcal{Y}_L$ transform in the necessary way to induce mass terms for each SN.

Here the dimensionful parameters $\mu_N$ and $\mu_S$ cannot be identified with bare Majorana mass terms. Rather, they arise from the unknown UV complete dynamics. As we remain agnostic about these dynamics, yet under the MLFV *ansatz* we must include such terms, we choose to fix the values of $\mu_N$ and $\mu_S$ in some plausible way. For example, it seems reasonable to take $\mu_i \simeq v^2/M_{\rm X}$, which would be true if $\mu_i$ arose from some effective coupling with the SM Higgs doublet mediated by a heavy new particle $X$, generating an operator similar to the Weinberg operator.

We fix these parameters to $\mu_N = \mu_S = 1$ GeV which, in the example given above, would arise if $m_X \simeq \mathcal{O}(10-1000)$ TeV depending on the strength of the relevant couplings. We also make the reasonable assumption that this mass scale is independent of any parameters appearing in the matrix $m_L$.

Figure 3.12 plots the asymmetry generated as a function of $\boldsymbol{m_L}$, which we define to be the average of the non-zero entries of $m_L$ in the three scenarios considered. Points in blue correspond to the asymmetry without including $\mathcal{N}_i$ and $\mathcal{S}_i$. As discussed previously near Eq. (3.47), in this regime (where all the SNs have identical masses) the self-energy contribution to the CP-asymmetry is switched off but a non-zero asymmetry is generated from the vertex contribution and differences in the decay widths of each SN. The most asymmetry (albeit much too small) is generated in the region where the washout is minimised, as shown Fig. 3.13, in agreement with [1] and Chapter 2.

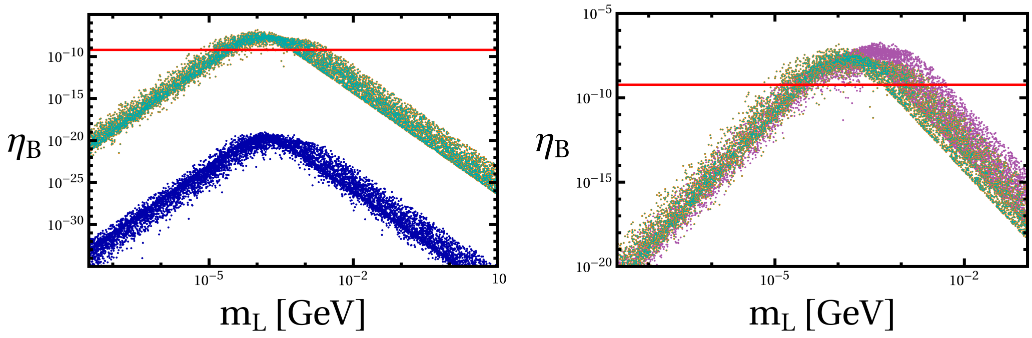


FIGURE 3.12: Plot of the asymmetry generated in the LSS for the three scenarios **(left)** and comparing the asymmetry generated from mixing to oscillations **(right)** as a function of $\boldsymbol{m_L}$, the average of the non-zero entries of the LNV matrix $m_L$ in GeV. Points in blue correspond to no radiative corrections, points in orange are when $\mathcal{N}_1$ and $\mathcal{S}_1$ are included and points in cyan include all terms. Contrary to the case of MLFV-ISS, corrections at leading order are sufficient to generate the necessary asymmetry. The case without any radiative corrections is highly suppressed as the self-energy contributions to $\varepsilon_i^\alpha$ are identically zero. However a non-zero asymmetry is generated due to the differences in the decay widths generating slight deviations in the vertex contribution for each SN, c.f. Eq. (3.47). Points in purple correspond to the estimated asymmetry generated due to oscillation effects between the heavy sterile neutrinos. The asymmetry due to oscillations is predicted to be of the same order as the asymmetry from standard thermal leptogenesis and modifies the predictions for the allowed range of couplings only slightly.

Points in orange correspond to spurion insertions at lowest order and points in cyan include all relevant terms. Now, due to the inclusion of the radiative Majorana masses, mass splittings occur between the six heavy SNs. The self-energy component of Eq. (3.43) turns on and increases the overall CP-asymmetry (due to a resonance between the SN masses) by several orders of magnitude. Here, including the next-to-leading order contributions does not change the size of the asymmetry generated. By contrast with with MLFV-ISS, the flavour mis-alignment between the matrix structure of $m_D^\nu$ and $m_L$ generates non-diagonal real entries in Eq. (3.39) at lowest order which also allows for larger values of $\varepsilon_i^\alpha$.

The right side of Fig. 3.12 estimates the contribution to the asymmetry arising from coherent oscillations with the spurion contributions included. For the entire region of parameter space we considered, the asymmetry generated from coherent oscillations is of similar size to that generated from conventional thermal leptogenesis. The inclusion of oscillation effects will therefore increase the total asymmetry, but we find no region where the effects of coherent oscillations dominate to a point where the region of viable parameter space significantly expands.

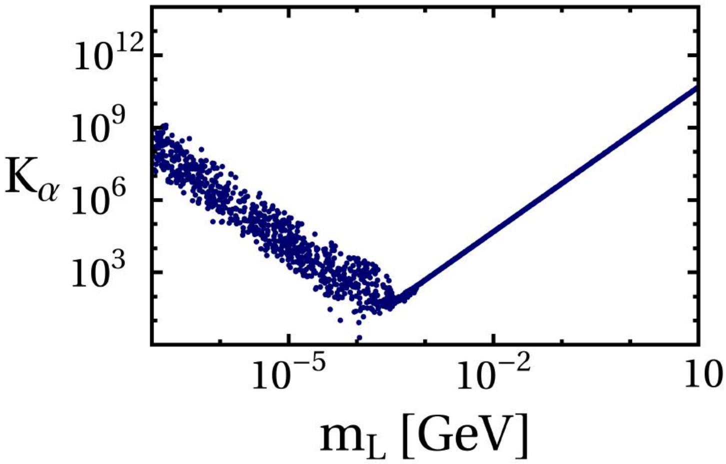


FIGURE 3.13: Plot of the effective washout to a specific lepton flavour $K_\alpha$ generated in the LSS as defined in Eq. (3.69). We find the washout is minimised for $\boldsymbol{m_L} \simeq \mathcal{O}(10^{-5}-10^{-3})$ GeV in agreement with [1]. The washout which is related to the Yukawa couplings in the mass basis of the heavy SNs from Eq. (3.39), is dominantly controlled by the parameters of $m_L(m_D^\nu)$ when $\|m_L\| > \|m_D^\nu\|( \|m_D^\nu\| > \|m_L\|)$. For large values of $\boldsymbol{m_L}$ the washout is not dependent on the size of the complex parameter $a_2^c$ whereas for small values where the parameters of $m_D^\nu$ dominate, different values of $a_2^c$ can produce different values of washout for the same choices in $m_L$.

Figure 3.14 plots the CP-asymmetry into a specific lepton flavour $\alpha$ in the three scenarios, where once again due to the anarchic nature each flavour has the same behaviour and overall size. It is clear that, for all values of $\boldsymbol{m_L}$, the CP-asymmetry is orders of magnitude larger when the radiative Majorana masses are included. In other words, for the entire region of the parameter space, roughly the same resonant enhancement is occurring. This forced-resonance is occurring as the mass splitting between the heavy SNs is related to the small Majorana parameters,

$$\begin{aligned} m_{N_j} &\simeq m_R + \frac{\tilde{\mu}_N}{2} + \frac{\tilde{\mu}_S}{2} \\ m_{N_i} &\simeq m_R - \frac{\tilde{\mu}_N}{2} - \frac{\tilde{\mu}_S}{2} \end{aligned} \tag{3.87}$$

leading to

$$\Delta m_{ij} = m_{N_i} - m_{N_j} = \tilde{\mu}_N + \tilde{\mu}_S = \mu_N \, n_1 \left( (\mathcal{Y}_D^\nu)^\dagger \mathcal{Y}_D^\nu \right) + \mu_S \, s_1 \left( \mathcal{Y}_L^\dagger \mathcal{Y}_L \right) \propto \Gamma_{i,j}, \tag{3.88}$$

where we take the parameters $\tilde{\mu}_N$ and $\tilde{\mu}_S$ to be independent of the parameters of $m_L$. Therefore the same level of resonant enhancement occurs for the entire parameter space. Unlike with MLFV-ISS, both $\Delta m_{i,j}^{\rm OS} \neq 0$ and $\Delta m_{i,j}^{\rm SS} \neq 0$ occurs at lowest order in the

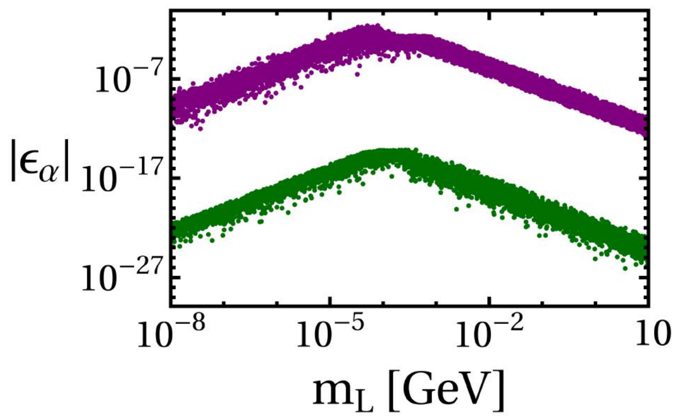


FIGURE 3.14: Plot of the CP-asymmetry to a specific lepton flavour $\alpha$ as a function of $\boldsymbol{m_L}$. Points in green correspond to when $\mathcal{N}_i$ and $\mathcal{S}_i$ are not included and points in purple correspond to when they are included (at lowest order and next-to-leading order the points are identical). Clearly a resonance due to their inclusion increases the overall CP-asymmetry by many orders of magnitude. The mass splittings induced in this scenario are directly proportional to the decay widths and therefore for any choice of the parameters within $m_L$ the mass splittings will always be in a resonant regime.

corrections and they both contribute to the asymmetry generated.

To illustrate this, Fig. 3.15 plots the mass splitting $\Delta m_{ij}$ and the decay width $\Gamma_i$ as a function of $\mathbf{m_L}$. The parameter which most significantly impacts the level of resonance (where the mass splitting overlaps with the decay width) is the combination of $\mu_N\, n_i$ and $\mu_S\, s_i$. The resonant enhancement is maximised when

$$\Delta m_{i,j} \simeq \Gamma_{i,j} = \frac{\left(h^\dagger h\right)}{8\pi} m_{N_i} \simeq 40 \left(h^\dagger h\right) \text{ GeV}. \tag{3.89}$$

This places constraints on the overall size of the combination $\mu_N\, n_i$ and $\mu_S\, s_i$ required in order for enough asymmetry to be generated. While this forced resonance occurs, in order for it to significantly impact the asymmetry, it relies on the radiative Majorana masses generated arising from a scale around $\mathcal{O}(1-1000)$ GeV.

In Fig. 3.16 we vary the lightest neutrino mass $m_{\nu_1}$ and the Wilson coefficients for fixed choices of the other parameters as described in the figure caption. We find similar conclusions to MLFV-ISS where large values of the light neutrino mass $m_{\nu_1}$ correspond to smaller asymmetry generation. Masses less than $\mathcal{O}(10^{-3})$ eV maximise the asymmetry generated. Larger values for the Wilson coefficient leads to a larger asymmetry and allows for a wider range of values within the parameters of $m_L$ to produce the necessary asymmetry along with smaller values for the CPV parameters.

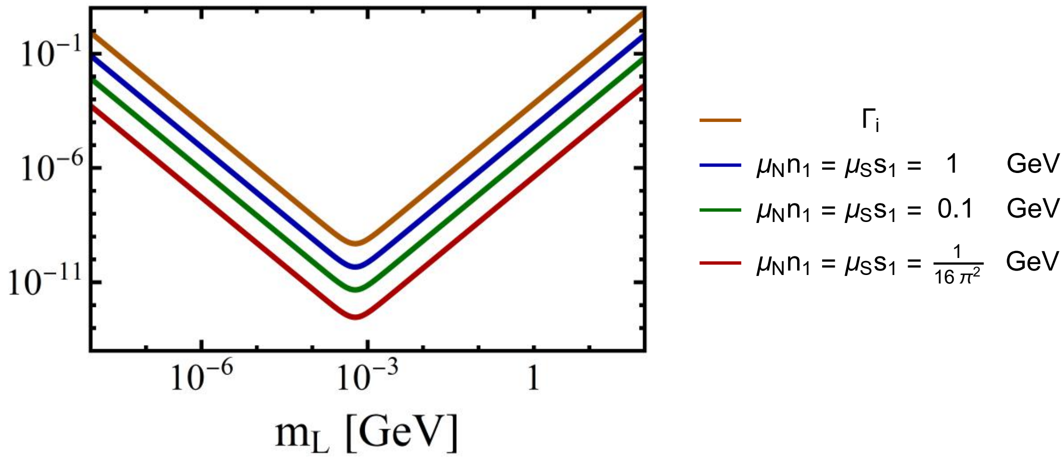


FIGURE 3.15: Plot of the mass splitting $\Delta m_{ij}$ as a function of $\boldsymbol{m_L}$ in GeV when $\mathcal{N}_1$ and $\mathcal{S}_1$ are included. In red $\mu_N\, n_i = \mu_S\, s_i = 1/(4\pi)^2$ GeV, in green $\mu_N n_i = \mu_S s_i = 0.1$ GeV and in blue $\mu_N n_i = \mu_S s_i = 1$ GeV. This is plotted against the decay width $\Gamma_{i,j}$ in brown. As the combination $\mathcal{N}_1 + \mathcal{S}_1 \propto \Gamma_{i,j}$ the mass splitting induced will always be on resonance independent of the value of $m_L$. Here there is no distinction between $\Delta m_{i,j}^{\rm SS}$ and $\Delta m_{i,j}^{\rm OS}$ and they both behave in a similar way.

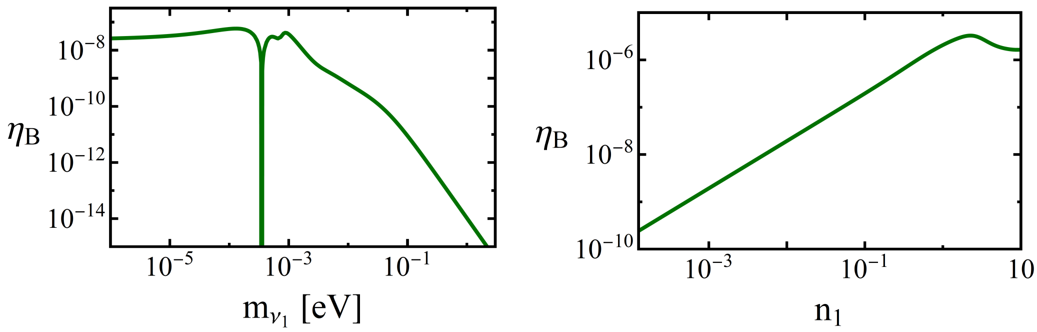


FIGURE 3.16: Variation in the baryon asymmetry as a function of the lightest active neutrino mass $m_{\nu_1}$ **(left)** and varying the Wilson coefficients $n_i$ and $s_i$ **(right)** for the case where all radiative spurion effects are included. In this scan we fixed $a_2^c = 0.7$ and in the left plot set $n_i,\, s_i = 1/16\pi^2$ whereas we fixed $m_{\nu_1} = 0.01$ eV in the right plot. In both plots similar behaviour compared to MLFV-ISS is found.

Based on these two scenarios, we conclude that successful MLFV resonant leptogenesis will also occur if the ISS and LSS were operative together. Appropriate choices for the now three LNV parameters based on the two scenarios here will allow for minimised washout with mass splittings related to the heavy SN decay widths for the necessary resonance to occur. However as the preceding chapter showed that resonant leptogenesis is already feasible [1] in this scenario without the need for radiative resonant leptogenesis, we do not consider this scenario further.

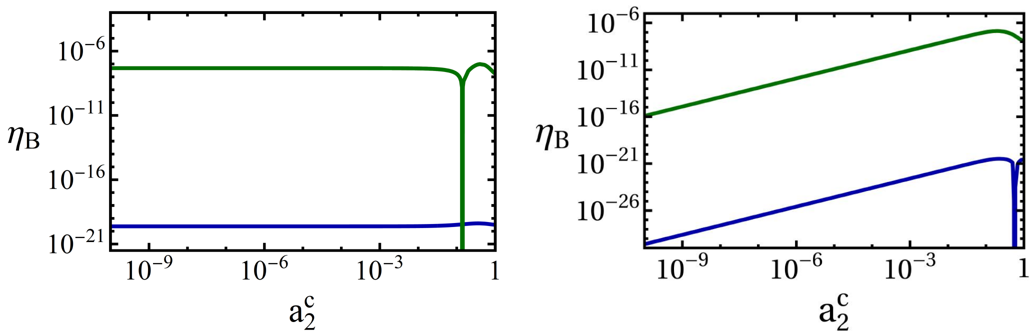


FIGURE 3.17: Plot of the baryon asymmetry as a function of the complex parameter $a_2^c$ for $\delta_{CP} = 3\pi/2$ **(let)** and $\delta_{CP} = 0$ **(right)**. Here we have fixed $m_L \simeq 10^{-4} \times \mathrm{diag}(1, 2, 5)$ GeV to be in a region with sufficient washout suppression for necessary asymmetry generation. In blue no radiative effects are included and in green is the scenario where spurion effects are included. The behaviour of the asymmetry as a function of the complex angle has consistent behaviour as it is taken to zero. As before asymmetry generation is possible both with low-energy phases as well as complex entries of the $C$ matrix where smaller values of $a_2^c$ are allowed compared to the ISS scenario.

Finally, in Fig. 3.17 we plot the behaviour of the asymmetry as a function of the complex component of the $C$ matrix when low-energy CPV is included and when it is not. Similarly to the ISS case, asymmetry generation can be predominately due to either the Dirac phase, $\delta_{CP}$, or the complex component $a_2^c$ of the $C$ matrix. We find consistent behaviour for the baryon asymmetry as these CPV parameters are taken to zero. It is clear from both Figs. 3.12 and 3.17 that a larger portion of the parameter space provides the necessary asymmetry generation allowing for smaller sizes of the CPV parameters, decreasing their contribution to flavour-violating processes.

### 3.4.4 $\ell_i \to \ell_j \gamma$ and MLFV-LSS

Once again we briefly consider the prospects of detection of MLFV-LSS through cLFV processes. Unlike in the MLFV-ISS scenario a much less tuned region of parameter space is required in order to generate the necessary baryon asymmetry which may lead to improved detection prospects.

As before we require insertions of spurions transforming as a $(\mathbf{3}, \overline{\mathbf{3}}, \mathbf{1}, \mathbf{1})$ in order to make the necessary dimension six effective operators invariant. Off-diagonal terms are required in order for LFV processes to occur. The lowest order combination which satisfies this is once again

$$\Delta\mathcal{Y}_e = \mathcal{Y}_D^\nu (\mathcal{Y}_D^\nu)^\dagger \mathcal{Y}_e + \mathcal{Y}_L \mathcal{Y}_L^\dagger \mathcal{Y}_e. \tag{3.90}$$

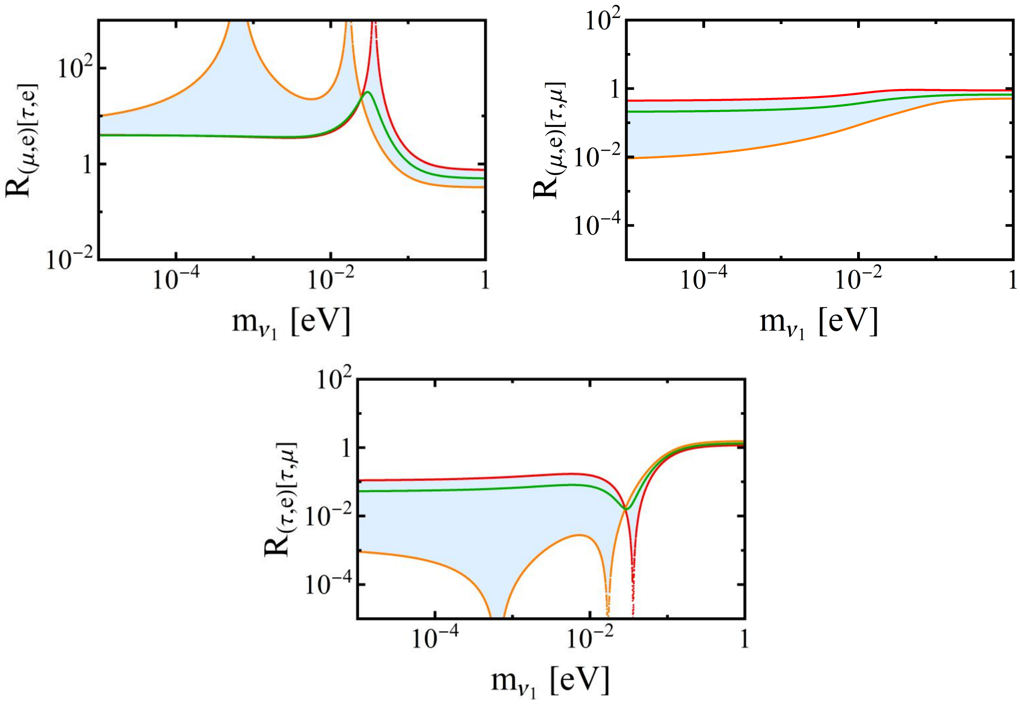


FIGURE 3.18: Plot of the ratios $R_{(i,j)[k,l]}$ for various combinations of flavour initial and final states as a function of the lightest neutrino mass $m_{\nu_1}$. Here the complex parameter $a_2^c$ has been switched off but the low-energy phase $\delta_{CP}$ is varied. Lines in red and orange correspond to the CP-conserving cases $\delta_{CP} = \{0, 2\pi\}$ and $\delta_{CP} = \pi$ respectively. In green is the maximally violating case of $\delta_{CP} = \pi/2$ or $\delta_{CP} = 3\pi/2$. The shaded blue region corresponds to $\delta_{CP} = (0, 2\pi)\backslash\{\pi/2,\, \pi,\, 3\pi/2\}$.

While the combination $\mathcal{Y}_L\mathcal{Y}_L^\dagger$ may transform in the correct way, it does not contain the necessary off-diagonal terms in our scan and therefore cLFV will once again be controlled by $(\mathcal{Y}_D^\nu)^\dagger$.

Figure 3.18 plots the three ratios of cLFV observables as in the ISS case for the scenario where $a_2^c = 0$ while $\delta_{CP}$ is varying. Similar predictions on the ratio $R_{(\mu,e)[\tau,\mu]}$ are made compared to the ISS scenario and therefore the branching ratio $\mathrm{BR}(\tau \to \mu\gamma)$ should be larger by one or two orders of magnitude compared to $\mathrm{BR}(\mu \to e\gamma)$. Here there is a cancellation in $\tau \to e\gamma$ for specific values of the lightest neutrino $m_{\nu_1}$ and the phase $\delta_{CP}$. In these regions a strong suppression of this channel is predicted. Outside the regions of strong cancellation the LSS similarly predicts $R_{(\tau,e)[\tau,\mu]} < 1$ but always predicts $R_{(\mu,e)[\tau,e]} > 1$ unlike the type-I and ISS case where this varied depending on the value of $\delta_{CP}$. As before the introduction of CPV appears to bring the ratios closer together.

Figure 3.19 plots the ratios of cLFV observables in the scenario where $\delta_{CP} = 0$ and $a_2^c$ is varied. We find that overall the presence of the CPV parameter becomes more impactful

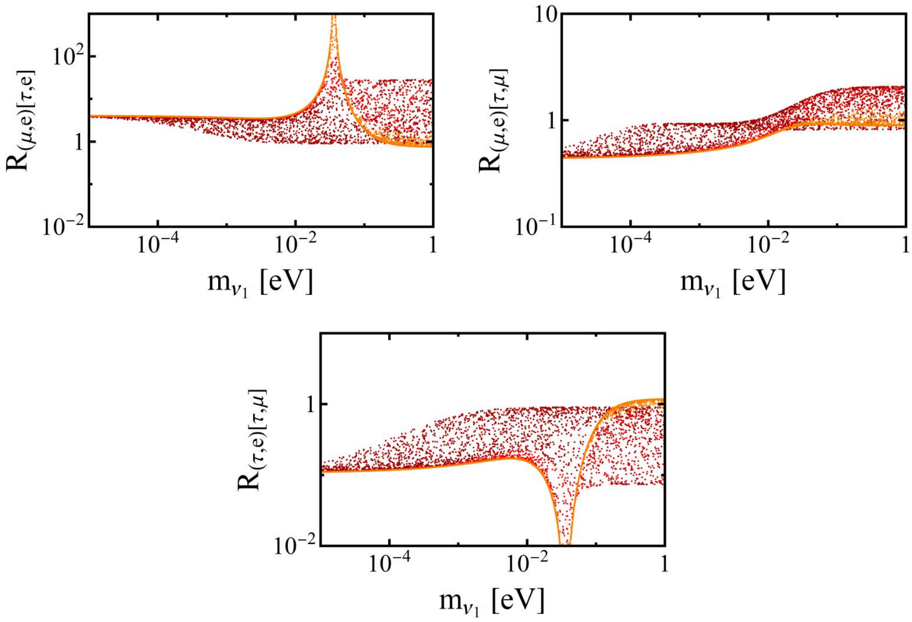


FIGURE 3.19: Plot of the ratios $R_{(i,j)[k,l]}$ for various combinations of flavour initial and final states as a function of the lightest neutrino mass $m_{\nu_1}$. Here the low-energy phase $\delta_{CP}$ has been switched off but the complex parameter $a_2^c$ is varied. We find the same generic predictions as in the CP-conserving case of $R_{(\mu,e)[\tau,e]} > 1$ **(top-left)** $R_{(\mu,e)[\tau,\mu]} \lesssim 1$ **(top-right)** and $R_{(\tau,e)[\tau,\mu]} \lesssim 1$ **(bottom)**. Similar to the scenario above a cancellation occurs for the process $\tau \to e\gamma$ for specific values of the lightest neutrino mass $m_{\nu_1}$. In orange $a_2^c < 0.1$, in red $0.1 < a_2^c < 0.3$ and in burgundy $a_2^c > 0.3$.

for larger values of the lightest neutrino mass, while for a hierarchical spectrum its impact is less significant. Overall similar predictions to the case where $\delta_{CP}$ was varied are obtained and a significant portion of the parameter space is not strongly sensitive to the presence of CPV. This implies the inclusion of CPV necessary for leptogenesis does not significantly modify the predictions given by the CP-conserving case.

Finally, Fig. 3.20 plots the predictions for the branching ratio $\mathrm{BR}(\mu \to e\gamma)$ as a function of the LNV parameter $m_L$ for $\Lambda_{\mathrm{LFV}} = 1$ TeV. As before, we plot cases with no CPV violation and cases in which CPV is present. The dotted(solid) red line corresponds to the current(future) limit placed by MEG(MEG-II). Due to the LSS parameterisation in Eq. (3.59), the Dirac-mass matrix $m_D^\nu$ is now inversely related to $m_L$ and is more senesitive to parameters within $m_L$ changing compared to the Majorana masses in the ISS scenario. While small values of $m_L$ are currently constrained, the region $10^{-5} \lesssim \boldsymbol{m_L}/\mathrm{GeV} \lesssim 10^{-3}$ required in order to account for baryogenesis will not be probed in near-future experiments. This roughly corresponds with the LNV scale $\Lambda_{\mathrm{LNV}} \simeq (10^6 - 10^4)$ GeV. This is in agreement with the estimates found in [169] for the necessary LNV scale for a given LFV scale to be probed. A future measurement of the process

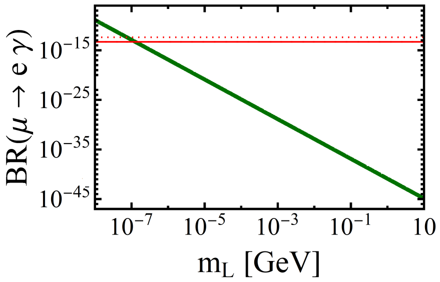


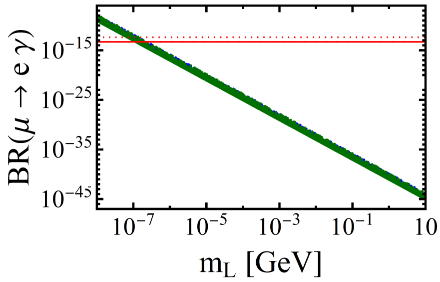


FIGURE 3.20: Plot of the branching ratio of $\mu \to e\gamma$ for $\theta_2^c = 0$ **(left)** and $0.1 < a_2^c < 1$ **(right)** as a function of $m_L$. Points in blue correspond to the choice $\delta_{CP} = 0$ whereas points in green correspond to $\delta_{CP} = 3\pi/2$. The red dotted(solid) line corresponds to the current(future) sensitivity of MEG and MEG-II [148, 150] respectively for this decay mode. Currently very small values of the LNV parameter are probed for MLFV-LSS which correspond to a very large seperation of the LNV and LFV scales. In order to allow for necessary asymmetry generation we require approximately $10^{-5} \lesssim m_L/\mathrm{GeV} \lesssim 10^{-3}$ which will not be probed by MEG-II in the near future. The inclusion of CPV of any type does not significantly impact the predictions.

$\mu \to e\gamma$ may rule out LSS as a leptogenesis candidate in the absence of additional physics introduced to lower the overall strength of the washout present for smaller values of $m_L$.

## 3.5 Summary

We have studied a well-motivated way in which small mass splittings between heavy SNs from different families may arise, within both the ISS and LSS frameworks, such that leptogenesis is possible despite the strong washout present in the theory. In the preceeding chapter we found that while a mass splitting naturally exists for the ISS, it is unable generate sufficient asymmetry. For the LSS, the mass degeneracy amongst the SN masses at the high scale prevents significant asymmetry generation. While Chapter 2 demonstrates that leptogenesis is feasible when all LNV terms are switched on (the ISS+LSS case) we explore the potential for ISS or LSS leptogenesis to occur independently, where additional symmetries may prevent both mass terms from simultaneously existing.

In the context of broken flavour symmetries and the MLFV hypothesis, a degeneracy amongst the heavy SNs is naturally produced, for the purposes of having a predictive theory. The degeneracy is then broken by higher-order spurion vev contributions, leading to a parameter region consistent with resonant asymmetry generation. In order for the desired splitting to occur in the intended way during cosmological evolution, the critical temperature at which the spurions acquire their non-zero vevs must be assumed to be above the scale of thermal leptogenesis.

We found that for MLFV-ISS only a small region of very large Majorana masses is able to generate the required asymmetry. Here asymmetry generation requires next-to-leading order corrections to be included, therefore suppressing the overall size of the CP-asymmetry generated per decay of SN. We briefly discussed the impact of CPV on potential low-energy observables, in particular how various ratios of cLFV decays are impacted compared to the CP conserving MLFV scenario. The region compatible with leptogenesis will not, however, be probed by current and near future cLFV experiments.

For MLFV-LSS a large region of parameter space is capable of satisfying the resonance condition simultaneously with the minimised washout required for successful asymmetry generation. Here corrections at lowest order are not flavour aligned and therefore much larger values of the CP-asymmetry are possible compared to the ISS. Similarly, we studied the impact of CPV on cLFV observables and find that small deviations occur due to their inclusion. In this case, relatively small values of the CPV parameters allow for sufficient asymmetry generation allowing for even smaller deviations as compared to the ISS case.

The viable regions of parameter space for ISS and LSS resonant leptogenesis found in this chapter should apply to other possible models in which small inter-family mass splittings are produced, provided that the mass splittings generated are of a sufficient size. The region of viable parameter space in both cases occurs when the naïve washout is minimised. This corresponds to large Majorana masses for $\mu_N$ or $\mu_S$ in the case of the ISS and much smaller relative values of the linear mass term, $m_L$, in the case of the LSS.

In both cases we estimated the impact of the lightest neutrino mass $m_{\nu_1}$ on the asymmetry generated. We find a clear preference for small values where the light neutrinos are hierarchical and estimate that $m_{\nu_1} \lesssim 10^{-2}$ eV is required to maximise asymmetry generation. Unsurprisingly we find that MLFV leptogenesis favours larger values for the Wilson coefficients related to the Majorana mass corrections in both scenarios.

# Chapter 4

# Lowering the scale of Pati-Salam breaking through low-scale seesaws

## 4.1 Introduction

The quark-lepton unifying Pati-Salam (PS) gauge symmetry [115, 116] is an interesting modification of the Standard Model (SM) for a number of reasons. For example, it requires the introduction of a right-handed neutrino state and therefore naturally can incorporate neutrino mass (in a number of ways). It unifies the now six seemingly disparate multiplets in each generation of the SM into two which, in the minimal variant of PS, only leads to two Yukawa couplings. It also appears as a subgroup of a number of possible grand unified theories (GUTs). An important property of the model is that it unifies quarks and leptons of the same $SU(2)$ isospin.

Although the PS symmetry is usually considered to be broken at high scales, the theory naturally can accommodate a conserved global baryon number. Therefore, and unlike many models of gauge coupling unification in which quark-lepton unification occurs, the PS breaking can occur at scales only a few orders of magnitude above the electroweak scale. Low-scale and high-scale variants of PS differ in very few ways, traditionally through a modification of the scalar sector and the inclusion of fermion singlets. However as with all models which unify the SM multiplets, the PS symmetry in its minimal form necessarily predicts two important mass equalities not observed experimentally:

$$m_\nu^{\text{Dirac}} = m_u \qquad \text{and} \qquad m_d = m_e. \tag{4.1}$$

The scalar content required in high-scale PS models to break the PS symmetry naturally leads to a seesaw within the neutrino sector (and not the up-quark sector), breaking the first mass relation; see e.g. [200]. Low-scale variants can be modified very simply in order to achieve a similar effect, although this requires extending the matter sector with, at a minimum, fermionic singlets. The second mass equality $m_d = m_e$ between the down-isospin partners also needs to be modified to produce a realistic theory

Any explanation of the broken mass degeneracy in the down-isospin sector requires a modification of the particle content of the theory. By far the most commonly considered modification is to introduce an additional scalar whose couplings to the down-quarks and charged-leptons differs by group theoretic factors; see e.g. [116]. This introduces enough free parameters such that all the masses of SM can arise without issue. An alternative idea, which we pursue further in this chapter, was first proposed in [201, 202] where additional fermionic states are introduced which mix with the charged-leptons inducing additional seesaw mixing. This similarly allows for a viable mass spectrum for all particles but additionally can attractively lead to phenomenologically viable PS models at much lower breaking scales than usually considered.

The limits on the PS breaking scale arise from rare meson decay processes mediated by leptoquarks. In particular the theory requires the existence of a gauge-boson leptoquark, $X_\mu$, which mediates these rare meson decays at tree level and with coupling strength similar to the strong coupling constant $g_c$. As $X_\mu$ couples quarks and fermions of the same isospin, the dominant decay modes that constrain PS breaking arise from the interactions of $X_\mu$ to the down-quarks and charged-leptons. Signals from up-isospin interactions result in neutrino (or missing energy) final states which are more difficult to constrain.

Interestingly, the introduction of new physics to break the down-isospin mass degeneracy can further modify the meson decay rates and hence also the limits on the PS breaking scale. Ordinarily the PS breaking limits vary between $\mathcal{O}(100-1000)$ TeV. However these mixing effects can reduce these limits down to $\mathcal{O}(10-100)$ TeV. Lower PS limits are of obvious interest as they allow for potential experimental probes of these models at scales lower than previously anticipated.

Additionally there has been a recent resurgence in interest in low-scale PS models as the leptoquarks predicted by the theory are promising candidates as explanations of anomalies in low-energy flavour-physics experiments [203–206]. The vector leptoquark $X_\mu$ itself is an attractive candidate to explain a portion of these anomalies. However, this requires a mass around $\Lambda \simeq 30$ TeV [207] which is naïvely ruled out from rare meson-decay experiments. Modifications to the PS gauge group itself have been proposed [208–210] in order to allow for lighter masses of $X_\mu$ by modifying the gauge coupling to the different generations or by embedding the theory in a Randall-Sundrum background allowing for PS breaking in the TeV range [211]. Alternatively the scalar leptoquark content of the theory has been considered as a candidate to explain the anomalies [207] in the standard PS scenario, by assuming some scalars develop significantly smaller masses than the PS breaking scale. This potentially leads to a hierarchy problem.

The use of charged-lepton mixing in order to both break the down-isospin mass degeneracy and reduce the allowed scale of PS breaking has already been considered in the context of the B anomalies for a specific model [212, 213] . The aim of this chapter is to thoroughly analyse which PS multiplets are viable candidates in breaking the aforementioned mass degeneracy, and to evaluate the requirements on the couplings introduced in each case such that this also leads to lower experimentally allowed PS breaking scales. Therefore while we are motivated by different appealing reasons for low-scale PS, we will only focus on the requirements such that a reduction in the limits occurs.

This chapter is organised as follows. Section 4.2 is an overview of the minimal PS scenario including an examination of the gauge boson and fermion masses. Section 4.3 evaluates the experimental limits on PS breaking as a function of the free parameters in the theory and determines the impact that fermionic mixing can have on the limits. Section 4.4 identifies all possible PS multiplets of low dimensionality that contain states such that mixing is induced. Finally, Section 4.5 evaluates the requirements on the couplings involving viable multiplets which achieve both the desired suppression in the PS limits and a viable values for all relevant SM masses.

## 4.2 Pati-Salam models

### 4.2.1 Basic Setup

The Pati-Salam gauge group $G_{\rm PS}$ extends the SM by identifying the $SU(3)$ colour group as a subgroup of an $SU(4)$ gauge group and extending the electroweak sector to be left-right symmetric:

$$G_{\rm PS} = SU(4)_{\rm c} \otimes SU(2)_{\rm L} \otimes SU(2)_{\rm R}. \tag{4.2}$$

Often a discrete symmetry between the $SU(2)_{\rm L}$ and $SU(2)_{\rm R}$ sectors is imposed but is not necessary. Under this gauge symmetry the five SM fermion multiplets of each generation can be unified into two simple multiplets[1] under $G_{\rm PS}$

$$f_L \sim (\mathbf{4}, \mathbf{2}, \mathbf{1}) \quad \text{and} \quad f_R \sim (\mathbf{4}, \mathbf{1}, \mathbf{2}), \tag{4.3}$$

where $L/R$ indicates both which $SU(2)$ the fields are charged under as well as the chirality. The breaking of $SU(4)$ to the maximal subgroup $SU(3) \otimes U(1)_X$ is phenomenologically required and under this breaking the fundamental of $SU(4)$ decomposes as

$$\mathbf{4} \to \mathbf{1}_{-1} \oplus \mathbf{3}_{1/3} \tag{4.4}$$

indicating that the SM quarks and leptons can be unified by identifying $U(1)_X$ with a gauged $B-L$. The SM fermions are embedded into the multiplets given in Eq. (4.3) as[2]

$$f_L = \begin{pmatrix} u_r & d_r \\ u_b & d_b \\ u_g & d_g \\ \nu_e & e \end{pmatrix}_L \quad \text{and} \quad f_R = \begin{pmatrix} u_r & d_r \\ u_b & d_b \\ u_g & d_g \\ \nu_e & e \end{pmatrix}_R , \tag{4.5}$$

with similar embeddings for the other generations. Therefore the gauge transformation rules for the fields, written as matrix multiplication, are

$$f_{L/R} \to U_4 \left(f_{L/R}\right) U_{L/R}^T \tag{4.6}$$

[1] With the necessary addition of a right-handed neutrino.

[2] For simplicity we choose to identify the first generation of leptons with the first generation of quarks and so forth, however alternative assignments are possible [214].

where $U_{4,L,R}$ are special unitary matrices for the groups $SU(4)_{\rm c}$, $SU(2)_{\rm L}$ and $SU(2)_{\rm R}$ respectively. There are multiple choices of scalars which give the correct breaking patterns. A common and near-minimal choice for electroweak symmetry breaking is a complex bidoublet

$$\phi \sim (\mathbf{1},\mathbf{2},\mathbf{2}) = \begin{pmatrix} \phi_1^0 & \phi_2^+ \\ \phi_1^- & \phi_2^0 \end{pmatrix}, \quad \langle\phi\rangle = \begin{pmatrix} v_1 & 0 \\ 0 & v_2 \end{pmatrix} \tag{4.7}$$

where the superscripts indicate the electric charge $Q$ of each field and $\phi$ is written such that it transforms as

$$\phi \to U_L \phi U_R^\dagger. \tag{4.8}$$

Two different combinations of scalar multiplets are usually considered for the breaking of $G_{\rm PS}$ down to $G_{\rm SM}$. Firstly, and most commonly, two scalars $\Delta_L \sim (\mathbf{10},\mathbf{3},\mathbf{1})$ and $\Delta_R \sim (\mathbf{10},\mathbf{1},\mathbf{3})$ are employed, where

$$\Delta^\alpha_{L/R} = \frac{1}{\sqrt{2}} \begin{pmatrix} \sqrt{2}\Delta_{11}^{\alpha+1/3} & \Delta_{12}^{\alpha+1/3} & \Delta_{13}^{\alpha+1/3} & \Delta_{14}^{\alpha-1/3} \\ \Delta_{12}^{\alpha+1/3} & \sqrt{2}\Delta_{22}^{\alpha+1/3} & \Delta_{23}^{\alpha+1/3} & \Delta_{24}^{\alpha-1/3} \\ \Delta_{13}^{\alpha+1/3} & \Delta_{23}^{\alpha+1/3} & \sqrt{2}\Delta_{33}^{\alpha+1/3} & \Delta_{34}^{\alpha-1/3} \\ \Delta_{14}^{\alpha-1/3} & \Delta_{24}^{\alpha-1/3} & \Delta_{34}^{\alpha-1/3} & \sqrt{2}\Delta_{44}^{\alpha-1} \end{pmatrix}_{L/R} \tag{4.9}$$

are symmetric matrices in $SU(4)$ space (written in the defining representation), $\alpha = (-1,0,1)$ corresponds to the non-trivial $SU(2)$ charge of the scalar (in the adjoint representation) and the superscripts on each component again corresponds to its electric charge[3]. The breaking $G_{\rm PS} \to G_{\rm SM}$ occurs with a non-zero vev in the following components

$$\left\langle \left(\Delta^{\alpha=1}_{L/R}\right)_{44} \right\rangle = v_{L/R}. \tag{4.10}$$

Alternatively, the scalars $\chi_L \sim (\mathbf{4},\mathbf{2},\mathbf{1})$ and $\chi_R \sim (\mathbf{4},\mathbf{1},\mathbf{2})$ can be used:

$$\chi_{L/R} = \begin{pmatrix} \chi_r^{2/3} & \chi_r^{-1/3} \\ \chi_b^{2/3} & \chi_b^{-1/3} \\ \chi_g^{2/3} & \chi_g^{-1/3} \\ \chi^0 & \chi^- \end{pmatrix}_{L,R}, \quad \left\langle \chi_{L/R} \right\rangle = \begin{pmatrix} 0 & 0 \\ 0 & 0 \\ 0 & 0 \\ v_{L/R} & 0 \end{pmatrix} \tag{4.11}$$

where the gauge transformation rules for these scalars are the same as $f_{L/R}$.

[3]Unless stated otherwise superscripts on fields making up a PS multiplet will correspond to its electric charge $Q$ under $U(1)_{\rm EM}$.

In both cases, $\Delta_R$ and $\chi_R$ would be sufficient without their $SU(2)_L$ counterparts as long as the bidoublet $\phi$ is included. Their inclusion however allows for the possibility of imposing a discrete symmetry between the left and right gauge sectors which would lead to partial unification of the gauge couplings, $g_L = g_R$, at the relevant breaking scale. An analysis of the renormalisation group running of the gauge coupling constants has shown that the inclusion of a parity symmetry requires a PS breaking scale of $\mathcal{O}(10^{12})$ GeV in order for consistency with low-energy measurements of electroweak observables [200], unless the parity breaking scale is decoupled from the scale of PS breaking [215]. In order to allow for the scale of PS breaking to be as low as possible we assume that if such a discrete symmetry exists, then its breaking occurs independently at a higher scale to the breaking of $G_{\text{PS}}$ which allows for the scale of PS breaking to be significantly lowered. However for generality we will include the $SU(2)_L$ scalars which may be predicted by specific GUTs or lead to unique phenomenology.

In addition to the scalars in Eq. (4.11) often $\Phi \sim (\mathbf{15}, \mathbf{1}, \mathbf{1})$ is included where

$$\Phi = \frac{1}{2}\begin{pmatrix} \Phi^0_\pi + \frac{1}{\sqrt{3}}\Phi^0_\eta + \frac{1}{\sqrt{6}}\Phi^0_{15} & \sqrt{2}\Phi^0_{12} & \sqrt{2}\Phi^0_{13} & \sqrt{2}\Phi^{2/3}_r \\ \sqrt{2}\left(\Phi^0_{12}\right)^* & -\Phi^0_\pi + \frac{1}{\sqrt{3}}\Phi^0_\eta + \frac{1}{\sqrt{6}}\Phi^0_{15} & \sqrt{2}\Phi^0_{23} & \sqrt{2}\Phi^{2/3}_b \\ \sqrt{2}\left(\Phi^0_{13}\right)^* & \sqrt{2}\left(\Phi^0_{23}\right)^* & -\frac{2}{\sqrt{3}}\Phi^0_\eta + \frac{1}{\sqrt{6}}\Phi^0_{15} & \sqrt{2}\Phi^{2/3}_g \\ \sqrt{2}\Phi^{-2/3}_{\bar{r}} & \sqrt{2}\Phi^{-2/3}_{\bar{b}} & \sqrt{2}\Phi^{-2/3}_{\bar{g}} & -\frac{3}{\sqrt{6}}\Phi^0_{15} \end{pmatrix}$$

$$\langle\Phi\rangle = v_\Phi \,\text{diag}\left(\frac{1}{2\sqrt{6}}, \frac{1}{2\sqrt{6}}, \frac{1}{2\sqrt{6}}, -\sqrt{\frac{3}{8}}\right) \tag{4.12}$$

such that $\Phi$ transforms as

$$\Phi \to U_4 \Phi\, U_4^\dagger. \tag{4.13}$$

As this scalar transforms in the adjoint representation of $SU(4)_{\text{c}}$, a non-zero vev for $\Phi$ will break this symmetry down to one of its maximal subgroups such as $SU(3)_{\text{c}} \otimes U(1)_{B-L}$. The inclusion of $\Phi$ therefore allows for all possible scales of symmetry breaking[4] starting from $G_{\text{PS}}$ down to the broken SM but is only necessary in scenarios where the $SU(2)_R$ gauge boson masses are desired to be smaller than the PS breaking scale.

[4]The vevs of the scalars $\chi_R$ and $\Delta_R$ directly break $SU(4)_{\text{c}} \otimes SU(2)_{\text{L}} \otimes SU(2)_{\text{R}}$ down to $SU(3)_{\text{c}} \otimes SU(2)_{\text{L}} \otimes U(1)_{\text{Y}}$.

The scalar content described above leads to the following symmetry breaking chain

$$\begin{gathered} SU(4)_c \otimes SU(2)_L \otimes SU(2)_R \\ \Big\downarrow_{\langle\Phi\rangle} \\ SU(3)_c \otimes SU(2)_L \otimes SU(2)_R \otimes U(1)_{B-L} \\ \Big\downarrow_{\langle\chi_R/\Delta_R\rangle} \\ SU(3)_c \otimes SU(2)_L \otimes U(1)_Y \\ \Big\downarrow_{\langle\phi,\chi_L/\Delta_L\rangle} \\ SU(3)_c \otimes U(1)_{\mathrm{EM}} \end{gathered} \tag{4.14}$$

where $Y = T_{3R} + \frac{B-L}{2}$, $Q = T_{3L} + Y$ and the order of breaking is determined by the relative size of each vev.

We now describe in more detail how the first mass relation of Eq. (4.1) can be avoided. The equality between down-isospin partners will be addressed further below, however the equality between up-isospin partners allows us to restrict the scalar content of the theory. If $\Delta_{L/R}$ are present, a Majorana mass term for the neutrinos will be generated via $y_{L/R}\overline{f_{L/R}}(f_{L/R})^c\Delta_{L/R}$ and will lead to a see-saw mechanism between the neutral fermions as the hierarchy $\langle\Delta_L\rangle \ll \langle\phi\rangle \ll \langle\Delta_R\rangle$ is required due to electroweak precision tests and the Yukawa couplings are fixed by the masses of the up-type quarks. This leads to light, predominantly left-handed neutrinos, with masses given by

$$m_\nu \simeq y_L\langle\Delta_L\rangle + \frac{m_u^2}{y_R\langle\Delta_R\rangle}. \tag{4.15}$$

Considering the third generation of fermions alone, $m_u = m_t \simeq 175$ GeV, requires PS breaking at large scales in order to achieve a viable low-energy neutrino mass spectrum. Setting $\langle\Delta_L\rangle = 0$ gives a rough lower-bound $\langle\Delta_R\rangle \gtrsim 10^{12}$ GeV and therefore the scalars $\Delta_{L/R}$ are not viable as models of low-scale PS.[5]

If $\chi_{L/R}$ are present, a viable neutrino mass spectrum is only possible with the inclusion of additional particles, for example a left-handed gauge-singlet fermion $S_L \sim (\mathbf{1},\mathbf{1},\mathbf{1})$ for each fermion generation, as otherwise $\nu_{L/R}$ are predicted to be Dirac particles with masses similar to those of the up-type quarks. Light neutrinos can arise due to the

[5]A viable neutrino mass spectrum with $\langle\Delta_R\rangle \ll 10^{12}$ GeV may be possible with a fine-tuned cancellation between the two terms appearing in Eq. (4.15) if $y_{L/R}$ have opposite sign, although we will not consider this possibility further.

| | $\Phi$ | $\phi$ | $\chi_L$ | $\chi_R$ |
|---|---|---|---|---|
| $SU(4)_{\rm c}$ | **15** | **1** | **4** | **4** |
| $SU(2)_{\rm L}$ | **1** | **2** | **2** | **1** |
| $SU(2)_{\rm R}$ | **1** | **2** | **1** | **2** |

TABLE 4.1: The scalar content which we utilise and their respective dimensions under each PS gauge group.

ISS and LSS mechanisms if small but non-zero lepton number violating mass terms are included as in Chapters 2 and 3. This scenario can allow for the PS breaking scale to be much lower, as we describe below, while allowing for light neutrino masses and therefore we restrict ourselves to the scalar content described in Table 4.1.

### 4.2.2 Yukawa sector

The full Yukawa Lagrangian for the fermions $f_L$, $f_R$ and $S_L$ and the scalars $\phi, \chi_L$ and $\chi_R$ is

$$\mathcal{L}_{\rm YUK} = {\rm Tr}\left[y_1 \overline{f_L} \phi\, (f_R)^T + y_2 \overline{f_L}\, \phi^c (f_R)^T + y_R \overline{S_L} \chi_R^\dagger f_R + y_L \overline{f_L} \chi_L (S_L)^c\right] + \frac{1}{2}\mu_S \overline{S_L} (S_L)^c + {\rm H.c} \tag{4.16}$$

where generational indices are suppressed, $\phi^c = \tau_2\, \phi^* \tau_2$ and $\tau_2 = \epsilon^{ab}$ is the two-dimensional Levi-Civita symbol.

After spontaneous symmetry breaking, charged-fermion masses arise from $\langle\phi\rangle$

$$\begin{aligned} m_u &= y_1 v_1 + y_2 v_2^* \\ m_d &= y_1 v_2 + y_2 v_1^* \\ m_e &= m_d, \end{aligned} \tag{4.17}$$

whereas, within the neutrino sector, mixing between the neutral fermions leads to

$$\frac{1}{2}\begin{pmatrix} \overline{\nu_L} & \overline{\nu_R^c} & \overline{S_L} \end{pmatrix} \begin{pmatrix} 0 & m_u & y_L v_L \\ m_u & 0 & y_R v_R^* \\ y_L v_L & y_R v_R^* & \mu_S \end{pmatrix} \begin{pmatrix} \nu_L^c \\ \nu_R \\ S_L^c \end{pmatrix}. \tag{4.18}$$

Adopting the hierarchy $|\mu_S,\, y_L\, v_L| < |m_u| < |y_R\, v_R|$ and setting all parameters to be real for simplicity leads to

$$\begin{aligned} m_{\nu_1} &\simeq \mu_S \left(\frac{m_u}{y_R v_R}\right)^2 + 2\frac{y_L v_L}{y_R v_R} m_u \\ m_{\nu_{2,3}} &\simeq y_R v_R \pm \mu_S \end{aligned} \tag{4.19}$$

if only one generation is considered, where the light state is predominantly made up of $\nu_L$ and the two heavy states predominantly made up of $\nu_R$ and $S_L$. A viable neutrino mass spectrum is possible for sufficiently small values of the lepton number violating mass terms $\mu_S$ and $y_L v_L$. These choices are technically natural and allow for the breaking scale $v_R$ (which breaks PS) to be lowered to $\mathcal{O}(1000)$ TeV or lower.

### 4.2.3 Gauge Sector

The kinetic term for each scalar is given by

$$\mathcal{L}^{\mathrm{S}}_{\mathrm{KIN}} = (D_\mu \phi)^\dagger (D^\mu \phi) + \left(D_\mu \chi_R\right)^\dagger \left(D^\mu \chi_R\right) + \left(D_\mu \chi_L\right)^\dagger \left(D^\mu \chi_L\right) + \frac{1}{2}\mathrm{Tr}\left(D_\mu \Phi\right)\left(D^\mu \Phi\right), \tag{4.20}$$

the covariant derivatives are given by

$$\begin{aligned} D_\mu \phi &= \partial_\mu \phi + i g_L \hat{W}_{L\mu} \phi - i g_R \phi \hat{W}_{R\mu} \\ D_\mu \chi_L &= \partial_\mu \chi_L + i g_4 \hat{G}_\mu \chi_L + i g_L \chi_L (\hat{W}_{L\mu})^T \\ D_\mu \chi_R &= \partial_\mu \chi_R + i g_4 \hat{G}_\mu \chi_R + i g_R \chi_R (\hat{W}_{R\mu})^T \\ D_\mu \Phi &= \partial_\mu \Phi + i g_4 \left[\hat{G}_\mu,\, \Phi\right] \end{aligned} \tag{4.21}$$

and $\hat{W}_{L[R]\mu}/\hat{G}_\mu$ are the $SU(2)_{L[R]}/SU(4)$ gauge fields respectively, written as matrices transforming in their defining representation and are explicitly written down in Appendix C.

After spontaneous symmetry breaking the spectrum of masses and mixings for the different gauge fields can be calculated. We find

$$m_X^2 = g_4^2 \left(\frac{1}{3}v_\Phi^2 + \frac{1}{2}v_L^2 + \frac{1}{2}v_R^2\right) \tag{4.22}$$

where $X_\mu$ corresponds to a colour-triplet vector leptoquark with electric charge 2/3,

$$\mathcal{L}^{\mathrm{S}}_{\mathrm{KIN}} \supset \frac{1}{2}\begin{pmatrix} W_L^+ & W_R^+ \end{pmatrix}_\mu \underbrace{\begin{pmatrix} g_L^2\left(v_\phi^2+v_L^2\right) & -2g_Lg_Rv_1v_2 \\ -2g_Lg_Rv_1v_2 & g_R^2\left(v_\phi^2+v_R^2\right)\end{pmatrix}}_{M^2_{W^\pm}} \begin{pmatrix} W_L^- \\ W_R^- \end{pmatrix}^\mu \tag{4.23}$$

which corresponds to the mixing matrix between the two colour-neutral, electrically-charged gauge bosons with $v_\phi^2 = v_1^2 + v_2^2$ and

$$\mathcal{L}^{\mathrm{S}}_{\mathrm{KIN}} \supset \frac{1}{2}\begin{pmatrix} G_{15} & W_{3L} & W_{3R} \end{pmatrix}_\mu \underbrace{\begin{pmatrix} \frac{3}{2}g_4^2\left(v_L^2+v_R^2\right) & -\sqrt{\frac{3}{2}}g_4g_Lv_L^2 & -\sqrt{\frac{3}{2}}g_4g_Rv_R^2 \\ -\sqrt{\frac{3}{2}}g_4g_Lv_L^2 & g_L^2\left(v_\phi^2+v_L^2\right) & -g_Lg_Rv_\phi^2 \\ -\sqrt{\frac{3}{2}}g_4g_Rv_R^2 & -g_Lg_Rv_\phi^2 & g_R^2\left(v_\phi^2+v_R^2\right)\end{pmatrix}}_{M_0^2} \begin{pmatrix} G_{15} \\ W_{3L} \\ W_{3R} \end{pmatrix}^\mu \tag{4.24}$$

which corresponds to the mixing matrix between the three colour- and electrically-neutral gauge bosons.

While the above equations can be solved numerically, simple analytic expressions can be derived in certain limits. Assuming a hierarchy in the scales of symmetry breaking, $v_{\mathrm{EW}} = \sqrt{v_\phi^2 + v_L^2} < v_R$, leads to the following spectrum of gauge boson masses:

$$\begin{aligned} m_\gamma^2 = 0, \quad m_Z^2 \simeq \frac{1}{2}\frac{3g_R^2g_4^2+3g_L^2g_4^2+2g_R^2g_L^2}{3g_4^2+2g_R^2}v_{\mathrm{EW}}^2, \quad m_{Z'}^2 \simeq \frac{1}{2}\left(g_R^2+\frac{3}{2}g_4^2\right)v_R^2 \\ m_W^2 \simeq \frac{1}{2}g_L^2v_{\mathrm{EW}}^2, \quad m_{W'}^2 \simeq \frac{1}{2}g_R^2\left(v_R^2+v_{\mathrm{EW}}^2\right) \\ m_X^2 = \frac{1}{2}\left(\frac{2}{3}v_\Phi^2+v_L^2+v_R^2\right)g_4^2. \end{aligned} \tag{4.25}$$

where the hypercharge gauge coupling is given by

$$g_Y^2 = \frac{3g_R^2g_4^2}{3g_4^2+2g_R^2}. \tag{4.26}$$

Note that $\langle\Phi\rangle$ only contributes to the mass of the vector leptoquark $X_\mu$ and otherwise is completely decoupled from the remaining gauge bosons and fermions.

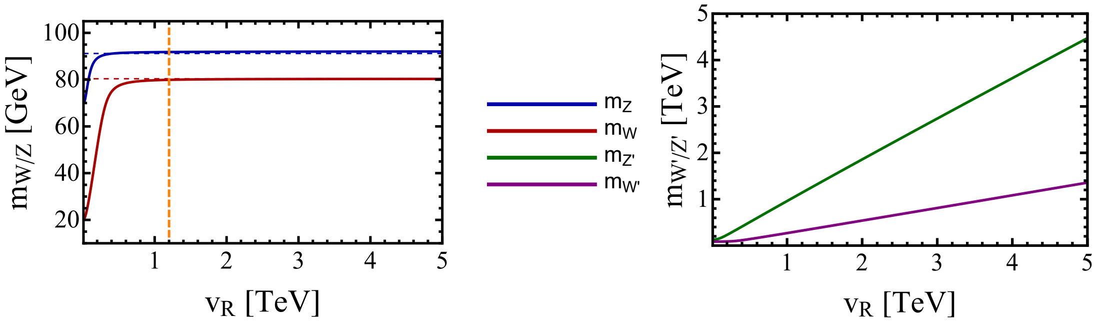


FIGURE 4.1: Plot of the masses of the SM-like gauge bosons $m_Z$ and $m_W$ **(left)** and the heavy gauge bosons $m_{Z'}$ and $m_{W'}$ **(right)** as a function of the $SU(2)_R$ breaking scale $v_R$. Here the masses were found by numerically solving Eqs. (4.23) and (4.24) with gauge couplings given by Eq. (4.27) assuming the normal running of the SM gauge couplings at these energy scales described in Appendix E. We roughly find that $v_R > 1.2$ TeV is required for Eq. (4.25) to be valid and to ensure the light gauge fields remain SM-like as indicated by the dashed vertical line, the dashed horizontal lines correspond to the measured masses of the electroweak gauge fields. We find that the $Z'$ gauge field will be significantly heavier than the $W'$ field and a ratio of $m_{Z'}/m_{W'} \simeq 3.5$. This is due to the additional mixing effects occurring between the neutral gauge bosons compared to the charged ones.

The gauge couplings of $G_{\text{PS}}$ ($g_4$, $g_L$ and $g_R$) are related to those of the SM ($g_c$, $g_w$ and $g_Y$) at the scale of PS breaking:

$$g_4^2(\mu) = g_c^2(\mu), \quad g_L^2(\mu) = g_w^2(\mu) \quad \text{and} \quad g_R^2(\mu) = \frac{3g_Y^2(\mu)g_c^2(\mu)}{3g_c^2(\mu) - 2g_Y^2(\mu)}. \tag{4.27}$$

As the $SU(4)$ coupling constant is given by the usual colour gauge coupling, at low scales $g_c(\mu) > g_Y(\mu)$ and therefore $g_R(\mu) \simeq g_Y(\mu)$. Figure 4.1 plots the masses of the electroweak gauge bosons of the theory as a function of the $SU(2)_R$ breaking scale $v_R$. In order to decouple $v_R$ from significantly impacting the masses of the light, SM-like gauge bosons we roughly find that $v_R > 1200$ GeV is required in order for Eq. (4.25) to be a valid approximation. The heavy neutral gauge boson $Z'$ is significantly heavier compared to the heavy charged gauge boson $W'$ and we roughly find a ratio of $m_{Z'}/m_{W'} \simeq 3.5$ at TeV scales. Adoption of the hierarchy $v_\Phi \gg v_R$ would imply that the leptoquark $X$ is heavier than both the $Z'$ and $W'$ fields such that $m_{W'} < m_{Z'} \ll m_X$. However, were $\Phi$ to be absent or have $v_\Phi < v_R$, the spectrum of heavy gauge bosons masses would be $m_{W'} < m_X < m_{Z'}$ with the ratio $m_{Z'}/m_X \simeq 1.3$ at TeV scales.

### 4.2.4 Baryon number violation

In order to assess the implications for baryon number violation arising from the unification of quarks and leptons within PS we consider the Yukawa and kinetic portion of the Lagrangian, and the scalar potential separately. Consider first the electroweak sector of the Yukawa Lagrangian:

$$\mathcal{L}_{\text{YUK,EW}} = \text{Tr}\left[y_1 \overline{f_L} \phi \left(f_R\right)^T + y_2 \overline{f_L}\, \phi^c (f_R)^T\right] + \text{H.c.} \tag{4.28}$$

This Lagrangian is invariant under a single global $U(1)_J$ transformation

$$f_L \to e^{i\theta J} f_L, \quad f_R \to e^{i\theta J} f_R \quad \text{and} \quad \phi \to \phi \tag{4.29}$$

and therefore the J charge of each field can be chosen such that

$$J(f_L) = J(f_R) = 1 \text{ and } J(\phi) = 0. \tag{4.30}$$

As $\phi$ is uncharged under the $SU(4)$ of Pati-Salam and the global symmetry $J$, the vev $\langle\phi\rangle$ also does not break either symmetry e.g. $J(\langle\phi\rangle) = T(\langle\phi\rangle) = 0$, where T corresponds to the fifteenth generator of $SU(4)$ identified with $B - L$. Baryon and lepton number can be identified as different linear combinations of $J$ and $T$

$$B = \frac{1}{4}(J + T) \text{ and } L = \frac{1}{4}(J - 3T) \tag{4.31}$$

such that

$$B(f_L) = B(f_R) = \begin{pmatrix} 1/3 & 1/3 \\ 1/3 & 1/3 \\ 1/3 & 1/3 \\ 0 & 0 \end{pmatrix} \text{ and } L(f_L) = L(f_R) = \begin{pmatrix} 0 & 0 \\ 0 & 0 \\ 0 & 0 \\ 1 & 1 \end{pmatrix} \tag{4.32}$$

as required for the embeddings of SM fermion in $f_L$ and $f_R$ defined in Eq. (4.5). As the electroweak Yukawa Lagrangian is invariant under both $J$ and $T$ independently in both the broken and unbroken phase, it is clearly also invariant under a linear combination of the two and therefore all interactions conserve both $B$ and $L$.

Turning to the remaining terms in the Yukawa Lagrangian[6],

$$\mathcal{L}_{\text{YUK,PS}} = \text{Tr}\left[y_R \overline{S_L} \chi_R^\dagger f_R + y_L \overline{f_L} \chi_L (S_L)^c\right] + \frac{1}{2}\mu_S \overline{S_L} S_L^c + \text{H.c} \tag{4.33}$$

the global symmetry $U(1)_J$ is unbroken with the additional charge assignments

$$J(\chi_L) = J(\chi_R) = 1 \text{ and } J(S_L) = 0 \tag{4.34}$$

where the $B$ and $L$ numbers of each component of $\chi_{L/R}$ are identical to those of $f_{L/R}$. The scalars $\chi_L$ and $\chi_R$ are charged under both $J$ and $T$, such that $\frac{1}{4}(J+T)(\langle\chi_{L/R}\rangle) = B(\langle\chi_{L/R}\rangle) = 0$, whereas $\frac{1}{4}(J-3T)(\langle\chi_{L/R}\rangle) = L(\langle\chi_{L/R}\rangle) \neq 0$. Therefore $B$ is conserved by the Yukawa Lagrangian at all scales whereas lepton number is spontaneously broken at the scale of $SU(2)_\text{R}$ breaking. Baryon number being an accidental symmetry of the PS Yukawa Lagrangian is a feature which appears to be insensitive to the choice of scalars used to break the PS symmetry. If the scalars $\Delta^\alpha_{L/R}$ defined in Eq. (4.9) were present instead of $\chi_{L/R}$ (often considered in high-scale PS models) identical conclusions are reached with baryon number remaining an accidental symmetry of the Yukawa sector while lepton number is spontaneously broken.

The kinetic portion of the Lagrangian

$$\mathcal{L}_{\text{KIN}} = i\sum_F \overline{F} \not{D} F + \sum_S (D_\mu S)^\dagger (D^\mu S), \tag{4.35}$$

where $F = (f_L, f_R, S_L)$ and $S = (\chi_L, \chi_R, \phi, \Phi)$, does not violate $B - L = T$ as it is a gauge symmetry. However it is easy to show that it also conserves a global $B + L = \frac{1}{2}(J-T)$ symmetry where

$$(B+L)(\hat{G}_\mu) = \begin{pmatrix} 0 & 0 & 0 & -2/3 \\ 0 & 0 & 0 & -2/3 \\ 0 & 0 & 0 & -2/3 \\ 2/3 & 2/3 & 2/3 & 0\,, \end{pmatrix} \tag{4.36}$$

as every gauge field is uncharged under $U(1)_J$ and $\hat{G}_\mu$ corresponds to the $SU(4)_\text{c}$ gauge fields. The gauge fields of $SU(2)_\text{L}$ and $SU(2)_\text{R}$ are uncharged under $J$ and $T$ and therefore uncharged under $B$ and $L$. As the gauge interactions conserve both $B-L$ and $B+L$

[6] Adopting the scalar and fermion particle content detailed in Section 4.2.1.

simultaneously they necessarily conserve $B$ and $L$ separately and therefore there is no gauge-mediated baryon- or lepton-number violation predicted by PS, though these may appear if PS is embedded into some GUT at a higher scale, with the effects suppressed by the relevant unification scale (see e.g. [216]).

A comprehensive analysis of the scalar potential including minimisation of the potential is beyond the scope of this work. Of all the possible gauge invariant terms within the scalar potential, we find only one term[7] which will violate $U(1)_J$ for the charge assignments imposed by the Yukawa Lagrangian:

$$V(\phi, \Phi, \chi_L, \chi_R) \supset \widetilde{\lambda}_{LR} \, (\chi_L)^{Aa} (\chi_L)^{Bb} (\chi_R)^{C\alpha} (\chi_R)^{D\beta} \epsilon_{ABCD} \epsilon_{ab} \epsilon_{\alpha\beta}, \tag{4.37}$$

where $(A, B, \dots)/(a, b, \dots)/(\alpha, \beta, \dots)$ correspond to $SU(4)/SU(2)_L/SU(2)_R$ indices respectively. As $J(\chi_{L/R}) = 1$ is required by the Yukawa sector, the existence of this term in the scalar potential violates $J$ by four units and therefore violates $B$ by one unit.

Therefore proton and neutron decay diagrams can exist within low-scale PS and will involve a combination of the couplings $y_R$, $y_L$ and $\widetilde{\lambda}_{LR}$. This requires the existence of both $\chi_L$ and $\chi_R$. Models with only $\chi_R$ included (required for PS breaking) have exact proton stability assuming no additional particle content. Additionally, baryon number can be easily imposed when both scalars are present by setting $\widetilde{\lambda}_{LR} \to 0$ which is not constrained by any other phenomenology and is technically natural and therefore insensitive to quantum corrections. Constraining the allowed size of $\widetilde{\lambda}_{LR}$ from the current experimental constraints on rare proton and neutron decays is beyond the scope of this work. However, this was briefly looked at in [202] for a similar model where they found $\widetilde{\lambda}_{LR} \leq 10^{-5}$ as a constraint arising from $N \to ee\nu$. PS models therefore are relatively unconstrained by baryon number violating decays compared to GUT scenarios and other experimental measurements (or lack thereof) are required in order to constrain the scale of PS breaking.

We note that the scalar potential must satisfy additional phenomenological bounds beyond the suppression of baryon number violation. In particular, due to the multiple $SU(2)_L$ doublets which appear in the theory, the masses of the physical scalars which

[7] Additionally there are two extra possible terms $\widetilde{\lambda}_L (\chi_L)^4 = \widetilde{\lambda}_L \, (\chi_L)^{Aa} (\chi_L)^{Bb} (\chi_L)^{Cc} (\chi_L)^{Dd} \epsilon_{ABCD} \epsilon_{ab} \epsilon_{cd}$ and $\widetilde{\lambda}_R (\chi_R)^4 = \widetilde{\lambda}_R \, (\chi_R)^{A\alpha} (\chi_R)^{B\beta} (\chi_R)^{C\gamma} (\chi_R)^{D\delta} \epsilon_{ABCD} \epsilon_{\alpha\beta} \epsilon_{\gamma\delta}$ which would also break $U(1)_J$ however we find them to be identically zero once contracted.

arise after minimisation of the scalar potential must be sufficiently heavy as they mediate various flavour-changing processes at tree-level, for example neutral-meson mixing. These constraints are identical for *all* left-right symmetric extensions of the SM which contain, at a minimum, a scalar bi-doublet and have been extensively studied [217–221]. Recent studies on the masses of the additional physical scalar fields [222] with flavour changing couplings puts a lower bound on its mass scale of $\mathcal{O}(20)$ TeV. Although this limit requires masses to be somewhat larger than the electroweak scale, it has been pointed out [221] that quartic couplings in the scalar potential can generate mass contributions proportional to the $SU(2)_R$ breaking scale for these scalars and therefore large masses can naturally be generated. Regardless, while such constraints are important for low-scale left-right symmetric models, of which PS is an example, they have no impact on the experimental limits on the scale of PS breaking and therefore we do not consider them further.

## 4.3 Probing Pati-Salam models through rare meson decays

A promising probe of the scale of Pati-Salam breaking is through the contributions of the gauge and scalar leptoquarks predicted by different realisations of the model to low-energy hadronic processes. Of particular significance is the gauge boson leptoquark $X_\mu$ which must couple universally to all three generations of fermions. This is unlike the various possible scalar leptoquarks for which the Yukawa couplings to the lighter generations could be suppressed, perhaps through a flavour symmetry. Additionally as $SU(3)_\mathrm{c}$ is a subgroup of the $SU(4)$ appearing in $G_\mathrm{PS}$, the coupling strength of the leptoquark $X_\mu$ to the SM quarks is related to that of $g_c$ and cannot be treated as a free parameter. Therefore precision flavour experiments involving the lighter generations provide stringent limits[8] on the mass of the gauge leptoquark $X_\mu$ which directly limits the scale of PS breaking (either $v_\Phi$ or $v_R$) through Eq. (4.25).

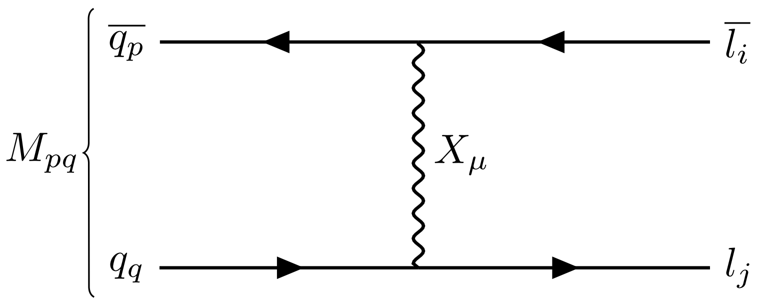


FIGURE 4.2: Tree-level Feynman diagram of the leptonic decay of a scalar meson $M_{pq}$, where $q_p$ and $q_q$ correspond to the valence quarks of the meson, to the lepton pair $l_{i,j}$ $(i, j = e, \mu, \tau)$ mediated by the PS gauge leptoquark $X_\mu$. PS unifies quarks and leptons of similar isospin, therefore the processes mediated by $X_\mu$ at tree-level are easily predicted, e.g. if $q_q$ corresponds to an up-type quark then $l_j$ must be a neutrino. The strongest limits on the mass of $X_\mu$ arise in the case where $p$ and $q$ are both down-type quarks, where $M_{pq} = (K_L^0, B_d^0, B_s^0, \dots)$, and therefore the final state comprises of charged leptons with opposite sign.

### 4.3.1 Neutral Pseudoscalar meson decays induced by $X_\mu$

The most stringent constraint on the mass of $X_\mu$ arises from limits on rare leptonic decays of pseudoscalar mesons, mediated at tree level by $X_\mu$ as shown in Fig. 4.2. As Pati-Salam unifies quarks and leptons with the same $SU(2)_{L/R}$ isospin into the same $SU(4)$ multiplet, as shown by Eq. (4.5), it couples up-type quarks to neutrinos and down-type quarks to the charged leptons. Therefore the leptonic decay channels induced by $X_\mu$ at tree-level can be predicted based on the valence quark content of the relevant meson. For example, $X_\mu$ will mediate the leptonic decay $D^0 \to \overline{\nu}\nu$ as both valence quarks are up-type but not $D^0 \to \ell^+\ell^-$. Unsurprisingly the meson decay channels which lead to the most stringent limits on the mass of $X_\mu$ arise from opposite-sign charged-lepton final states where there is no missing energy, which only occurs in PS for neutral mesons with down-type valence quarks. As a result, the mass of $X_\mu$ is most constrained by measurements of the decays of $K_L^0$, $B_d^0$ and $B_s^0$ mesons whose leptonic decay channels are well measured.

The leptoquark $X_\mu$ couples to the fermions through their kinetic terms in the Lagrangian

$$\mathcal{L}_{\text{KIN}}^{\text{F}} = i\overline{f_L}\not{D} f_L + i\overline{f_R}\not{D} f_R \tag{4.38}$$

[8] If a scalar leptoquark is present which also mediates the same decay, destructive interference between the gauge and scalar contribution to the hadronic process can somewhat lower the limits on the mass of $X$ by up to a factor of 2 [223] depending on the mass(es) and couplings of the relevant scalar(s). In our analysis we will focus solely on the contribution from the gauge leptoquark and neglect possible regions of destructive interference with scalar contributions by assuming the masses of the scalars to be heavier than the gauge leptoquark.

where the covariant derivatives for $f_{L/R}$ are defined similarly to $\chi_{L/R}$ given in Eq. (4.21). Expanding out Eq. (4.38) explicitly with the fermion multiplets given in Eq. (4.5) and leaving only the interactions of interest gives

$$\mathcal{L}^{\text{F}}_{\text{KIN}} \supset \frac{g_4}{\sqrt{2}} \left( \overline{d} \not{X} P_L e + \overline{d} \not{X} P_R e \right) + \text{ H.c,} \tag{4.39}$$

where colour and generational indices have been suppressed. Here the fields $d$ and $e$ represent the gauge eigenstates. Rotating to the mass eigenstates leads to

$$\mathcal{L}_{Xde} = \frac{g_4}{\sqrt{2}} \left( \overline{d'_i} \, (K_L^{de})_{ij} \not{X} P_L e'_j + \overline{d'_i} \, (K_R^{de})_{ij} \not{X} P_R e'_j \right) + \text{ H.c.} \tag{4.40}$$

where now the generational indices are explicitly shown and primed fields represent mass eigenstates[9]. The matrices $K^{de}_{L/R}$ are CKM-like mixing matrices between the down-type quarks and charged leptons. The existence of both left- and right-handed couplings to $X_\mu$ leads to two different mixing matrices which, without a parity symmetry, are not necessarily equal. The matrices can be expressed in terms of the unitary matrices used to diagonalise the mass matrices e.g. $(U_L^i)^\dagger M_i U_R^i = M_i^d = \text{diag}(\dots)$. For the case of $G_{\text{PS}}$ in total there are eight different physical mixing matrices (compared to the two of the SM) given by

$$\begin{aligned}
V_L^{\text{CKM}} &= (U_L^u)^\dagger \, U_L^d, \quad & V_R^{\text{CKM}} &= (U_R^u)^\dagger \, U_R^d, \qquad & K_L^{de} &= (U_L^d)^\dagger \, U_L^e, \quad & K_R^{de} &= (U_R^d)^\dagger \, U_R^e \\
U_L^{\text{LEPT}} &= (U_L^\nu)^\dagger \, U_L^e, \quad & U_R^{\text{LEPT}} &= (U_R^\nu)^\dagger \, U_R^e, \qquad & K_L^{u\nu} &= (U_L^u)^\dagger U_L^\nu, \quad & K_R^{u\nu} &= (U_R^u)^\dagger \, U_R^e
\end{aligned} \tag{4.41}$$

where $U^\nu_{L/R}$ is a $3 \times (3+n)$ matrix due to the possible seesaw nature of the neutrino sector and the upper-left $3 \times 3$ block of $U_L^{\text{LEPT}}$ is given by the (now non-unitary) PMNS matrix.

For a pseudo-scalar meson $M_{pq}$, where $q_p$ and $q_q$ correspond to the valence quarks of the meson e.g. $B_d^0 = M_{bd}$, the partial width for the two-body decay $M_{pq} \to \ell_i^+ \ell_j^-$ is given by [223, 224]

$$\Gamma_{M_{pq} \to \ell_i^+ \ell_j^-} = \frac{m_{M_{pq}}}{16\pi} \, \lambda(m_{M_{pq}}, m_{\ell_i}, m_{\ell_j}) \sum_h |\mathcal{M}_{pq,ij}|^2 \tag{4.42}$$

[9]For the remainder of this chapter, where there is no chance of confusion between gauge and mass eigenstates, fields will remain unprimed for both basis.

where

$$\lambda(m_{M_{pq}}, m_{\ell_i}, m_{\ell_j}) = \sqrt{\left[1 - \left(\mu_{\ell_i} + \mu_{\ell_j}\right)^2\right]\left[1 - \left(\mu_{\ell_i} - \mu_{\ell_j}\right)^2\right]} \tag{4.43}$$

and $\mu_X = m_X/m_{M_{pq}}$. For the decay of a scalar to two fermions the sum over helicity states is given by

$$\begin{aligned}\sum_h |\mathcal{M}_{pq,ij}|^2 = \left(1 - \mu_{\ell_i}^2 - \mu_{\ell_j}^2\right)\left[|\mathcal{M}^L_{pq,ij}|^2 + |\mathcal{M}^R_{pq,ij}|^2\right] \\ - 2\,\mu_{\ell_i}\mu_{\ell_j}\left[\mathcal{M}^L_{pq,ij}\left(\mathcal{M}^R_{pq,ij}\right)^* + \mathcal{M}^R_{pq,ij}\left(\mathcal{M}^L_{pq,ij}\right)^*\right]\end{aligned} \tag{4.44}$$

where

$$\mathcal{M}_{pq,ij} \equiv \mathcal{M}^L_{pq,ij}\,\overline{u}(p_{\ell_j})P_L\,v(p_{\ell_i}) + \mathcal{M}^R_{pq,ij}\,\overline{u}(p_{\ell_j})P_R\,v(p_{\ell_i}). \tag{4.45}$$

The matrix elements of the axial and pseudoscalar currents for the relevant mesons are given by [214, 223]

$$\begin{aligned}\langle 0|\overline{d_p}\gamma^\mu\gamma^5 d_q|M_{pq}\rangle &= i f_{M_{pq}}(p^\mu_{\ell_j} + p^\mu_{\ell_i}) \\ \langle 0|\overline{d_p}\gamma^5 d_q|M_{pq}\rangle &= -i f_{M_{pq}}\overline{m}_{pq}\end{aligned} \tag{4.46}$$

where $f_{M_{pq}}$ is the meson's decay constant and $\overline{m}_{pq} = m^2_{M_{pq}}/(m_{q_p} + m_{q_q})$. Combining these matrix elements with Fig. 4.2 and Eq. (4.40) leads to

$$\mathcal{M}^{L/R}_{pq,ij} = f_{M_{pq}}\left[R_{pq}\,\overline{m}_{pq}(M_P^{L/R})_{pq,ij} - \left\{m_{\ell_j}(M_A^{L/R})_{pq,ij} - m_{\ell_i}(M_A^{R/L})_{pq,ij}\right\}\right] \tag{4.47}$$

where

$$\begin{aligned}\left(M_A^{L/R}\right)_{pq,ij} &= \mp\frac{g_4^2}{4m_V^2}\left(K^{de}_{L/R}\right)_{pi}\left(K^{de}_{L/R}\right)^*_{qj} \\ \left(M_P^{L/R}\right)_{pq,ij} &= \mp\frac{g_4^2}{2m_V^2}\left(K^{de}_{L/R}\right)_{pi}\left(K^{de}_{R/L}\right)^*_{qj}\end{aligned} \tag{4.48}$$

and $R_{pq}$ is a factor introduced to account for the running of the strong coupling from the high scale, $\mu \sim m_X$, down to the relevant hadron mass scale, $\mu \sim m_{M_{pq}}$. This leads to an enhancement in the pseudoscalar-current matrix element in Eq. (4.46) [223, 225] but no enhancement for the axial current which does not run due to the Ward identity of QCD [226].

To demonstrate, for the leptonic decays of $K_L^0$ the correction factor is given by

$$R_{K_L^0}(m_{K_L^0},\, m_X) = R(m_{K_L^0},\, m_c;\, 3)R(m_c,\, m_b;\, 4)R(m_b,\, m_t;\, 5)R(m_t,\, m_X;\, 6) \tag{4.49}$$

where

$$R(\mu_1,\, \mu_2;\, n_f) = [g_c(\mu_1)/g_c(\mu_2)]^{8/b(n_f)}, \tag{4.50}$$

$b(n_f) = 11 - (2/3)n_f$ and $n_f$ corresponding to the number of active quark flavours in each energy regime.

As $X_\mu$ couples to both left- and right-handed quarks and leptons, two different types of contributions can be seen in Eq. (4.47). The first term does not depend on the masses of the final state leptons and corresponds to the helicity-unsuppressed contribution and only exists if both $K^{de}_{L/R}$ exist, which is only possible if $X_\mu$ couples to both fermion chiralities. The last two terms are proportional to the final state charged lepton masses. This corresponds to the helicity-suppressed contribution which arises from a mass insertion and only requires one of $K^{de}_{L/R}$ to exist. It is forbidden in the limit of massless final-state leptons, in complete analogy to weak meson decays in the SM. If the final state particle masses are ignored, the decay width is given purely by the helicity-unsuppressed contribution, and can be simplified to [223, 227, 228]

$$\Gamma^{\rm HU}_{M_{pq}\to\ell_i^+\ell_j^-} = \frac{m_{M_{pq}}\left[g_4(m_X)\right]^4 f^2_{M_{pq}}\overline{m}^2_{pq}}{64\,\pi\, m_X^4} R^2_{pq}\left(\left|K_L^{de}\right|^2_{pi}\left|K_R^{de}\right|^2_{qj} + \left|K_R^{de}\right|^2_{pi}\left|K_L^{de}\right|^2_{qj}\right). \tag{4.51}$$

In the limit where $X_\mu$ couples to only one chirality of fermions[10] similar to the weak force, $M_P^{L/R} = 0$ but one of $M_A^{L/R}$ remains nonzero. This results in the total decay width depending only on the helicity-suppressed terms appearing in Eq. (4.47). The usual result for helicity-suppressed meson decays is recovered

$$\begin{aligned}\Gamma^{\rm HS}_{M_{pq}\to\ell_i^+\ell_j^-} = \frac{m_{M_{pq}}\left[g_4(m_X)\right]^4 f^2_{M_{pq}}}{256\,\pi\, m_X^4}&\sqrt{\left[1-\left(\mu_{\ell_i}+\mu_{\ell_j}\right)^2\right]\left[1-\left(\mu_{\ell_i}-\mu_{\ell_j}\right)^2\right]} \\ &\times\left[\left(1-\mu^2_{\ell_i}-\mu^2_{\ell_j}\right)\left(m^2_{\ell_i}+m^2_{\ell_j}\right) - 4\mu_{\ell_i}\mu_{\ell_j}m_{\ell_i}m_{\ell_j}\right]\end{aligned} \tag{4.52}$$

[10] This is a special case of the general case which occurs for example by setting $K_R^{de} = 0_{3\times3}$ but $K_L^{de}$ remains unitary.

which, in the limit $m_{\ell_j} > m_{\ell_i}$, valid for the SM charged leptons, is well approximated by

$$\Gamma^{\text{HS}}_{M_{pq}\to\ell_i^+\ell_j^-} \simeq \frac{m_{M_{pq}}\left[g_4(m_X)\right]^4 f^2_{M_{pq}}}{256\,\pi\, m_X^4}\, m^2_{\ell_j}\left(1-\frac{m^2_{\ell_j}}{m^2_{M_{pq}}}\right)^2\left(\left|K^{de}\right|^2_{pi}\left|K^{de}\right|^2_{qj}\right), \tag{4.53}$$

where $K^{de}$ corresponds to either $K^{de}_L$ or $K^{de}_R$ depending on which chirality of fermions $X_\mu$ couples to. Comparing Eqs. (4.51) and (4.53) unsuprisingly suggests that generically the helicity-unsuppressed contribution is expected to dominate:

$$R_{\text{HU/HS}} = \frac{\Gamma^{\text{HU}}}{\Gamma^{\text{HS}}} \simeq \frac{4\,\overline{m}^2_{pq}R^2_{pq}}{m^2_{\ell_j}}\underbrace{\left(\frac{\left|K^{de}_L\right|^2_{pi}\left|K^{de}_R\right|^2_{qj}+\left|K^{de}_R\right|^2_{pi}\left|K^{de}_L\right|^2_{qj}}{\left|K^{de}_L\right|^2_{pi}\left|K^{de}_L\right|^2_{qj}+\left|K^{de}_R\right|^2_{pi}\left|K^{de}_R\right|^2_{qj}}\right)}_{\kappa}. \tag{4.54}$$

For example, for $K_L^0 \to \mu e$ we roughly find $R_{\text{HU/HS}} \simeq 10^4\,\kappa$ where $\kappa$ corresponds to the combination of mixing matrices involving $K^{de}_{L/R}$ above. However the helicity unsuppressed contribution can be sub-dominant if the couplings are strongly suppressed for one chirality over the other e.g. $|K^{de}_L|_{pi/qj} \simeq 1$ and $|K^{de}_R|_{pi/qj} \simeq 0$. In such scenarios the limits for the vector leptoquark mass (and therefore the PS breaking scale) will be significantly decreased due to a reduction in the decay rate with $R_{\text{HU/HS}} < 1$. However this would require the hierarchy

$$\frac{4\,\overline{m}^2_{pq}R^2_{pq}}{m^2_{\ell_j}} < \frac{1}{\kappa} \tag{4.55}$$

implying a difference in the couplings of $X_\mu$ to $f_L$ and $f_R$ of several order of magnitude at least.

The contribution to the decay widths from the PS gauge leptoquark in Eq. (4.42) depends on both the mass of the leptoquark $m_X$ as well as to the different elements of $K^{de}_{L/R}$. These physical mixing matrices are currently unconstrained and different textures within each matrix can significantly change the relative strength of specific lepton flavour decay channels over others for a given meson. As limits and measurements of different processes differ in sensitivity, the limits on the leptoquark mass (and therefore the scale of PS breaking) can vary significantly for different choices of the mixing matrices $K^{de}_{L/R}$.

To demonstrate this, we define general unitary matrices for $K^{de}_{L/R}$,

$$K^{de}_{L/R} = K_{23}(\theta^{L/R}_{23}, \delta^{L/R})\, K_{13}(\theta^{L/R}_{13})\, K_{12}(\theta^{L/R}_{12})$$
$$= \begin{pmatrix} c_{12}\, c_{13} & c_{13}\, s_{12} & s_{13} \\ -c_{23}\, s_{12} - e^{i\delta} c_{12}\, s_{13}\, s_{23} & c_{12}\, c_{23} - e^{i\delta} s_{12}\, s_{13}\, s_{23} & e^{i\delta} c_{13}\, s_{23} \\ -c_{12}\, c_{23}\, s_{13} + e^{-i\delta} s_{12}\, s_{23} & -c_{23}\, s_{12}\, s_{13} - e^{-i\delta} c_{12}\, s_{23} & c_{13}\, c_{23} \end{pmatrix}^{L/R} . \tag{4.56}$$

In principle the matrix $K^{de}_L$ should contain all six possible phases as by convention rephasing of quark and lepton fields fixes the phases appearing in $V^{\text{CKM}}_L$ and $U^{\text{LEPT}}_L$ and therefore no rephasing[11] can occur for $K^{de}_L$ or $K^{u\nu}_L$. However only one complex phase is important for the discussion below and therefore we ignore all other possible complex phases which can appear in $K^{de}_{L/R}$.

Table 4.2 lists the meson decay channels of interest[12] alongside either their measured branching fractions or the current experimental upper limit. Additionally we indicate which two matrix elements of $K^{de}_{L/R}$ are required to be non-zero in order for $X_\mu$ to mediate this process through Fig. 4.2. Note that for lepton-flavour violating decays there are two possible combinations of non-zero matrix elements which mediate a decay which is taken into account in our calculations. It is clear from Table 4.2 that the decays of $K^0_L$ are currently the most experimentally probed channels, with the lepton-flavour violating decay $K^0_L \to \mu e$ having the most sensitive upper limit of any process.

In contrast the current experimental precision for the decays of $B^0_{d/s}$ is, for most channels, significantly weaker and will lead to weaker limits. Therefore the lower mass bound on $X_\mu$ will vary most depending on whether the structure of $K^{de}_{L/R}$ leads to decays of $K^0_L$ or not. A thorough analysis for general unitary matrices similar to Eq. (4.56) for the PS gauge leptoquark has been performed [228] to find what conditions are required on $K^{de}_{L/R}$ in order to suppress the decays of $K^0_L$, either preventing them completely or significantly reducing the predicted decay width by removing the helicity-unsuppressed contribution.

[11] In contrast $K^{de}_R$ could be chosen to contain one complex phase if the other right-handed physical mixing matrices are left as general unitary matrices. However a more natural choice of basis would be to rephase the fields appearing in $V^{\text{CKM}}_R$ and $U^{\text{LEPT}}_R$ in analogy with the left-handed mixing matrices.

[12] All neutral-pesudoscalar mesons will receive a similar contribution however in the cases of other mesons not listed (such as the $\pi^0$, $\eta$, $\eta'$, $\Upsilon$ etc) we find the limits on $m_X$ are subdominant compared to the mesons listed in Table 4.2 when comparing the predicted branching fraction induced by $X_\mu$ compared to the experimental sensitivity.

| Hadronic Process | Measured value or upper limit | $(p,i)(q,j)$ |
|---|---|---|
| $\mathcal{B}(K_L^0 \to ee)$ | $9.0^{+6.0}_{-4.0} \times 10^{-12}$ | (1,1)(2,1) |
| $\mathcal{B}(K_L^0 \to \mu\mu)$ | $6.84^{+0.11}_{-0.11} \times 10^{-12}$ | (1,2)(2,2) |
| $\mathcal{B}(K_L^0 \to \mu e)$ | $< 4.7 \times 10^{-12}$ | (1,2)(2,1)/(1,1)(2,2) |
| $\mathcal{B}(B_d^0 \to ee)$ | $< 8.3 \times 10^{-8}$ | (1,1)(3,1) |
| $\mathcal{B}(B_d^0 \to \mu\mu)$ | $< 3.6 \times 10^{-10}$ | (1,2)(3,2) |
| $\mathcal{B}(B_d^0 \to \tau\tau)$ | $< 2.1 \times 10^{-3}$ | (1,3)(3,3) |
| $\mathcal{B}(B_d^0 \to \mu e)$ | $< 1.0 \times 10^{-9}$ | (1,2)(3,1)/(1,1)(3,2) |
| $\mathcal{B}(B_d^0 \to \tau e)$ | $< 2.8 \times 10^{-5}$ | (1,3)(3,1)/(1,1)(3,3) |
| $\mathcal{B}(B_d^0 \to \tau\mu)$ | $< 2.2 \times 10^{-5}$ | (1,3)(3,2)/(1,2)(3,3) |
| $\mathcal{B}(B_s^0 \to ee)$ | $< 2.8 \times 10^{-7}$ | (2,1)(3,1) |
| $\mathcal{B}(B_s^0 \to \mu\mu)$ | $3.0^{+0.4}_{-0.4} \times 10^{-9}$ | (2,2)(3,2) |
| $\mathcal{B}(B_s^0 \to \tau\tau)$ | $< 6.8 \times 10^{-3}$ | (2,3)(3,3) |
| $\mathcal{B}(B_s^0 \to \mu e)$ | $< 5.4 \times 10^{-9}$ | (2,2)(3,1)/(2,1)(3,2) |
| $\mathcal{B}(B_s^0 \to \tau e)$ | – | (2,3)(3,1)/(2,1)(3,3) |
| $\mathcal{B}(B_s^0 \to \tau\mu)$ | – | (2,2)(3,3)/(3,2)(2,3) |

Table 4.2: Experimental measurements and upper limits on rare leptonic decays of various pseudo-scalar mesons which form the dominant constraint on the scale of Pati-Salam breaking. The third column represents which entries of the matrices $(K^{de}_{L/R})_{pi}$ and $(K^{de}_{L/R})_{qj}$ need to be non-zero for the given decay channel to occur via $X_\mu$ where $p$, $q$ correspond to the valence down-type quarks, $(d, s, b) = (1, 2, 3)$ and $i$, $j$ to the final state charged leptons $(e, \mu, \tau) = (1, 2, 3)$ for the diagram in Fig. 4.2. Lepton-flavour violating decay modes can occur via two different possible diagrams. For example the process $B_d^0 \to \mu e$ can arise from the $(3,1)$ and $(1,2)$ entries which corresponds to the couplings $\bar{b}\not{X}e$ and $\bar{d}\not{X}\mu$ leading to $B_d^0 \to \mu^- e^+$, but can also have a contribution from $(3,2)$ and $(1,1)$ which corresponds to $\bar{b}\not{X}\mu$ and $\bar{d}\not{X}e$ and leads to $B_d^0 \to e^-\mu^+$.

Two possible scenarios were found. Firstly if

$$\theta^L_{23} = \theta^R_{23} = \frac{\pi}{2}, \quad \theta^L_{13} = \theta^R_{13} = \theta, \quad \delta^L = \delta \quad \text{and} \quad \delta^R = \pi - \delta \tag{4.57}$$

is satisfied by Eq. (4.56), this leads to

$$K^{de}_L = \begin{pmatrix} c^L_{12}\, c_\theta & s^L_{12}\, c_\theta & s_\theta \\ -e^{i\delta} c^L_{12}\, s_\theta & -e^{i\delta} s^L_{12}\, s_\theta & e^{i\delta} c_\theta \\ e^{-i\delta} s^L_{12} & -e^{-i\delta} c^L_{12} & 0 \end{pmatrix} \text{ and } K^{de}_R = \begin{pmatrix} c^R_{12}\, c_\theta & s^R_{12}\, c_\theta & s_\theta \\ e^{-i\delta} c^R_{12}\, s_\theta & e^{-i\delta} s^R_{12}\, s_\theta & -e^{-i\delta} c_\theta \\ -e^{i\delta} s^R_{12} & e^{i\delta} c^R_{12} & 0 \end{pmatrix}. \tag{4.58}$$

These matrix structures will not completely prevent the decays of $K_L^0$. However, they will prevent the helicity-unsuppressed terms from contributing and therefore will be suppressed by the final-state lepton masses similar to weak decays in the SM. Note that all the entries of the upper-left $2 \times 2$ block of $K^{de}_{L/R}$ are non-zero, but an important cancellation in the amplitude arises as $\delta^{L/R}$ are exactly out of phase. Additionally the $(3,3)$ entry of both matrices is zero and therefore for this scenario the decays $B^0_d \to \tau\tau$ and $B^0_s \to \tau\tau$ cannot occur. Interestingly, if $\delta$ is maximally CP violating then the helicity unsuppressed contribution completely disappears and therefore there is no contribution to the decay of $K^0_L$, whereas the helicity-suppressed contribution to this decay is maximised for CP conserving choices for $\delta$.

Alternatively the desired decays can be completely prevented with the simple condition

$$\theta^L_{13} = \theta^R_{13} = \frac{\pi}{2} \tag{4.59}$$

which leads to

$$K^{de}_{L/R} = \begin{pmatrix} 0 & 0 & 1 \\ -c_{23}\, s_{12} - e^{i\delta} c_{12}\, s_{23} & c_{12}\, c_{23} - e^{i\delta} s_{12}\, s_{23} & 0 \\ -c_{12}\, c_{23} + e^{-i\delta} s_{12}\, s_{23} & -c_{23}\, s_{12} - e^{-i\delta} c_{12}\, s_{23} & 0 \end{pmatrix}^{L/R} . \tag{4.60}$$

Here the decays of $K^0_L$ trivially do not occur as both the $(1,1)$ and $(1,2)$ entries of $K^{de}_{L/R}$ are exactly zero and, as can be seen in Table 4.2, $X_\mu$ will not mediate the relevant decays. Similar to the previous scenario the decays $B^0_d \to \tau\tau$ and $B^0_s \to \tau\tau$ do not occur. Additionally, the processes $B^0_d \to (ee,\, \mu\mu,\, \tau e)$ and $B^0_s \to (\tau e,\, \tau\mu)$ will not occur as the $(2,3)$ entry is also zero. Therefore, for low-scale PS, the suppressed decay channels for $B^0_{d/s} \to \tau\tau$ are directly correlated with suppressed decays of $K^0_L$. Increasing the experimental sensitivity of these channels could therefore provide a powerful test of PS, especially if a non-SM signal was detected in these channels as no such signal has been seen in the decays of $K^0_L$.

In both scenarios above which lead to the lowest possible limits on the PS gauge leptoquark, the matrices $K^{de}_L$ and $K^{de}_R$ are required to have a similar structure to each other. The first scenario allows for only four free parameters between the two matrices whereas in the second scenario six free parameters exist. In order for both these matrices (which are naïvely unrelated) to have the same structure suggests that a parity symmetry must be enforced at some scale. The two matrices do not have to be exactly equal to each other, although this is also possible. However in both scenarios at least one angle has to be identical for both matrices. As discussed previously it has been found that enforcing a parity symmetry alongside the PS gauge groups requires parity to be broken at $\mathcal{O}(10^{12})$ GeV or higher [200, 215]. As we are interested in minimising the scale of PS breaking it would seem quite coincidental for both $K_L^{de}$ and $K_R^{de}$ to be so similar at low scales (and rather unlikely for them to be exactly equal) with such a high scale of parity breaking. However, this requires a full analysis of the running of the relevant mixing angles which we will not explore further. It may be possible that at some high scale $K_{L/R}^{de}$ are equal to each other and after parity breaking some angles are insensitive to running effects whereas others run significantly, leading to the desired form for the mixing matrices.

In addition to the two scenarios above which completely prevent $X_\mu$ from inducing decays of $K_L^0$ we identify two additional scenarios which would prevent the LFV decay $K_L^0 \to \mu e$ but not necessarily the decays $K_L^0 \to ee$ or $K_L^0 \to \mu\mu$. For example if the conditions

$$\theta_{12}^L = \theta_{12}^R = 0 \quad \text{and} \quad \theta_{23}^L = \theta_{23}^R = \frac{\pi}{2} \tag{4.61}$$

are satisfied, this leads to

$$K_{L/R}^{de} = \begin{pmatrix} c_{13} & 0 & s_{13} \\ -e^{i\delta} s_{13} & 0 & e^{i\delta} c_{13} \\ 0 & -e^{-i\delta} & 0 \end{pmatrix}^{L/R} , \tag{4.62}$$

and the decays $K_L^0 \to \mu e$ and $K_L^0 \to \mu\mu$ do not occur via $X_\mu$. However the decay $K_L^0 \to ee$ does occur as suggested by Table 4.2. Similarly if

$$\theta_{12}^L = \theta_{12}^R = \frac{\pi}{2} \quad \text{and} \quad \theta_{23}^L = \theta_{23}^R = \frac{\pi}{2} \tag{4.63}$$

is satisfied, this leads to

$$K_{L/R}^{de} = \begin{pmatrix} 0 & c_{13} & s_{13} \\ 0 & -e^{i\delta} s_{13} & e^{i\delta} c_{13} \\ e^{-i\delta} & 0 & 0 \end{pmatrix}^{L/R} . \tag{4.64}$$

The decays $K_L^0 \to \mu e$ and $K_L^0 \to ee$ will not occur, but $K_L^0 \to \mu\mu$ will, forming a strong constraint on the mass of $X_\mu$.

Finally as the decay channel $K_L^0 \to \mu e$ is currently the most precisely constrained of all relevant meson decay channels the *largest* lower bound on the mass of $X_\mu$ will occur for $K_{L/R}^{de}$ which have a form that maximises this particular decay channel. Table 4.2, which indicates which entries of $K_{L/R}^{de}$ mediate this decay, suggests that if for example the mixing matrices were given by

$$K_{L/R}^{de} = \begin{pmatrix} 1 & 0 & 0 \\ 0 & 1 & 0 \\ 0 & 0 & 1 \end{pmatrix} \tag{4.65}$$

then the contribution to this decay channel would be maximised. Therefore the current mass limits on the PS gauge leptoquark (and the breaking scale) can fluctuate between the mass limits obtained if the mixing matrices are given by Eqs. (4.58) and (4.60) up to the limits obtained if the matrices are given by Eq. (4.65).

In order to numerically find the lower-bound mass range for $X_\mu$ we fix the values of the total decay width of each relevant meson to the experimentally observed central values

$$\Gamma_{K_L^0}^{\text{TOT}} = 1.29 \times 10^{-17}\ \text{GeV}, \quad \Gamma_{B_d^0}^{\text{TOT}} = 4.33 \times 10^{-13}\ \text{GeV} \quad \text{and} \quad \Gamma_{B_s^0}^{\text{TOT}} = 4.36 \times 10^{-13}\ \text{GeV}, \tag{4.66}$$

which we take from the PDG [229]. The parameter $R_{pq}$ which appears in the helicity-unsuppressed contribution to a given decay and is defined in Eq. (4.49) requires running from the scale $\mu = m_X$ down to $\mu = m_{M_{pq}}$ and the gauge coupling constant $g_4$ is related to the strong coupling constant at the scale of PS breaking:

$$\begin{aligned} g_4(m_X) = g_c(m_X) &= 2\sqrt{\pi}\left(\frac{17}{2} + \frac{7}{2\pi}\log\left[\frac{m_X}{90}\right]\right)^{-1/2} \\ R_{K_L^0} &\simeq 0.51\left(\frac{17}{2} + \frac{7}{2\pi}\log\left[\frac{m_X}{90}\right]\right)^{4/7} \\ R_{B_s^0} \simeq R_{B_d^0} &\simeq 0.37\left(\frac{17}{2} + \frac{7}{2\pi}\log\left[\frac{m_X}{90}\right]\right)^{4/7} \end{aligned} \tag{4.67}$$

where $m_X$ is in units of GeV and for simplicity we assume the one-loop SM running of the gauge coupling constant $g_c$ which can be found in Appendix E. We calculate lower bound limits on the leptoquark mass by numerically solving Eqs. (4.42) and (4.67) as a function of the leptoquark mass and comparing to the experimental limits listed in Table 4.2.

Table 4.3 shows the calculated lower bound on the gauge leptoquark masses for the relevant decay channel with different choices of $K^{de}_{L/R}$ corresponding to the five scenarios above. Maximising the leptoquark's contribution to $K^0_L \to \mu e$ as in Eq. (4.65) leads to limits on the gauge leptoquark mass of roughly 2500 TeV, similar to previous studies [214, 225, 227]. The other non-zero decays in this case indicate which other channels will occur in this scenario: $B^0_d \to \tau e$ and $B^0_s \to \tau\mu$. More realistically we would expect the matrices $K^{de}_{L/R}$ to be approximately diagonal rather than exactly, and therefore other processes which are listed would also be mediated by $X_\mu$, but the three listed would have the strongest signals.

If $K^{de}_{L/R}$ is of the form described in Eq. (4.58), decays of $K^0_L$ still occur but are helicity suppressed. This reduces the limits obtained from 2500 TeV down to $\mathcal{O}(100)$ TeV (with some sensitivity to the free mixing angles) where notably the channel $K^0_L \to ee$ leads to limits on the gauge leptoquark mass of $\mathcal{O}(10)$ TeV. This significant reduction compared to other channels of $K^0_L$ is due to the helicity-suppression of electron final states being significantly larger than for muon final states. For this scenario neglecting the electron and muon mass, as was done in [228], would suggest that $X_\mu$ does not mediate $K^0_L$ decays. However, we find when included they lead to comparable limits for $m_X$ to the helicity-unsuppressed $B^0_d$ and $B^0_s$ decays. This is due to the larger experimental precision obtained for $K^0_L$ decays and therefore we find that the muon mass cannot be ignored. As mentioned previously, if $\delta$ is maximally violating the helicity-unsuppressed decays of $K^0_L$ are forbidden and in this limit the results of [228] remain valid.

If the mixing matrices are given by Eq. (4.60), decays of $K^0_L$ do not occur via $X_\mu$ either helicity-suppressed or -unsuppressed. Only five decay channels are non-zero in this scenario and the dominant mass limit will arise from decays of $B^0_s$ and are of similar order to the previous scenario: $m_X \sim \mathcal{O}(100)$ TeV. The final two scenarios described by Eqs. (4.62) and (4.64) completely suppress the channel $K^0_L \to \mu e$ but does not suppress the lepton-flavour conserving channels of $K^0_L$. Here the resulting mass limits are $\mathcal{O}(1900)$ TeV unless the mixing angles in $\kappa$ were significantly tuned (e.g. $\theta^L_{12} \simeq -\theta^R_{12}$) in order to suppress these channels. In all cases the last two channels $B^0_s \to \tau e$ and $B^0_s \to \tau\mu$ are currently unconstrained by measurement and therefore do not lead to limits on $m_X$. In cases were a scenario predicts a contribution to these channels, future measurement will be a relevant constraint which we indicate in Table 4.3 by '$-$'.

| | $K_L^{de} = K_R^{de} = \mathbb{1}_{3\times 3}$ | SCENARIO 1 | SCENARIO 2 | SCENARIO 3 | SCENARIO 4 |
|---|---|---|---|---|---|
| $\mathcal{B}(K_L^0 \to ee)$ | 0 | $13\,\kappa_1^{Kee}$ TeV | 0 | $1817\,\kappa_3^{Kee}$ TeV | 0 |
| $\mathcal{B}(K_L^0 \to \mu\mu)$ | 0 | $177\,\kappa_1^{K\mu\mu}$ TeV | 0 | 0 | $1900\,\kappa_4^{K\mu\mu}$ TeV |
| $\mathcal{B}(K_L^0 \to \mu e)$ | 2467 TeV | $230\,\kappa_1^{K\mu e}$ TeV | 0 | 0 | 0 |
| $\mathcal{B}(B_d^0 \to ee)$ | 0 | $39.7\,\kappa_1^{Bee}$ TeV | 0 | 0 | 0 |
| $\mathcal{B}(B_d^0 \to \mu\mu)$ | 0 | $151\,\kappa_1^{B\mu\mu}$ TeV | 0 | 0 | 0 |
| $\mathcal{B}(B_d^0 \to \tau\tau)$ | 0 | 0 | 0 | 0 | 0 |
| $\mathcal{B}(B_d^0 \to \mu e)$ | 0 | $140\,\kappa_1^{B\mu e}$ TeV | 0 | $140\,\kappa_3^{B\mu e}$ TeV | $140\,\kappa_4^{B\mu e}$ TeV |
| $\mathcal{B}(B_d^0 \to \tau e)$ | 12.1 TeV | $10.6\,\kappa_1^{B\tau e}$ TeV | $10.6\,\kappa_2^{B\tau e}$ TeV | 0 | $10.6\,\kappa_4^{B\tau e}$ TeV |
| $\mathcal{B}(B_d^0 \to \tau\mu)$ | 0 | $11.3\,\kappa_1^{B\tau\mu}$ TeV | $11.3\,\kappa_2^{B\tau\mu}$ TeV | $11.3\,\kappa_3^{B\tau\mu}$ TeV | 0 |
| $\mathcal{B}(B_s^0 \to ee)$ | 0 | $29.5\,\kappa_1^{B_s^{ee}}$ TeV | $29.5\,\kappa_2^{B_s^{ee}}$ TeV | 0 | 0 |
| $\mathcal{B}(B_s^0 \to \mu\mu)$ | 0 | $90.0\,\kappa_1^{B_s^{\mu\mu}}$ TeV | $90.0\,\kappa_2^{B_s^{\mu\mu}}$ TeV | 0 | |
| $\mathcal{B}(B_s^0 \to \tau\tau)$ | 0 | 0 | 0 | 0 | 0 |
| $\mathcal{B}(B_s^0 \to \mu e)$ | 0 | $92.3\,\kappa_1^{B_s^{\mu e}}$ TeV | $92.3\,\kappa_2^{B_s^{\mu e}}$ TeV | $92.3\,\kappa_3^{B_s^{\mu e}}$ TeV | $92.3\,\kappa_4^{B_s^{\mu e}}$ TeV |
| $\mathcal{B}(B_s^0 \to \tau e)$ | 0 | – | 0 | 0 | – |
| $\mathcal{B}(B_s^0 \to \tau\mu)$ | – | – | 0 | – | 0 |

TABLE 4.3: Limits on the gauge leptoquark mass $m_X$ compared to current measurements (or upper limits) for the mesons $K_L^0$, $B_d^0$ and $B_s^0$. Each column represents different choices for the matrices $K_{L/R}^{de}$ where scenarios 1-4 are given by Eqs. (4.58), (4.60), (4.62) and (4.64) respectively. Each scenario corresponds to possible structures of the mixing matrices which would in some way suppress the decays of $K_L^0$. In scenario 1 the decays to $K_L^0$ are non-zero albeit helicity-suppressed, leading to mass limits similar to what is obtained from decays of $B_d^0$ and $B_s^0$. Scenario 2 completely suppresses the decays of $K_L^0$ and the most significant mass limits now come from the decays of $B_s^0$. Scenario 3 and 4 correspond to examples of mixing matrices which would suppress the decay channel $K_L^0 \to \mu e$ but not $K_L^0 \to ee$ or $K_L^0 \to \mu\mu$ which would form the dominant limit. The first column represents a scenario which maximises the rate of $K_L^0 \to \mu e$ decays leading to the largest mass limit on $X_\mu$. In all the scenarios above the parameter $\kappa_\alpha^X$ corresponds to the combination of mixing angles relevant to that decay chain. We find the lower bound on the PS breaking scale to be no smaller than $\mathcal{O}(100)$ TeV. For the final two channels $B_s^0 \to \tau e/\tau\mu$ there are currently no measured upper bounds, however non-zero contributions to these channels are indicated by '–' and their future measurement will form a constraint for a given choice of $K_{L/R}^{de}$.

For simplicity, the interference between the SM and PS contributions to the decay channels with lepton-flavour conserving final states has not been calculated. As the PS contribution to the decay rate is inversely proportional to the fourth power of $m_X$, the decay rate will decrease by orders of magnitude for small increases in $m_X$. The derived lower bound on $m_X$ from such channels should be understood as a conservative lower bound and will slightly change by order one factors once the SM contribution is incorporated. Obviously when the dominant limit arises from a LFV decay channel no such interference occurs and the derived limit can be considered even more robust.

In all cases, non-zero decay channels listed in Table 4.3 come with factors of $\kappa$ corresponding to the combination of mixing angles arising from $K^{de}_{L/R}$. These expressions, particularly in the cases of scenario 1 and 2, are quite complicated due to the large number of free parameters allowed. Therefore minimising the decay widths as a function of the free mixing angles is difficult. Instead, we perform a numerical scan of the free parameters in order to estimate the maximum and minimum lower bound on the mass of $X_\mu$ for a given scenario.

Tables 4.4 and 4.5 explicitly calculate the leptoquark mass limits for different choices of the mixing angles appearing in scenario 1 and 2 ordered from largest to smallest limits. The limit on the leptoquark mass varies for different choices but not significantly. The decay channel which forms the dominant constraint also varies for different choices of angles, which we indicate. A numerical scan over the parameter space shows that for scenario 1 the mass limits on $X_\mu$ vary from $81 - 177$ TeV for different values of the mixing angles. The fourth entry of Table 4.4 is a benchmark taken from [228] who found in their case a lower bound mass limit of 86 TeV compared to the 117 TeV we find. In their analysis they neglected the final-state muon mass and therefore assumed no induced decays of $K^0_L$ from $X_\mu$, whereas we find, when included, it forms the dominant constraint. When neglected we find a limit of 84 TeV from the process $B^0_{d/s} \to \mu\mu$ in full agreement with [228]. For Table 4.4 we find that, though helicity-suppressed, decays of $K^0_L$ are important to consider for PS breaking limits. For the case of scenario 2 we conducted a similar scan of parameters and found the mass limits on $X_\mu$ varies roughly from $84 - 102$ TeV as indicated by Table 4.5.

| SCENARIO 1 | Limit on $m_X$ | Dominant channel |
|---|---|---|
| $\theta_{12}^L = \frac{3\pi}{2}$, $\theta_{12}^R = 2\pi$, $\theta = \frac{7\pi}{4}$, $\delta = \pi$ | 177 TeV | $K_L^0 \to \mu\mu$ |
| $\theta_{12}^L = \frac{\pi}{4}$, $\theta_{12}^R = \frac{\pi}{4}$, $\theta = \frac{\pi}{4}$, $\delta = 0$ | 164 TeV | $K_L^0 \to \mu e$ |
| $\theta_{12}^L = \frac{\pi}{2}$, $\theta_{12}^R = \frac{\pi}{8}$, $\theta = 0$, $\delta = \frac{\pi}{2}$ | 145 TeV | $B_d^0 \to \mu\mu$ |
| $\theta_{12}^L = 0$, $\theta_{12}^R = 0.81$, $\theta = 1.183$, $\delta = 0$ | 117 TeV | $K_L^0 \to \mu e$ |
| $\theta_{12}^L = \frac{\pi}{4}$, $\theta_{12}^R = \frac{\pi}{4}$, $\theta = \frac{\pi}{4}$, $\delta = \frac{\pi}{2}$ | 107 TeV | $B_d^0 \to \mu\mu$ |
| $\theta_{12}^L = 2.06$, $\theta_{12}^R = 2.4$, $\theta = 5.11$, $\delta = 4.58$ | 81 TeV | $B_s^0 \to \mu e$ |

TABLE 4.4: Limits obtained for the gauge leptoquark mass $X_\mu$ for different choices of the mixing angles appearing in Eq. (4.58) ordered from largest to smallest. The decay process from which the dominant limit arises is also listed. In some cases, even though it is helicity-supressed, the dominant limit will still arise from $K_L^0$ decays. The angles in the fourth row were first used in [228] from which they obtained a limit of 86 TeV from $B_{d/s}^0 \to \mu\mu$ when the muon and electron mass were neglected. We find similar limits however we highlight the importance of including the muon mass as the channel $K_L^0 \to \mu e$ still forms the dominant limit for this scenario. A numerical scan finds the limits in this scenario can vary from $81 - 177$ TeV.

| SCENARIO 2 | Limit on $m_X$ | Dominant channel |
|---|---|---|
| $\theta_{12}^L = 2.4$, $\theta_{12}^R = 2.3$, $\theta_{23}^L = \frac{\pi}{2}$, $\theta_{23}^R = 0$, $\delta^L = 2\pi$, $\delta^R = 2.77$ | 102 TeV | $B_s^0 \to \mu e$ |
| $\theta_{12}^L = \frac{\pi}{9}$, $\theta_{12}^R = \frac{\pi}{2}$, $\theta_{23}^L = 1$, $\theta_{23}^R = 0$, $\delta^{L/R} = 0$ | 100 TeV | $B_s^0 \to \mu e$ |
| $\theta_{12}^L = \frac{\pi}{3}$, $\theta_{12}^R = \frac{\pi}{6}$, $\theta_{23}^L = \frac{\pi}{2}$, $\theta_{23}^R = 1$, $\delta^{L/R} = 0$ | 92 TeV | $B_s^0 \to \mu\mu$ |
| $\theta_{12}^L = \frac{\pi}{3}$, $\theta_{12}^R = \frac{\pi}{6}$, $\theta_{23}^L = \frac{\pi}{2}$, $\theta_{23}^R = 1$, $\delta^{L/R} = \frac{\pi}{2}$ | 86 TeV | $B_s^0 \to \mu\mu$ |
| $\theta_{12}^L = \frac{\pi}{4}$, $\theta_{12}^R = \frac{\pi}{8}$, $\theta_{23}^L = 0$, $\theta_{23}^R = 0$, $\delta^{L/R} = 0$ | 85 TeV | $B_s^0 \to \mu e$ |
| $\theta_{12}^L = 0.72$, $\theta_{12}^R = 3.05$, $\theta_{23}^L = 4.02$, $\theta_{23}^R = 2\pi$, $\delta^L = 0$, $\delta^R = \frac{3\pi}{2}$ | 84 TeV | $B_s^0 \to \mu e$ |

TABLE 4.5: Limits obtained for the gauge leptoquark mass $X_\mu$ for some different choices of mixing angles appearing in Eq. (4.60) ordered from largest to smallest. The decay process from which the dominant limit arises is also listed. Here the decays of $K_L^0$ are completely forbidden and the dominant limit will always arise either from $B_s^0 \to \mu\mu$ or $B_s^0 \to \mu e$. Through a numerical scan we find the mass of the PS leptoquark varies between roughly $84 - 102$ TeV depending on different choices of mixing angles, a much closer range compared to the results of Scenario 2.

### 4.3.2 Fermion mass degeneracy

Although the dominant constraint on the PS breaking scale arises from pseudoscalar meson decays, a secondary requirement for a viable Pati-Salam model is to address the lack of mass degeneracy between fermion pairs with the same $SU(2)_{L/R}$ isospin. As

| | $\mu = m_Z$ | $\mu = 1$ TeV | $\mu = 10$ TeV | $\mu = 100$ TeV | $\mu = 1000$ TeV |
|---|---|---|---|---|---|
| $m_e/m_d$ | 0.177 | 0.205 | 0.230 | 0.251 | 0.271 |
| $m_\mu/m_s$ | 1.891 | 2.195 | 2.454 | 2.688 | 2.902 |
| $m_\tau/m_b$ | 0.612 | 0.724 | 0.823 | 0.913 | 0.997 |

TABLE 4.6: Measured mass ratios $m_e/m_d$ for each generation at fixed energy scales $\mu$ at one-loop and assuming SM running of the Yukawas. Additional details of the running calculations performed can be found in Appendix E.

indicated by Eq. (4.17) the simplest PS models lead to the fermion mass relations

$$m_d = m_e \qquad \text{and} \qquad m_u = m_\nu^{\text{Dirac}} \tag{4.68}$$

for all three generations of SM fermions.

Comparing this prediction to the measured masses of the down-isospin fermions shown in Table 4.6 for the different generations at different energy scales demonstrates that this tree-level relation must be broken. As discussed previously, the mass relation between the up-isospin components can be easily broken due to seesaw mixing in the neutral fermion sector as demonstrated in Section 4.2.2. In the case of the down-isospin components, with no additional particle content, the mass relation is unbroken at tree level and holds at the scale of PS breaking. In scenarios where PS is broken at high scales, this relation could potentially be viable as threshold effects as well as renormalisation group running can potentially be sufficient to explain the observed mass differences of the different generations. PS breaking scales as low as $\mathcal{O}(1000)$ TeV can explain the bottom and tau lepton mass differences [230] as the two Yukawa couplings unify at around this scale. It therefore could be possible for high-scale PS models to explain the mass differences between all three generations in the same way. Table 4.6 shows that for PS breaking scales below 1000 TeV the different generations of down-quark and charged-lepton Yukawa couplings cannot be equal at the PS breaking scale and therefore there should be some tree-level explanation for their difference.

The mass relations can be broken at tree level by the existence of additional particle content, either scalar or fermion, necessarily transforming as complete PS multiplets above the scale of PS breaking. For example, the inclusion of a scalar $(\mathbf{15}, \mathbf{2}, \mathbf{2})$ Higgs particle, sometimes referred to as the Minimal Quark-Lepton Symmetric Model (MQLS), which has a non-zero vev will induce a Georgi-Jarlskog like texture [231] lifting the degeneracy between the down quark and charged lepton masses [115, 116]. The additional Yukawa couplings results in enough freedom such that the mass ratios measured and shown in Table 4.6 can arise.

We explore an alternative possibility first noted in [201, 202] where additional anomaly-free fermion multiplets transforming under the PS gauge group are introduced. If the additional multiplets contain components with the same quantum numbers as the down quarks or charged leptons, mixing effects could induce a see-saw which can decouple the down-quark and charged-lepton Yukawas, breaking the tree-level mass relations obtained without their inclusion. In this scenario, both the up- and down-isospin components have their PS mass relations broken due to see-saw effects, so the breaking of the mass relations between all SM fermions is explained by a similar mechanism.

An additional consequence of introducing extra fermionic states is that they can cause the gauge boson leptoquark $X_\mu$ to couple in a chiral-like way to the light SM-like fermions. As an example, consider the introduction of the fermion multiplets $F_{L/R}$ that contain components $E^-_{L/R}$ that have the same quantum numbers as the SM charged leptons:

$$f_{L/R} = \begin{pmatrix} u_r & d_r \\ u_b & d_b \\ u_g & d_g \\ \nu_e & e \end{pmatrix}_{L/R} \quad \oplus \quad F_{L/R} = \begin{pmatrix} & \cdots & & \\ \vdots & \ddots & & \\ & & E^-_{L/R} & \\ & & & \ddots \end{pmatrix}. \tag{4.69}$$

Here both $E^-_L$ and $E^-_R$ are required phenomenologically such that no massless charged fermion states appear and the exotic multiplets $F_L$ and $F_R$ need not transform in the same way. However, the combination must be anomaly free.

If Yukawa interactions connecting the multiplets $F_{L/R}$ and $f_{L/R}$ exist, mass mixing will be induced as per

$$\mathcal{L}_{eE} = \begin{pmatrix} \overline{e_L} & \overline{E_L} \end{pmatrix} \begin{pmatrix} m_{ee} & m_{eE} \\ m_{Ee} & m_{EE} \end{pmatrix} \begin{pmatrix} e_R \\ E_R \end{pmatrix} + \text{H.c.} \tag{4.70}$$

Diagonalising into the mass basis for the charged fermions leads to

$$(e'_{L/R})_\ell = c_{\theta_{L/R}} e_{L/R} + s_{\theta_{L/R}} E_{L/R} \qquad (E'_{L/R})_\hbar = -s_{\theta_{L/R}} e_{L/R} + c_{\theta_{L/R}} E_{L/R} \tag{4.71}$$

where the subscripts $\ell$ and $\hbar$ indicate the light and heavy eigenstates respectively. The pseudoscalar meson decays discussed above are induced by the gauge leptoquark interactions between the colour triplet $d$ and charged lepton $e$ from the multiplet $f_{L/R}$.

Expanding Eq. (4.39) with Eq. (4.71) leads to

$$\mathcal{L}_{Xde} = \frac{g_4}{\sqrt{2}}\left(\overline{d'}\, K_L^{de}\, \not{X} P_L(c_{\theta_L} e' - s_{\theta_L} E')) + \overline{d'}\, K_R^{de}\, \not{X} P_R(c_{\theta_R} e' - s_{\theta_R} E')\right) + \text{ H.c} \quad (4.72)$$

for the gauge interactions in the mass basis where generational indices have been suppressed for simplicity. Because of phenomenological constraints, any exotic fermions with SM quantum numbers must be significantly heavier than the pseudoscalar mesons whose decays supply the dominant constraint on PS breaking; therefore, processes such as $K_L^0 \to EE$ or $K_L^0 \to eE$ are kinematically forbidden. The decay $K_L^0 \to ee$ will exist as before, but now suppressed by the relevant mass mixing angles. Therefore the only relevant interactions in Eq. (4.72) for meson decay are

$$\mathcal{L}_{Xde} \supset \frac{g_4}{\sqrt{2}}\left(\overline{d'}\,(c_{\theta_L} K_L^{de})\, \not{X} P_L e' + \overline{d'}\,(c_{\theta_R} K_R^{de})\, \not{X} P_R e'\right) + \text{ H.c} \quad (4.73)$$

which will lead to a decay rate given by Eqs. (4.51) and (4.53) with the replacement $K_{L/R}^{de} \to \mathcal{K}_{L/R}^{de} = c_{\theta_{L/R}} K_{L/R}^{de}$. As the mixing angles $\theta_L$ and $\theta_R$ can significantly differ, this can effectively lead to a chiral coupling between $X_\mu$ and the fermions $d$ and $e$ causing a suppression in the helicity-unsupressed contribution of the total meson decay rates in Eq. (4.42). This therefore allows for an overall weaker lower bound on the leptoquark mass compared to those in Table 4.3 and therefore the scale of PS breaking. As noted previously, however, in order to significantly helicity-suppress the decays mediated by $X_\mu$, one of the angles $\theta_{L/R}$ is required to be very small e.g. $\theta_R \lesssim 10^{-4}$ in the case of $K_L^0 \to \mu e$ decays.

Table 4.7 demonstrates the impact this can have on the mass limits in the extreme case of an exactly chiral theory ($m_E \to \infty$) where for example $c_{\theta_L} = 1$ and $c_{\theta_R} = 0$ for all three generations[13], assuming the same matrix textures for $K_{L/R}^{de}$ as in Table 4.3. The leptoquark mass limits are significantly lowered compared to Table 4.3 as the helicity

[13] These limits are also valid for scenarios where quark-lepton unification occurs for only one chirality of fermions, e.g. a gauge group given by $SU(4)_L \otimes SU(3)_R \otimes SU(2)_L \otimes SU(2)_R \to SU(3)_c \otimes SU(2)_L \otimes SU(2)_R$ where the vector leptoquark $X$ couples to only one chirality of fermions.

| | $K_L^{de} = \mathbb{1}_{3\times 3}$ | SCENARIO 1 | SCENARIO 2 | SCENARIO 3 | SCENARIO 4 |
|---|---|---|---|---|---|
| $\mathcal{B}(K_L^0 \to ee)$ | 0 | $13\,\kappa_1^{Kee}$ TeV | 0 | $13\,\kappa_3^{Kee}$ TeV | 0 |
| $\mathcal{B}(K_L^0 \to \mu\mu)$ | 0 | $177\,\kappa_1^{K\mu\mu}$ TeV | 0 | 0 | $177\,\kappa_4^{K\mu\mu}$ TeV |
| $\mathcal{B}(K_L^0 \to \mu e)$ | 194 TeV | $230\,\kappa_1^{K\mu e}$ TeV | 0 | 0 | 0 |
| $\mathcal{B}(B_d^0 \to ee)$ | 0 | $0.2\,\kappa_1^{Bee}$ TeV | 0 | 0 | 0 |
| $\mathcal{B}(B_d^0 \to \mu\mu)$ | 0 | $10.8\,\kappa_1^{B\mu\mu}$ TeV | 0 | 0 | 0 |
| $\mathcal{B}(B_d^0 \to \tau\tau)$ | 0 | 0 | 0 | 0 | 0 |
| $\mathcal{B}(B_d^0 \to \mu e)$ | 0 | $10.0\,\kappa_1^{B\mu e}$ TeV | 0 | $10.0\,\kappa_3^{B\mu e}$ TeV | $10.0\,\kappa_4^{B\mu e}$ TeV |
| $\mathcal{B}(B_d^0 \to \tau e)$ | 2.7 TeV | $3.2\,\kappa_1^{B\tau e}$ TeV | $3.2\,\kappa_2^{B\tau e}$ TeV | 0 | $3.2\,\kappa_4^{B\tau e}$ TeV |
| $\mathcal{B}(B_d^0 \to \tau\mu)$ | 0 | $3.2\,\kappa_1^{B\tau\mu}$ TeV | $3.2\,\kappa_2^{B\tau\mu}$ TeV | $3.2\,\kappa_3^{B\tau\mu}$ TeV | 0 |
| $\mathcal{B}(B_s^0 \to ee)$ | 0 | $0.2\,\kappa_1^{B_s^{ee}}$ TeV | $0.2\,\kappa_2^{B_s^{ee}}$ TeV | 0 | 0 |
| $\mathcal{B}(B_s^0 \to \mu\mu)$ | 0 | $6.5\,\kappa_1^{B_s^{\mu\mu}}$ TeV | $6.5\,\kappa_2^{B_s^{\mu\mu}}$ TeV | 0 | |
| $\mathcal{B}(B_s^0 \to \tau\tau)$ | 0 | 0 | 0 | 0 | 0 |
| $\mathcal{B}(B_s^0 \to \mu e)$ | 0 | $6.7\,\kappa_1^{B_s^{\mu e}}$ TeV | $6.7\,\kappa_2^{B_s^{\mu e}}$ TeV | $6.7\,\kappa_3^{B_s^{\mu e}}$ TeV | $6.7\,\kappa_4^{B_s^{\mu e}}$ TeV |
| $\mathcal{B}(B_s^0 \to \tau e)$ | 0 | – | 0 | 0 | – |
| $\mathcal{B}(B_s^0 \to \tau\mu)$ | – | – | 0 | – | 0 |

TABLE 4.7: Limits on the gauge leptoquark mass $m_X$ compared to current measurements (or upper limits) for the mesons $K_L^0$, $B_d^0$ and $B_s^0$ in the chiral limit (e.g. $c_{\theta_R} = 0$) where all decays are now helicity suppressed. Each scenario is given by Eqs. (4.58), (4.60), (4.62) and (4.64) respectively. As *all* decays are now helicity-suppressed, the dominant decay channel in scenario 1 will now arise from $K_L^0 \to \mu e$ (unless forbidden by a specific choice of $\kappa$). As Scenario 2 completely suppresses the decays of $K_L^0$ and now the decays of $B_{d/s}^0$ are helicity-suppressed, the limits on the leptoquark mass quite substantially decrease. Similarly the limits from scenarios 3 are significantly reduced. In particular scenario 3 allows for incredibly low mass scales due to the large helicity-suppression present for electron final-states. The first column represents a scenario which maximises the rate of $K_L^0 \to \mu e$ decays leading to the largest mass limit on $X_\mu$ which in this case is roughly 200 TeV. In all the scenarios above the parameter $\kappa_\alpha^X$ corresponds to the combination of mixing angles relevant to that decay chain. We find the lower bound on the PS breaking scale to be no smaller than $\mathcal{O}(10)$ TeV. For the final two channels $B_s^0 \to \tau e/\tau\mu$ there are currently no measured upper bounds, however non-zero contributions to these channels are indicated by '–' and their future measurement will form a constraint for a given choice of $K_{L/R}^{de}$.

unsuppressed contribution from Eq. (4.51) no longer contributes and therefore the decay rate is suppressed by the charged lepton masses. Scenario 1, which already had helicity-suppressed $K_L^0$ decays, will have its limits largely unchanged except for when the dominant channel arises from $B^0_{d/s}$. If there are no contributions to the decays of $K_L^0$, as in scenario 2, then the helicity suppression on the other decay channels allows for PS breaking scales as low as $\mathcal{O}(10)$ TeV. Interestingly, in these scenarios with a chiral-like coupled $X_\mu$, if there is a significant contribution to $K_L^0 \to ee$, then the limits are significantly reduced compared to the reduction for the processes $K_L^0 \to \mu\mu[\mu e]$ due to the much larger helicity-suppression present for the electron compared to the muon. Therefore with the presence of exotic fermion multiplets, a signficant contribution to $K_L^0$ decays can be possible with small leptoquark masses provided it only couples $K_L^0$ to electrons. This is unlike the case without mass mixing where any induced decay for $K_L^0$ by $X_\mu$ causes mass limits larger than 1000 TeV irrespective of the final decay product. In such a chiral scenario only one of $K_L^{de}$ and $K_R^{de}$ is required to have a matrix structure given by each indicated scenario as the other is significantly suppressed through seesaw effects. Therefore for scenarios involving charged-lepton or down-quark seesaws, $K^{de}_{L/R}$ do not need to be related and therefore no parity symmetry needs to be imposed at a high scale.

In Tables 4.8 and 4.9 the limits on $m_X$ are re-evaluated for the same benchmark scenarios in Tables 4.4 and 4.5 now assuming an exact helicity suppression. In both scenarios a significant reduction in the mass limits can occur. This reduction occurs for any choice of mixing angles in scenario 2, whereas in scenario 1, a significant reduction occurs only when the dominant decay channel comes from either $B_d^0$ or $B_s^0$. In general a reduction in the limits on $m_X$ by a factor of $0.05-0.07$ naturally occurs compared to the scenario without additional mass mixing. We find that the limits on $m_X$ can be as low as 5 TeV potentially allowing for discovery signals of different PS particles comfortably within reach of current and possible future hadron colliders.

Exotic fermion multiplets are therefore an attractive feature for low scale Pati Salam models. It is curious that they allow for significantly lighter PS breaking scales whilst also potentially breaking the mass degeneracy amongst the down-isospin fermions. This effect is possible not only for mixing between the charged leptons as discussed above, but also if heavy versions of the down quarks, $D$, were to be included which mix with

| SCENARIO 1 | Limit on $m_X$ | Reduction | Dominant channel |
|---|---|---|---|
| $\theta_{12}^L = \frac{3\pi}{2}$, $\theta = \frac{7\pi}{4}$, $\delta = \pi$ | 177 TeV | 1 | $K_L^0 \to \mu\mu$ |
| $\theta_{12}^L = \frac{\pi}{4}$, $\theta = \frac{\pi}{4}$, $\delta = 0$ | 139 TeV | 0.85 | $K_L^0 \to \mu e$ |
| $\theta_{12}^L = 2.06$, $\theta = 5.11$, $\delta = 4.58$ | 51 TeV | 0.63 | $K_L^0 \to \mu\mu$ |
| $\theta_{12}^L = 0$, $\theta = 1.183$, $\delta = 0$ | 11 TeV | 0.09 | $K_L^0 \to ee$ |
| $\theta_{12}^L = \frac{\pi}{2}$, $\theta = 0$, $\delta = \frac{\pi}{2}$ | 8.5 TeV | 0.06 | $B_d^0 \to \mu e$ |
| $\theta_{12}^L = \frac{\pi}{4}$, $\theta = \frac{\pi}{4}$, $\delta = \frac{\pi}{2}$ | 7.8 TeV | 0.07 | $B_d^0 \to \mu\mu$ |

TABLE 4.8: Limits obtained for the gauge leptoquark mass $X_\mu$ for different choices of the mixing angles appearing in Eq. (4.58) with an exact helicity suppression where we have chosen $K_R^{de} = 0_{3\times 3}$. The decay process from which the dominant limit arises is also listed as well as the percentage reduction from the non-helicity suppressed scenario given in Table 4.4. In some cases only a small reduction in the mass limits occurs, this is a result of the Kaon decay channels being helicitiy suppressed as a result of the structure of the mixing matrices instead of due to a chiral coupling of $X_\mu$. Only the benchmark scenarios which initially had dominant decay channels arising from $B_d$ or $B_s$ experience a significant reduction in their limits as they were initially not helicity suppressed.

| SCENARIO 2 | Limit on $m_X$ | Reduction | Dominant channel |
|---|---|---|---|
| $\theta_{12}^L = 2.4$, $\theta_{23}^L = \frac{\pi}{2}$, $\delta^L = 2\pi$ | 6.2 TeV | 0.06 | $B_s^0 \to \mu e$ |
| $\theta_{12}^L = \frac{\pi}{9}$, $\theta_{23}^L = 1$, $\delta^L = 0$ | 6.0 TeV | 0.06 | $B_s^0 \to \mu e$ |
| $\theta_{12}^L = \frac{\pi}{4}$, $\theta_{23}^L = 0$, $\delta^L = 0$ | 6.0 TeV | 0.07 | $B_s^0 \to \mu e$ |
| $\theta_{12}^L = 0.72$, $\theta_{23}^L = 4.02$, $\delta^L = 0$ | 5.9 TeV | 0.07 | $B_s^0 \to \mu e$ |
| $\theta_{12}^L = \frac{\pi}{3}$, $\theta_{23}^L = \frac{\pi}{2}$, $\delta^L = 0$ | 5.6 TeV | 0.06 | $B_s^0 \to \mu\mu$ |
| $\theta_{12}^L = \frac{\pi}{3}$, $\theta_{23}^L = \frac{\pi}{2}$, $\delta^L = \frac{\pi}{2}$ | 5.6 TeV | 0.065 | $B_s^0 \to \mu\mu$ |

TABLE 4.9: Limits obtained for the gauge leptoquark mass $X_\mu$ for some different choices of mixing angles appearing in Eq. (4.60) with an exact helicity suppression where we have chosen $K_R^{de} = 0_{3\times 3}$. The decay process from which the dominant limit arises is also listed as well as the percentage reduction from the non helicity-suppressed scenarios in Table 4.5. Each benchmark experiences a significant reduction in their mass limits of over an order of magnitude allowing for extremely light masses of $X_\mu$ and significantly lower scales of PS breaking.

the light $d$ quarks. This would lead to a similar reduction in the mass limits on $X_\mu$ as above for the same reasons.

## 4.4 Exotic PS fermion multiplets

As discussed above, exotic PS fermion multiplets which contain states with the correct quantum numbers to mix with the charged leptons or down quarks can simultaneously explain the experimentally observed mass non-degeneracy between these two types of fermions as well as lower the phenomenologically-allowed scale of PS breaking. A number of different viable PS multiplets are possible; for consistency we require that the multiplets added do not introduce anomalies and that they allow for a phenomenologically valid mass spectrum. For simplicity we focus on small multiplets which transform with no more than two indices total under all three gauge groups when written in their defining representations. All possible combinations satisfying this requirement are listed in Table 4.10. We take the scalar content of the theory to remain unchanged but will note where additional exotic scalars may be required for a viable model in some cases. Although the PS gauge group is an attractive subgroup of some GUTs e.g. $SO(10)$ or $E_6$, we will not require successful gauge-coupling unification or partial unification. We will not consider the location of Landau poles[14] or require that the extra exotic fermions fit into complete GUT multiplets. We simply focus on the specific particle content required at low scales sufficient to lift the mass degeneracy between $\ell$ and $d$ and simultaneously lower the scale of PS breaking.

### 4.4.1 Fermion extensions

Considering the relevant exotic multiplets indicated in Table 4.10, below we study basic phenomenological implications of introducing each given multiplet. We indicate heavy, exotic versions of down quarks, charged leptons and neutrinos by $D$, $E$ and $N$ respectively. We will also briefly comment on the implications for baryon number violation in each case. As we are only introducing exotic fermions, the Yukawa sector of the Lagrangian is the only possible area where additional violation could arise.

[14]These would further motivate considering multiplets of small dimensionality as large multiplets will have a much more significant impact on RGE evolution relevant for viable GUT theories.

| | PS multiplet | $A(R)$ | $SU(3)\otimes U(1)_{\rm EM}$ decomposition | Candidate |
|---|---|---|---|---|
| $f^a$ | $(\mathbf{1},\mathbf{2},\mathbf{1})$ | 0 | $\mathbf{1}_{-1/2}\oplus\mathbf{1}_{+1/2}$ | ✖ |
| $f^\alpha$ | $(\mathbf{1},\mathbf{1},\mathbf{2})$ | 0 | $\mathbf{1}_{-1/2}\oplus\mathbf{1}_{+1/2}$ | ✖ |
| $f^A$ | $(\mathbf{4},\mathbf{1},\mathbf{1})$ | $\pm1$ | $\mathbf{1}_{-1/2}\oplus\mathbf{3}_{+1/6}$ | ✖ |
| $f^a{}_b$ | $(\mathbf{1},\mathbf{3},\mathbf{1})$ | 0 | $\mathbf{1}_{-1}\oplus\mathbf{1}_{0}\oplus\mathbf{1}_{+1}$ | ✔ |
| $f^\alpha{}_\beta$ | $(\mathbf{1},\mathbf{1},\mathbf{3})$ | 0 | $\mathbf{1}_{-1}\oplus\mathbf{1}_{0}\oplus\mathbf{1}_{+1}$ | ✔ |
| $f^{AB}$ | $(\mathbf{6},\mathbf{1},\mathbf{1})$ | 0 | $\mathbf{3}_{-1/3}\oplus\overline{\mathbf{3}}_{+1/3}$ | ✔ |
| $f^{AB}$ | $(\mathbf{10},\mathbf{1},\mathbf{1})$ | $\pm8$ | $\mathbf{1}_{-1}\oplus\mathbf{3}_{-1/3}\oplus\mathbf{6}_{+1/3}$ | ✔ |
| $f^A{}_B$ | $(\mathbf{15},\mathbf{1},\mathbf{1})$ | 0 | $\overline{\mathbf{3}}_{-2/3}\oplus\mathbf{1}_{0}\oplus\mathbf{8}_{0}\oplus\mathbf{3}_{+2/3}$ | ✖ |
| $f^{a\alpha}$ | $(\mathbf{1},\mathbf{2},\mathbf{2})$ | 0 | $\mathbf{1}_{-1}\oplus\mathbf{1}_{0}\oplus\mathbf{1}_{0}\oplus\mathbf{1}_{+1}$ | ✔ |
| $f^{Aa}$ | $(\mathbf{4},\mathbf{2},\mathbf{1})$ | $\pm2$ | $\mathbf{1}_{-1}\oplus\mathbf{3}_{-1/3}\oplus\mathbf{1}_{0}\oplus\mathbf{3}_{+2/3}$ | ✔ |
| $f^{A\alpha}$ | $(\mathbf{4},\mathbf{1},\mathbf{2})$ | $\pm2$ | $\mathbf{1}_{-1}\oplus\mathbf{3}_{-1/3}\oplus\mathbf{1}_{0}\oplus\mathbf{3}_{+2/3}$ | ✔ |

TABLE 4.10: Different dimensional representations of fermions $f$ (with indices in their defining representation) under PS where $a$, $\alpha$ and $A$ correspond to $SU(2)_L$, $SU(2)_R$ and $SU(4)_c$ indices respectively. Multiplets are considered good candidates if they contain states with the same quantum numbers as either the down quarks or charged leptons, which will mix with its SM counterpart, when broken to $SU(3)_c\otimes U(1)_{\rm EM}$ . Additionally the $SU(4)$ anomaly coefficient $A(R)$ for each fermion is indicated where the sign depends on whether the fermion is left- or right-handed.

#### 4.4.1.1 $SU(2)_{L/R}$ Triplets

If a triplet fermion is added, for example $\Psi_3^R\sim(\mathbf{1},\mathbf{1},\mathbf{3})$, the extra terms appearing in the Yukawa Lagrangian are

$$\mathcal{L}_{\rm YUK}\supset {\rm Tr}\left[\sqrt{2}\,y_{\Psi_3}\overline{(\Psi_3^R)^c}\chi_R^\dagger f_R+\frac{1}{2}\mu_{\Psi_3}\overline{(\Psi_3^R)^c}\,(\Psi_3^R)^T\right]+{\rm H.c.} \tag{4.74}$$

As $\Psi_3^R$ is uncharged under the colour group $SU(4)_c$, it contains no quark states. However, it contains components which can mix with both the charged and neutral SM leptons

$$f_{L/R}=\begin{pmatrix} \cdot & \cdot \\ \cdot & \cdot \\ \cdot & \cdot \\ \nu & e\end{pmatrix}_{L/R}\quad,\qquad \Psi_3^R=\frac{1}{\sqrt{2}}\begin{pmatrix} N_R & \sqrt{2}\,(E_L^-)^c \\ \sqrt{2}\,E_R^- & -N_R\end{pmatrix} \tag{4.75}$$

where the dotted components of $f_{L/R}$ do not mix with $\Psi_3^R$ but the undotted do and $\Psi_3^R\to U_R\,\Psi_3^R\,U_R^\dagger$. Here we have assigned $\Psi_3^R$ to be a right-handed fermion without loss of generality. Expanding out Eqs. (4.16) and (4.74) with the parameterisation given in

Eq. (4.75) leads to a mixing matrix given by

$$\mathcal{L}_{eE} = \begin{pmatrix} \overline{e_L} & \overline{E_L} \end{pmatrix} \begin{pmatrix} m_e & 0 \\ \sqrt{2}\, y^R_{\Psi_3} v^*_R & \mu_{\Psi^R_3} \end{pmatrix} \begin{pmatrix} e_R \\ E_R \end{pmatrix} \tag{4.76}$$

for the charged lepton states and

$$\mathcal{L}_{\nu N} = \frac{1}{2} \begin{pmatrix} \overline{\nu_L} & \overline{\nu^c_R} & \overline{N^c_R} \end{pmatrix} \begin{pmatrix} 0 & m_u & 0 \\ m_u & 0 & y^R_{\Psi_3} v^*_R \\ 0 & y^R_{\Psi_3} v^*_R & \mu_{\Psi^R_3} \end{pmatrix} \begin{pmatrix} \nu^c_L \\ \nu_R \\ N_R \end{pmatrix} \tag{4.77}$$

for the neutral states. If $f_L$, $f_R$ and $\Psi$ are the only fermions introduced, the PS symmetry enforces that the singular values of $m_d$ and $m_u$ are given by the down and up quark masses respectively. Equation (4.77) assumes that the fermion singlets $S_L$ discussed in Section 4.2, appearing in the usual low-scale PS scenario, are not included. As can be seen from the neutrino mass mixing matrix, $S_L$ may no longer be necessary for light neutrino masses as an inverse seesaw arises naturally with the triplet. We therefore neglect $S_L$, and if it were to be included Eq. (4.77) would be trivially extended by the last row and column of Eq. (4.18).

The terms introduced in Eq. (4.74) do not violate the global $U(1)_J$ symmetry which Eq. (4.16) obeys and is the only global accidental symmetry of this Yukawa Lagrangian. These terms unsurprisingly enforce the assignment

$$J(\Psi^R_3) = 0 \tag{4.78}$$

as $\Psi^R_3$ transforms as a real representation. Therefore baryon number remains an unbroken global symmetry of the Yukawa sector similar to the vanilla scenario described in Section 4.2.4. Interestingly if the singlet $S_L$ is not included, the scalar $\chi_L$ no longer Yukawa couples to any of the fermions and the relevant term of the scalar potential given in Eq. (4.37) no longer violates the $U(1)_J$ global symmetry as we are free to choose $J(\chi_L) = -1$. The proton would therefore remain absolutely stable (assuming no additional particle content) after breaking of the PS symmetry, whereas lepton number would be broken.

If instead an $SU(2)_L$ triplet fermion $\Psi^L_3$ was introduced, similar conclusions are reached related to the leptonic mass mixing matrices and baryon number violation[15]. The Yukawa Lagrangian in this case is similar to the one appearing in Eq. (4.74) with the replacements $\Psi_3^R \to (\Psi_3^L)^c$, $\chi_R \to (\chi_L)^*$ and $f_R \to (f_L)^c$ leading to the mixing matrix

$$\mathcal{L}_{eE} = \begin{pmatrix} \overline{e_L} & \overline{E_L} \end{pmatrix} \begin{pmatrix} m_e & \sqrt{2}\, y^L_{\Psi_3} v_L \\ 0 & \mu_{\Psi_3^L} \end{pmatrix} \begin{pmatrix} e_R \\ E_R \end{pmatrix} \tag{4.79}$$

for the charged lepton states and

$$\mathcal{L}_{\nu N} = \frac{1}{2} \begin{pmatrix} \overline{\nu_L} & \overline{\nu_R^c} & \overline{N_L} \end{pmatrix} \begin{pmatrix} 0 & m_u & y^L_{\Psi_3} v_L \\ m_u & 0 & 0 \\ y^L_{\Psi_3} v_L & 0 & \mu_{\Psi_3^L} \end{pmatrix} \begin{pmatrix} \nu_L^c \\ \nu_R \\ N_L^c \end{pmatrix} \tag{4.80}$$

for the neutral states.

If both $\Psi_3^L$ and $\Psi_3^R$ are included simultaneously the mass mixing matrices for the charged and neutral sectors are simply a combination of Eqs. (4.76), (4.77), (4.79) and (4.80). Explicitly writing out the mass mixing matrices gives

$$\mathcal{L}_{eE\mathcal{E}} = \begin{pmatrix} \overline{e_L} & \overline{E_L} & \overline{\mathcal{E}_L} \end{pmatrix} \begin{pmatrix} m_e & 0 & \sqrt{2}\, y^L_{\Psi_3} v_L \\ \sqrt{2}\, y^R_{\Psi_3} v_R & \mu_{\Psi_3^R} & 0 \\ 0 & 0 & \mu_{\Psi_3^L} \end{pmatrix} \begin{pmatrix} e_R \\ E_R \\ \mathcal{E}_R \end{pmatrix} \tag{4.81}$$

for the charged leptons, where $E_{L/R}$ and $\mathcal{E}_{L/R}$ correspond to the charged lepton states appearing in $\Psi_3^R$ and $\Psi_3^L$ respectively, and

$$\mathcal{L}_{\nu N} = \frac{1}{2} \begin{pmatrix} \overline{\nu_L} & \overline{\nu_R^c} & \overline{N_L} & \overline{N_R^c} \end{pmatrix} \begin{pmatrix} 0 & m_u & y^L_{\Psi_3} v_L & 0 \\ m_u & 0 & 0 & y^R_{\Psi_3} v_R^* \\ y^L_{\Psi_3} v_L & 0 & \mu_{\Psi_3^L} & 0 \\ 0 & y^R_{\Psi_3} v_R^* & 0 & \mu_{\Psi_3^R} \end{pmatrix} \begin{pmatrix} \nu_L^c \\ \nu_R \\ N_L^c \\ N_R \end{pmatrix} \tag{4.82}$$

for the neutral states.

[15] However if both $\Psi_3^L$ and $\Psi_3^R$ are included simultaneously, the Yukawa Lagrangian enforces $J(\chi_L) = J(\chi_R) = 1$ and the relevant quartic term of the scalar potential would once again violate $U(1)_J$ and therefore $B$ regardless of the existence of $S_L$.

#### 4.4.1.2 $SU(2)_L/SU(2)_R$ Bi-doublet

If a fermion transforming as a bi-doublet under the two $SU(2)$ gauge groups of PS, $\Psi_{22} \sim (\mathbf{1}, \mathbf{2}, \mathbf{2})$, is introduced the Yukawa Lagrangian is extended by

$$\mathcal{L}_{\text{YUK}} \supset \mathrm{Tr}\Big[y^R_{\Psi_{22}} \overline{f_L} \chi_R (\Psi^T_{22})^c (i\tau_2) + y^L_{\Psi_{22}} \overline{\Psi_{22}} (i\tau_2) \chi^\dagger_L f_R + \mu_{\Psi_{22}} \overline{\Psi_{22}} (i\tau_2)(\Psi_{22})^c (i\tau_2)\Big] + \text{H.c.} \tag{4.83}$$

As before, $\Psi_{22}$ is uncharged under the $SU(4)_c$ colour group and therefore only contains uncoloured states which can mix with the SM leptons:

$$f_{L/R} = \begin{pmatrix} \cdot & \cdot \\ \cdot & \cdot \\ \cdot & \cdot \\ \nu & e \end{pmatrix}_{L/R} , \qquad \Psi_{22} = \begin{pmatrix} -(E^-_R)^c & N^0_L \\ (N^0_R)^c & E^-_L \end{pmatrix} \tag{4.84}$$

where $\Psi_{22}$ is written with two raised indices and therefore transforms as $\Psi_{22} \to U_L \Psi_{22} U^T_R$. Expanding out Eqs. (4.16) and (4.83) with Eq. (4.84) leads to

$$\mathcal{L}_{eE} = \begin{pmatrix} \overline{e_L} & \overline{E_L} \end{pmatrix} \begin{pmatrix} m_e & y^R_{\Psi_{22}} v_R \\ y^L_{\Psi_{22}} v^*_L & \mu_{\Psi_{22}} \end{pmatrix} \begin{pmatrix} e_R \\ E_R \end{pmatrix} \tag{4.85}$$

for the charged lepton mass mixing matrix and

$$\mathcal{L}_{\nu N} = \frac{1}{2} \begin{pmatrix} \overline{\nu_L} & \overline{\nu^c_R} & \overline{N_L} & \overline{N^c_R} \end{pmatrix} \begin{pmatrix} 0 & m_u & 0 & y^R_{\Psi_{22}} v_R \\ m_u & 0 & 0 & y^L_{\Psi_{22}} v^*_L \\ 0 & 0 & 0 & \mu_{\Psi_{22}} \\ y^R_{\Psi_{22}} v_R & y^L_{\Psi_{22}} v^*_L & \mu_{\Psi_{22}} & 0 \end{pmatrix} \begin{pmatrix} \nu^c_L \\ \nu_R \\ N^c_L \\ N_R \end{pmatrix} \tag{4.86}$$

for the neutral mass mixing.

Similar to the case of the triplet, Eq. (4.83) does not violate the global $U(1)_J$ symmetry (which, recall, is the only accidental symmetry in this Yukawa Lagrangian) and implies

$$J(\Psi_{22}) = 0. \tag{4.87}$$

Therefore $U(1)_J$ is not violated in the Yukawa Lagrangian and baryon number violation proceeds through the scalar sector as before. Unlike the scenarios involving only one triplet, in the absence of the fermion $S_L$, Eq. (4.83) still enforces the choice $J(\chi_L) = J(\chi_R) = 1$ and therefore baryon number will remain violated if both scalars are included and will proceed via similar diagrams to those presented in Section 4.2.4.

#### 4.4.1.3 $SU(4)_c/SU(2)_{L/R}$ Bi-fundamentals

In the case where additional copies of the usual PS fermions exist, there are a number of different possible scenarios depending on the chirality of the fermions introduced. An even number of fermion bi-fundamentals needs to be introduced, as can be seen in Table 4.10, for anomaly cancellation and therefore we focus on the minimal scenario where a pair of bi-fundamentals are added. If two exact copies of $f_L$ and $f_R$ are added, that is a left-handed fermion transforming as $(F_L)_\alpha \sim (\mathbf{4},\mathbf{2},\mathbf{1})$ under PS and a right-handed fermion transforming as $(F_R)_{\dot\alpha} \sim (\mathbf{4},\mathbf{1},\mathbf{2})$ where we explicitly show the dotted and undotted Lorentz indices for clarity, then the Yukawa Lagrangian is extended by the terms

$$\begin{aligned}\mathcal{L}_{\text{YUK}} = \mathrm{Tr}\Big[\Big\{ & y_{f_L f_R}\overline{f_L}\,\phi\,(f_R)^T + \widetilde{y}_{f_L f_R}\overline{f_L}\,\phi^c(f_R)^T + y_{f_R}\overline{S_L}\,\chi_R^\dagger\, f_R + y_{f_L}\overline{f_L}\,\chi_L(S_L)^c \\ & + (f_L \to F_L) + (f_R \to F_R)\Big\}\Big] + \frac{1}{2}\mu_S\overline{S_L}\,S_L^c + \text{H.c}\end{aligned} \tag{4.88}$$

with the additional fermion multiplets

$$f_{L/R} = \begin{pmatrix} u_r & d_r \\ u_b & d_b \\ u_g & d_g \\ \nu & e \end{pmatrix}_{L/R}, \qquad F_{L/R} = \begin{pmatrix} U_r & D_r \\ U_b & D_b \\ U_g & D_g \\ N^0 & E^- \end{pmatrix}_{L/R} \tag{4.89}$$

where $U_i$ and $D_i$ ($i = r, b, g$) have electric charge $+2/3$ and $-1/3$ respectively. Note that no bare mass terms are present in Eq. (4.88) and therefore the expansion will be similar to that of Eq. (4.16) in the vanilla PS scenario. In particular all mass terms between the SM and exotic charged fermions will be related to the electroweak vevs $v_1$ and $v_2$ implying that the heavy exotic charged fermions $E$, $D$ and $U$ would be expected to appear near the electroweak scale which is ruled out phenomenologically.

Alternatively two fermions with the same PS representations but *opposite* chirality to the bi-fundamentals already included in PS could be added, that is a right-handed fermion transforming as $(F_L)_{\dot{\alpha}} \sim (\mathbf{4}, \mathbf{2}, \mathbf{1})$ under PS and a left-handed fermion transforming as $(F_R)_\alpha \sim (\mathbf{4}, \mathbf{1}, \mathbf{2})$. In this case the Yukawa Lagrangian will be similar, albeit with additional bare mass and Yukawa terms:

$$\begin{aligned}\mathcal{L}_{\text{YUK}} = \text{Tr}\Big[\Big\{ & y_{f_L f_R}\overline{f_L}\,\phi\,(f_R)^T + \widetilde{y}_{f_L f_R}\overline{f_L}\,\phi^c(f_R)^T + y_{f_R}\overline{S_L}\,\chi_R^\dagger\,f_R + y_{f_L}\overline{f_L}\,\chi_L(S_L)^c \\ & + (f_{L/R} \to F_{R/L}\ \&\ \chi_R \to \chi_L)\Big\} + \mu_L\,\overline{f_L}\,F_L + \mu_R\,\overline{F_R}\,f_R + y_\Phi^L\,\overline{f_L}\Phi F_L + y_\Phi^R\,\overline{F_R}\Phi f_R\Big] \\ & + \frac{1}{2}\mu_S\overline{S_L}\,S_L^c + \text{H.c.}\end{aligned} \tag{4.90}$$

Now the exotic charged fermions can have their masses decoupled from the electroweak scale for large bare mass terms. However as the exotic fermion multiplets transform in the exact same way as the multiplets containing the SM fields, large values for the bare mass terms $\mu_L$ and $\mu_R$ will not decouple the masses of the down-quarks and charged-leptons. However, if the $SU(4)$ adjoint scalar, $\Phi$, is included in the scalar spectrum, its allowed Yukawa couplings between $f_{L/R}$ and $F_{L/R}$ will lead to a breaking of the mass degeneracy since $\langle\Phi\rangle \propto (1, 1, 1, -3)$. Therefore, in order for such a scenario to be even remotely feasible, additional scalars beyond that of $\phi$, $\chi_L$ and $\chi_R$ are required so that the down-isospin mass degeneracy can be broken: a seesaw mechanism *as well as* the addition of scalars which induce a Georgi-Jarlskog-like texture are simultaneously required.

The charged-lepton mixing matrix will then be given by

$$\mathcal{L}_{eE} = \begin{pmatrix} \overline{e_L} & \overline{E_L} \end{pmatrix} \begin{pmatrix} m_f & \mu_L - \sqrt{\frac{3}{2}}y_\Phi^L v_\Phi \\ \mu_R - \sqrt{\frac{3}{2}}y_\Phi^R v_\Phi & M_F \end{pmatrix} \begin{pmatrix} e_R \\ E_R \end{pmatrix} \tag{4.91}$$

where $m_f = \widetilde{y}_{f_L f_R} v_1 + y_{f_L f_R} v_2^*$ and $M_F = \widetilde{y}_{F_R F_L} v_1 + y_{F_R F_L} v_2^*$. The down quark mixing matrix is given similarly and only differs by group theoretic factors introduced by the allowed Yukawa couplings of the fermions to $\Phi$:

$$\mathcal{L}_{dD} = \begin{pmatrix} \overline{d_L} & \overline{D_L} \end{pmatrix} \begin{pmatrix} m_f & \mu_L + \sqrt{\frac{1}{6}}y_\Phi^L v_\Phi \\ \mu_R + \sqrt{\frac{1}{6}}y_\Phi^R v_\Phi & M_F \end{pmatrix} \begin{pmatrix} d_R \\ D_R \end{pmatrix}. \tag{4.92}$$

Similar matrices can be written down for the mass mixing between the neutral fermions:

$$\mathcal{L}_{\nu N} = \overline{n_L}\, M_{\nu NS}\, (n_L^c)^T \tag{4.93}$$

with $n_L = \begin{pmatrix} \nu_L & \nu_R^c & N_L & N_R^c & S_L \end{pmatrix}$ and

$$M_{\nu NS} = \begin{pmatrix} 0 & m_x & 0 & \mu_L - \sqrt{\frac{3}{2}} y_\Phi^L v_\Phi & y_{f_L} v_L \\ m_x & 0 & \mu_R - \sqrt{\frac{3}{2}} y_\Phi^R v_\Phi & 0 & y_{f_R} v_R^* \\ 0 & \mu_R - \sqrt{\frac{3}{2}} y_\Phi^R v_\Phi & 0 & M_X & y_{F_R} v_L \\ \mu_L - \sqrt{\frac{3}{2}} y_\Phi^L v_\Phi & 0 & M_X & 0 & y_{F_L} v_R^* \\ y_{f_L} v_L & y_{f_R} v_R^* & y_{F_R} v_R^* & y_{F_L} v_R^* & \mu_S \end{pmatrix}. \tag{4.94}$$

The mass mixing between $u_{L/R}$ and $U_{L/R}$ is instead given by

$$\mathcal{L}_{uU} = \begin{pmatrix} \overline{u_L} & \overline{U_L} \end{pmatrix} \begin{pmatrix} m_x & \mu_L + \sqrt{\frac{1}{6}} y_\Phi^L v_\Phi \\ \mu_R + \sqrt{\frac{1}{6}} y_\Phi^R v_\Phi & M_X \end{pmatrix} \begin{pmatrix} u_R \\ U_R \end{pmatrix}. \tag{4.95}$$

The only difference between the up-quark and down-quark mass mixing matrices being $m_x = y_{f_L f_R} v_1 + \widetilde{y}_{f_L f_R} v_2^*$ and $M_X = y_{F_R F_L} v_1 + \widetilde{y}_{F_R F_L} v_2^*$ compared to $m_f$ and $M_F$ defined above.

Two other possible combinations can occur when pairs of bi-fundamentals are introduced, e.g. two fermions of opposite chirality transforming under $SU(2)_R$: $(F_R^{(1)})_\alpha \sim (\mathbf{4},\mathbf{1},\mathbf{2})$ and $(F_R^{(2)})_{\dot\alpha} \sim (\mathbf{4},\mathbf{1},\mathbf{2})$ which will lead to a mass mixing matrix similar to above with a zero entry appearing on one of the off diagonal terms. Note that in all possible cases, the diagonal entries of $M_{eE}$ and $M_{dD}$ will contain mass terms tied to the electroweak scale whereas the off-diagonal entries (if they exist) will contain bare mass terms and terms tied to the scale of PS breaking generated by $\langle\Phi\rangle$.

Let us briefly comment on the implications for such models where mass mixing matrices occur for all SM fermion types as in Eqs. (4.91) to (4.93) and (4.95). Due to the additional mixing within the up-isospin sector, which have very similar mixing matrices to the down-isospin sector, we find it very difficult to achieve a viable mass spectrum for all SM fermions in this scenario. It appears highly unlikely that the inclusion of a pair of bi-fundamental fermions is able to achieve a chiral-suppression on the experimental limits on $m_X$ as well as a phenomenologically-viable mass spectrum for the SM fermions.

Due to the number of coupled mass mixing matrices as well as the large number of mass parameters, we do not try to prove this statement. Note, however, that if one of the off-diagonal entries of $M_{dD}$ is made large (required such that the $D'$ states do not gain electroweak masses), this also implies the same thing for $M_{uU}$. Assuming that this occurs for the bottoem-left entry, we have that

$$m_{u/d} \simeq (\mu_L + \sqrt{\frac{1}{6}} y_\Phi^L v_\Phi) - m_{x/f} \left( \mu_R + \sqrt{\frac{1}{6}} y_\Phi^R v_\Phi \right)^{-1} M_{X/F} \tag{4.96}$$

which would imply that the up-quarks and down-quarks have similar masses if the first term is dominant compared to the second. If instead the second term was dominant compared to the first, at a minimum, it would be difficult to generate the correct top mass considering that $m_{x/X}$ are tied to the electroweak scale.

A chiral suppression along with a viable mass spectrum of SM fermions is possible with the addition of *two pairs* of $SU(4) \otimes SU(2)_{L/R}$ PS bi-fundamental fermions on top of the usual fermions $f_L$ and $f_R$ as has already been shown in [209]. As two pairs of bi-fundamentals are introduced, more freedom in the mixing matrices allows for a viable mass spectrum as well as allowing for chiral couplings of $X_\mu$ to the light SM-like fermions. As a variant of this model has already been studied within the literature we do not consider this possibility any further and simply conclude that this model, in its minimal form, does not appear viable.

It is easy and unsurprising to see that for both Eqs. (4.88) and (4.90) the accidental global symmetry $U(1)_J$ is unbroken and therefore for these scenarios all baryon number violating interactions will proceed similarly to Section 4.2.4.

#### 4.4.1.4 $SU(4)_c$ Sextet

Adding a fermion which transforms as an $SU(4)$ sextet $\Psi_6 \sim (\mathbf{6}, \mathbf{1}, \mathbf{1})$, extends the Yukawa Lagrangian by[16]

$$\mathcal{L}_{\text{YUK}} \supset \text{Tr}\Big[ y_\Psi^L \overline{f_L} (i\tau_2) \chi_L^\dagger \Psi_6 + y_\Psi^R \overline{(\Psi_6)^c}\, \chi_R (i\tau_2) (f_R)^T + \frac{1}{2} \mu_{\Psi_6} \overline{(\Psi_6)^c}\, \Psi_6 \Big] + \text{H.c} \tag{4.97}$$

[16] Note that for one generation of sextet fermions, no Yukawa coupling exists between $\Psi_6$ and the adjoint scalar $\Phi$ due to the antisymmetric nature of the sextet.

where $(\tilde{\Psi}_6)_{mn} = (\Psi_6)^{ij}\epsilon_{ijmn}$. As this multiplet is uncharged under $SU(2)_{L/R}$, the electric charge of each component is given by the diagonal generator of $SU(4)$ identified with $B-L$. The branching rule for this multiplet is therefore

$$(\mathbf{6},\mathbf{1},\mathbf{1}) \to \overline{\mathbf{3}}_{+1/3} \oplus \mathbf{3}_{-1/3} \tag{4.98}$$

when broken to $SU(3)_c \otimes U(1)_{\text{EM}}$ of the SM. This irreducible representation therefore contains the correct states to mix with the down quarks of the standard model:

$$f_{L/R} = \begin{pmatrix} \cdot & d_r \\ \cdot & d_b \\ \cdot & d_g \\ \cdot & \cdot \end{pmatrix}_{L/R}, \qquad \Psi_6 = \begin{pmatrix} 0 & (D_{L,g})^c & -(D_{L,b})^c & D_{R,r} \\ -(D_{L,g})^c & 0 & (D_{L,r})^c & D_{R,b} \\ (D_{L,b})^c & -(D_{L,r})^c & 0 & D_{R,g} \\ -D_{R,r} & -D_{R,b} & -D_{R,g} & 0 \end{pmatrix} \tag{4.99}$$

where the components $D_{(L/R),i}$ $(i = r,g,b)$ have electric charge $-1/3$ and $\Psi_6 \to U_4\,\Psi_6\,U_4^T$.

The resulting mixing matrix for the down quark and its partners can be found by expanding Eqs. (4.16) and (4.97) with Eq. (4.99), giving

$$\mathcal{L}_{dD} = \begin{pmatrix} \overline{d_L} & \overline{D_L} \end{pmatrix} \begin{pmatrix} m_d & y^L_{\Psi_6} v_L^* \\ y^R_{\Psi_6} v_R & \mu_{\Psi_6} \end{pmatrix} \begin{pmatrix} d_R \\ D_R \end{pmatrix}, \tag{4.100}$$

and, in the absence of additional fermionic states which mix with $\ell$, the singular values of $m_d$ are given by the charged-lepton masses.

The additional Yukawa interactions involving $\Psi_6$ lead to explicit violation of the global symmetry $U(1)_J$: the bare mass term requires $J(\Psi_6) = 0$, while the two Yukawa terms of Eq. (4.97) imply $J(\Psi_6) = 2$ and $J(\Psi_6) = -2$ respectively, assuming the singlet $S_L$ is included for neutrino mass and therefore $J(\chi_{L/R}) = J(f_{L/R}) = 1$ is enforced. Therefore any two of the three terms in Eq. (4.97) in combination with the Yukawa couplings of $f_{L/R}$ to $S_L$ in Eq. (4.16) leads to baryon number violating interactions. Interestingly for a more minimal PS model where the only scalars[17] present are $\chi_R$ and $\phi$, a global

[17] Therefore the Yukawa terms $y^L_\Psi f_L \chi_L^\dagger \Psi_6$ and $y_L \overline{f_L} \chi_L (S_L)^c$ will not be present.

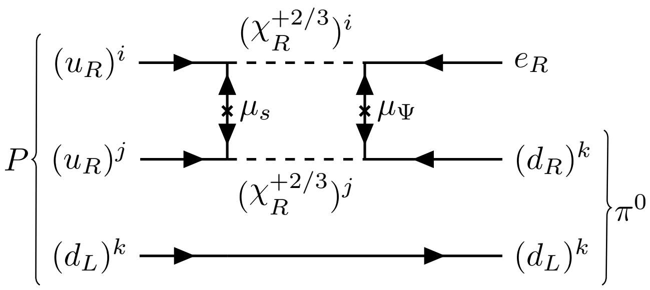


FIGURE 4.3: An example box diagram of proton decay implied by a PS model extended by a fermionic $SU(4)$ sextet fermion. The $p \to \pi^0 e^+$ diagram above is similar to the coloured Higgsino mediated proton decay, $p \to K^+\overline{\nu}$, predicted by the minimal SUSY $SU(5)$ GUT model which typically requires GUT scale masses for the Higgsinos, see e.g. [232].

baryon number is restored in the limit $\mu_{\psi_6} \to 0$ which therefore could be argued to be small from technical naturalness.

Evaluating the full implications of baryon number violation with a realistic mass spectrum for the SM particles is quite complicated for the sextet and beyond the scope of this work. However, an example diagram for $p \to \pi^0 e^+$ is shown in Fig. 4.3 in the case where $\chi_L$ is removed. The diagram involves the couplings

$$\mathcal{L} \supset y_R \overline{S_L}(\chi_R^{+2/3})_i^*(u_R)^i + y_\Psi^R \left((\overline{D_L})_k e_R + \epsilon_{ijk}(\overline{D_R^c})^i (d_R)^j\right)(\chi_R^{+2/3})^k + \mu_{\Psi_6}(\overline{D_L})_i (D_R)^i + \text{H.c} \tag{4.101}$$

where $SU(3)$ indices are explicitly shown and the above couplings are found by expanding out Eqs. (4.16) and (4.97). This decay diagram leads to an effective four-fermion interaction very similar to the coloured Higgsino mediated $p \to K^+\overline{\nu}$ in minimal SUSY $SU(5)$, see e.g. [232]. As this usually requires very large Higgsino masses (at or larger than the GUT scale) and the SM quantum numbers of $D_L$ and $D_R$ are the same as the coloured Higgsino, we expect that in scenarios where baryon number is not imposed (by setting $\mu_\Psi$ to be small), this diagram alone would likely lead to significant limits on the masses of the particles running in the loop which would translate into large limits on the PS breaking scale. An additional suppression factor of $\mu_S$ appears in Fig. 4.3, and is required to be small for neutrino mass generation, which may interestingly connect the large proton lifetime to the smallness of neutrino mass in this potential minimal model.

#### 4.4.1.5 $SU(4)_c$ Decuplets

Finally we consider the possibility that two fermions of opposite handedness[18] transforming as $\Psi^{10}_{L/R} \sim (\mathbf{10},\mathbf{1},\mathbf{1})$ are added. The relevant, non-zero terms added to the Yukawa Lagrangian are

$$\mathcal{L}_{\text{YUK}} \supset \text{Tr}\Big[\sqrt{2}\, y^R_{\Psi_{10}} \overline{\Psi^{10}_L}\, \chi_R (i\tau_2)(f_R)^T - \sqrt{2}\, y^L_{\Psi_{10}} (\overline{f_L})^T (i\tau_2)\chi^\dagger_L \Psi^{10}_R \\ + \mu_{\Psi_{10}} \overline{\Psi^{10}_L}\, \Psi^{10}_R + \sqrt{6}\, y_\Phi \overline{\Psi^{10}_L}\, \Phi\, \Psi^{10}_R\Big] + \text{H.c.} \tag{4.102}$$

Similar to the case of the sextet above, these multiplets are uncharged under $SU(2)_{L/R}$ and therefore the branching rule for their breaking to $SU(3)_c \otimes U(1)_{\text{EM}}$ is simply given by

$$(\mathbf{10},\mathbf{1},\mathbf{1}) \to \mathbf{6}_{1/3} \oplus \mathbf{3}_{-1/3} \oplus \mathbf{1}_{-1}. \tag{4.103}$$

These multiplets therefore contain the necessary states to mix with both the down quarks and the charged leptons:

$$f_{L/R} = \begin{pmatrix} \cdot & d_r \\ \cdot & d_b \\ \cdot & d_g \\ \cdot & e \end{pmatrix}_{L/R}, \quad \Psi^{10}_{L/R} = \frac{1}{\sqrt{2}} \begin{pmatrix} \cdot & \cdot & \cdot & D_r \\ \cdot & \cdot & \cdot & D_b \\ \cdot & \cdot & \cdot & D_g \\ D_r & D_b & D_g & \sqrt{2}\, E^- \end{pmatrix}_{L/R} \tag{4.104}$$

where the components $D_{(L/R),i}$ $(i = r, b, g)$ have electric charge $-1/3$. Contained in $\Psi^{10}_{L/R}$ is an exotic colour sextet Dirac fermion, which is embedded in the upper-left $3 \times 3$ block of the second multiplet in Eq. (4.104). If such a sextet was discovered alongside heavy copies of the charged leptons and down quarks it would suggest the existence of these exotic fermion multiplets within a PS symmetry.

In this scenario, the mixing matrices for the charged leptons and down quarks are related to each other as they exist in the same multiplet. The charged lepton mixing matrix is

[18] Both are required for anomaly cancellation.

given by

$$\mathcal{L}_{eE} = \begin{pmatrix} \overline{e_L} & \overline{E_L} \end{pmatrix} \begin{pmatrix} m_F & \sqrt{2}\, y^L_{\Psi_{10}} v^*_L \\ \sqrt{2}\, y^R_{\Psi_{10}} v_R & \mu_{\Psi_{10}} - \sqrt{\frac{1}{6}} y_\Phi v_\Phi \end{pmatrix} \begin{pmatrix} e_R \\ E_R \end{pmatrix} \tag{4.105}$$

and the down quark mixing matrix is of a similar form and only differs by some group theoretic factors

$$\mathcal{L}_{dD} = \begin{pmatrix} \overline{d_L} & \overline{D_L} \end{pmatrix} \begin{pmatrix} m_F & y^L_{\Psi_{10}} v^*_L \\ y^R_{\Psi_{10}} v_R & \mu_{\Psi_{10}} - \sqrt{\frac{3}{2}} y_\Phi v_\Phi \end{pmatrix} \begin{pmatrix} d_R \\ D_R \end{pmatrix} \tag{4.106}$$

where $m_F$ is enforced by the PS symmetry to appear in both mass matrices and its singular values are no longer necessarily given by the charged-lepton or down-quark masses individually. Note that, similar to the case of the bi-fundamental, a Georgi-Jarlskog like texture will occur with the inclusion of the scalar $\Phi$. Unlike the bi-fundamental scenario however, extra group theoretic factors between the two mass matrices exist even without the inclusion of $\Phi$ and therefore it is not required for a breaking of the down-isospin mass degeneracy (though it may be needed to achieve a phenomenologically viable spectrum of masses). Additionally as $E$ and $D$ are contained in the same multiplet, there will be gauge interactions between the two mediated by $X_\mu$ similar to $e$ and $d$.

The colour sextet fermion $\psi$ develops a mass given by $m_\psi = \mu_{\Psi_{10}} + \sqrt{\frac{1}{6}} y_\Phi v_\Phi$ and therefore the mass spectrum of the exotic states depends on the relative sizes of the dimensionful parameters $y^R_{\Psi_{10}} v_R$, $\mu_{\Psi_{10}}$ and $y_\Phi v_\Phi$[19]. For example assuming $\mu_{\Psi_{10}} > y_\Phi v_\Phi \gg y^R_{\Psi_{10}} v_R$ leads to a mass spectrum where the colour sextet would be the heaviest of the three exotics and the heavy, charged leptons would be the lightest.

The global symmetry $U(1)_J$ remains unbroken in the Yukawa sector and enforces the charge assignment

$$J(\Psi^{10}_L) = J(\Psi^{10}_R) = 2 \tag{4.107}$$

regardless of whether $S_L$ is included or not and therefore baryon number remains an accidental symmetry of the Yukawa sector. The additional multiplets $\Psi^{10}_{L/R}$ do not contain any neutral states under $U(1)_{\text{EM}}$ and there are no lepton number violating terms present in Eq. (4.102). This is easy to see as in the absence of $S_L$ the Yukawa Lagrangian

[19]For phenomenological reasons the parameters $m_e$ and $y^L_{\Psi_{10}} v^*_L$ are required to be smaller in size than these parameters.

obeys a secondary global symmetry

$$J'(\phi,\,\Phi)=0,\;\; J'(f_L,\,f_R)=1,\;\; J'(\chi_L,\,\chi_R)=-3\;\text{ and }\; J'(\Psi^{10}_L,\Psi^{10}_R)=-2. \tag{4.108}$$

Lepton number can be identified as $L=\frac{1}{4}(J'-3T)$ such that

$$L(f_{L/R})=\begin{pmatrix}0 & 0\\ 0 & 0\\ 0 & 0\\ 1 & 1\end{pmatrix}\;\text{ and }\; L(\Psi^{10}_{L/R})=\begin{pmatrix}-1 & -1 & -1 & 0\\ -1 & -1 & -1 & 0\\ -1 & -1 & -1 & 0\\ 0 & 0 & 0 & 1\end{pmatrix} \tag{4.109}$$

which is unbroken by $\langle\chi_L,\chi_R\rangle$ and therefore $\nu_L$ and $\nu_R$ develop a Dirac mass of order $m_u$. Therefore, for a realistic model, $S_L$ or some other lepton number violating physics needs to be included in order to break $L=\frac{1}{4}(J'-3T)$ and allow for small neutrino masses. If $S_L$ is included the neutrino mass matrix is given by Eq. (4.19) as before. Baryon number violation will therefore proceed similarly to Section 4.2.4 and therefore will lead to the same order of magnitude limits on the relevant quartic coupling of the scalar potential.

## 4.5 Fermion mixing

From the results of Section 4.4.1 only a few PS multiplets lead to mass mixing in the charged-lepton and/or down-quark sectors in the desired way. Table 4.11 summarises viable multiplets from the ones considered and indicates in which sector mixing will occur. Charged-lepton mixing exclusively will occur with the addition of $SU(2)_{L/R}$ triplets or bidoublets and in the down-sector exclusively with the addition of $SU(4)$ sextets[20]. Mixing will occur in both sectors either through a combination of the aforementioned multiplets or with[21] the addition of a pair of $SU(4)$ decuplets, with opposite chiralities.

We analyse, where possible, the conditions necessary on the parameters of the Lagrangian which lead to the desired effects of decreasing the experimentally allowed PS breaking scale through helicity suppression and generating a viable fermion mass spectrum through

[20] With the caveat that the additional baryon number violating Yukawa interactions do not lead to proton and neutron decay rates larger than the experimental bounds.

[21] Note that in this case the mass mixing between $d-D$ and $e-E$ will be 'coupled' and the mass mixing matrices only differ by group theoretic factors.

| PS multiplet | $e-E$ mixing | $d-D$ mixing |
|---|---|---|
| $(\mathbf{1},\mathbf{1},\mathbf{3})$ | ✔ | ✖ |
| $(\mathbf{1},\mathbf{3},\mathbf{1})$ | ✔ | ✖ |
| $(\mathbf{1},\mathbf{2},\mathbf{2})$ | ✔ | ✖ |
| $(\mathbf{6},\mathbf{1},\mathbf{1})$ | ✖ | ✔ |
| $(\mathbf{10},\mathbf{1},\mathbf{1})$ | ✔ | ✔ |

TABLE 4.11: Summary of the results of Section 4.4.1 which indicates which viable fermion extensions lead to a seesaw with the charged leptons by adding heavy states $E$ or with the down quarks by adding heavy states $D$, required to explain the lack of mass-degeneracy predicted by PS. Including an $SU(2)_{L/R}$ triplet or bi-doublet will induce $e-E$ mixing and including an $SU(4)$ sextet will lead to $d-D$ mixing. Including two $SU(4)$ decouplet fermions of opposite chirality or will lead to 'coupled' $e-E$ and $d-D$ mixing.

mixing for all SM-like particles. We will separately consider the validity of charged-lepton mixing and down-quark mixing and finally comment on the more general scenarios where mixing occurs for both fermion types.

### 4.5.1 $e-E$ mixing

Mixing with heavy exotics within the charged-lepton sector will arise if at least one $SU(2)_{L/R}$ triplet or $SU(2)_{L/R}$ bi-doublet is included. As the minimal low-scale PS model already requires an additional singlet $S_L$ for viable neutrino mass, it would be attractive if these more complicated multiplets could allow for a viable mass spectrum for the neutral and charged leptons without the need for the singlet $S_L$. In this situation we parametrise the general mass mixing matrix for the charged leptons as

$$\mathcal{L}_{eE} = \begin{pmatrix} \overline{e_L} & \overline{E_L} \end{pmatrix} \underbrace{\begin{pmatrix} m_{ee} & m_{eE} \\ m_{Ee} & m_{EE} \end{pmatrix}}_{M_{eE}} \begin{pmatrix} e_R \\ E_R \end{pmatrix} + \text{H.c}, \tag{4.110}$$

where the different elements of $M_{eE}$ in terms of Lagrangian parameters are given in Sections 4.4.1.1 and 4.4.1.2 for each possible case we have considered. Additionally we parametrise the diagonalisation matrices for $M_{eE}$

$$U_L^\dagger\, M_{eE}\, U_R = \text{diag}(\dots) = M_{eE}^{\text{diag}}, \tag{4.111}$$

by

$$U_{L/R} = \begin{pmatrix} V & W \\ X & Y \end{pmatrix}_{L/R} \tag{4.112}$$

where the unitarity condition on $U$ implies $VV^\dagger + WW^\dagger = XX^\dagger + YY^\dagger = \mathbb{1}$ and $V^\dagger V + X^\dagger X = W^\dagger W + Y^\dagger Y = \mathbb{1}$. Therefore the relationship between the interaction and mass eigenstates for the charged leptons is given by

$$e_{L/R} = V_{L/R}\, e'_{L/R} + W_{L/R}\, E'_{L/R} \tag{4.113}$$

with $e'_{L/R}$ ($E'_{L/R}$) corresponding to the light (heavy) mass eigenstate. The fields $e_{L/R}$ correspond to the uncoloured components of $f_{L/R}$ charged under $SU(4)$ which couple to $d_{L/R}$ via $X_\mu$.

Therefore the relevant physical mixing matrices between the light, SM-like states and down quarks relevant for meson decays is given similarly to the vanilla PS scenario by

$$K_L^{de} = (U_L^d)^\dagger\, V_L, \quad K_R^{de} = (U_R^d)^\dagger\, V_R \tag{4.114}$$

where now the matrices $V_{L/R}$ are no longer unitary. The condition required for a chiral suppression to occur in the relevant pseudoscalar meson decays is for one of $K_{L/R}^{de}$ to satisfy

$$\|K_{L/R}^{de}\| \ll 1 \tag{4.115}$$

such that the helicity-unsuppressed contribution to each decay is sufficiently reduced as discussed in Section 4.3.2.

The limits on heavy charged-leptons are model-dependent but in all cases far exceed the masses of the SM charged leptons. For example for an $SU(2)_L$ triplet the limits are roughly 800 GeV [233] and reduce down to 300 GeV in the case of vector-like lepton doublets [234]. We will conservatively assume that the masses of the heavy charged-lepton states all exceed 1 TeV, this obviously requires at least one block appearing in $M_{eE}$ to have all its singular values larger than 1 TeV.

Comparing the general form of $M_{eE}$ in Eq. (4.110) to those derived for the cases of either $SU(2)_{L/R}$ triplet or the bi-doublet given in Eqs. (4.76), (4.79) and (4.85) respectively, we see that two possible mass terms can be significantly larger than the electroweak scale: either the Yukawa couplings $y^R_{\Psi_3} v_R$ or $y^R_{\Psi_{22}} v_R$ proportional to the scale of $SU(2)_R$ breaking (which is absent in the case of the $SU(2)_L$ triplet), or the bare mass terms $\mu_{\Psi_3}$ and $\mu_{\Psi_{22}}$ which are completely unconstrained. Therefore the correct phenomenological masses for the heavy charged leptons are possible in the scenarios where $\|y^R_{\Psi_3} v_R,\, y^R_{\Psi_{22}} v_R\| \geq 1$ TeV or $\|\mu_{\Psi_3},\, \mu_{\Psi_{22}}\| \geq 1$ TeV. In all cases the mass term generated by $v_R$ appears on the off-diagonal of $M_{eE}$, either in the top-right entry in the case of the bi-doublet extension and in the bottom-left entry for the case of an $SU(2)_R$ triplet. Although this term is absent in the case of the $SU(2)_L$ triplet, it may be generated in the bottom-left entry of $M_{eE}$ by assuming a modified scalar sector, which we discuss further below, and therefore the discussion below remains relevant for this exotic fermion choice. The bare mass terms $\mu_{\Psi_3}$ and $\mu_{\Psi_{22}}$ appear in the bottom-right entry in all three cases. We suppress the labels $\Psi_3$ and $\Psi_{22}$ below and write $y^R_\Psi v_R$ and $\mu_\Psi$ for simplicity.

Consider first the scenario where $\mu_\Psi$ is taken to be larger than all other mass terms, e.g. $\mu_\Psi = m_{EE} > m_{eE}, m_{Ee}, m_{ee}$. Following the results from Appendix D.0.1 the resultant masses for the seesaw states are approximated by

$$m_\ell \simeq \left| m_{ee} - \frac{m_{eE}\, m_{Ee}}{m_{EE}} \right| \qquad \text{and} \qquad m_{\hbar} \simeq m_{EE}. \tag{4.116}$$

Using Eq. (D.4) the mass eigenstates relate to the interaction eigenstates by

$$e_L \simeq \underbrace{\left(1 - \frac{1}{2}\left(\frac{m_{eE}}{m_{EE}}\right)^2\right)}_{V_L} e'_L + \underbrace{\left(\frac{m_{eE}}{m_{EE}}\right)}_{W_L} E'_L \tag{4.117}$$

for the left-handed states and

$$e_R \simeq \underbrace{\left(1 - \frac{1}{2}\left(\frac{m_{Ee}}{m_{EE}}\right)^2\right)}_{V_R} e'_R + \underbrace{\left(\frac{m_{Ee}}{m_{EE}}\right)}_{W_R} E'_R \tag{4.118}$$

for the right-handed states. One generation of fermions with real parameters has been assumed for simplicity in order to establish viability. Similar conclusions are reached for multi-generational scenarios where each entry of $M_{eE}$ is promoted to a block matrix of appropriate dimension. The one-dimensional equivalents of $V_{L/R}$ and $W_{L/R}$ are indicated and, as can be seen in this scenario where the bare mass is the dominant term in the charged-lepton seesaw, both the left- and right-handed light charged lepton mass states are predominantly made up of the fields $e_{L/R}$ embedded in $f_{L/R}$. Therefore, while this would lead to a very mild suppression in the PS mass limits as $V_{L/R}$ are slightly suppressed compared to the scenario without charged-lepton mass mixing (where $V_{L/R} = 1$), the mass limits obtained for $X_\mu$ will be of similar size to those appearing in Table 4.4 and therefore the limits will remain at around $\mathcal{O}(100 - 1000)$ TeV depending on the structure of $K^{de}_{L/R}$.

Alternatively, $y^R_\Psi v_R$ can be the dominant mass term within $M_{eE}$ which corresponds to one of the off-diagonal terms in our parametrisation. Following a similar procedure we find

$$m_\ell \simeq \left| m_{Ee} - \frac{m_{ee}\, m_{EE}}{m_{eE}} \right| \tag{4.119}$$

and

$$\begin{aligned} e_L &\simeq \underbrace{-\left(\frac{m_{EE}}{m_{eE}}\right)}_{V_L} e'_L + \underbrace{\left(1 - \frac{1}{2}\left(\frac{m_{EE}}{m_{eE}}\right)^2\right)}_{W_L} E'_L \\ e_R &\simeq \underbrace{\left(1 - \frac{1}{2}\left(\frac{m_{ee}}{m_{eE}}\right)^2\right)}_{V_R} e'_R + \underbrace{\left(\frac{m_{ee}}{m_{eE}}\right)}_{W_R} E'_R \end{aligned} \tag{4.120}$$

for the scenario where $m_{eE}$ is dominant and

$$m_\ell \simeq \left| m_{eE} - \frac{m_{ee}\, m_{EE}}{m_{Ee}} \right| \tag{4.121}$$

and

$$\begin{aligned} e_L &\simeq \underbrace{\left(1 - \frac{1}{2}\left(\frac{m_{ee}}{m_{Ee}}\right)^2\right)}_{V_L} e'_L + \underbrace{\left(\frac{m_{ee}}{m_{Ee}}\right)}_{W_L} E'_L \\ e_R &\simeq \underbrace{-\left(\frac{m_{EE}}{m_{Ee}}\right)}_{V_R} e'_R + \underbrace{\left(1 - \frac{1}{2}\left(\frac{m_{EE}}{m_{Ee}}\right)^2\right)}_{W_R} E'_R \end{aligned} \tag{4.122}$$

if $m_{Ee}$ is dominant. In both cases, one of $e_{L/R}$ is predominantly made up of the light mass state $e'_{L/R}$ while the opposite chirality is predominantly made up from the heavy mass state $E'_{R/L}$. $V_L$ or $V_R$ are now significantly different in size from each other, where one will be suppressed compared to the other. If $m_{eE}$ is the largest term then $V_L \ll V_R$ and the leptoquark $X_\mu$ will strongly couple $e'_R$ and $d'_R$ but not $e'_L$ and $d'_L$ and vice versa for $m_{Ee}$ dominance. Therefore the desired helicity suppression in meson decays induced by $X_\mu$ will occur for the hierarchy $y^R_\Psi v_R > \mu_\Psi$ leading to decreased PS breaking limits, potentially as low as those appearing in Table 4.7. Both an $SU(2)_R$ triplet or the $SU(2)_{L/R}$ bidoublet are therefore viable candidates as one off-diagonal term is proportional to $v_R$ and therefore can be large in size. In the case of an $SU(2)_L$ triplet, assuming no modification to the scalar fields, the only mass term not tied to the electroweak scale is $\mu_\Psi$ and therefore helicity suppression in the relevant meson decays will not occur as $\mu_\Psi$ must be dominant phenomenologically.

For a multi-generational scenario all terms in $M_{eE}$ are promoted to block matrices and using the results in Appendix D.0.2 we find for $\|m_{Ee}\| > \|m_{ee}, m_{eE}, m_{EE}\|$

$$m_L \simeq m_{eE} - m_{ee}\left(m_{Ee}^{-1}\right) m_{EE} \tag{4.123}$$

and

$$\begin{aligned} e'_L &\simeq \underbrace{\left(\mathbb{1} - \frac{1}{2}\left(m_{ee}m_{Ee}^{-1}\right)\left(m_{ee}m_{Ee}^{-1}\right)^\dagger\right) O_L}_{V_L}\, e_L + \underbrace{m_{ee}m_{Ee}^{-1}\mathcal{O}_L}_{W_L}\, E_L \\ e'_R &\simeq -\underbrace{m_{Ee}^{-1}m_{EE}\, O_R}_{V_R}\, e_R + \underbrace{\left(\mathbb{1} - \frac{1}{2}\left(m_{Ee}^{-1}m_{EE}\right)\left(m_{Ee}^{-1}m_{EE}\right)^\dagger\right)\mathcal{O}_R}_{W_R}\, E_R \end{aligned} \tag{4.124}$$

where $O_{L/R}$ and $\mathcal{O}_{L/R}$ are the unitary matrices which diagonalise the light and heavy mass blocks which appear after block diagonalisation, e.g. $O_L^\dagger m_L O_R = \mathrm{diag}(\dots)$. For obvious reasons these expressions are only valid when $m_{Ee}$ is nonsingular. Similar expressions for $m_{eE}$ dominance can be derived quite simply and the results only differ by the same permutations of parameters as between Eqs. (4.119) and (4.120).

One last potential scenario which will lead to the heavy lepton masses exceeding 1 TeV occurs for the tuned case $y_\Psi v_R \simeq \mu_\Psi$. Consider for example when $m_{Ee} \simeq m_{EE}$ and are both dominant in $M_{eE}$. We find for one generation

$$m_\ell \simeq \left| \frac{m_{ee} - m_{eE}}{\sqrt{2}} \right| \tag{4.125}$$

and

$$\begin{aligned} e_L &\simeq -\underbrace{\left(1 - \frac{1}{4}\left(\frac{m_{eE}+m_{ee}}{m_{Ee}}\right)^2\right)}_{V_L} e'_L + \underbrace{\frac{1}{2}\left(\frac{m_{eE}+m_{ee}}{m_{Ee}}\right)}_{W_L} E'_L \\ e_R &\simeq \underbrace{\frac{1}{\sqrt{2}}}_{V_R} e'_R + \underbrace{\frac{1}{\sqrt{2}}}_{W_R} E'_R \end{aligned} \tag{4.126}$$

with similar results if $m_{eE} \simeq m_{EE}$ except for the reassignments $L \leftrightarrow R$ on the fields above. Here the mass eigenstate $e'_R$ is made up of a roughly equal amount of the fields $e_R$ and $E_R$ and therefore while the mixing parameter $V_R$ is decreased, it remains an order one number. The overall strength of $K_R^{de}$ will be lowered, however the helicity-unsuppressed contribution for each meson decay will remain dominant as it is several orders of magnitude larger than the helicity-unsuppressed contribution, as discussed in Section 4.3.2. Therefore we find that in order for helicity suppression to allow for decreased experimental limits on the PS breaking scale, the hierarchy $y_\Psi^R v_R \gg \mu_\Psi$ is required.

We will therefore adopt the hierarchy $\|y_\Psi^R v_R\| > \|y_\Psi v_L,\, m_e,\, \mu_\Psi\|$ below in order to helicity suppress the mass limits of $X_\mu$, further requiring the correct down-quark and charged-lepton masses with appropriate SM-like weak couplings as a secondary condition will further restrict the parameters in each mass mixing matrix.

Specifically for the case of an $SU(2)_R$ triplet, adopting the above hierarchy in $M_{eE}$ leads to the light-mass block approximately given by

$$m_\ell \simeq -\frac{1}{v_R} m_d \left(Y_{\Psi_3}\right)^{-1} \mu_{\Psi_3} \tag{4.127}$$

where we have introduced three generations of the triplet $\Psi_3^R$ and $Y_{\Psi_3}$ corresponds to a $3 \times 3$ matrix further assumed to be nonsingular. Unless stated otherwise, and for the remainder of the chapter, $y_\Psi$ and $Y_\Psi$ will distinguish between when one or three generations of exotic fermions are introduced respectively. Within Eq. (4.127) we have used the relation $m_e = m_d$ which is enforced by the PS symmetry and therefore the singular values of $m_d$ are given by the down-quark masses run up to the PS breaking scale. Similarly the singular values of the light block $m_\ell$ must be given by the masses of the charged-leptons at the same scale. An unavoidable consequence of Eq. (4.127) is that it necessarily predicts that all generations of charged leptons have masses strictly lighter than their corresponding generation of down-quark. We prove this result in Appendix D.0.3. While this is accurate for the first and third generations, this mass hierarchy is flipped in the second generation as shown in Table 4.6 where the muon is heavier than the strange quark at least for energy scales below 1000 TeV which we are considering.

Therefore we find that Eq. (4.127) is unable to reproduce the correct charged-lepton masses if $m_e = m_d$ is enforced by the PS symmetry to give the down-quark masses. The alternative seesaw scenario where $\|\mu_{\Psi_3}\| > \|Y_{\Psi_3} v_R\|$, although unable to lead to the desired chiral suppression in the PS breaking scale, is also unable to reproduce the correct muon and strange masses as it requires $m_\ell \simeq m_d$. Therefore a potential hybrid scenario where the hierarchy in the singular values between $Y^R_{\Psi_3} v_R$ and $\mu_{\Psi_3}$ flips for the second generation compared to the first and third would also not be viable. Similar arguments apply to the $SU(2)_L$ triplet, which was already unable to give sufficiently heavy masses to the charged-lepton partners. Therefore both triplet scenarios are unable to reproduce the correct charged-lepton masses in their minimal form. This is a direct consequence of the zero entry appearing in the mass matrix $M_{eE}$ but applies to any similar scenario with quark-lepton mass unification and exotic mass mixing. Similar arguments apply to the scenario where both an $SU(2)_L$ and $SU(2)_R$ triplet are added as in Eqs. (4.81) and (4.82) and therefore we find that $SU(2)_{L/R}$ triplets require a more exotic scalar sector such that all mass terms in the Yukawa Lagrangian can be generated.

#### 4.5.1.1 Top-right dominance: Bi-doublet fermions

Turning to the case of the $SU(2)_{L/R}$ bi-doublet, now each entry of the charged-lepton mass matrix $M_{eE}$ is non-zero. The choice $\|Y_{\Psi_{22}} v_R\| > \|\mu_{\Psi_{22}}\|$, such that the desired suppression in the PS limits occurs, implies that the top-right entry of $M_{eE}$ is the dominant block, as can be seen in Eq. (4.85). Therefore the light mass block is given by

$$m_\ell \simeq Y^L_{\Psi_{22}} v_L - \frac{1}{v_R} \mu_{\Psi_{22}} (Y^R_{\Psi_{22}})^{-1} m_d \tag{4.128}$$

where again the PS symmetry enforces $m_e = m_d$. Now with the addition of the mass term $Y^L_{\Psi_{22}} v_L$ the correct charged-lepton masses can be generated. For example in the limit $\mu_{\Psi_{22}} \to 0_{3\times 3}$ the charged lepton masses are simply given by

$$m_\ell \simeq Y^L_{\Psi_{22}} v_L \tag{4.129}$$

and therefore the effect of the seesaw in $M_{eE}$ is to completely disassociate the mass origin of the SM-like charged leptons from the down quarks as now they arise from different Yukawa couplings and vevs and implies that $v_L \gtrsim m_\tau$ for perturbative couplings.

Using Appendix D.0.2, the mass states of the light leptons relate to the interaction states by

$$\begin{aligned} e'_L &\simeq -(O^e_L)^\dagger \mathcal{X} e_L + (O^e_L)^\dagger \left(\mathbb{1} - \frac{1}{2}\mathcal{X}\mathcal{X}^\dagger\right) E_L \\ e'_R &\simeq (O^e_R)^\dagger \left(\mathbb{1} - \frac{1}{2}\mathcal{Z}^\dagger\mathcal{Z}\right) e_R - (O^e_R)^\dagger \mathcal{Z}^\dagger E_R \end{aligned} \tag{4.130}$$

where $O^e_{L/R}$ diagonalise the light mass block and

$$\begin{aligned} \mathcal{X} &\simeq \frac{1}{v_R}\mu_{\Psi_{22}} \left(Y^R_{\Psi_{22}}\right)^{-1} + \frac{v_L}{v_R^2} Y^L_{\Psi_{22}} m_d^\dagger [(Y^R_{\Psi_{22}})^\dagger]^{-1} (Y^R_{\Psi_{22}})^{-1}, \\ \mathcal{Z} &\simeq \frac{1}{v_R}(Y^R_{\Psi_{22}})^{-1} m_d + \frac{v_L}{v_R^2}(Y^R_{\Psi_{22}})^{-1}[(Y^R_{\Psi_{22}})^\dagger]^{-1}\mu^\dagger_{\Psi_{22}} Y^L_{\Psi_{22}} \end{aligned} \tag{4.131}$$

and we have expanded up to second order in $\mathcal{X}$ and $\mathcal{Z}$. In this seesaw regime, the light left-handed lepton states measured in experiments are predominately made up of $E_L$ appearing in the bi-doublet whereas the right-handed light states are predominately made up of $e_R$ appearing in $f_R$ which interacts with $X_\mu$.

For clarity, the relevant physical mixing matrices are given by

$$K^{de}_L \simeq -(U^d_L)^\dagger \mathcal{X}^\dagger O^e_L,\ K^{de}_R \simeq (U^d_R)^\dagger \left(\mathbb{1} - \frac{1}{2}\mathcal{Z}^\dagger\mathcal{Z}\right) O^e_R \text{ and } U_{\text{PMNS}} \simeq N^\dagger_\nu \left(\mathbb{1} - \frac{1}{2}\mathcal{X}\mathcal{X}^\dagger\right) O^e_L, \tag{4.132}$$

where $N_\nu$ corresponds to the relevant non-unitary submatrix of the neutral fermion diagonalising matrix for the active neutrinos. Therefore in this scenario the deviation from unitarity of the PMNS matrix arising from mixing in the charged lepton sector *and* the suppression of the matrix $K^{de}_L$ is determined by the smallness of the matrix $\mathcal{X}$. In Eq. (4.131) we have included the second order terms in the expansion as for sufficiently small values in the matrix $\mu_{\Psi_{22}}$ this deviation will be dominated by the second-order term. As $Y^L_{\Psi_{22}} v_L$ and $m_d$ are fixed to give the correct SM charged-lepton and down-quark masses respectively, the second order term is therefore fixed for a given choice of $Y^R_{\Psi_{22}} v_R$ and therefore can place a lower bound on the scale $v_R$ required to satisfy both PMNS unitarity constraints and lead to the desired chiral suppression in the rare meson decays which constrain PS.

The neutrino mass matrix with the addition of the fermion bi-doublets is given by the block matrix equivalent of Eq. (4.86) which specifically for the hierarchy $\|Y^R_{\Psi_{22}} v_R\| > \|m_u, Y^L_{\Psi} v_L\| > \|\mu_{\Psi_{22}}\|$ leads to the following four mass blocks (after block diagonalisation):

$$\begin{aligned} m_{1,2} &\simeq v_R\, Y^R_{\Psi_{22}} & \nu_{1/2} &\simeq \frac{1/i}{\sqrt{2}}(\nu_L \pm N^c_R) \\ m_3 &\simeq \frac{v_L}{v_R}\left(Y^L_{\Psi_{22}}(Y^R_{\Psi_{22}})^{-1} m_u + m_u^T\left[Y^L_{\Psi_{22}}(Y^R_{\Psi_{22}})^{-1}\right]^T\right) & \nu_3 &\simeq \nu^c_R \\ m_4 &\simeq \frac{1}{v_L v_R}\mu_{\Psi_{22}}\left[(Y^L_{\Psi_{22}})^T m_u^{-1} Y^R_{\Psi_{22}} + (Y^R_{\Psi_{22}})^T (m_u^T)^{-1} Y^L_{\Psi_{22}}\right]^{-1}\mu^T_{\Psi_{22}} & \nu_4 &\simeq N_L. \end{aligned} \tag{4.133}$$

Here there is a heavy pseudo-Dirac pair with degenerate masses to the heavy charged leptons, a light neutrino block with mass arising from a linear seesaw mechanism whose mass eigenstate is predominantly made up of $\nu_R$. and an even-lighter neutrino mass block which is predominantly made up of $N_L$ appearing in the bi-doublet. Therefore

$$m_{\nu_4} \ll m_{\nu_3} \ll m_{\nu_1}, m_{\nu_2} \tag{4.134}$$

where $m_{\nu_4}$ corresponds to the three light neutrinos observed through oscillation experiments. A more complete expression for the relationship between the neutrino mass and interaction eigenstates can be found at the end of Appendix D.0.4. In Appendix D.0.4 we argue that the above scenario where $\mu_{\Psi_{22}}$ is significantly smaller than all other mass parameters, which will lower the experimental limits on PS breaking, is the only scenario which allows for an experimentally valid spectrum of active neutrino masses unless a PS breaking scale larger than $10^{11}$ GeV is adopted. It is quite striking that the only hierarchy of parameters which allows for both low scale PS breaking and appropriately light active neutrino masses, when bi-doublet fermions are introduced, is the same hierarchy that will lead to a suppression in the experimental limits on the PS breaking scale. Additionally, in the limit $\mu_{\Psi_{22}} \to 0_{3\times 3}$ where the lightest neutrinos are massless at tree-level, there is an additional global symmetry conserved in the Yukawa Lagrangian and therefore taking this mass matrix to be small is technically natural.

The correct charged-lepton masses for each generation and the active neutrino mass limits and differences can both be achieved with the addition of the bi-doublet without needing to introduce any additional states, such as the singlet $S_L$. Equations (4.128) and (4.133) can be solved simultaneously for the three unknown blocks $Y^R_{\Psi_{22}}$, $Y^L_{\Psi_{22}}$ and $\mu_{\Psi_{22}}$ with the assumed hierarchy between each block. In the one generational scenario, the masses of the two lightest neutrino states and the light charged lepton state are given by

$$m_{\nu_3} \simeq \frac{v_L}{v_R}\frac{2y^L_{\Psi_{22}} m_t}{y^R_{\Psi_{22}}} \tag{4.135}$$

$$m_{\nu_4} \simeq \frac{1}{v_L v_R}\frac{\mu^2_\Psi m_t}{2y^L_{\Psi_{22}} y^R_{\Psi_{22}}} \tag{4.136}$$

$$m_\ell \simeq v_L y^L_{\Psi_{22}} - \frac{\mu_\Psi m_b}{v_R y^R_{\Psi_{22}}} \tag{4.137}$$

where we have fixed the masses of the quarks to the top- and bottom-quark respectively. Setting $m_\ell \simeq 1$ GeV in order to reproduce the correct tau mass and $m_b \simeq 4$ GeV and $m_t \simeq 173$ GeV leads to Fig. 4.4 where we find the required size of $\mu_{\Psi_{22}}$ as a function of $y^R_{\Psi_{22}} v_R$ for different choices of the light neutrino mass. We find for sub-eV neutrino masses, setting $v_R$ to be between $1 - 100$ TeV requires $\mu_{\Psi_{22}}$ to be below the MeV scale. Due to the small size of $\mu_{\Psi_{22}}$ required from neutrino mass limits, the term $\mu_{\Psi_{22}} m_d / y^R_{\Psi_{22}} v_R$ entering the charged lepton masses is negligible compared to $y^L_{\Psi_{22}} v_L$ and therefore the correct charged-lepton masses are easily possible. As discussed, such small values of $\mu_{\Psi_{22}}$ required for neutrino mass quite conveniently also lead to a chiral suppression in the PS breaking scale. The mass of the intermediately heavy neutrino, $\nu_3$, will vary only with the size of $y^R_{\Psi_{22}} v_R$ as all other parameters are related to SM masses. The predicted mass of $m_{\nu_3}$ lies roughly between the MeV and GeV scales depending on the $v_R$ breaking scale, with larger scales of $SU(2)_R$ breaking corresponding to lighter masses as demonstrated in the second plot of Fig. 4.4. We note that for this proposed scenario, the quark masses arise from the vevs $v_1$ and $v_2$ from $\phi$ whereas the charged-lepton masses predominately arise from the vev $v_L$ appearing in $f_L$.

The lightest neutrino mass eigenstate arises predominantly from the state $N_L$ appearing in the bi-doublet fermion $\Psi_{22}$ and therefore, as phenomenologically required, will have

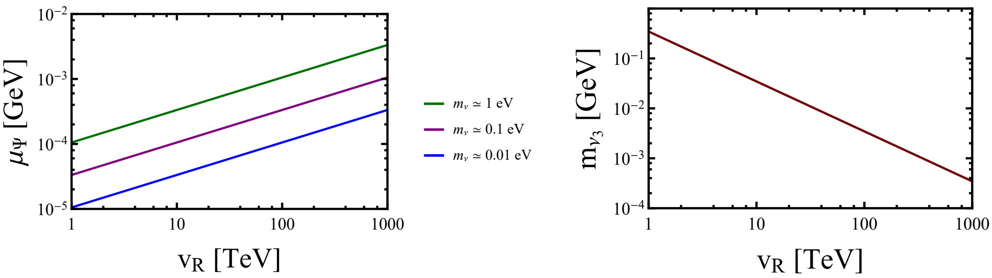


FIGURE 4.4: Plot of the required size of $\mu_{\Psi_{22}}$ in GeV as a function of $v_R$ in TeV in the one generational scenario where $y^R_{\Psi_{22}} = 1$ has been assumed **(left)** and the masses of the intermediately heavy neutrino as a function of the same scale **(right)**. Different lines correspond to different choices for the value of the neutrino masses and we have fixed $m_\ell \simeq 1$ GeV, $m_b \simeq 4$ GeV and $m_t \simeq 173$ GeV in order to reproduce the correct tau, bottom- and top-quark masses. Requiring sufficiently light neutrinos is only possible when $\mu_{\Psi_{22}}$ is sufficiently small which also happens to be the requirement in order to helicity-suppress the experimental limits on PS breaking.

SM-like weak interactions. The left-handed charged-lepton mass eigenstates arise predominantly from the state $E_L$ which appears in the same bi-doublet as $N_L$, as shown in Eq. (4.84), additionally they form an $SU(2)_L$ doublet with each other after $SU(2)_R$ breaking. The (pseudo-unitary) PMNS matrix is identified from the coupling of $W_L^\pm$ to $N_L$ and $E_L$ as

$$U_L = (\mathbb{1} - \eta')\, U_N^\dagger\, (\mathbb{1} - \eta')\, O_L^e \tag{4.138}$$

where

$$\eta' \simeq \frac{1}{2}\mathcal{X}\mathcal{X}^\dagger \tag{4.139}$$

measures the deviation from unitarity arising from mixing. We find the deviation to be the same in both sectors, at least at the lowest order, as explained in Appendices D.0.2 and D.0.4. As usual $U_N$ and $O_L^e$ are the unitary matrices which diagonalise the light mass blocks in each sector of the block-diagonal mass matrices.

Writing

$$\begin{aligned} U_L &= \left[(\mathbb{1} - \eta')\, U_N^\dagger\, (\mathbb{1} - \eta')\, O_L^e\right] \left[(O_L^e)^\dagger U_N U_N^\dagger O_L^e\right] \\ &= \left[(\mathbb{1} - \eta')\, U_N^\dagger\, (\mathbb{1} - \eta')\, U_N\right] U_N^\dagger O_L^e \\ &\simeq \left(\mathbb{1} - \eta' - U_N^\dagger \eta' U_N\right) U_N^\dagger O_L^e \\ &= (\mathbb{1} - \eta)\, U_{\mathrm{PMNS}} \end{aligned} \tag{4.140}$$

allows us to estimate the deviation from unitarity by $(\mathbb{1} - \eta)$, as is usually done, where

$$\eta \simeq \eta' + U_N^\dagger \eta' U_N \tag{4.141}$$

and we identify the combination $U_N^\dagger O_L^e$ with the unitary PMNS matrix as usual.

The left plot of Fig. 4.5 shows the deviation from unitarity as a function of $\mathcal{X} \simeq \mu_{\Psi_{22}}(Y^R_{\Psi_{22}})^{-1}$ where we have fixed $U_N = \mathbb{1}$ for simplicity. We further assumed that $Y^R_{\Psi_{22}}$ was diagonal with entries close to unity such that the vev of $v_R$ can be as small as possible[22]. We then performed two scans over different values of $v_R$ ranging from 1 TeV to $10^4$ TeV. In the first scan (in blue) we randomly scanned over the entries of $\mu_{\Psi_{22}}$ and therefore do not generate the correct neutrino mass spectrum but establishes the relationship between $\eta$ and $\mu_{\Psi_{22}}$. The second scan (in red) had $\mu_{\Psi_{22}}$ fixed for a given $v_R Y^R_{\Psi_{22}}$ through a Casas-Ibarra parametrisation in order to generate the correct charged lepton and neutrino masses. The resultant PMNS matrix was compared to the experimental limits on the deviation from unitarity, $\eta^{\text{exp}}$ which we take from [147], and we find that the region which leads to a viable mass spectrum for the SM leptons predicts a deviation of unitary many orders of magnitude below the current limit. This is due to the deviation being proportional to the small matrix $\mu_{\Psi_{22}}$. For alternative models where, for example, the size of $\mu_{\Psi_{22}}$ and therefore $\|\mathcal{X}\|_F$ is not fixed to be small by requiring small neutrino masses (through the introduction of additional neutral lepton mass mixing), deviation from unitarity limits constrain

$$\|\mathcal{X}\|_F \lesssim 10^{-1}. \tag{4.142}$$

Fig. 4.6 plots the experimental limits on the mass of $X_\mu$ as a function of $\mathcal{X}$ where again points in blue have the entries of $\mu_{\Psi_{22}}$ randomly scanned over and points in red correspond to where $\mu_{\Psi_{22}}$ has been fixed by through a Casas-Ibarra parameterisation. We find that the only region of parameter space which allows for a low-scale seesaw in the charged lepton and neutrino masses also happens to be the region where the limits on the mass of $X_\mu$ have been completely helicity suppressed to their lowest values. The plot on the left and right represent two different choices of $K^{de}_{L/R}$ where we find the same behaviour regardless of the form of $K^{de}_{L/R}$. For some more complicated scenario where the entries of $\mathcal{X}$ are not related to the smallness of neutrino mass, deviation from

[22] For a non-degenerate spectrum of singular values in $Y_{\Psi_{22}}$, requiring all the masses of the heavy charged leptons to be larger than 1 TeV requires larger $v_R$ breaking scales, e.g. if $\sigma_1(Y_{\Psi_{22}}) = 1/100$ then this requires $v_R \geq 100$ TeV.

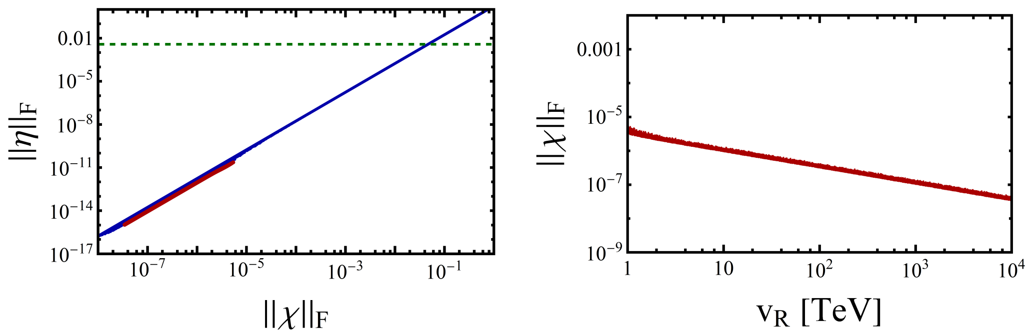


FIGURE 4.5: Plot of the deviation of unitarity **(left)** as a function of $\mathcal{X}$ where points in blue correspond to a random scan on the entries of $\mu_{\Psi_{22}}$ and $Y^R_{\Psi_{22}}$ whereas points in red correspond to the region which gives the correct charged-lepton and neutrino masses through a Casas-Ibarra parameterisation. We find that there are no limits on the scale $v_R$ from unitarity violation and furthermore the region with a viable neutrino mass spectrum predicts a deviation of unitarity many orders of magnitude less than the experimental precision. The **(right)** plot shows the generated $\mathcal{X}$ through the Casas-Ibarra parameterisation as a function of $v_R$ which leads to a viable charged-lepton and neutrino mass spectrum. As the deviation of unitary is given by $\eta \simeq \mathcal{X}^2$, the deviation at all scales is significantly smaller than the current experimental limits. $\|\cdot\|_F$ corresponds to the Frobenius norm of the given matrix which we use to present the data and the limits on the deviation indicated by the dashed green line is taken from [147].

unitarity limits require $\|\mathcal{X}\|_F \lesssim 10^{-1}$ and therefore would at a minimum lead to the limits decreasing by about a factor of a half compared to the limits obtained without any charged-lepton mixing. For values where $\|\mathcal{X}\|_F \lesssim 10^{-2}$ the limits on the mass of $X_\mu$ are decreased by about an order of magnitude and for $\|\mathcal{X}\|_F \lesssim 10^{-3}$ the limits are completely helicity suppressed to their lowest values.

Therefore we find that with the addition of fermionic $SU(2)_{L/R}$ bi-doublets to the usual PS fermions the singlet $S_L$ is no longer necessary for the generation of neutrino masses. The down-quark, charged-lepton and neutrino masses can all be successfully generated for low scales of PS breaking only in the region where $\|\mu_{\Psi_{22}}\|$ is smaller than all other mass parameters, and this region also leads to an order of magnitude reduction in the limits on $m_X$ through helicity suppression. The smallness of the entries of $\mu_{\Psi_{22}}$ can be justified through technical naturalness, since a new global symmetry is recovered (which can be identified with a type of lepton number) when they are taken to zero. In this limit the active neutrino become massless, however other massive Majorana neutrinos are present.

A number of predictions for the exotic fermions can be made in the scenario where only $f_{L/R}$ and $\Psi_{22}$ are present. Firstly heavy charged-lepton partners and pseudo-Dirac pairs of heavy neutrinos are predicted to have the same masses as each other at the

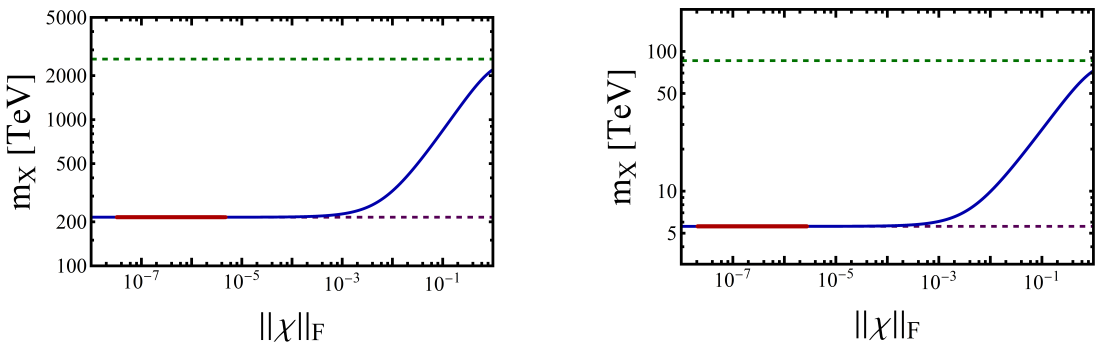


FIGURE 4.6: Plot of the experimental limits on $m_X$ as a function of $\mathcal{X}$ where we have assumed $K^{de}_{L/R} = \mathbb{1}$ **(left)** and mixing angles given by the fifth row of Tables 4.5 and 4.9 **(right)**. Points in blue correspond to a random scan over $\mu_{\Psi_{22}}$ in order to establish its variation whereas points in red correspond to where the entries of $\mu_{\Psi_{22}}$ are fixed through a Casas-Ibarra parameterisation to give a valid neutrino mass spectrum. We find that all regions which lead to a viable neutrino mass spectrum also imply that the limits on the mass of $X_\mu$ are completely helicity suppressed. This remains true for any choices of the physical mixing matrices $K^{de}_{L/R}$. The horizontal dashed green lines corresponds to the limits obtained without helicity suppression, as in Tables 4.3 to 4.5, and the horizontal dashed purple lines corresponds to the limits calculated with exact helicity suppression as in Tables 4.7 to 4.9. For large values of $\|\mathcal{X}\|_F$ the limits on the mass of $X_\mu$ approach their usual values whereas for values where $\|\mathcal{X}\|_F \lesssim 10^{-3}$ the limits on $m_X$ are almost identical to the limits obtained with exact helicity suppression.

scale of $SU(2)_R$ breaking and additional, intermediately heavy neutrinos are predicted to exist with masses between MeV to GeV which are sufficiently heavy to not violate any cosmological bounds. For more complicated scenarios with additional fermions (but the same charged-lepton mass mixing matrix), where the size of $\mathcal{X}$ is not tied to the smallness of neutrino mass, we find that unitarity deviation constraints begin to constrain the overall size of $\mathcal{X}$ and imply that the limits on $m_X$ must be reduced by at least a factor of a half.

#### 4.5.1.2 Bottom-left dominance: $SU(2)_{L/R}$ Triplet fermions

The analysis of the alternative scenario where the mass matrix $Y^R_\Psi v_R$ appears in the bottom-left entry of $M_{eE}$ (such as when an $SU(2)_R$ triplet is added) follows very similarly to the above, with only a few key differences. As mentioned previously, the scalar content we have chosen is unable to generate a viable charged lepton mass spectrum in the case of the triplets due to the lack of an $e_L E_R$ or $E_L e_R$ mass term in the Yukawa sector, as per Eqs. (4.76) and (4.79). However, these missing mass terms can be generated through a modified scalar sector. For example, if $\chi_L \sim (\mathbf{4}, \mathbf{2}, \mathbf{1})$ is replaced with $\chi' \sim (\mathbf{4}, \mathbf{2}, \mathbf{3})$ then, as was first noted in [213], the missing mass term in the top-right entry of $M_{eE}$ in

Eq. (4.76), proportional to $v_L$, is generated for the case of an $SU(2)_R$ triplet. Similarly, if $\chi_R \sim (\mathbf{4},\mathbf{1},\mathbf{2})$ is replaced with $\chi'' \sim (\mathbf{4},\mathbf{3},\mathbf{2})$ then the missing mass term in the bottom-left entry of $M_{eE}$, proportional to $v_R$, is generated for the case of an $SU(2)_L$ triplet. We therefore assume that all mass terms are generated in what follows, with a $Y^R_{\Psi_3} v_R$ mass matrix appearing in the bottom-left entry of $M_{eE}$ in Eq. (4.79), but remain agnostic about the scalar sector which generates it.

We shall also not undertake a detailed study of the requirements for neutrino masses in these modified scenarios, but make the following brief observations: A crucial difference between the triplet and bi-doublet scenarios is that the neutral lepton mass mixing matrix in the case of triplets is given by an inverse/linear seesaw similar to Eq. (4.18), with the exception that the terms are also related to the charged-lepton mass mixing matrix. In Appendix D.0.5 we argue that, unlike the bi-doublet case, the mass mixing matrices in this scenario are such that low-scale seesaws for the neutrinos and charged leptons are unable to correctly reproduce the SM lepton masses. A viable setup therefore requires additional physics to further decouple the charged- and neutral-lepton mass mixing matrices, for example with the addition of singlet fermions $S_L$ [213] which also appear in the usual low-scale PS particle spectrum. Introducing $SU(2)_L$ or $SU(2)_R$ triplets therefore requires both a modification of the scalar content of the theory (to generate a viable charged-lepton mass spectrum), as well as *additional* fermionic states to generate sufficiently light neutrinos for low scales of PS breaking.

We therefore assume some additional physics is included in the neutrino sector to allow for a viable mass spectrum and simply comment on the implications of a charged-lepton mass matrix of the form

$$\mathcal{L}_{eE} = \begin{pmatrix} \overline{e_L} & \overline{E_L} \end{pmatrix} \begin{pmatrix} m_d & Y^L_{\Psi_3} v_L \\ \sqrt{2}\, Y^R_{\Psi_3} v_R^* & \mu_{\Psi_3} \end{pmatrix} \begin{pmatrix} e_R \\ E_R \end{pmatrix}, \tag{4.143}$$

where the dominant seesaw term is in the bottom-left entry has on the limits on PS breaking through $m_X$.

Adopting the hierarchy $\|Y^R_{\Psi_3}\| > \|m_d,\, \mu_{\Psi_3},\, Y^L_{\Psi_3} v_L\|$, necessary for a chiral suppression to occur, leads to

$$m_\ell \simeq v_L Y^L_{\Psi_3} - \frac{1}{v_R} m_d (Y^R_{\Psi_3})^{-1} \mu_\Psi \tag{4.144}$$

for the light states after diagonalisation. The relationship between the interaction and mass eigenstates is now given by

$$
\begin{aligned}
e'_L &\simeq (O^e_L)^\dagger \left(\mathbb{1} - \frac{1}{2}\mathcal{X}\mathcal{X}^\dagger\right) e_L - (O^e_L)^\dagger \mathcal{X}\, E_L \\
e'_R &\simeq -(O^e_R)^\dagger \mathcal{Z}^\dagger\, e_R + (O^e_R)^\dagger \left(\mathbb{1} - \frac{1}{2}\mathcal{Z}^\dagger \mathcal{Z}\right) E_R
\end{aligned}
\tag{4.145}
$$

where $O^e_{L/R}$ diagonalises the light mass block,

$$
\begin{aligned}
\mathcal{X} &\simeq \frac{1}{v_R} m_d \left(Y^R_{\Psi_3}\right)^{-1} + \frac{v_L}{v_R^2} Y^L_{\Psi_3} \mu^\dagger_{\Psi_3} [(Y^R_{\Psi_3})^\dagger]^{-1} (Y^R_{\Psi_3})^{-1} \\
\mathcal{Z} &\simeq \frac{1}{v_R} (Y^R_{\Psi_3})^{-1} \mu_{\Psi_3} + \frac{v_L}{v_R^2} (Y^R_{\Psi_3})^{-1} [(Y^R_{\Psi_3})^\dagger]^{-1} m_d^\dagger Y^L_{\Psi_3}
\end{aligned}
\tag{4.146}
$$

and we have expanded up to second order. The physical mixing matrices are now given by

$$
K^{de}_L \simeq -(U^d_L)^\dagger \left(\mathbb{1} - \frac{1}{2}\mathcal{X}\mathcal{X}^\dagger\right) O^e_L,\ K^{de}_R \simeq -(U^d_R)^\dagger \mathcal{Z} O^e_R \text{ and } U_{\text{PMNS}} \simeq N^\dagger_\nu \left(\mathbb{1} - \frac{1}{2}\mathcal{X}\mathcal{X}^\dagger\right) O^e_L.
\tag{4.147}
$$

The notable differences to the results in the previous section where the top-right entry of $M_{eE}$ is dominant are: (i) the leptoquark $X_\mu$ now effectively only couples to the left-handed states (compared with right-handed previously), and (ii) the parameter controlling the deviation from unitarity for the PMNS and the parameter determining the degree of helicity suppression in meson decays are different. Unitarity deviation is determined by $\mathcal{X}$, which is given at lowest order by $\mathcal{X} \simeq m_d (Y^R_{\Psi_3} v_R)^{-1}$, while the degree of helicity suppression in the $X_\mu$ couplings is given by $\mathcal{Z} \simeq (Y^R_{\Psi_3} v_R)^{-1} \mu_{\Psi_3}$. In the previous scenario of top-right entry dominance, both are controlled by $\mathcal{X}$ which in that case was given by $\mathcal{X} \simeq (Y^R_{\Psi_3} v_R)^{-1} \mu_{\Psi_3}$. Unlike before where $\mu_{\Psi_3}$ could be lowered, the only way to decrease the deviation from unitarity is by increasing the scale $v_R$ as $m_d$ is fixed by the SM down-quark masses. This leads to larger masses for the leptoquark $X_\mu$, and thus experimental limits on the deviation will more strongly constrain the allowed scales of $SU(2)_R$ breaking. As before, the degree of helicity suppression is controlled by $\mathcal{Z} \sim (Y^R_{\Psi_3} v_R)^{-1} \mu_{\Psi_3}$ but now there are no constraints on $\mathcal{Z}$ from unitarity deviation.

The two plots of Fig. 4.7 show the size of $\mathcal{X}$ as a function of $v_R$ where as before we consider the singular values in $Y^R_{\Psi_3}$ to vary between 0.1 and 1. Points in blue correspond to $\mathcal{X}$ at first order where

$$\mathcal{X}^{(1)} \simeq m_d(Y^R_{\Psi_3} v_R)^{-1} \tag{4.148}$$

and points in light purple correspond to where $\mathcal{X}$ has been calculated up to second order where

$$\mathcal{X}^{(2)} \simeq \mathcal{X}^{(1)} + \frac{v_L}{v_R^2} Y^L_{\Psi_3} \mu^\dagger_{\Psi_3} [(Y^R_{\Psi_3})^\dagger]^{-1} (Y^R_{\Psi_3})^{-1}. \tag{4.149}$$

As $\mu_{\Psi_3}$ is a free parameter – it is not fixed from the requirement of a viable neutrino mass spectrum – for regions where $\|\mu_{\Psi_3}\| \gg \|m_d\|$ the second order term in $\mathcal{Z}$ can dominate leading to larger levels of unitarity deviation. Of course for larger values of $\mu_{\Psi_3}$ the degree of helicity suppression in the limits on $m_X$ also decreases leading to larger limits on the PS breaking scale. The right plot of Fig. 4.7 shows the level of unitarity deviation in the most experimentally constrained entry of $\eta$ and it shows that for all values of $v_R$ the deviation is below the current experimental limit. Unlike the previous scenario, as $\mu_{\Psi_3}$ enters $\mathcal{X}$ at second order, large values of $\mu_{\Psi_3}$ are not constrained by requiring $|\eta_{ij}| < |\eta^{\text{exp}}_{ij}|$. For $v_R \sim 1$ TeV and large values in the entries of $\mu_{\Psi_3}$, the deviation from unitarity in the most constrained entry of $\eta$ is roughly one order of magnitude below the current experimental limits. For small values of $\mu_{\Psi_3}$ (which correspond to the region which helicity suppresses the limits on $m_X$) the predicted deviation in unitarity is roughly an order of magnitude smaller. Unlike the previous scenario, however, Fig. 4.7 demonstrates that as the constraints on $\eta^{\text{exp}}$ get stronger, they will lead to constraints on the allowed magnitude of $v_R$. This will require limits several orders of magnitude stronger than the current ones.

Similarly to the scenario with top-right dominance, the level of chiral suppression in the couplings of $X_\mu$ is controlled by $\mathcal{Z} \simeq \mu_{\Psi_3}(Y^R_{\Psi})^{-1}$. The left plot of Fig. 4.8 demonstrates that the variation in the limits on $m_X$ vary in the exact same way as Fig. 4.6 and requiring complete helicity suppression in the limits on $m_X$ requires $\|\mathcal{Z}\|_F \lesssim 10^{-3}$ as before.

Whereas in the bi-doublet scenario the smallness of $\mu_{\Psi_{22}}$ could be directly connected to the light neutrino masses, here we find additional physics is required for a phenomenologically-viable neutrino mass spectrum. Therefore the relationship between the bare mass term $\mu_{\Psi_3}$ and the light neutrino masses cannot be established without properly considering the possible hierarchies of parameters in the full neutrino mass matrix, which is itself model dependent. While we do not thoroughly analyse the neutrino

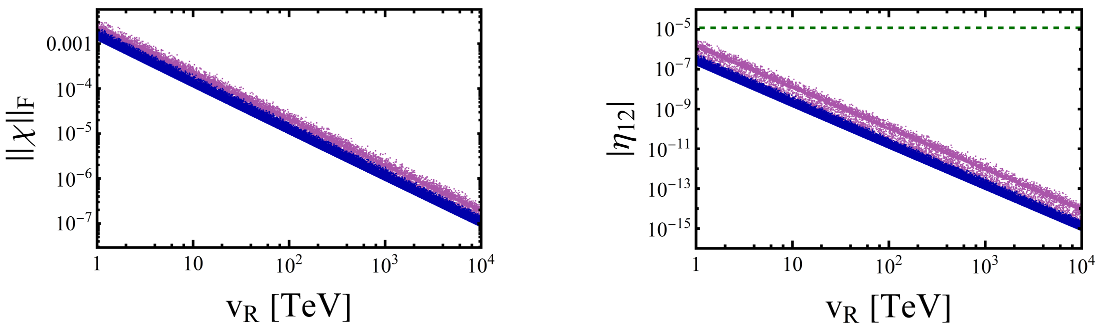


FIGURE 4.7: Plots of the variation of $\mathcal{X}$ **(left)** and the variation of the most experimentally constrained entry of $\eta$ **(right)** as a function of $v_R$. Points in blue correspond to where $\|\mu_{\Psi_3}\| < \|m_d\|$ and therefore $\mathcal{X} \simeq \mathcal{X}^{(1)}$ and points in purple correspond to the opposite regime where $\mathcal{X} \simeq \mathcal{X}^{(2)}$ where we have scanned over the entries of $\mu_{\Psi_3}$ only requiring $\|\mu_{\Psi_3}\| < \|Y^R_{\Psi_3} v_R\|$ such that the seesaw assumption is satisfied. Here there are no current experimental constraints on $\mathcal{X}$ from unitarity deviation however future constraints on $\eta$ will begin to constrain $v_R$.

mass matrix of a more complete model, we note that [213] found that if an $SU(2)_R$ triplet, $\Psi_3$, was extended with additional fermionic singlets (such that the full Yukawa Lagrangian was given by a combination of Eqs. (4.16) and (4.74)) a viable neutrino mass spectrum was recovered for $\|\mu_{\Psi_3}\| \lesssim 1$ GeV which would suggest that $\mathcal{Z} \ll 10^{-3}$ and therefore the limits on $m_X$ will be helicity suppressed to their lowest values. However we note that the limit $\mu_{\Psi_3} \to 0$ does not recover a global symmetry of the Lagrangian as it does in the bi-doublet case and therefore it is unlikely that the smallness of $\mu_{\Psi_3}$ can be related to the smallness of neutrino mass. It may be possible that there are multiple regions in which viably light neutrino masses are recovered, some of which require the entries of $\mu_{\Psi_3}$ to be large, which would not lead to a reduction in the limits on $m_X$. While the smallness of $\mu_{\Psi_3}$ cannot be guaranteed by the smallness of the active neutrino masses, as in the bi-doublet scenario, the work in [213] at least indicates that there is a region of parameter space which recovers all SM fermion masses with $\mu_{\Psi_3}$ small enough to reduce fully the limits on $m_X$.

Therefore exotic PS fermion multiplets which introduce additional states which mix with the SM charged and neutral leptons are an attractive method for reducing the limits on PS breaking. As both multiplets considered contain both charged and neutral states, the mixings within both sectors are now coupled. Requiring a valid neutrino-mass spectrum leads to a chiral suppression in the limits on $m_X$. In the case of additional $SU(2)_{L/R}$ bi-doublets, a chiral suppression can be motivated through technical naturalness arguments. In the case of additional $SU(2)_{L/R}$ triplets, the usual PS scalar content is ruled

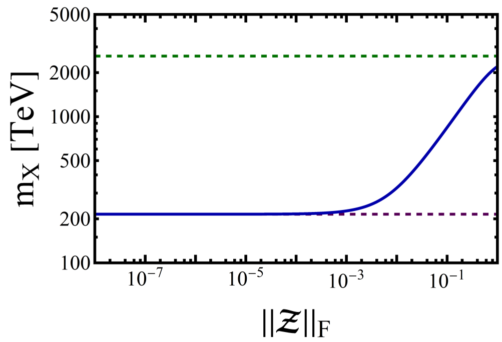


FIGURE 4.8: Plot of the limits on $m_X$ as a function of $\|\mathcal{Z}\|_F$ assuming that $K_L^{de} = \mathbb{1}$. As the extent of chiral suppression in the couplings of $X_\mu$ to $e'_R$ and $d'_R$ is controlled by $\mathcal{Z}$, requiring full helicity suppression in the limits on $m_X$ requires $\|\mathcal{Z}\|_F \lesssim 10^{-3}$ as in the previous section. Unlike the previous section $\mathcal{Z}$ is not constrained by limits on unitarity deviation.

out phenomenologically. However, if the scalar and fermion sectors are modified appropriately the desired masses and chiral suppression can be achieved. Although not linked to any technical naturalness arguments, previous studies with the triplets and more exotic scalar content suggest that a viable neutrino mass spectrum will still lead to a complete chiral suppression in the limits on $m_X$. Due to the fact that the mass hierarchy between the down quarks and charged leptons differs between the different generations, the correct masses are most naturally generated for the two fermion types by having their masses arise from different Yukawa couplings and vevs. In the two scenarios considered above, viable charged-lepton and down-quark masses implied that the masses of all quarks arise from couplings of $f_{L/R}$ to $\phi$ with vevs $v_1$ and $v_2$, whereas the lepton masses are related to couplings of the relevant fermions to $\chi_L$ with vev $v_L$, suggesting the hierarchy $v_{1,2} \gg v_L \gtrsim 1$ GeV.

### 4.5.2 $d - D$ mixing: Sextet fermions

Mixing between the down quarks and heavy exotic partners is similar to the scenarios above involving lepton mixing. A number of possible fermion extensions lead to $d - D$ mixing. Here we will focus on the feasibility of $d - D$ mixing alone in generating both a viable SM mass spectrum and a suppression of the mass limits on $m_X$ which occurs through the addition of the $SU(4)$ sextet fermions, but may also occur with higher dimensional PS multiplets. The results for down-quark mixing will follow very similarly to Section 4.5.1.2. As can be seen in Eq. (4.100), $y^R_{\Psi_6} v_R$ appears in the bottom-left entry of $M_{dD}$.

Writing the down-quark mass mixing matrix similarly to the case of the charged leptons

$$\mathcal{L}_{dD} = \begin{pmatrix} \overline{d_L} & \overline{D_L} \end{pmatrix} \underbrace{\begin{pmatrix} m_{dd} & m_{dD} \\ m_{Dd} & m_{DD} \end{pmatrix}}_{M_{dD}} \begin{pmatrix} d_R \\ D_R \end{pmatrix} + \text{H.c} \tag{4.150}$$

and noting that the entries of Eq. (4.100) appear similarly to the case of $M_{eE}$ above allows us to draw the same conclusions which we will summarise. Limits on exotic quark states exceed 1 TeV [235] and therefore for phenomenological reasons a seesaw in $M_{dD}$ is required. As before the only two entries of $M_{dD}$ not tied to the electroweak scale are $y_{\Psi_6} v_R$ and $\mu_{\Psi_6}$ and, as discussed, a significant chiral suppression in limits on the PS breaking scale will only occur for the scenario where $\|y^R_{\Psi_6} v_R\| > \|m_d, y^L_{\Psi_6} v_L, \mu_{\Psi_6}\|$.

This hierarchy implies the down-quark masses are given upon diagonalisation by

$$m_d \simeq y^L_{\Psi_6} v^*_L - m_e \, (y^R_{\Psi_6} v_R)^{-1} \mu_{\Psi_6} \tag{4.151}$$

where the PS symmetry enforces that the singular values of $m_e$ give the correct charged-lepton masses at the appropriate scale in the case where there are no additional multiplets that induce $e-E$ mixing. For the same reasons as with the $SU(2)_{L/R}$ triplets, the correct down-quark masses cannot be recovered in the limit $y^L_{\Psi_6} v_L \to 0$ as this would imply

$$m_d \simeq -m_e \, (y^R_{\Psi_6} v_R)^{-1} \mu_{\Psi_6} \tag{4.152}$$

suggesting all three generations of down-quarks are lighter than the corresponding generation of charged-lepton, as discussed in Appendix D.0.3. In Section 4.4.1.4 the constraint from baryon number violation suggested that imposing baryon number conservation required suppressing the Yukawa interactions of $\chi_L$ to the fermions (for example by removing the scalar). However as phenomenologically the mass term $y^L_{\Psi_6} v_L$ is required in order to generate a viable charged-lepton and down-quark mass spectrum, this suggests that models involving just $d-D$ mixing through the introduction of $SU(4)$ sextets are likely ruled out by proton lifetime measurements. An analysis of all possible proton and neutrino decay diagrams in the region where the correct down-quark and charged-lepton masses arise is beyond the scope of this work. If the dominant decay channels are two-body decays which proceed via $d = 6$ effective four-fermi interactions similar to Fig. 4.3, estimates from [236] suggest that for TeV scale new physics the product of Yukawa couplings within the relevant loop diagram must satisfy $Y \lesssim 10^{-6}$. As $y^L_{\Psi_6} v_L$ is related to the down-quark masses in this case and for low scales of $v_R$, $y^R_{\Psi_6}$ is required to be close to unity such that the heavy $D$ states are sufficiently heavy naïvely suggests difficulty in suppressing the decays.

If a viable model involving the $SU(4)$ sextets exists which can suppress the dangerous proton decay diagrams whilst generating the appropriate charged-lepton and down-quark masses in the regime where the mass term $|y^R_{\Psi_6}|$ is dominant, the requirements for a chiral suppression in the limits on $m_X$ would follow almost identically to the $e-E$ mixing case above. For small values of $\mu_{\Psi_6}$ the couplings of $X_\mu$ to $d'_R$ and $e'_R$ will be suppressed and decreasing the experimental limits to their lowest value would roughly require

$$\|\mathcal{Z}\|_F \simeq (Y^R_{\Psi_6})^{-1}\mu_{\Psi 6} \lesssim 10^{-3}. \tag{4.153}$$

The only difference between $d-D$ and $e-E$ mixing will be in the deviation of unitarity, where $e-E$ mixing is constrained by deviation of unitarity in the PMNS whereas $d-D$ mixing is constrained by deviation within the measured CKM matrix,

$$V_{\text{CKM}} \simeq (U^u_L)^\dagger \left(\mathbb{1} - \frac{1}{2}\mathcal{X}\mathcal{X}^\dagger\right) O^d_L \tag{4.154}$$

where

$$\begin{aligned} d'_L &\simeq (O^d_L)^\dagger \left(\mathbb{1} - \frac{1}{2}\mathcal{X}\mathcal{X}^\dagger\right) d_L - (O^d_L)^\dagger \mathcal{X}\, D_L \\ d'_R &\simeq -(O^d_R)^\dagger \mathcal{Z}^\dagger\, d_R + (O^d_R)^\dagger \left(\mathbb{1} - \frac{1}{2}\mathcal{Z}^\dagger\mathcal{Z}\right) D_R \end{aligned} \tag{4.155}$$

and

$$\begin{aligned} \mathcal{X} &\simeq \frac{1}{v_R} m_X \left(Y^R_\Psi\right)^{-1} + \frac{v_L}{v_R^2} Y^L_\Psi \mu^\dagger_\Psi [(Y^R_\Psi)^\dagger]^{-1} (Y^R_\Psi)^{-1} \\ \mathcal{Z} &\simeq \frac{1}{v_R}(Y^R_\Psi)^{-1}\mu_\Psi + \frac{v_L}{v_R^2}(Y^R_\Psi)^{-1}[(Y^R_\Psi)^\dagger]^{-1} m_d^\dagger Y^L_\Psi . \end{aligned} \tag{4.156}$$

In Section 4.5.3 which involves coupled $e-E$ and $d-D$ mixing we find that limits from CKM unitarity deviation lead to very similar constraints on the level of mixing within the theory and therefore we find that $d-D$ mixing would be equally viable to the $e-E$ mixing above in the absence of proton decay issues.

### 4.5.3 Coupled $e - E$ and $d - D$ mixing: Decuplet fermions

Coupled mass mixing, which we define as scenarios which involve the introduction of exotic PS multiplets which contain both $D$ and $E$ states within the same multiplet, occurs with the addition of a pair of opposite-chirality $SU(4)$ decuplets. There is an additional subtlety for such coupled scenarios compared to the previous analyses. Due to the coupled nature of the exotic states $D$ and $E$ there exist additional relevant gauge interactions with the leptoquark $X_\mu$.

Consider the full fermion kinetic Lagrangian with the addition of $SU(4)$ decuplet fermions $\Psi^{10}_{L/R}$:

$$\mathcal{L}^{\text{F}}_{\text{KIN}} = i\overline{f_{L/R}}\not{D} f_{L/R} + i\,\overline{\Psi^{10}_{L/R}}\,\not{D}\Psi^{10}_{L/R} \tag{4.157}$$

with covariant derivative given by

$$\not{D}\Psi^{10}_{L/R} = \partial_\mu \Psi^{10}_{L/R} + ig_4 \hat{G}_\mu \Psi^{10}_{L/R} + ig_4 \Psi^{10}_{L/R}(\hat{G}_\mu)^T \tag{4.158}$$

for the decuplets, which transform as $\Psi^{10}_{L/R} \to U_4 \Psi^{10}_{L/R} U_4^T$. Expanding out Eq. (4.158) and leaving only the interactions of interest gives

$$\mathcal{L}^{\text{F}}_{\text{KIN}} \supset \frac{g_4}{\sqrt{2}}\left(\overline{d}\not{X} P_{L/R} e + \sqrt{2}\,\overline{D}\not{X} P_{L/R} E\right) + \text{H.c} \tag{4.159}$$

and therefore the exotic states $D$ and $E$ within $\Psi^{10}_{L/R}$ have similar gauge interactions to $X_\mu$ as the states $d$ and $e$ within $f_{L/R}$. Due to the mass mixing present in $M_{dD}$ and $M_{eE}$ in Eqs. (4.105) and (4.106) between the states $f_{L/R}$ and $\Psi^{10}_{L/R}$, the physical mass states $e'$, $E'$, $d'$ and $D'$ are admixtures as before. Writing

$$\begin{pmatrix} e \\ E \end{pmatrix}_{L/R} = \begin{pmatrix} V^e_{L/R} {e'}_{L/R} + W^e_{L/R} {E'}_{L/R} \\ X^e_{L/R} {e'}_{L/R} + Y^e_{L/R} {E'}_{L/R} \end{pmatrix} \text{ and } \begin{pmatrix} d \\ D \end{pmatrix}_{L/R} = \begin{pmatrix} V^e_{L/R} {d'}_{L/R} + W^e_{L/R} {D'}_{L/R} \\ X^e_{L/R} {d'}_{L/R} + Y^e_{L/R} {D'}_{L/R} \end{pmatrix} \tag{4.160}$$

for the unitary diagonalisation matrices as usual leads to

$$\frac{g_4}{\sqrt{2}}\left(\overline{d'_L}\left((V^d_L)^\dagger V^e_L + \sqrt{2}(X^d_L)^\dagger X^e_L\right)\not{X} e'_L + (L \leftrightarrow R)\right) \tag{4.161}$$

for the gauge interactions between the physical SM-like states $d'$ and $e'$. We have once again neglected to write the similar gauge interactions which contain the heavy states $D'$

or $E'$ as by assumption the relevant mesons are kinematically forbidden from decaying into them.

Therefore the relevant mixing matrices are now given by

$$K^{de}_{L/R} = (V^d_{L/R})^\dagger V^e_{L/R} + \sqrt{2}\,(X^d_{L/R})^\dagger X^e_{L/R}. \tag{4.162}$$

Due to the second term which now appears in Eq. (4.162) (which arises from the components of $d'$ and $e'$ contained within the states $D$ and $E$), the resultant mixing matrix can only be made helicity-suppressed if and only if a hierarchy in both $V$ and $X$ occurs, e.g. $\|V^d_R\| \ll \|V^e_R\|$ *and* $\|X^d_R\| \ll \|X^e_R\|$. This is unlike the previous scenarios where the additional multiplets included did not induce any new interactions between $X_\mu$ and exotic states with down-quark and charged-lepton quantum numbers. For scenarios where the $D$ and $E$ states are introduced through two different PS multiplets, no such gauge interactions will occur and the requirements for a helicity suppression in the relevant meson decays will be given by a combination of the results in Sections 4.5.1 and 4.5.2. Therefore what follows will be specific to 'coupled' scenarios where the new states $D$ and $E$ transform within the same multiplet.

Consider the mass mixing matrices between the down-quark and charged-lepton states, in the three-generational scenario, which arises from the inclusion of a pair of $SU(4)$ decuplets:

$$M_{eE} = \begin{pmatrix} m_F & \sqrt{2}\,Y^L_{\Psi_{10}} v^*_L \\ \sqrt{2}\,Y^R_{\Psi_{10}} v_R & \mu_{\Psi_{10}} - \sqrt{\frac{3}{2}}\,Y_\Phi v_\Phi \end{pmatrix} \quad \text{and} \quad M_{dD} = \begin{pmatrix} m_F & Y^L_{\Psi_{10}} v^*_L \\ Y^R_{\Psi_{10}} v_R & \mu_{\Psi_{10}} - \sqrt{\frac{1}{6}}\,Y_\Phi v_\Phi \end{pmatrix}. \tag{4.163}$$

Previously it was found that a hierarchy where $\|Y^R_{\Psi_{10}} v_R\|$ is larger than all other entries of $M_{dD}$ or $M_{eE}$ is required for a helicity suppression to occur, and therefore for a reduction in the experimental mass limits of $X_\mu$. If such a hierarchy is assumed for the entries of $M_{dD}$ and $M_{eE}$ above, the unitary block diagonalisation matrices are given by

$$U^{e,d}_L \simeq \begin{pmatrix} \mathbb{1}_{3\times3} - \frac{1}{2}\mathcal{X}\mathcal{X}^\dagger & \mathcal{X} \\ -\mathcal{X}^\dagger & \mathbb{1}_{3\times3} - \frac{1}{2}\mathcal{X}^\dagger\mathcal{X} \end{pmatrix} \quad \text{and} \quad U^{e,d}_R \simeq \begin{pmatrix} -\mathcal{Z} & \mathbb{1}_{3\times3} - \frac{1}{2}\mathcal{Z}\mathcal{Z}^\dagger \\ \mathbb{1}_{3\times3} - \frac{1}{2}\mathcal{Z}^\dagger\mathcal{Z} & \mathcal{Z}^\dagger \end{pmatrix} \tag{4.164}$$

where the explicit forms for $\mathcal{X}$ and $\mathcal{Z}$ in the case of $U^e_{L/R}$ and $U^d_{L/R}$ can be easily derived from Appendix D.0.2. As always, due to the assumption that there is a seesaw where $\|Y^R_{\Psi_{10}} v_R\|$ is dominant in both $M_{dD}$ and $M_{eE}$, the parameters $\mathcal{X}$ and $\mathcal{Z}$ are small: $\|\mathcal{X},\, \mathcal{Z}\| \ll 1$. Comparing Eq. (4.164) with Eq. (4.160) implies

$$\|V^e_L\| \simeq \|V^d_L\| \simeq 1,\; \|V^e_R\| \simeq \|V^d_R\| \simeq 0 \tag{4.165}$$

and

$$\|X^e_L\| \simeq \|X^d_L\| \simeq 0,\; \|X^e_R\| \simeq X^d_R \simeq 1. \tag{4.166}$$

Therefore under the assumption that the mass term proportional to the $SU(2)_R$ breaking is dominant for both $M_{dD}$ and $M_{eE}$ (which previously led to a helicity-suppression with $\|K^{de}_R\| \ll 1$ for cases of uncoupled $e-E$ or $d-D$ mixing), we find no suppression in the relevant mixing matrices:

$$\|K^{de}_L\| \simeq \|K^{de}_R\| \simeq 1 \tag{4.167}$$

which is due to the second contribution to $K^{de}_{L/R}$ appearing in Eq. (4.162). Physically it is very simple to see why this occurs. Assuming that the bottom-left entries of $M_{dD}$ and $M_{eE}$ are both dominant in a seesaw implies that the light mass states $d'_L$, $d'_R$, $e'_L$ and $e'_R$ are predominately composed of $d_L$, $D_R$, $e_L$ and $E_R$ respectively. However $d_L$ and $e_L$ are contained in the same PS multiplet *and* $D_R$ and $E_R$ are also contained within a PS multiplet together. As such, the gauge leptoquark $X_\mu$ couples to both chiralities of fermion mass states with little suppression. If instead the bottom-right entries of $M_{dD}$ and $M_{eE}$ are assumed dominant, for the same reasons as presented in Section 4.5.1, the desired helicity suppression in the relevant meson decays will not occur.

From the above arguments it is clear that, for scenarios with coupled mixing in the down-quark and charged-lepton sectors, a chiral-suppression in the relevant meson decays is not possible if both mixing matrices $M_{dD}$ and $M_{eE}$ in Eq. (4.163) are assumed to have the same seesaw structure. However, note that the entries of the two mixing matrices differ by combinations of group theoretic factors from the Yukawa couplings of the adjoint scalar $\Phi$. Therefore it is in principle possible for there to be sufficient tuning of the mass parameters, particularly the parameters in the second row of $M_{eE}$ and $M_{dD}$, such that the seesaw structure in the two mass matrices differs.

To demonstrate this for for one-generation of fermions, assume that the hierarchy of parameters in $\mu_{\Psi_{10}}$, $y^R_{\Psi_{10}} v_R$ and $y_\Phi v_\Phi$ is such that

$$\mu_{\Psi_{10}} - \sqrt{\frac{1}{6}} y_\Phi v_\Phi \geq 10\, y^R_{\Psi_{10}} v_R \geq 100 \left( \sqrt{\frac{1}{2}} \mu_{\Psi_{10}} - \sqrt{\frac{3}{4}} y_\Phi v_\Phi \right) \tag{4.168}$$

is satisfied (taking each combination to be real and positive). This corresponds to the hierarchy $m_{DD} > m_{Dd}, m_{Ee} > m_{EE}$. Under this assumption, the *bottom-left* entry of $M_{eE}$ is at least an order of magnitude larger than the other entries of the charged-lepton mass mixing matrix. In addition, the *bottom-right* entry of $M_{dD}$ is dominant in the down-quark mass mixing matrix. This certainly requires a degree of tuning between the mass parameters $\mu_{\Psi_{10}}$ and $y_\Phi\, v_\Phi$ and also implies that the adjoint scalar $\Phi$ is required in such a theory in order to introduce the required Georgi-Jarlskog-like factors. Now the unitary block diagonalisation matrices differ from Eq. (4.164):

$$\begin{aligned} U^e_L &\simeq \begin{pmatrix} \mathbb{1}_{3\times3} - \frac{1}{2}\mathcal{X}\mathcal{X}^\dagger & \mathcal{X} \\ -\mathcal{X}^\dagger & \mathbb{1}_{3\times3} - \frac{1}{2}\mathcal{X}^\dagger\mathcal{X} \end{pmatrix}, U^e_R \simeq \begin{pmatrix} -\mathcal{Z} & \mathbb{1}_{3\times3} - \frac{1}{2}\mathcal{Z}\mathcal{Z}^\dagger \\ \mathbb{1}_{3\times3} - \frac{1}{2}\mathcal{Z}^\dagger\mathcal{Z} & \mathcal{Z}^\dagger \end{pmatrix}, \\ U^d_L &\simeq \begin{pmatrix} \mathbb{1}_{3\times3} - \frac{1}{2}\mathcal{X}\mathcal{X}^\dagger & \mathcal{X} \\ -\mathcal{X}^\dagger & \mathbb{1}_{3\times3} - \frac{1}{2}\mathcal{X}^\dagger\mathcal{X} \end{pmatrix}, U^d_R \simeq \begin{pmatrix} \mathbb{1}_{3\times3} - \frac{1}{2}\mathcal{Z}^\dagger\mathcal{Z} & \mathcal{Z}^\dagger \\ -\mathcal{Z} & \mathbb{1}_{3\times3} - \frac{1}{2}\mathcal{Z}\mathcal{Z}^\dagger \end{pmatrix}. \end{aligned} \tag{4.169}$$

Consequently

$$\|V^e_L\| \simeq \|V^d_L\| \simeq 1,\ \|V^e_R\| \simeq 0,\ \|V^d_R\| \simeq 1 \tag{4.170}$$

and

$$\|X^e_L\| \simeq \|X^d_L\| \simeq 0,\ \|X^e_R\| \simeq 1,\ \|X^d_R\| \simeq 0 \tag{4.171}$$

and therefore $\|K^{de}_L\| \simeq 1$ and $\|K^{de}_R\| \simeq 0$ as required. Again this is simple to see given that in this case the light mass states are predominately composed of $e_L$, $E_R$, $d_L$ and $d_R$, due to the seesaw assumption. Therefore the leptoquark $X_\mu$ will strongly couple to left-handed states[23] (as $e_L$ and $d_L$ are in the same PS multiplet) whereas there will be a suppression in its right-handed couplings (as $E_R$ and $d_R$ are not within the same PS multiplet). Therefore, scenarios with coupled mass mixing matrices between the down-quark and charged-lepton sectors are able to generate the desired chiral couplings of $X_\mu$ for a tuned selection of certain mass parameters within the theory. To reiterate, this

[23] The light left-handed mass states will therefore also behave correctly in weak interactions.

kind of tuning is required only when the extra states, $D$ and $E$, reside in the same PS multiplet. A similar tuning was required in [209], such that the mass mixing matrices in the down-quark and charged-lepton sectors had different seesaw structures, in order to achieve a chiral suppression the limits on $m_X$ for the case where multiple pairs of bi-fundamental PS fermions were introduced. We therefore find this to be a general requirement for models with coupled $e-E$ and $d-D$ mixing, when a chiral suppression in the couplings of $X_\mu$ is desired.

Importantly, the addition of $\Psi^{10}_{L/R}$ implies the existence of a Dirac colour-sextet fermion with electric charge 1/3. Its mass is given by

$$m_\psi = \mu_{\Psi_{10}} + \sqrt{\frac{1}{6}} y_\Phi v_\Phi \tag{4.172}$$

and therefore requiring that the sextet is sufficiently heavy leads to constraints on the singular values of $\mu_{\Psi_{10}}$. The mass limits for a colour sextet fermion vary from roughly 100 GeV if stable on collider length scales [229] up to a TeV [237] for large couplings and possibly in the multi-TeV range [238]. However if a hierarchy similar to

$$\mu_{\Psi_{10}} - \sqrt{\frac{1}{6}} y_\Phi v_\Phi \gg y^R_{\Psi_{10}} v_R \gg \sqrt{\frac{1}{2}} \mu_{\Psi_{10}} - \sqrt{\frac{3}{4}} y_\Phi v_\Phi \tag{4.173}$$

is required, $m_\psi$ is already required to be at least at the multi-TeV scale considering the limits on the $SU(2)_R$ breaking scale. Therefore regions of parameter space which lead to the desired chiral suppression of $X_\mu$ will naturally require the colour-sextet masses to be sufficiently large.

Let us estimate whether this hierarchy of mass parameters, though somewhat tuned, is able to successfully reproduce the correct SM fermion mass hierarchies as well as generate a chiral suppression in the couplings of $X_\mu$ in the multi-generational scenario. For simplicity, put the bottom-right entry of $M_{eE}$ to be exactly zero (the maximally tuned case), that is:

$$\mu_{\Psi_{10}} - \sqrt{\frac{3}{2}} Y_\Phi v_\Phi = 0_{3\times 3}. \tag{4.174}$$

This implies that the bottom-right entry of $M_{dD}$ is given by

$$\mu_{\Psi_{10}} - \sqrt{\frac{1}{6}} Y_\Phi v_\Phi = \frac{2}{3} \mu_{\Psi_{10}} \tag{4.175}$$

and consequently

$$m_\psi = \frac{4}{3}\mu_{\Psi_{10}}. \tag{4.176}$$

The two mass mixing matrices, $M_{eE}$ and $M_{dD}$, now simplify to

$$M_{eE} = \begin{pmatrix} m_F & \sqrt{2}\,Y^L_{\Psi_{10}} v^*_L \\ \sqrt{2}\,Y^R_{\Psi_{10}} v_R & 0_{3\times 3} \end{pmatrix} \quad \text{and} \quad M_{dD} = \begin{pmatrix} m_F & Y^L_{\Psi_{10}} v^*_L \\ Y^R_{\Psi_{10}} v_R & \frac{2}{3}\mu_{\Psi_{10}} \end{pmatrix}. \tag{4.177}$$

We require that $\|\sqrt{\frac{1}{2}}\, m_F,\, Y^L_{\Psi_{10}} v_L\| < \|Y^R_{\Psi_{10}} v_R\| < \frac{2}{3}\|\mu_{\Psi_{10}}\|$ in order for the dominant entries of each mass matrix to be different. This hierarchy leads to

$$m_\ell \simeq \sqrt{2}\,Y^L_{\Psi_{10}} v_L \tag{4.178}$$

for the charged-lepton mass matrix and

$$m_d \simeq m_F - \frac{3}{2} v_L v_R Y^L_{\Psi_{10}} \left(\mu_{\Psi_{10}}\right)^{-1} Y^R_{\Psi_{10}} \tag{4.179}$$

for the down-quark mass mixing matrix.

As the dominant block is in the bottom-left entry, the relationship between the interaction and mass eigenstates for the SM-like charged leptons is given identically to Section 4.5.1.2:

$$\begin{aligned} e'_L &\simeq (O^e_L)^\dagger \left(\mathbb{1} - \frac{1}{2}\mathcal{X}^e (\mathcal{X}^e)^\dagger\right) e_L - (O^e_L)^\dagger \mathcal{X}^e\, E_L \\ e'_R &\simeq -(O^e_R)^\dagger (\mathcal{Z}^e)^\dagger\, e_R + (O^e_R)^\dagger \left(\mathbb{1} - \frac{1}{2}(\mathcal{Z}^e)^\dagger \mathcal{Z}^e\right) E_R \end{aligned} \tag{4.180}$$

with $\mathcal{X}^e \simeq m_F (Y_{\Psi_{10}} v_R)^{-1}$ and $\mathcal{Z}^e \simeq \frac{v_L}{v_R^2}(Y^R_{\Psi_{10}})^{-1}((Y^R_{\Psi_{10}})^\dagger)^{-1} m_F Y^L_{\Psi_{10}}$ at leading order. The light down-quark mass eigenstates are instead given by

$$\begin{aligned} d'_L &\simeq (O^d_L)^\dagger \left(\mathbb{1} - \frac{1}{2}\mathcal{X}^d (\mathcal{X}^d)^\dagger\right) d_L - (O^d_L)^\dagger \mathcal{X}^d\, D_L \\ d'_R &\simeq (O^d_R)^\dagger \left(\mathbb{1} - \frac{1}{2}(\mathcal{Z}^d)^\dagger \mathcal{Z}^d\right) d_R + (O^d_R)^\dagger (\mathcal{Z}^d)^\dagger D_R \end{aligned} \tag{4.181}$$

with $\mathcal{X}^d \simeq \frac{3}{2} v_L Y^L_{\Psi_{10}} (\mu_{\Psi_{10}})^{-1}$ and $\mathcal{Z}^d \simeq \frac{3}{2} v_R (\mu_{\Psi_{10}})^{-1} Y^R_{\Psi_{10}}$. The physical mixing matrices are therefore given by

$$\begin{aligned}
K_L^{de} &\simeq (O_L^d)^\dagger \left[ \left( \mathbb{1} - \frac{1}{2}\mathcal{X}^d (\mathcal{X}^d)^\dagger \right) \left( \mathbb{1} - \frac{1}{2}\mathcal{X}^e (\mathcal{X}^e)^\dagger \right) + \mathcal{X}^d (\mathcal{X}^e)^\dagger \right] O_L^e, \\
&\simeq (O_L^d)^\dagger O_L^e \\
K_R^{de} &\simeq (O_R^d)^\dagger \left[ (\mathcal{Z}^d)^\dagger \left( \mathbb{1} - \frac{1}{2} (\mathcal{Z}^e)^\dagger \mathcal{Z}^e \right) - \left( \mathbb{1} - \frac{1}{2} (\mathcal{Z}^d)^\dagger \mathcal{Z}^d \right) \mathcal{Z}^e \right] O_R^e \\
&\simeq (O_R^d)^\dagger \left( (\mathcal{Z}^d)^\dagger - \mathcal{Z}^e \right) O_R^e \\
V_{\text{CKM}} &\simeq (U_L^u)^\dagger \left( \mathbb{1} - \frac{1}{2}\mathcal{X}^d (\mathcal{X}^d)^\dagger \right) O_L^d \text{ and } U_{\text{PMNS}} \simeq N_\nu^\dagger \left( \mathbb{1} - \frac{1}{2}\mathcal{X}^e (\mathcal{X}^e)^\dagger \right) O_L^e
\end{aligned} \tag{4.182}$$

where the two terms appearing in $K^{de}_{L/R}$ are generated from the gauge interactions $\overline{D}\not{X}E$ and $\overline{d}\not{X}e$ as explained above. This features the $X_\mu$ coupling being predominately to $d'_L$ and $e'_L$ as expected, with a strong suppression of its coupling to $d'_R$ and $e'_R$.

Additionally, the unitarity deviation in the PMNS mixing matrix is given almost identically to Section 4.5.1.2, where it was quantified by $\mathcal{X} \simeq \frac{1}{v_R} m_d (Y^R_{\Psi_3})^{-1}$, compared to the current scenario where $\mathcal{X}^e \simeq \frac{1}{v_R} m_F (Y^R_{\Psi_{10}})^{-1}$. Note also that combining Eqs. (4.178) and (4.179) leads to

$$m_d \simeq m_F - \frac{3}{2\sqrt{2}} v_R \, m_\ell \, (\mu_{\Psi_{10}})^{-1} \, Y^R_{\Psi_{10}}, \tag{4.183}$$

which, combined with $\|Y^R_{\Psi_{10}} v_R\| < \|\mu_{\Psi_{10}}\|$, implies that $m_F \simeq m_d$, since the singular values of $m_\ell$ are of similar order to $m_d$. Therefore the constraints on the $SU(2)_R$ breaking scale, $v_R$, from the deviation of the PMNS matrix follows essentially identically to Section 4.5.1.2 and therefore Fig. 4.7 is also valid for this scenario. Therefore for all values of $v_R$ which are at the TeV scale or higher, there are no constraints arising from the deviation of unitarity from the PMNS matrix.

Due to the additional down-quark mixing, there are also constraints from the deviation from unitarity of the CKM matrix. In this case, the deviation is determined by the matrix $\mathcal{X}^d \propto v_L Y^L_{\Psi_{10}} (\mu_{\Psi_{10}})^{-1}$ where again $v_L Y^L_{\Psi_{10}}$ is proportional to the charged-lepton mass matrix, $m_\ell$. Now, $\mu_{\Psi_{10}}$ is related to the colour-sextet fermion mass scale from Eq. (4.176). In Fig. 4.9 we measure the level of deviation through the parameters

$$\eta^r_j = 1 - \sum_i |(V_{\text{CKM}})_{ji}|^2 \quad \text{and} \quad \eta^c_k = 1 - \sum_i |(V_{\text{CKM}})_{ik}|^2. \tag{4.184}$$

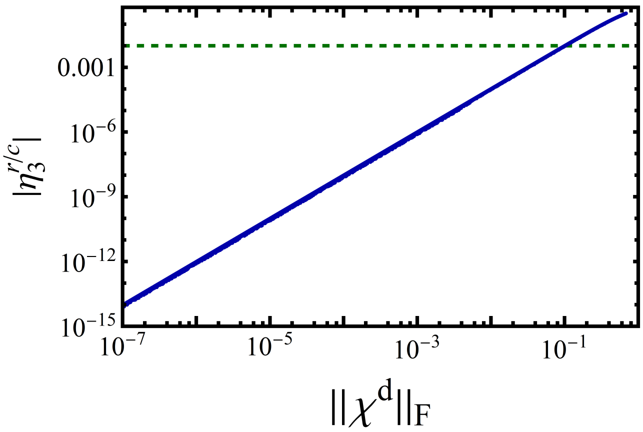


FIGURE 4.9: Plot of the deviation of unitarity in the CKM matrix as a function of $\|\mathcal{X}^d\|_F$ where the dashed green line roughly indicates the current experimental limit. The CKM matrix deviation is measured as the difference in the sum of the squares of each row and column. Even though it is currently the least constrained, the sum of the squares of the third row and column provide the strongest bounds on the deviation due to the large masses of the third generation of quarks compared to the first and second generation. This plot indicates that $\|\mathcal{X}^d\|_F \lesssim 10^{-1}$ is required. The limits for CKM matrix elements are taken from [14].

The strongest experimental limits on $\eta^{r/c}$ come from the sum of the squares of the first row or column of the CKM matrix. However, due to the much larger masses of the third generation of quarks, we find that deviations in the sum of the third row and column of the CKM matrix lead to stronger constraints on $\mathcal{X}^d$. We find that $\eta_3^r$ and $\eta_3^c$ place almost identical limits on the magnitude of $\|\mathcal{X}^d\|_F$ and therefore only plot one for brevity. Using [14] places the limit

$$-0.01 \lesssim \eta_3^{r/c} \lesssim 0.09 \tag{4.185}$$

and therefore we conservatively set the limit $|\eta_3^{r/c}| < 10^{-2}$ at the PS breaking scale. Figure 4.9 therefore sets a rough limit of $\|\mathcal{X}^d\|_F \lesssim 10^{-1}$ in order to prevent significant deviation occurring for the CKM matrix. This can be compared to the limits from PMNS deviation which currently lead to no derived limits on $v_R$.

The implications for the experimental limits on $m_X$ can also be very easily determined from the results derived in Section 4.5.1 and the explicit derivations of $K_{L/R}^{de}$ derived in Eq. (4.182). From the results in Fig. 4.8 it is clear that in order for a substantial chiral suppression to occur in the limits on $m_X$, where $K_R^{de} \simeq (O_R^d)^\dagger \mathcal{Z} O_R^e$, we roughly require $\|\mathcal{Z}\| \lesssim 10^{-2}$. The expression for $K_R^{de}$ given in Eq. (4.182) in this case is of a identical form with

$$K_R^{de} \simeq (O_R^d)^\dagger \left( (\mathcal{Z}^d)^\dagger - \mathcal{Z}^e \right) O_R^e \equiv (O_R^d)^\dagger \mathcal{Z}_{10} O_R^e. \tag{4.186}$$

Therefore we clearly require that $\|\mathcal{Z}_{10}\| \lesssim 10^{-2}$ in order for the desired chiral suppression to occur. This will clearly be satisfied if both $\mathcal{Z}^d$ and $\mathcal{Z}^e$ individually satisfy this requirement, and we do not consider a scenario with a tuned cancellation between the two matrices. By inspection, from the definitions of $\mathcal{Z}^d$ and $\mathcal{Z}^e$ in Eqs. (4.180) and (4.181) this will be trivially satisfied by $\mathcal{Z}^e$, as it contains terms which are at most at the GeV scaled which are suppressed by terms which are at a minimum at the TeV scale, but in the case of $\mathcal{Z}^d$ roughly implies the hierarchy

$$\frac{\|v_R Y^R_{\Psi_{10}}\|}{\|\mu_{\Psi_{10}}\|} \lesssim 10^{-2} \tag{4.187}$$

and therefore we require the colour-sextet masses to be at least two order of magnitude larger than the mass term proportional to the $SU(2)_R$ breaking term, if a full suppression in the experimental limits on $m_X$ is desired.

However note that here we are assuming that $\mu_{\Psi_{10}} = \sqrt{\frac{3}{2}} Y_\Phi v_\Phi$ where $v_\Phi$ is a vev which breaks $SU(4)$ and therefore contributes to the mass of $X_\mu$. Therefore the gauge leptoquark $m_X$ will roughly develop a mass at the same order as the colour-sextet fermion $m_\psi$, which will typically be a stronger limit on $m_X$ than the experimental constraints, for many choices of $K^{de}_R$. For example, if $v_R \simeq 5$ TeV, a large chiral suppression requires $\mu_{\Psi_{10}}$ to be roughly two order of magnitude larger than this, implying that $m_\psi \simeq m_X \gtrsim 500$ TeV. Therefore a mild suppression in the limits on $m_X$ is expected due to the required hierarchy between $Y_{\Psi_{10}} v_R$ and $\mu_{\Psi_{10}}$ (and therefore $Y_\Phi v_\Phi$). Only for situations where the mixing angles in $K^{de}_R$ are such that the experimental constraint on $m_X$ are initially close to their largest value, e.g. $K^{de}_R = \mathbb{1}_{3\times 3}$, will this lead to a suppression in the limits on $m_X$. We therefore find that it is possible for the leptoquark $X_\mu$ to develop a chiral coupling to the SM-like fermions and requires a tuning between the mass matrices $\mu_{\Psi_{10}}$ and $Y_\Phi v_\Phi$. However, while this may lead to a suppression in the decay rates of the relevant mesons, the large hierarchy required between $v_\Phi$ and $v_R$ requires $m_X \gtrsim 100$ TeV at a minimum. As the experimental limits on $v_R$ increase, this will subsequently decrease the already small parameter space for this scenario.

It is easy to estimate the minimum level of tuning between the parameters within $\mu_{\Psi_{10}}$ and $Y_\Phi v_\Phi$ in order to achieve the desired change in seesaw structure between $M_{dD}$ and

$M_{eE}$. Requiring

$$\left\|\mu_{\Psi_{10}} - \sqrt{\frac{3}{2}}Y_\Phi v_\Phi\right\| < \left\|Y^R_{\Psi_{10}} v_R\right\| < \left\|\mu_{\Psi_{10}} - \sqrt{\frac{1}{6}}Y_\Phi v_\Phi\right\| \tag{4.188}$$

in combination with the limits from unitarity violation within the CKM matrix from Fig. 4.9 requires that

$$\left\|Y^R_{\Psi_{10}} v_R \left(\mu_{\Psi_{10}} - \sqrt{\frac{1}{6}}Y_\Phi v_\Phi\right)^{-1}\right\| \lesssim 10^{-1} \tag{4.189}$$

at a minimum. This suggests that for anarchic values for the entries of each matrix:

$$\|\mu_{\Psi_{10}}, Y_\Phi v_\Phi\| \gtrsim 10\, \|Y^R_{\Psi_{10}} v_R\| \tag{4.190}$$

and therefore the left inequality of Eq. (4.188) requires that a cancellation between $\mu_{\Psi_{10}}$ and $\sqrt{\frac{3}{2}}Y_\Phi v_\Phi$ of at least two orders is required for the couplings of $X_\mu$ to become effectively chiral, and at least three orders for a full suppression in the couplings of $X_\mu$ to the right-handed SM-like fermions, such that $\|\mathcal{Z}\| \lesssim 10^{-3}$.

### 4.5.4 Connection to $SO(10)$

While we are motivated by the experimentally attractive prospect of lowering the scale of PS breaking to be as low as possible, here we briefly consider how the exotic fermionic multiplets proposed could fit into an $SO(10)$ GUT and mention any obvious problems. We note the smallest dimensional multiplets of $SO(10)$ which contain each exotic multiplet as well as additional states this would predict. It is well known that two standard PS fermion multiplets fit into the spinorial

$$\mathbf{16} \to (\mathbf{4}, \mathbf{1}, \mathbf{2}) \oplus (\mathbf{4}, \mathbf{2}, \mathbf{1}) = f_L \oplus f_R \tag{4.191}$$

of $SO(10)$. The fundamental representation of $SO(10)$,

$$\mathbf{10} \to (\mathbf{1}, \mathbf{2}, \mathbf{2}) \oplus (\mathbf{6}, \mathbf{1}, \mathbf{1}) = \Psi_{22} \oplus \Psi_6, \tag{4.192}$$

contains both the bi-doublet and sextet fermion states. While we find that the bi-doublet fermion is the most attractive candidate in lowering the PS breaking scale, the sextet fermion leads to undesirable proton decay diagrams. Some mechanism would therefore be desirable in order to significantly increase the masses of the $D$ states from the sextet, and not the $E$ and $N$ states from the bi-doublet, in order to prevent large proton decay widths. This cannot be through different bare mass terms, e.g. $\mu_{\Psi_{22}} \ll \mu_{\Psi_6} \simeq 10^{16}$ GeV, as the $SO(10)$ symmetry now enforces the two terms to be equal.

The adjoint representation

$$\mathbf{45} \to (\mathbf{1},\mathbf{3},\mathbf{1}) \oplus (\mathbf{1},\mathbf{1},\mathbf{3}) \oplus (\mathbf{15},\mathbf{1},\mathbf{1}) \oplus (\mathbf{6},\mathbf{2},\mathbf{2}) \supset \Psi_{3_L} \oplus \Psi_{3_R} \tag{4.193}$$

contains both the $SU(2)_L$ and $SU(2)_R$ triplet fermions. Interestingly, the additional $(\mathbf{15},\mathbf{1},\mathbf{1})$ fermion contains a neutral state and therefore will contribute to the full neutrino mass matrix. As we found that the triplets alone are unable to generate a viable neutrino mass spectrum, due to the various mass equalities predicted, it is convenient that the minimal $SO(10)$ multiplet which contains these states also contains additional neutrino states which could possibly generate a viable spectrum of masses. The $(\mathbf{6},\mathbf{2},\mathbf{2})$ fermion will likely require a similar mechanism to the $(\mathbf{6},\mathbf{1},\mathbf{1})$ fermion in order to significantly increase its mass compared to the triplets within the theory. Finally the $SU(4)$ decuplets first appear in the $\mathbf{120}$ representation of $SO(10)$. This representation also contains the bi-doublet fermion which will itself allow for the generation of chiral-like couplings of $X_\mu$ as well as generate neutrino masses, which the decuplet fermions do not. An interesting possible direction of future work is to analyse the feasibility of embedding such low-scale variants of PS into an $SO(10)$ GUT in such a way that the required fermion states do not develop GUT scale masses whereas any fermion in a given embedding which may mediate proton decay, or similar undesirable processes, have masses developed at the $SO(10)$ breaking scale.

## 4.6 Conclusion

We have studied the implications of introducing additional fermionic states to the usual Pati-Salam fermion multiplets. In particular we have focused on multiplets of relatively low dimensionality which contain partner states to the charged-leptons and/or down-quarks. The implications of mixing effects induced by these states were extensively studied, particularly with a focus on the feasibility of lowering the scale of PS breaking.

We identified four multiplets that allow for the possibility of a suppression in the PS limits. Of the four, the inclusion of an $SU(2)_{L/R}$ bi-doublet alone can lead to a valid mass spectrum for all SM particles and a significant reduction in the PS limits. The decuplet, requires the addition of extra singlet states (at a minimum) for neutrino mass, the inclusion of a scalar that induces a Georgi-Jarlskog like texture (such as $\Phi$) and is only able to reduce the limits on $m_X$ for some choices of $K^{de}_{L/R}$ and for a tuning between mass parameters. The remaining two multiplets, the $SU(2)_L$ and $SU(2)_R$ triplets, require both a modification of the scalar sector for a viable charged-lepton mass spectrum as well as additional fermionic states for a viable neutrino mass spectrum. A common feature of all scenarios was the existence of scalars $\chi_L$ and $\chi_R$ in order to generate a viable down-quark and charged-lepton mass spectrum. Therefore three $SU(2)_L$ Higgs doublets are predicted.

The most attractive models, the $SU(2)_{L/R}$ bidoublet or triplets, contain only additional leptonic states, inducing both $e-E$ mixing as well as mixing within the neutrino sector. While both these models have already appeared in the literature, we have extended these analyses by rigorously studying the requirements for viable mass spectra of the down-quarks, charged-leptons and neutrinos as well as the implications for the PS breaking scale limits. We identify an attractive connection between the smallness of neutrino mass and the helicity suppression of the limits on $m_X$ which, particularly in the case of the bi-doublet, necessarily has a chiral-like coupling of $X_\mu$ to the SM fermions.

The sextet option leads to mixing in the down-quark sector alone but we find that this likely leads to large proton decay widths in the only region which can generate a viable mass spectrum. Finally the scenario with fermion decouplets, which leads to both $d-D$ and $e-E$ mixing, was considered. It also includes additional exotic states potentially discoverable at current and future colliders. The regime of interest, where the limits on PS breaking can be lowered, is very sensitive to future experimental limits on $SU(2)_R$ breaking scale $v_R$ and relies on a tuning of mass parameters.

We find that a chiral suppression in the PS breaking limits can reduce the usual limits of $81-2467$ TeV, depending on the structure of $K^{de}_{L/R}$, down to as low as $5.6-194$ TeV. An attractive property of models which lead to a chiral suppression is that only one of $K^{de}_{L/R}$ is required to have a specific structure. Without a chiral suppression, the lowest PS limits obtained required both of $K^{de}_{L/R}$ to have a specific structure which might suggest a parity symmetry in conflict with the assumed low-scale setup.

The addition of $SU(2)$ triplets has already been explored in the context of the current B-anomalies [212, 213]. A more in-depth examination of baryon number violation implications in the case with $SU(4)$ sextets is required before it can be ruled out as a low-scale candidate. Additionally, due to the mass mixing induced, collider constraints for other particles predicted (such as the $W'$ and $Z'$) could lead to significantly smaller mass limits than what is usually expected. Exploring the reach of the LHC and future colliders for these extended PS scenarios with chiral-like gauge couplings may be required.

# Chapter 5

# Conclusion

The work within this thesis has extended the Standard Model in a number of well motivated ways in order to explore the possibility of new physics occurring at scales close to the electroweak scale. Two of the three areas explored, neutrino mass and the measured BAU, incontrovertibly require an extension to the SM from long established experimental evidence, whereas the last area explored, quark-lepton unification, is an example where extending the SM is motivated from the theoretical attractiveness of increasing the symmetries of the theory. The seesaw mechanism is a simple and attractive mechanism for generating neutrino mass with an important connection to both leptogenesis and the Pati-Salam gauge symmetry. Low-scale seesaw models of neutrino mass, and their implications for the BAU and quark-lepton unification, are highly motivated models that should be studied in detail due to to much more promising prospects of it's testability, either through direct on-shell production at colliders or from an observation of charged-lepton flavour violation, compared to the traditional high-scale variants. A generic prediction of most low-scale seesaw models is the pseudo-Dirac nature of the heavy sterile neutrino states predicted, and their detection can have significant implications for BSM theories beyond the simple possibility of explaining neutrino mass.

In Chapter 1 we described how the experimental observation of neutrino flavour oscillations is itself evidence for massive neutrinos and how a number of other indirect measurements fix all three generations of neutrino to have masses significantly smaller than the other SM fermions. The simplest method of incorporating neutrino mass into the SM was discussed, the seesaw mechanism, with examples of the different possible types of seesaws which may exist. The relationship between the light and heavy neutrino mass states and the LNV parameters of the theory were discussed in detail. The evidence for a baryon asymmetry as well as the motivations for considering a dynamic generation of this asymmetry were presented. In particular the idea of leptogenesis was introduced as a baryogenesis mechanism and the incredibly interesting connection between the seesaw mechanism of neutrino mass and baryogenesis was established. Finally, the Pati-Salam gauge symmetry was motivated and the connection between the scale of sterile neutrino masses and the scale of Pati-Salam breaking was discussed implying that low-scale models of PS are only possible if a low-scale seesaw is implemented.

In Chapter 2 we considered the leptogenesis implications for the SM which has been extended by two additional sterile fermions per generation of SM lepton. The focus within this chapter was on the feasibility of the inverse, linear or combined seesaw scenarios as the source of leptogenesis where small mass splittings occur between SNs within the same family. The possible resonant enhancement under this assumption is purely driven by LNV parameters, motivated to be small due to the observed small neutrino masses. In this scenario we find that both the ISS and LSS models alone are unable to generate a sufficient level of asymmetry by many order of magnitude. The combined scenario, where both the ISS and LSS terms are present simultaneously, contains parameter space for a viable generation of the baryon asymmetry. This study was the first to point out that asymmetry generation in the simplest low-scale model requires both LNV terms to present. This chapter also served as a proof of principle that, in this model, the asymmetry generation can occur purely from the CPV Dirac phase of the PMNS matrix, motivating the precise measurement of $\delta_{CP}$ in future oscillation experiments. Possible discovery signals in each model were also discussed briefly.

In Chapter 3 we point out that the inclusion of additional mass splitting terms within the neutrino mass matrix can modify the results of Chapter 2. In particular leptogenesis can be viable in both the ISS or LSS alone when the assumption that the mass splitting is driven only by LNV parameters is lifted. Here we assumed a MLFV hypothesis which had been extensively studied in the case of a minimal type-I seesaw, and find that both the ISS and LSS seesaws can lead to asymmetry generation albeit in a very narrow window in the case of the ISS. Importantly we find that the extended type-I seesaws do not suffer from the same flavour alignment issue which the minimal type-I seesaw experiences and therefore asymmetry generation can occur much more naturally with a

MLFV hypothesis in the ISS and LSS compared to the vanilla scenario. Chapter 2 and Chapter 3 therefore demonstrate that the linear seesaw term can very naturally generate the required baryon asymmetry provided that a mass splitting above the critical temperature can be generated, either from the accompanying inverse mass term or through additional effects if this term is forbidden in a given theory.

Chapter 4 explores the connection between low-scale seesaws and the Pati-Salam gauge group. In particular we extensively study the connection between a seesaw occurring within the down-quark or charged-lepton sectors and the experimental limits on PS breaking. We show that the traditional quoted experimental limit of $v_{PS} \simeq \mathcal{O}(1000)$ TeV, can be significantly lowered to even as low as 5 TeV in some scenarios where additional exotic fermionic states are included. We additionally analyse the different possible matrix textures required for the mixing matrix between $d$ and $e$ in charged-current interactions and how the experimental limits on the PS breaking scale vary for different choices. We find that only four possible exotic multiplets can lead to the desired suppression, two of which, the $SU(2)_L$ or $SU(2)_R$ triplet, require a modified scalar sector *and* additional singlet fermions at a minimum and one of which, the $SU(4)$ decuplets, that predict additional exotic coloured particles with direct implications for collider searches. The final viable multiplet, the $SU(2)_{L/R}$ bi-doublet, is able to generate all SM fermion masses without additional modifications to the scalar or fermion sectors. In the cases where exotic fermion multiplets introduced contain singlet states, the two triplets or the bi-doublet, we identify a well motivated connection between the reduced PS breaking scale and the smallness of neutrino mass.

Overall we have considered non minimal extension to the type-I seesaw and the interplay they have with aspects of early universe cosmology and BSM unification models. Such models can explain unresolved puzzles of the Standard Model at scales potentially accessible in future experiments with exciting potential discovery signals and therefore their importance extends well beyond the simple generation of non-zero neutrino mass for the neutral components of $\ell_\alpha$.

# Appendix A

# Decay and Scattering Rates entering the Boltzmann Equations.

The decay and scattering rates entering the Boltzmann equations used in the analyses of Chapters 2 and 3 are listed below. Following the literature, the following rescaled variables are used:

$$z = \frac{m_{N_1}}{T}\,, \quad x = \frac{s}{m_{N_1}^2}\,, \quad a_i = \left(\frac{m_{N_i}}{m_{N_1}}\right)^2\,, \quad a_r = \left(\frac{m_{\rm IR}}{m_{N_1}}\right)^2 \simeq 10^{-5}\,, \quad c_i \;=\; \left(\frac{\Gamma_{N_i}}{m_{N_1}}\right)^2 . \tag{A.1}$$

where $s$ is the Mandelstam variable, and $m_{\rm IR} = m_\Phi/M_{N_1}$ is an infrared mass regulator for the t-channel whose value is set to $10^{-5}$ as discussed in Refs. [239, 240].

The total decay width $\Gamma_{N_i}$ of the SNs is given by

$$\Gamma_{N_i} \;=\; \sum_{l=1}^{3} \Gamma^{\alpha}_{N_i} = \frac{m_{N_i}}{8\pi}\,\sum_{l=1}^{3} h^*_{li} h_{li}. \tag{A.2}$$

The collision terms for $1 \to 2$ and $2 \to 2$ processes which appear in Eqs. (2.45) and (2.46) are calculated in [84] for the unflavoured case and additional flavour-specific processes are calculated in [85]. These scattering rates will be summarised below without suppressed flavour indices. The rate for a generic process $X \to Y$ and its conjugate counterpart $\overline{X} \to \overline{Y}$ is defined as $\gamma^X_Y$. For the $1 \to 2$ process, $N_i \to L\Phi$ or $N_i \to L^C\Phi^\dagger$, $\gamma^X_Y$ is given by

$$\gamma^{N_i}_{L_\alpha \Phi} = \frac{m_{N_1} m^2_{N_i} \Gamma^\alpha_{N_i}}{\pi^2 z} K_1(z\sqrt{a_i}) , \tag{A.3}$$

in terms of the rescaled variables of Eq. (A.1) where $K_n(z)$ is an $n$th-order modified Bessel function. The $2 \to 2$ processes can be divided into $\Delta L = 0, 1, 2$ cases, each contributing to the washout of lepton flavour at different rates. For a generic $2 \to 2$ process the collision term is calculated through

$$\gamma^X_Y = \frac{m^4_{N_1}}{64\,\pi^4 z} \int\limits_{x_{\rm thr}}^{\infty} dx \sqrt{x}\, K_1(z\sqrt{x})\, \sigma^X_Y(x) \ , \tag{A.4}$$

where $x_{\rm thr}$ corresponds to $\text{Max}(m^2_x, m^2_y)$ with $m_{x(y)}$ corresponding to the sum of masses of particles in the initial(final) state such that the process is kinematically allowed. Each process is therefore calculated by substituting each reduced cross section $\sigma^X_Y$, numerically interpolating Eq. (A.4) over a range of $z$ values and then including them in the numerical Boltzmann Equations.

The relevant $\Delta L = 1$ processes and cross-sections are,

$$\begin{aligned}
\sigma^{N_i L_\alpha}_{Q u^C} &= \frac{3 y_t^2}{4\pi} (h^*_{\alpha i} h_{\alpha i}) \left(\frac{x - a_i}{x}\right)^2 , \\
\sigma^{N_i u^C}_{L_\alpha Q^C} &= \sigma^{N_i Q}_{L_\alpha u} \\
&= \frac{3 y_t^2}{4\pi} (h^*_{\alpha i} h_{\alpha i}) \left(1 - \frac{a_i}{x} + \frac{a_i}{x} \ln\left(\frac{x - a_i + a_r}{a_r}\right)\right), \\
\sigma^{N_i V_\mu}_{L_\alpha \Phi} &= \frac{3 g^2}{8\pi\, x} (h^*_{\alpha i} h_{\alpha i}) \left(\frac{(x + a_i)^2}{x - a_i + 2a_r} \ln\left(\frac{x - a_i + a_r}{a_r}\right)\right), \\
\sigma^{N_i L_\alpha}_{\Phi^\dagger V_\mu} &= \frac{3 g^2}{16\pi\, x^2} (h^*_{\alpha i} h_{\alpha i}) \left(5x - a_i)\,(a_i - x) + 2(x^2 + x a_i - a_i^2) \ln\left(\frac{x - a_i + a_r}{a_r}\right)\right), \\
\sigma^{N_i \Phi^\dagger}_{L_\alpha V_\mu} &= \frac{3 g^2}{16\pi\, x^2} (h^*_{\alpha i} h_{\alpha i})\,(x - a_i) \left(x - 3a_i + 4a_i \ln\left(\frac{x - a_i + a_r}{a_r}\right)\right) .
\end{aligned} \tag{A.5}$$

For the scatterings involving gauge bosons, only the $SU(2)_L$ processes were considered as the $U(1)_Y$ processes are expected to be subdominant.

The relevant $\Delta L = 2$ processes and cross-sections are,

$$
\begin{aligned}
\sigma^{L_\alpha \Phi}_{L^C_\beta \Phi^\dagger} = 2 \sum_{i,j=1}^{6} \mathrm{Re}\Big[ \left(h_{\alpha j} h_{\beta j} h^*_{\alpha i} h^*_{\beta i}\right) \mathcal{A}^{ss}_{ij} \quad &+ \quad \left(h_{\alpha j} h_{\beta j} h^*_{\alpha i} h^*_{\beta i}\right) \mathcal{A}^{tt}_{ij} \\
&+ \quad \left(h^*_{\alpha i} h_{\beta i} h^*_{\alpha j} h_{\beta j} + h_{\alpha i} h^*_{\beta i} h_{\alpha j} h^*_{\beta j}\right) \mathcal{A}^{(st)*}_{ij} \Big] \\
\sigma^{L_\alpha L_\beta}_{\Phi^\dagger \Phi^\dagger} \quad = \sum_{i,j=1}^{6} \mathrm{Re}\left(h_{\alpha j} h_{\beta j} h^*_{\alpha i} h^*_{\beta i}\right) \mathcal{B}_{ij} \;, & \qquad\qquad\qquad\qquad (\mathrm{A.6})
\end{aligned}
$$

where

$$
\begin{aligned}
\mathcal{A}^{(ss)}_{ij} \quad &= \quad \begin{cases} 0 & (i = j)\,, \\ \dfrac{x\sqrt{a_i\, a_j}}{4\pi P^*_i P_j} & (i \neq j)\,, \end{cases} \\
\mathcal{A}^{(tt)}_{ij} \quad &= \quad \begin{cases} \frac{a_i}{2\pi x}\left[ \frac{x}{a_i} \; - \; \ln\left(\frac{x+a_i}{a_i}\right)\right], & (i = j)\,, \\ \frac{\sqrt{a_i\, a_j}}{2\pi x\;(a_i - a_j)} \left[ (x + a_j)\; \ln\left(\frac{x+a_j}{a_j}\right) \; - \; (x + a_i)\; \ln\left(\frac{x+a_i}{a_i}\right)\right], & (i \neq j)\,, \end{cases} \\
\mathcal{A}^{(st)}_{ij} \quad &= \quad \frac{\sqrt{a_i\, a_j}}{2\pi P_i} \left[ 1 \; - \; \frac{x + a_j}{x}\; \ln\left(\frac{x + a_j}{a_j}\right)\right], \\
\mathcal{B}_{ij} \quad &= \quad \begin{cases} \frac{1}{2\pi}\left[ \frac{x}{x+a_i} \; + \; \frac{2\,a_i}{x+2a_i} \ln\left(\frac{x+a_i}{a_i}\right)\right], & (i = j)\,, \\ \frac{\sqrt{a_i\, a_j}}{2\pi}\left[ \frac{1}{a_i - a_j} \ln\left(\frac{a_i(x+a_j)}{a_j(x+a_i)}\right) \; + \; \frac{1}{x+a_i+a_j} \ln\left(\frac{(x+a_i)(x+a_j)}{a_i\, a_j}\right)\right]. & (i \neq j)\,, \end{cases}
\end{aligned}
\qquad (\mathrm{A.7})
$$

and

$$
P_i^{-1}(x) \quad = \quad \frac{1}{x - a_i + i\sqrt{a_i c_i}} \;. \qquad (\mathrm{A.8})
$$

Finally as flavoured leptogenesis is being considered there are also processes which do not violate lepton number but do violate lepton flavour [85]. The relevant $\Delta L = 0$ processes are,

$$
\begin{aligned}
\sigma^{L_\alpha \Phi}_{L_\beta \Phi} \quad &= \quad \sum_{i,j=1}^{6} \left(h^*_{\beta i} h_{\alpha i} h_{\beta j} h^*_{\alpha j} + h_{\beta i} h^*_{\alpha i} h^*_{\beta j} h_{\alpha j}\right) \mathcal{C}_{ij} \\
\sigma^{L_\alpha \Phi^\dagger}_{L_\beta \Phi^\dagger} \quad &= \quad \sum_{i,j=1}^{6} \mathrm{Re}\Big( h^{\nu *}_{l\alpha}\, h^{\nu}_{k\alpha}\, h^{\nu}_{l\beta}\, h^{\nu *}_{k\beta}\Big)\, \mathcal{D}_{ij}\;, \\
\sigma^{L_\alpha L^C_\beta}_{\Phi^\dagger \Phi} \quad &= \quad \sum_{i,j=1}^{6} \mathrm{Re}\Big( h^{\nu *}_{l\alpha}\, h^{\nu}_{k\alpha}\, h^{\nu}_{l\beta}\, h^{\nu *}_{k\beta}\Big)\, \mathcal{E}_{ij}\;,
\end{aligned}
\qquad (\mathrm{A.9})
$$

with

$$
\begin{aligned}
\mathcal{C}_{ij} &= \begin{cases} 0 & (i=j) \\ \dfrac{x\sqrt{a_i a_j}}{4\pi P_i^* P_j} & (i \neq j) \end{cases} \\
\mathcal{D}_{ij} &= \begin{cases} \frac{a_i}{\pi x}\left[\frac{x}{a_i} - \ln\left(\frac{x+a_i}{a_i}\right)\right] & (i=j) \\ \frac{\sqrt{a_i a_j}}{\pi x(a_i-a_j)}\left[(x+a_j)\ln\left(\frac{x+a_j}{a_j}\right) - (x+a_i)\ln\left(\frac{x+a_i}{a_i}\right)\right] & (i \neq j) \end{cases} \\
\mathcal{E}_{ij} &= \begin{cases} \frac{x}{\pi(x+a_i)} & (i=j) \\ \frac{\sqrt{a_i a_j}}{\pi(a_i-a_j)}\ln\left(\frac{a_i(x+a_j)}{a_j(x+a_i)}\right) & (i \neq j) \end{cases}
\end{aligned}
\tag{A.10}
$$

The scattering rates used in Eqs. (2.45) and (2.46) are then calculated as functions of the collision terms above,

$$
\begin{aligned}
\Gamma^{D(i\alpha)} &= \frac{1}{n_\gamma}\,\gamma^{N_i}_{L_\alpha\Phi} \\
\widehat{\Gamma}^{D(i\alpha)} &= \frac{1}{n_\gamma}\left(1+\frac{4}{21}\frac{\eta_{\Delta L}}{\eta_{\Delta L_\alpha}}\right)\gamma^{N_i}_{L_\alpha\Phi} \\
\widetilde{\Gamma}^{D(i\alpha)} &= \frac{1}{n_\gamma}\left(1+\frac{4}{21}\frac{\eta_{\Delta L}}{\eta_{\Delta L_\alpha}}\right)\gamma^{N_i}_{L_\alpha\Phi} \\
\Gamma^{S(i\alpha)}_{\mathrm{Y}} &= \frac{1}{n_\gamma}\left(\gamma^{N_i L_\alpha}_{Qu^C} + \gamma^{N_i u^C}_{L_\alpha Q^C} + \gamma^{N_i Q}_{L_\alpha u}\right), \\
\widehat{\Gamma}^{S(i\alpha)}_{\mathrm{Y}} &= \frac{1}{n_\gamma}\left[\left(-\frac{\eta_{N_i}}{\eta^{\mathrm{eq}}_{N_i}} + \frac{4}{21}\frac{\eta_{\Delta L}}{\eta_{\Delta L_\alpha}}\right)\gamma^{N_i L}_{Qu^C} + \left(1+\frac{1}{9}\frac{\eta_{\Delta L}}{\eta_{\Delta L_\alpha}} - \frac{5}{63}\frac{\eta_{N_i}}{\eta^{\mathrm{eq}}_{N_i}}\frac{\eta_{\Delta L}}{\eta_{\Delta L_\alpha}}\right)\gamma^{N_\alpha u^C}_{LQ^C}\right. \\
&\quad \left. + \left(1+\frac{5}{63}\frac{\eta_{\Delta L}}{\eta_{\Delta L_\alpha}} - \frac{1}{9}\frac{\eta_{N_i}}{\eta^{\mathrm{eq}}_{N_i}}\frac{\eta_{\Delta L}}{\eta_{\Delta L_\alpha}}\right)\gamma^{N_i Q}_{Lu}\right] \\
\widetilde{\Gamma}^{S(i\alpha)}_{\mathrm{Y}} &= \frac{1}{n_\gamma}\left[\left(\frac{\eta_{N_i}}{\eta^{\mathrm{eq}}_{N_i}} + \frac{4}{21}\frac{\eta_{\Delta L}}{\eta_{\Delta L_\alpha}}\right)\gamma^{N_i L}_{Qu^C} + \left(1+\frac{1}{9}\frac{\eta_{\Delta L}}{\eta_{\Delta L_\alpha}} + \frac{5}{63}\frac{\eta_{N_i}}{\eta^{\mathrm{eq}}_{N_i}}\frac{\eta_{\Delta L}}{\eta_{\Delta L_\alpha}}\right)\gamma^{N_i u^C}_{LQ^C}\right. \\
&\quad \left. + \left(1+\frac{5}{63}\frac{\eta_{\Delta L}}{\eta_{\Delta L_\alpha}} + \frac{1}{9}\frac{\eta_{N_i}}{\eta^{\mathrm{eq}}_{N_i}}\frac{\eta_{\Delta L}}{\eta_{\Delta L_\alpha}}\right)\gamma^{N_i Q}_{Lu}\right] \\
\Gamma^{S(i\alpha)}_{\mathrm{G}} &= \frac{1}{n_\gamma}\left(\gamma^{N_i L_\alpha}_{\Phi^\dagger V_\mu} + \gamma^{N_i V_\mu}_{L_\alpha\Phi} + \gamma^{N_i\Phi^\dagger}_{L_\alpha V_\mu}\right) \\
\widehat{\Gamma}^{S(i\alpha)}_{\mathrm{G}} &= \frac{1}{n_\gamma}\left[\left(-\frac{\eta_{N_i}}{\eta^{\mathrm{eq}}_{N_i}} + \frac{4}{21}\frac{\eta_{\Delta L}}{\eta_{\Delta L_\alpha}}\right)\gamma^{N_i L}_{\Phi^\dagger V_\mu} + \left(1+\frac{4}{21}\frac{\eta_{\Delta L}}{\eta_{\Delta L_\alpha}}\right)\gamma^{N_i V_\mu}_{L\Phi}\right. \\
&\quad \left. + \left(1-\frac{4}{21}\frac{\eta_{N_i}}{\eta^{\mathrm{eq}}_{N_i}}\frac{\eta_{\Delta L}}{\eta_{\Delta L_\alpha}}\right)\gamma^{N_i\Phi^\dagger}_{LV_\mu}\right]
\end{aligned}
$$

$$
\begin{aligned}
\widetilde{\Gamma}_{\rm G}^{S(i\alpha)} &= \frac{1}{n_\gamma}\Bigg[\left(\frac{\eta_{N_i}}{\eta_{N_i}^{\rm eq}}+\frac{4}{21}\,\frac{\eta_{\Delta L}}{\eta_{\Delta L_\alpha}}\right)\gamma^{N_iL}_{\Phi^\dagger V_\mu}+\left(1+\frac{4}{21}\,\frac{\eta_{\Delta L}}{\eta_{\Delta L_\alpha}}\right)\gamma^{N_iV_\mu}_{L\Phi} \\
&\quad +\left(1+\frac{4}{21}\frac{\eta_{N_i}}{\eta_{N_i}^{\rm eq}}\frac{\eta_{\Delta L}}{\eta_{\Delta L_\alpha}}\right)\gamma^{N_i\Phi^\dagger}_{LV_\mu}\Bigg] \\
\Gamma_{\rm Y}^{W(i\alpha)} &= \frac{1}{n_\gamma}\Bigg[\left(2+\frac{4}{21}\frac{\eta_{\Delta L}}{\eta_{\Delta L_\alpha}}\right)\gamma^{N_iL}_{Qu^C}+\left(1+\frac{17}{63}\frac{\eta_{\Delta L}}{\eta_{\Delta L_\alpha}}\right)\gamma^{N_iu^C}_{LQ^C} \\
&\quad +\left(1+\frac{19}{63}\frac{\eta_{\Delta L}}{\eta_{\Delta L_\alpha}}\right)\gamma^{N_\alpha Q}_{Lu}\Bigg] \\
\Gamma_{\rm G}^{W(i\alpha)} &= \frac{1}{n_\gamma}\;\Bigg[\left(2+\frac{4}{21}\,\frac{\eta_{\Delta L}}{\eta_{\Delta L_\alpha}}\right)\gamma^{N_iL}_{\Phi^\dagger V_\mu}+\left(1+\frac{4}{21}\,\frac{\eta_{\Delta L}}{\eta_{\Delta L_\alpha}}\right)\gamma^{N_iV_\mu}_{L\Phi} \\
&\quad +\left(1+\frac{8}{21}\frac{\eta_{\Delta L}}{\eta_{\Delta L_\alpha}}\right)\gamma^{N_i\Phi^\dagger}_{LV_\mu}\Bigg] \\
\Gamma_{\rm Y}^{\Delta L=2(\alpha\beta)} &= \frac{1}{n_\gamma}\;\left[\left(1+\frac{4}{21}\frac{\eta_{\Delta L}}{\eta_{\Delta L_\alpha}}\right)\left(\gamma^{L_\alpha\Phi}_{L_\beta^C\Phi^\dagger}+\gamma^{L_\alpha L_\beta}_{\Phi^\dagger\Phi^\dagger}\right)\right] \\
\Gamma_{\rm Y}^{\Delta L=0(\alpha\beta)} &= \frac{1}{n_\gamma}\;\left[\left(1+\frac{4}{21}\,\frac{\eta_{\Delta L}}{\eta_{\Delta L_\alpha}}\right)\gamma^{L_\alpha\Phi}_{L_\beta\Phi}+\gamma^{L_\alpha\Phi^\dagger}_{L_\beta\Phi^\dagger}+\gamma^{L_\alpha L_\beta^C}_{\Phi\Phi^\dagger}\right].
\end{aligned}
\tag{A.11}
$$

# Appendix B

# $\delta_{CP}$ dependence of $\eta_B$

Due to the flavoured nature of the Boltzmann equations, an inherent $\delta_{CP}$ dependence exists on the strength of certain flavoured scattering terms within them. It is interesting to note that, as a consequence, a maximally-violating phase, such as $\delta_{CP}$, actually does not necessarily result in a maximally generated net baryon asymmetry. Although maximal values of $\delta_{CP}$ will lead to maximised generation of asymmetry *per decay*, if the efficiency of the washout is greater here compared to some other values of $\delta_{CP}$ the net surviving asymmetry may end up being smaller. It is even possible for the net asymmetry to be minimised when the CP violating phase is maximised. This phenomenon was not explored further and the CP-violating phase $\delta_{CP}$ was simply fixed to the suggestive value of $\delta_{CP} = 3\pi/2$ in Chapter 2. Below are example plots of the absolute value of the net baryon asymmetry[1] $|\eta_B|$ as a function of $\delta_{CP}$ in the pure ISS scenario, chosen once again for computation convenience even though the asymmetry values are unrealistic. Alongside each plot is a contour plot of the sum of each $\Delta L = 0, 1, 2$ scattering term ($\sum_{X,i,\alpha} \Gamma^{X(i\alpha)}$) as a function of $\delta_{CP}$ and $z$ for a specific lepton flavour. As illustrated in Figs. B.1 to B.4, in scenarios where scattering terms without a $\delta_{CP}$ dependence dominate, the generated asymmetry behaves as naïvely expected. However, for some regions of parameter space the final asymmetry generated is maximised for values of $\delta_{CP}$ different to the maximal CPV case as in these cases, where the scattering terms which depend on $\delta_{CP}$ are dominant, the washout is stronger here comparative to other values of $\delta_{CP}$.

[1]The absolute value is plotted due to the sign change between $0 < \delta_{CP} < \pi$ and $\pi < \delta_{CP} < 2\pi$.

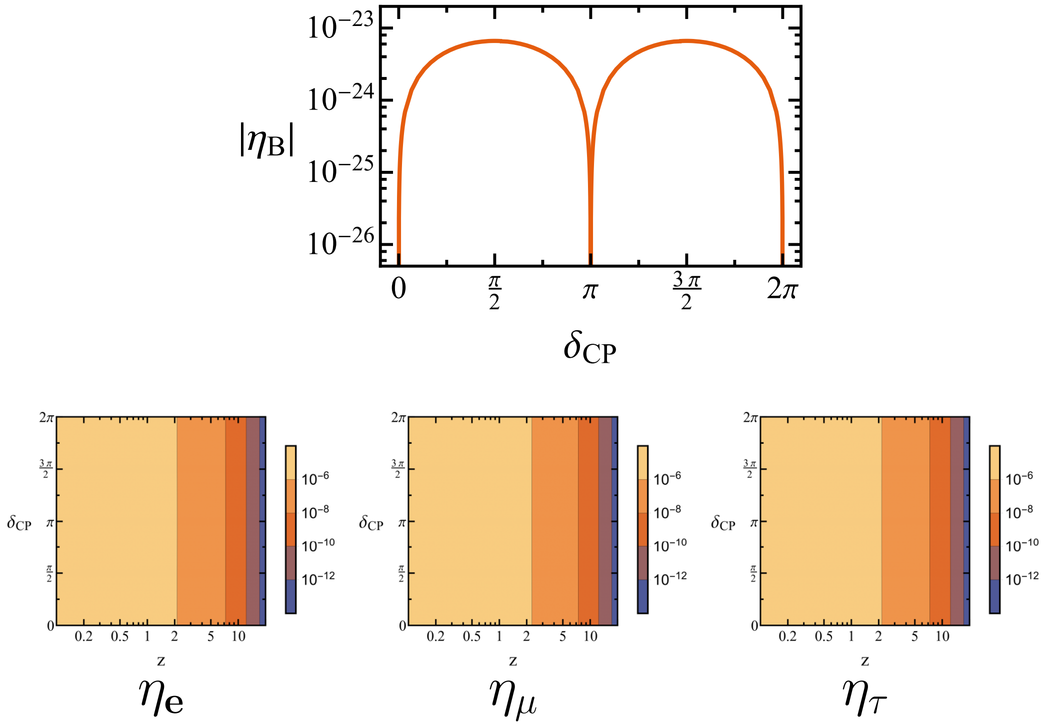


FIGURE B.1: In scenarios where the asymmetry is dominated by terms in the scatterings which do not have a net dependence on $\delta_{CP}$ the net asymmetry is maximised when the CP violation is maximised and as naïvely expected.

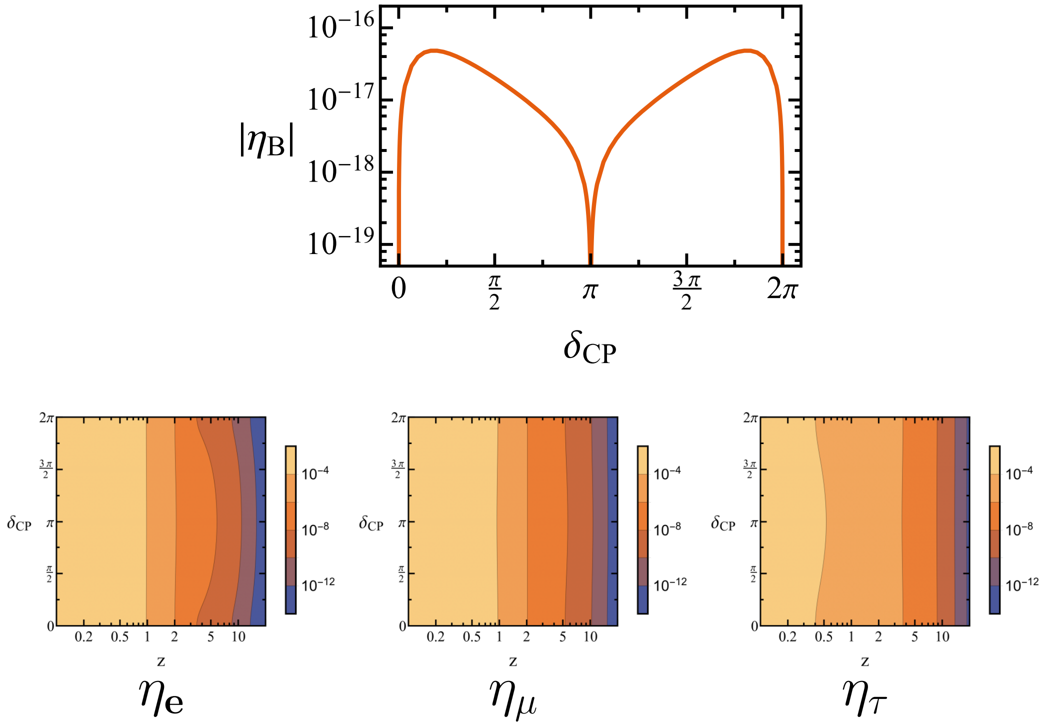


FIGURE B.2: If the total scattering rate is maximised for $\delta_{CP} = \pi$, more asymmetry is washed out in this region and the baryon asymmetry will be maximised for values of $\delta_{CP}$ closer to 0 and $2\pi$.

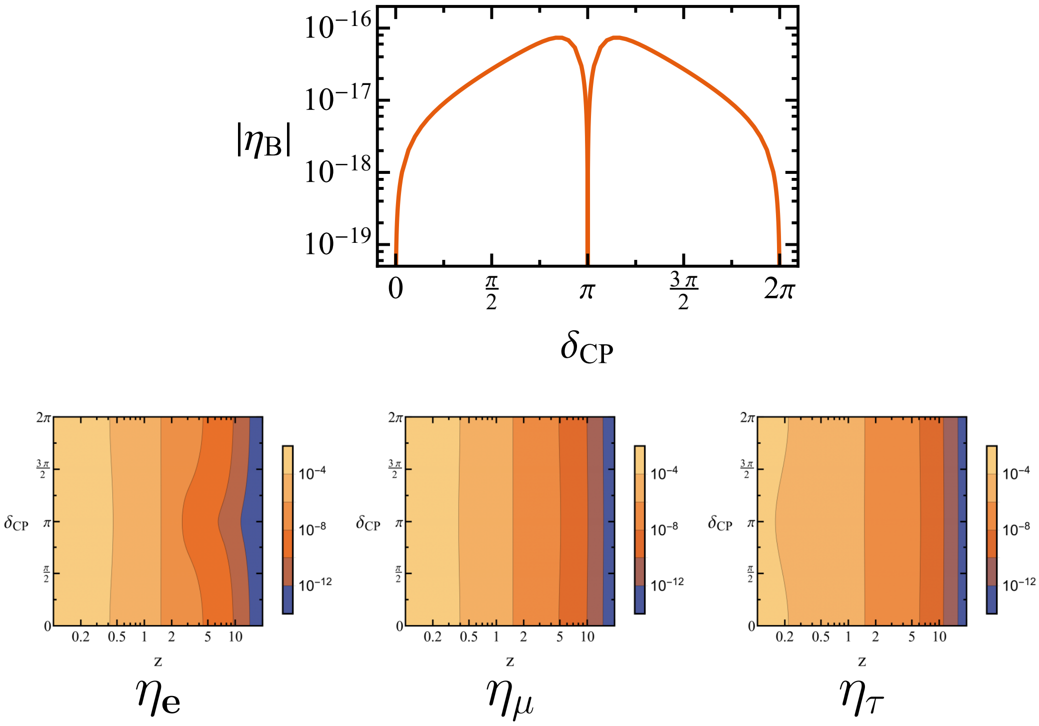


FIGURE B.3: If the total scattering is maximised around $\delta_{CP} \in \{0, 2\pi\}$, more asymmetry is washed out in this region and the baryon asymmetry will be maximised for values of $\delta_{CP}$ closer to $\pi$.

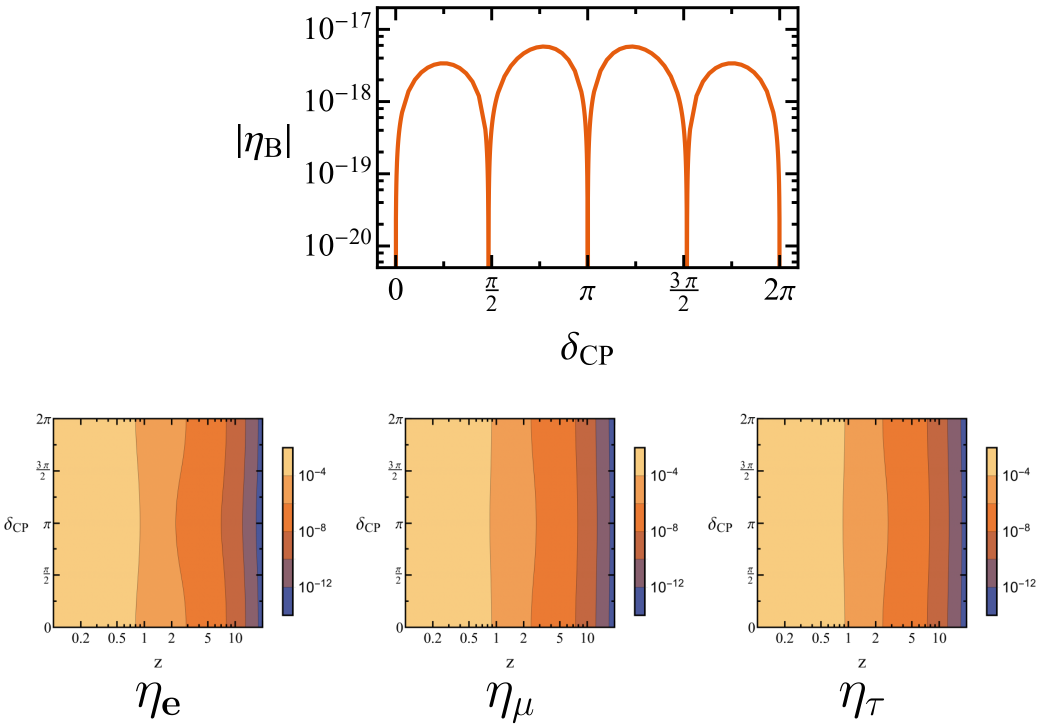


FIGURE B.4: In the unique scenario that the scattering rates have competing efficiencies, e.g. the efficiency to $e$ is maximal for $\delta_{CP} \in \{0, 2\pi\}$ and the efficiency to $\mu$ and $\tau$ is maximal for $\delta_{CP} = \pi$ as shown above, the net baryon asymmetry generated can actually be minimised for maximal CP violation.

# Appendix C

# SU(4) Generators

We use a basis for the $SU(4)$ generators (in their defining representation) given by

$$\lambda_1 = \begin{pmatrix} 0 & 1 & 0 & 0 \\ 1 & 0 & 0 & 0 \\ 0 & 0 & 0 & 0 \\ 0 & 0 & 0 & 0 \end{pmatrix} \quad \lambda_2 = \begin{pmatrix} 0 & -i & 0 & 0 \\ i & 0 & 0 & 0 \\ 0 & 0 & 0 & 0 \\ 0 & 0 & 0 & 0 \end{pmatrix} \quad \lambda_4 = \begin{pmatrix} 1 & 0 & 0 & 0 \\ 0 & -1 & 0 & 0 \\ 0 & 0 & 0 & 0 \\ 0 & 0 & 0 & 0 \end{pmatrix} \quad \lambda_5 = \begin{pmatrix} 0 & 0 & -i & 0 \\ 0 & 0 & 0 & 0 \\ i & 0 & 0 & 0 \\ 0 & 0 & 0 & 0 \end{pmatrix}$$

$$\lambda_6 = \begin{pmatrix} 0 & 0 & 0 & 0 \\ 0 & 0 & 1 & 0 \\ 0 & 1 & 0 & 0 \\ 0 & 0 & 0 & 0 \end{pmatrix} \quad \lambda_7 = \begin{pmatrix} 0 & 0 & 0 & 0 \\ 0 & 0 & -i & 0 \\ 0 & i & 0 & 0 \\ 0 & 0 & 0 & 0 \end{pmatrix} \quad \lambda_9 = \begin{pmatrix} 0 & 0 & 0 & 1 \\ 0 & 0 & 0 & 0 \\ 0 & 0 & 0 & 0 \\ 1 & 0 & 0 & 0 \end{pmatrix} \quad \lambda_{10} = \begin{pmatrix} 0 & 0 & 0 & -i \\ 0 & 0 & 0 & 0 \\ 0 & 0 & 0 & 0 \\ i & 0 & 0 & 0 \end{pmatrix}$$

$$\lambda_{11} = \begin{pmatrix} 0 & 0 & 0 & 0 \\ 0 & 0 & 0 & 1 \\ 0 & 0 & 0 & 0 \\ 0 & 1 & 0 & 0 \end{pmatrix} \quad \lambda_{12} = \begin{pmatrix} 0 & 0 & 0 & 0 \\ 0 & 0 & 0 & -i \\ 0 & 0 & 0 & 0 \\ 0 & i & 0 & 0 \end{pmatrix} \quad \lambda_{13} = \begin{pmatrix} 0 & 0 & 0 & 0 \\ 0 & 0 & 0 & 0 \\ 0 & 0 & 0 & 1 \\ 0 & 0 & 1 & 0 \end{pmatrix} \quad \lambda_{14} = \begin{pmatrix} 0 & 0 & 0 & 0 \\ 0 & 0 & 0 & 0 \\ 0 & 0 & 0 & -i \\ 0 & 0 & i & 0 \end{pmatrix}$$

$$\lambda_3 = \begin{pmatrix} 1 & 0 & 0 & 0 \\ 0 & -1 & 0 & 0 \\ 0 & 0 & 0 & 0 \\ 0 & 0 & 0 & 0 \end{pmatrix} \quad \lambda_8 = \begin{pmatrix} \frac{1}{\sqrt{3}} & 0 & 0 & 0 \\ 0 & \frac{1}{\sqrt{3}} & 0 & 0 \\ 0 & 0 & -\frac{2}{\sqrt{3}} & 0 \\ 0 & 0 & 0 & 0 \end{pmatrix} \quad \lambda_{15} = \begin{pmatrix} \frac{1}{\sqrt{6}} & 0 & 0 & 0 \\ 0 & \frac{1}{\sqrt{6}} & 0 & 0 \\ 0 & 0 & \frac{1}{\sqrt{6}} & 0 \\ 0 & 0 & 0 & -\sqrt{\frac{3}{2}} \end{pmatrix} \tag{C.1}$$

and similarly for the $SU(2)$ generators

$$\tau_1 = \begin{pmatrix} 0 & 1 \\ 1 & 0 \end{pmatrix} \quad \tau_2 = \begin{pmatrix} 0 & -i \\ i & 0 \end{pmatrix} \quad \tau_3 = \begin{pmatrix} 1 & 0 \\ 0 & -1 \end{pmatrix}. \tag{C.2}$$

Note that all generators are normalised such that $\mathrm{Tr}(\tau^i\tau^j) = \mathrm{Tr}(\lambda^i\lambda^j) = 2\delta^{ij}$ where $i$ and $j$ should be understood as summing over the appropriate indices in the $SU(4)$ and $SU(2)$ cases.

Therefore the $SU(4)$ gauge bosons, $G$, can be written as

$$\begin{aligned}\hat{G}_\mu &= \frac{1}{2}\lambda_a G^a_\mu \\ &= \frac{1}{2}\begin{pmatrix} G_{3\mu} + \frac{1}{\sqrt{3}}G_{8\mu} + \frac{1}{\sqrt{6}}G_{15\mu} & \sqrt{2}G^+_{(12)\mu} & \sqrt{2}G^+_{(45)\mu} & \sqrt{2}X^+_{r\mu} \\ \sqrt{2}G^-_{(12)\mu} & -G_{3\mu} + \frac{1}{\sqrt{3}}G_{8\mu} + \frac{1}{\sqrt{6}}G_{15\mu} & \sqrt{2}G^+_{(67)\mu} & \sqrt{2}X^+_{b\mu} \\ \sqrt{2}G^-_{(45)\mu} & \sqrt{2}G^-_{(67)\mu} & -\frac{2}{\sqrt{3}}G_{8\mu} + \frac{1}{\sqrt{6}}G_{15\mu} & \sqrt{2}X^+_{g\mu} \\ \sqrt{2}X^-_{r\mu} & \sqrt{2}X^-_{b\mu} & \sqrt{2}X^-_{g\mu} & -\frac{3}{\sqrt{6}}G_{15\mu} \end{pmatrix}\end{aligned} \tag{C.3}$$

where $G^\pm_{(ij)\mu} = \frac{1}{\sqrt{2}}\left(G_{i\mu} \mp iG_{j\mu}\right)$, $G_{3\mu}$ and $G_{8\mu}$ correspond to the SM gluons, $X^\pm_{r\mu} = \frac{1}{\sqrt{2}}\left(G_{9\mu} \mp iG_{10\mu}\right)$, $X^\pm_{b\mu} = \frac{1}{\sqrt{2}}\left(G_{11\mu} \mp iG_{12\mu}\right)$ and $X^\pm_{g\mu} = \frac{1}{\sqrt{2}}\left(G_{13\mu} \mp iG_{14\mu}\right)$ form a colour-triplet electric-charge $2/3$ vector leptoquark and $G_{15\mu}$ is the gauge field of the $U(1)_{B-L}$ subgroup.

Similarly the $SU(2)_{L/R}$ gauge fields, $W_{L/R}$, are written in this basis as

$$\begin{aligned}\hat{W}_{L\mu} &= \frac{1}{2}\tau_a W^a_{L\mu} = \frac{1}{2}\begin{pmatrix} W_{3\mu} & \sqrt{2}W^+_\mu \\ \sqrt{2}W^-_\mu & -W_{3\mu} \end{pmatrix}_L \\ \hat{W}_{R\mu} &= \frac{1}{2}\tau_a W^a_{R\mu} = \frac{1}{2}\begin{pmatrix} W_{3\mu} & \sqrt{2}W^+_\mu \\ \sqrt{2}W^-_\mu & -W_{3\mu} \end{pmatrix}_R\end{aligned} \tag{C.4}$$

with $W^\pm_{(L/R)\mu} = \frac{1}{\sqrt{2}}\left(W_{1\mu} \mp iW_{2\mu}\right)_{(L/R)}$ as usual.

# Appendix D

# Various Seesaw Properties

### D.0.1 Singular Values in One Generation

Consider the matrix $M \in M_2(\mathbb{C})$ given by

$$M = \begin{pmatrix} a & b \\ c & d \end{pmatrix}. \tag{D.1}$$

This matrix can be diagonalised via its singular value decomposition:

$$U_L^\dagger \, M \, U_R = M_d = \begin{pmatrix} m_\ell & 0 \\ 0 & m_\hbar \end{pmatrix}. \tag{D.2}$$

There exists exact analytic expressions for $U_L$, $U_R$, $m_\ell$ and $m_\hbar$ for this $2 \times 2$ matrix, however in the seesaw limit where the absolute value of one entry of Eq. (D.1) is significantly larger than the others, these expressions can be significantly simplified by writing it as a perturbation series. For example, in the limit where $|d| \gg |a|, |b|, |c|$ we find for the unitary-diagonalisation matrices

$$\begin{aligned} U_L &= \underbrace{\begin{pmatrix} 1 - \frac{1}{2}\left|\frac{ac^*+bd^*}{|d|^2}\right|^2 & \frac{ac^*+bd^*}{|d|^2} \\ -\left(\frac{ac^*+bd^*}{|d|^2}\right)^* & 1 - \frac{1}{2}\left|\frac{ac^*+bd^*}{|d|^2}\right|^2 \end{pmatrix}}_{Q_L} \underbrace{\begin{pmatrix} \sqrt{\frac{m_\ell}{|m_\ell|}} & 0 \\ 0 & \sqrt{\frac{m_\hbar}{|m_\hbar|}} \end{pmatrix}}_{K_L} + \mathcal{O}(\epsilon^3) \\ U_R &= \underbrace{\begin{pmatrix} 1 - \frac{1}{2}\left|\frac{ab^*+cd^*}{|d|^2}\right|^2 & \left(\frac{ab^*+cd^*}{|d|^2}\right)^* \\ -\frac{ab^*+cd^*}{|d|^2} & 1 - \frac{1}{2}\left|\frac{ab^*+cd^*}{|d|^2}\right|^2 \end{pmatrix}}_{Q_R} \underbrace{\begin{pmatrix} \sqrt{\frac{m_\ell^*}{|m_\ell|}} & 0 \\ 0 & \sqrt{\frac{m_\hbar^*}{|m_\hbar|}} \end{pmatrix}}_{K_R} + \mathcal{O}(\epsilon^3) \end{aligned} \tag{D.3}$$

where $Q_{L/R}$ removes the off-diagonal entries of $M$, $K_{L/R}$ is required to ensure the remaining diagonal entries are real and positive and $\epsilon \sim \frac{1}{|d|}$. The singular values of $M$ written up to sub-subleading order are

$$\begin{aligned} m_\ell &= \left| a - \frac{bc}{d} - \frac{a}{2}\left(\frac{|b|^2+|c|^2}{|d|^2}\right)\right| + \mathcal{O}(\epsilon^3) \\ m_\hbar &= \left| d + \frac{1}{2}\left(\frac{|b|^2+|c|^2}{d^*}\right) + \frac{a^* bc}{|d|^2}\right| + \mathcal{O}(\epsilon^3). \end{aligned} \tag{D.4}$$

Note that in the type-I seesaw scenario ($a = 0$, $b = c = m_D$, $d = M_R$), Eq. (D.3) implies $U_L^\dagger = U_R^T$ and therefore the (now symmetric) matrix M can be diagonalised either by $U_R^T M U_R$ or $U_L^\dagger M U_L^*$ with the singular values of Eq. (D.4) simplifying to

$$\begin{aligned} m_\ell &= \left|\frac{m_D^2}{M_R}\right| + \mathcal{O}(\epsilon^2) \\ m_\hbar &= \left| M_R + \frac{|m_D|^2}{M_R}\right| + \mathcal{O}(\epsilon^2) \end{aligned} \tag{D.5}$$

as expected.

The results above can applied to find similar expressions for $U_L$, $U_R$, $m_\ell$ and $m_\hbar$ in scenarios where different entries of $M$ are the largest in the seesaw through appropriate permutations. For example consider when $|c| \gg |a|, |b|, |d|$, as before there exist $U_L$ and $U_R$ which diagonalise $M$ however we note that Eq. (D.2) can be rewritten,

$$U_L^\dagger \begin{pmatrix} a & b \\ c & d \end{pmatrix} U_R = U_L^\dagger \begin{pmatrix} b & a \\ d & c \end{pmatrix} \tau_1 U_R = (U_L')^\dagger \begin{pmatrix} b & a \\ d & c \end{pmatrix} U_R' = \mathrm{diag}(m_\ell, m_\hbar) \tag{D.6}$$

where $\tau_1$ corresponds to the first Pauli matrix.

The results in Eqs. (D.3) and (D.4) can now be applied to Eq. (D.6) as $c$ is assumed to be the largest entry of $M$. Therefore $m_\ell$ and $m_\hbar$ are given by the expressions in Eq. (D.4) with the permutations $a \leftrightarrow b$ and $c \leftrightarrow d$, and the unitary diagonalisation matrices are given by $U_L' = U_L$ and $U_R' = \tau_1 U_R$ taken from Eq. (D.3) with similar permutations. Applying a similar procedure for $|b| \gg |a|, |c|, |d|$ we find that $U_L' = \tau_1 U_L$ and $U_R' = U_R$ and the results from Eqs. (D.3) and (D.4) are valid with permutations $a \leftrightarrow c$ and $b \leftrightarrow d$. Finally when $|a| \gg |b|, |c|, |d|$ we find $U_L' = \tau_1 U_L$ and $U_R' = \tau_1 U_R$ with the permutations $a \leftrightarrow d$ and $b \leftrightarrow c$ applied to Eqs. (D.3) and (D.4).

### D.0.2 Singular Values for Multiple Generations

Consider now a general matrix $M_{\rm B} \in \mathbb{C}^{m\times n}$ which can be partitioned into a $2\times 2$ block matrix of the form

$$M_{\rm B} = \begin{pmatrix} A_{m_1\times n_1} & B_{m_1\times l_1} \\ C_{l_1\times n_1} & D_{l_1\times l_1} \end{pmatrix} \tag{D.7}$$

where the subscripts on the matrix blocks correspond to their dimensions, $m_1 + l_1 = m$, $n_1 + l_1 = n$ and $D$ is restricted to be nonsingular. This matrix can be *block* diagonalised by

$$Q_L^\dagger M_{\rm B}\, Q_R = M_{\mathscr{D}} = \mathrm{diag}(m_L,\, m_H) = \begin{pmatrix} m_L & 0_{m_1\times l_1} \\ 0_{l_1\times n_1} & m_H \end{pmatrix} \tag{D.8}$$

where $m_L$ and $m_H$ now correspond to $m_1\times n_1$ and $l_1\times l_1$ block matrices respectively and $0_{n_1\times l_1}$ corresponds to a matrix of zeroes with dimension $n_1\times l_1$. Unlike in the $2\times 2$ case, exact analytical expressions for the block matrices $m_L$ and $m_H$ or the diagonalisation matrices $Q_L$ and $Q_R$ do not exist. However in the seesaw limit, where the lightest singular value of the square block $D$ is assumed to be significantly larger than the largest singular value of all other blocks, a similar perturbative expansion can be derived. This is done by assuming, as an *ansatz*, that the block matrices $U_L$ and $U_R$ have a similar form to the matrices appearing in Eq. (D.3)[1] in combination with the conditions $U_L^\dagger (M_{\rm B} M_{\rm B}^\dagger)\, U_L = \mathrm{diag}(m_L m_L^\dagger,\, m_H m_H^\dagger)$ and $U_R^\dagger (M_{\rm B}^\dagger M_{\rm B})\, U_R = \mathrm{diag}(m_L^\dagger m_L,\, m_H^\dagger m_H)$ which allows $U_{L/R}$ to be solved separately from each other.

In this limit, $||D|| \gg ||A, B, C||$, we find $M_{\rm B}$ can be *fully* diagonalised at sub-subleading order by

$$\begin{aligned} U_L &\simeq \underbrace{\begin{pmatrix} \mathbb{1}_{n\times n} - \frac{1}{2}XX^\dagger & X \\ -X^\dagger & \mathbb{1}_{n\times n} - \frac{1}{2}X^\dagger X \end{pmatrix}}_{Q_L} \underbrace{\begin{pmatrix} V_L & 0 \\ 0 & W_L \end{pmatrix}}_{K_L} \\ U_R &\simeq \underbrace{\begin{pmatrix} \mathbb{1}_{n\times n} - \frac{1}{2}Z^\dagger Z & Z^\dagger \\ -Z & \mathbb{1}_{n\times n} - \frac{1}{2}ZZ^\dagger \end{pmatrix}}_{Q_R} \underbrace{\begin{pmatrix} V_R & 0 \\ 0 & W_R \end{pmatrix}}_{K_R} \end{aligned} \tag{D.9}$$

[1] In other words that $U_L$ and $U_R$ can be written perturbatively in terms of an expansion parameter $\epsilon$ related to the seesaw in $M$.

where

$$X = (AC^\dagger + BD^\dagger)(DD^\dagger)^{-1} \simeq BD^{-1}$$
$$Z = (D^\dagger D)^{-1}(B^\dagger A + D^\dagger C) \simeq D^{-1}C. \tag{D.10}$$

Similar to the $2\times 2$ case, $Q_{L/R}$ remove the off-diagonal entries of $M_{\rm B}$, $K_{L/R}$ diagonalise the blocks $m_{L/H}$ via $(V/W)_L^\dagger\, m_{L/H}\, (V/W)_R = m^d_{L/H} = \text{diag}(\dots)$ and the expression for $V_{L/R}$ and $W_{L/R}$ depends on the structure of the submatrices $m_L$ and $m_H$.

Applying Eqs. (D.9) and (D.10) to Eq. (D.8) gives the light and heavy submatrices at sub-subleading order as per

$$\begin{aligned} m_L &\simeq \left(A - BD^{-1}C - \frac{1}{2}\left(BD^{-1}(D^\dagger)^{-1}B^\dagger A + A\,C^\dagger(D^\dagger)^{-1}D^{-1}C\right)\right) \\ m_H &\simeq D + \frac{1}{2}\left(CC^\dagger(D^\dagger)^{-1} + (D^\dagger)^{-1}B^\dagger B\right) \\ &\quad + \frac{1}{2}\left((D^\dagger)^{-1}D^{-1}CA^\dagger B + CA^\dagger BD^{-1}(D^\dagger)^{-1}\right). \end{aligned} \tag{D.11}$$

Note that Eq. (D.11) agrees with Eq. (D.4) in the special case where $M_{\rm B} \in \mathbb{C}^{2\times 2}$, i.e. all the blocks of $M_{\rm B}$ are just complex numbers, $A \to a \dots D \to d$.

In the special case of Eq. (D.7) where $B = C^T = m_D$ (implying $n_1 = m_1$), $A = 0_{n_1\times n_1}$ and $D = M_R$ is a symmetric matrix, which occurs in the n-dimensional type-I seesaw model of neutrino mass, $U_L^\dagger = U_R^T$ and $m_L$ and $m_H$ simplify to at sub-subleading order

$$\begin{aligned} m_L &\simeq -\, m_D M_R^{-1} m_D^T \\ m_H &\simeq \quad M_R + \frac{1}{2}\left(m_D^T m_D^* (M_R^*)^{-1} + (M_R^*)^{-1} m_D^\dagger m_D\right) \end{aligned} \tag{D.12}$$

where $M_R = M_R^T$ has been used. Therefore the usual results are recovered in this case and we find them to be in full agreement[2] with [241] which derived an algorithm to find the light and heavy mass matrices in neutrino seesaw models at arbitrary order.

In a similar way to the case with $M \in \mathbb{C}^{2\times 2}$, the results above can be extended to find $m_L$, $m_H$, $U_L$ and $U_R$ in situations where the norm of different blocks in Eq. (D.7) are dominant[3]. Once again consider a scenario where $||C|| \gg ||A, B, D||$ (and C is square)

[2]We also find agreement in the case where $A = A^T \neq 0_{n\times n}$ which for example is relevant in hybrid type-I+II models.

[3]This is with the caveat that $M_{\rm B}$ can be partitioned such that the dominant block has a well defined inverse.

| Dominant Block | Permutations | $(U'_L,\, U'_R)$ |
|---|---|---|
| $A$ | $A \leftrightarrow D$ & $B \leftrightarrow C$ | $(\not{1}(l_1, m_1)\, U_L,\, \not{1}(n_1, l_1)\, U_R)$ |
| $B$ | $A \leftrightarrow C$ & $B \leftrightarrow D$ | $(\not{1}(l_1, m_1)\, U_L,\, U_R)$ |
| $C$ | $A \leftrightarrow B$ & $C \leftrightarrow D$ | $(U_L,\, \not{1}(n_1, l_1)\, U_R)$ |
| $D$ | – | $(U_L,\, U_R)$ |

TABLE D.1: Required rotations on $U_L$ and $U_R$ and permutations of block elements for the formulas in Eqs. (D.9) to (D.11) to be valid for different block elements assumed to be the nonsingular-square dominant block of $M_{\rm B}$ in seesaw scenarios. $\not{1}(l_1, m_1)$ is defined in Eq. (D.13) and here $l_1$ is taken to be the dimension of the dominant square matrix block and $(m_1, n_1)$ corresond to the dimensions of the matrix block diagonally opposite.

and note that

$$M_{\rm B} = \begin{pmatrix} A_{m_1\times l_1} & B_{m_1\times n_1} \\ C_{l_1\times l_1} & D_{l_1\times n_1} \end{pmatrix} = \begin{pmatrix} B_{m_1\times n_1} & A_{m_1\times l_1} \\ D_{l_1\times n_1} & C_{l_1\times l_1} \end{pmatrix} \underbrace{\begin{pmatrix} 0_{n_1\times l_1} & \mathbb{1}_{n_1\times n_1} \\ \mathbb{1}_{l_1\times l_1} & 0_{l_1\times n_1} \end{pmatrix}}_{\not{1}(n_1, l_1)} . \tag{D.13}$$

Therefore Eqs. (D.9) to (D.11) are valid if $U'_L = U_L$, $U'_R = \not{1}(n_1, l_1)\, U_R$ and the permutations $A \leftrightarrow B$ and $C \leftrightarrow D$ are performed, where $(U'_L)^\dagger\, M_{\rm B}\, U'_R = \mathrm{diag}(m_L,\, m_H)$. This can be performed for any of the four blocks of $M_{\rm B}$ being dominant and the results for this are summarised in Table D.1.

### D.0.3 Gap properties between the charged leptons and down quarks

Below we briefly prove the claim that, in the triplet scenario, the charged-lepton mass matrices defined in Eqs. (4.76) and (4.79) imply that the SM-like charged lepton masses must be lighter than the down-quark masses for all generations. This arises due to the zero block appearing in their mass matrices diagonally opposite the dominant block in the seesaw. Unlike the previous section which relied on an approximate block diagonalisation technique with neglected higher-order terms, the results below are exact statements that do not rely on any perturbative arguments. We closely follow the work presented in [242] which proved a similar gap property specifically for the type-I seesaw symmetric mass matrix, which we will generalise to an arbitrary complex matrix relevant to our charged-lepton seesaw.

We state without proof three matrix properties related to the Courant-Fischer-Weyl min-max theorem:

- For two hermitian $n \times n$ matrices $A$ and $B$, if $C = A + B$ then

$$a_k + b_1 \leq c_k \leq a_k + b_n \tag{D.14}$$

  where $x_i$ corresponds to the i-th largest eigenvalue of the matrix X and $k \leq n$. For $k = 1$ this reduces to the special case

$$\min(A) + \min(B) \leq \min(A + B) \tag{D.15}$$

  where $\min(X) = x_1$.

- For all $A \geq 0$ and $B \in M_n(\mathbb{C})$, if $C = B^\dagger A B$ then

$$a_k \min(B^\dagger B) \leq c_k. \tag{D.16}$$

- If $Q$ is an $n \times n$ submatrix of the $N \times N$ matrix $M$ then

$$m_k \leq q_k \leq m_{N-n+k} \tag{D.17}$$

  for every $k \leq n$, this is known as the Cauchy interlacing theorem.

Additional details including proofs for some of these properties can be found in [242].

We take the mass mixing matrix $M_{eE}$ to have the same structure as the case of an $SU(2)_R$ triplet defined in Eq. (4.76):

$$M_{eE} = \begin{pmatrix} m_{ee} & 0_{3\times3} \\ m_{Ee} & m_{EE} \end{pmatrix}, \tag{D.18}$$

where we are assuming three generations of the exotic triplet fermion and therefore each block is $3 \times 3$ and we further assume $m_{Ee}$ is nonsingular. As discussed in Section 4.5.1, in order to achieve the desired helicity-suppression in the PS limits we require the hierarchy $\|m_{Ee}\| > \|m_{ee}, m_{EE}\|$ to be satisfied which implies

$$\sigma_n(m_{ee}), \sigma_n(m_{EE}) < \sigma_1(m_{Ee}) \tag{D.19}$$

where $\sigma_i(X)$ corresponds to the i-th largest singular value of the matrix $X$ and $n = 3$. This defines a seesaw in $M_{eE}$ with $m_{Ee}$ as the dominant block.

The bottom-right sub-matrix of

$$\left(M_{eE}M_{eE}^\dagger\right)^{-1} = \begin{pmatrix} \cdot & \cdot \\ \cdot & m_{EE}^{-1}m_{Ee}m_{ee}^{-1}(m_{ee}^\dagger)^{-1}m_{Ee}^\dagger(m_{EE}^\dagger)^{-1} + m_{EE}^{-1}(m_{EE}^\dagger)^{-1} \end{pmatrix} \tag{D.20}$$

which we will label as $X$ satisfies the property defined in Eq. (D.17), where the dots correspond to sub-matrices which are not relevant. As the sub-matrix X has dimensions $n \times n$ and the full matrix has dimensions $2n \times 2n$ the interlacing theorem implies

$$x_{n-k} \leq m_{2n-k} \tag{D.21}$$

where we have chosen $k = n - k$ in Eq. (D.17). As $M_{eE}(M_{eE}^\dagger)^{-1}$ is Hermitian, its eigenvalues correspond to the squared singular values of $M_{eE}$. Furthermore, from simple properties of eigenvalues, the i-th *largest* eigenvalue of an $n \times n$ matrix $M^{-1}$ corresponds to the (n-i)-th *smallest* eigenvalue of $M$. Therefore Eq. (D.21) implies

$$x_{n-k} \leq \frac{1}{\sigma_k(M_{eE})^2}. \tag{D.22}$$

Applying Eq. (D.15) to $x_{n-k}$ leads to the inequality

$$\left[m_{EE}^{-1}m_{Ee}m_{ee}^{-1}(m_{ee}^\dagger)^{-1}m_{Ee}^\dagger(m_{EE}^\dagger)^{-1}\right]_{n-k} + \min(m_{EE}^{-1}(m_{EE}^\dagger)^{-1}) \leq x_{n-k} \tag{D.23}$$

and now with repeated applications of Eq. (D.16) to the first term of Eq. (D.23) leads to

$$\left(\left[m_{ee}^{-1}(m_{ee}^\dagger)^{-1}\right]_{n-k} \min\left(m_{Ee}m_{Ee}^\dagger\right) + \mathbb{1}\right) \min(m_{EE}^{-1}(m_{EE}^\dagger)^{-1}) \leq x_{n-k} \tag{D.24}$$

which implies

$$\frac{1}{\sigma_n(m_{EE})^2}\left(\frac{\sigma_1(m_{Ee})^2}{\sigma_k(m_{ee})^2}\right) \leq \frac{1}{(\sigma_k(M_{eE}))^2} \tag{D.25}$$

and therefore

$$\sigma_k(M_{eE}) \leq \sigma_k(m_{ee})\frac{\sigma_n(m_{EE})}{\sqrt{\sigma_1(m_{Ee})^2 + \sigma_k(m_{ee})^2}} < \sigma_k(m_{ee})\frac{\sigma_n(m_{EE})}{\sigma_1(m_{Ee})} \tag{D.26}$$

where we have used the seesaw assumption that $\sigma_n(m_{ee}, m_{EE}) < \sigma_1(m_{Ee})$.

The exact same procedure can be applied to the matrix $(M_{eE}^\dagger)^{-1}M_{eE}$ which instead leads to the inequality

$$\sigma_k(M_{eE}) \leq \sigma_k(m_{EE})\frac{\sigma_n(m_{ee})}{\sqrt{\sigma_1(m_{Ee})^2+\sigma_k(m_{EE})^2}} < \sigma_k(m_{EE})\frac{\sigma_n(m_{ee})}{\sigma_1(m_{Ee})}. \tag{D.27}$$

Combining Eqs. (D.26) and (D.27) leads to an upper-bound on the k-th largest *light* singular value of $M_{eE}$

$$\sigma_k(M_{eE}) < \frac{\min\left[\sigma_k(m_{ee})\sigma_n(m_{EE}),\sigma_k(m_{EE})\sigma_n(m_{ee})\right]}{\sigma_1(m_{Ee})} \leq \frac{\sigma_n(m_{ee})\sigma_n(m_{EE})}{\sigma_1(m_{Ee})}. \tag{D.28}$$

Comparing Eq. (D.28) to the charged-lepton mass matrix in the case of the $SU(2)_R$ triplet in Eq. (4.76) leads to the strict inequality

$$\sigma_k(m_\ell) < \sigma_k(m_d)\left(\frac{\sigma_3(\mu_\Psi)}{v_R\,\sigma_1(Y_\Psi)}\right) \tag{D.29}$$

and as the singular values of each matrix correspond to the physical masses, each light lepton mass of a given generation must be strictly lighter than the corresponding down-quark mass of the same generation. This is due to the seesaw assumption which enforces the fraction in brackets to be strictly smaller than one. As shown in Table 4.6 the charged-lepton and down-quark mass hierarchies change between generations at low scales, therefore due the PS symmetry, a matrix of the form in Eq. (D.18) is phenomenologically ruled out.

Although not relevant in our analysis, a similar procedure can be applied to the Hermitian matrices $(M_{eE}^\dagger)M_{eE}$ and $M_{eE}(M_{eE}^\dagger)$ to derive inequalities on the masses of the $n$ heavy states of $M_{eE}$ and for example leads to

$$\sigma_{n+1}(M_{eE}) \geq \max\left(\sqrt{\sigma_1(m_{Ee})^2+\sigma_1(m_{ee})^2},\sqrt{\sigma_1(m_{Ee})^2+\sigma_1(m_{EE})^2}\right) > \sigma_1(m_{Ee}) \tag{D.30}$$

Therefore the strict hierarchy implied by these inequalities leads to the 'gap property'

$$\sigma_1(M_{eE}) \leq ... \leq \sigma_n(M_{eE}) \leq \frac{\sigma_n(m_{ee})\sigma_n(m_{EE})}{\sigma_1(m_{Ee})} \ll \sigma_1(m_{Ee}) < \sigma_{n+1}(M_{eE}) \leq ... \leq \sigma_{2n}(M_{eE}) \tag{D.31}$$

which does not rely on any perturbative arguments and we emphasise that these results are only valid for 'type-I like' scenarios where the entry diagonally opposite the dominant block is zero. Our results agree with the gap properties derived in [242] in the type-I limit which assumes $m_{ee} = (m_{EE})^T = m_D$ and $m_{Ee} = M_R$ and recovers the usual type-I hierarchy.

### D.0.4 Lepton masses with additional bi-doublets

The neutrino mass matrix which arises with the addition of an $SU(2)_{L/R}$ bi-doublet to the usual PS fermions $f_{L/R}$ is given by

$$\mathcal{L}_{\nu N} = \frac{1}{2}\begin{pmatrix} \overline{\nu_L} & \overline{\nu_R^c} & \overline{N_L} & \overline{N_R^c} \end{pmatrix} \begin{pmatrix} 0 & m_u & 0 & y^R_{\Psi_{22}} v_R \\ m_u & 0 & 0 & y^L_{\Psi_{22}} v_L^* \\ 0 & 0 & 0 & \mu_{\Psi_{22}} \\ y^R_{\Psi_{22}} v_R & y^L_{\Psi_{22}} v_L^* & \mu_{\Psi_{22}} & 0 \end{pmatrix} \begin{pmatrix} \nu_L^c \\ \nu_R \\ N_L^c \\ N_R \end{pmatrix} \tag{D.32}$$

where we have labelled the fields as in Eq. (4.84). A phenomenologically viable mass spectrum for the heavy charged lepton states requires either $y^R_{\Psi_{22}} v_R$ or $\mu_{\Psi_{22}}$ to have masses at a TeV or above, as discussed in Section 4.5.1, due to the charged lepton mass mixing matrix

$$\mathcal{L}_{eE} = \begin{pmatrix} \overline{e_L} & \overline{E_L} \end{pmatrix} \begin{pmatrix} m_d & y^R_{\Psi_{22}} v_R \\ y^L_{\Psi_{22}} v_L^* & \mu_{\Psi_{22}} \end{pmatrix} \begin{pmatrix} e_R \\ E_R \end{pmatrix}. \tag{D.33}$$

The parameter $m_u$ is fixed by the up-quark masses due to the PS symmetry, $m_d$ is fixed by the down-quark masses, $y^L_{\Psi_{22}} v_L$ is tied to the electroweak scale, $y^R_{\Psi_{22}} v_R$ can at most be the size of $SU(2)_R$/PS breaking and $\mu_{\Psi_{22}}$ is unconstrained.

Different hierarchies between the parameters appearing in Eq. (D.32) lead to different neutrino mass phenomenology and here we show that only one possibility allows for a viable mass spectrum for the charged leptons as well as sufficiently light neutrino masses assuming a low scale PS breaking. We will use a one-generational example for illustrative purposes as the same statements hold true for the more complicated multi-generational scenario. As discussed in Section 4.5.1 at least one of $y^R_{\Psi_{22}} v_R$ or $\mu_{\Psi_{22}}$ must have masses at least an order of magnitude larger than the electroweak scale such that the charged lepton partners are sufficiently heavy phenomenologically.

Firstly in the scenario where $|\mu_{\Psi_{22}}| \gg |y^R_{\Psi_{22}} v_R,\, y^L_{\Psi_{22}} v_L,\, m_u|$ the light, charged-lepton masses are given by

$$m_\ell \simeq m_d - v_L v_R\, y^L_{\Psi_{22}} (\mu_{\Psi_{22}})^{-1} y^R_{\Psi_{22}} \tag{D.34}$$

and diagonalising Eq. (D.32) leads to two different pairs of pseudo-Dirac neutrinos with masses given at first order by

$$\begin{aligned} m_{1,2} &\simeq \mu_{\Psi_{22}} & \nu_{1,2} &\simeq \frac{1}{\sqrt{2}} N_L \pm \frac{1}{\sqrt{2}} N^c_R \\ m_{3,4} &\simeq m_u & \nu_{3,4} &\simeq \frac{1}{\sqrt{2}} \nu_L \pm \frac{1}{\sqrt{2}} \nu^c_R. \end{aligned} \tag{D.35}$$

Therefore the lightest neutrino masses would be predicted to have masses and splittings similar to the up-quark sector. The above equation is true irrespective of the hierarchy between the non-dominant parameters $y^R_{\Psi_{22}} v_R$, $y^L_{\Psi_{22}} v_L$ and $m_u$. Therefore we find that this hierarchy of couplings does not lead to the desired seesaw required to explain the lightness of the active neutrino masses for any scale of PS breaking.

Turning to the alternate possibility where $|y^R_{\Psi_{22}} v_R| \gg |\mu_{\Psi_{22}},\, y^L_{\Psi_{22}} v_L,\, m_u|$ the charged lepton masses are now given by

$$m_\ell \simeq y^L_{\Psi_{22}} v_L - \frac{m_d \mu_{\Psi_{22}}}{y^R_{\Psi_{22}} v_R}. \tag{D.36}$$

Here we find two different neutrino mass regimes depending on the hierarchy between the non-dominant parameters $|\mu_{\Psi_{22}}|$ and $|y^L_{\Psi_{22}} v_L|$.

For the hierarchy $|y^R_{\Psi_{22}} v_R| \gg |\mu_{\Psi_{22}}| > 2|y^L_{\Psi_{22}} v_L|$ the physical neutrino states have masses given at first order by

$$\begin{aligned} m_{1,2} &\simeq y^R_{\Psi_{22}} v_R & \nu_{1,2} &\simeq \frac{1}{\sqrt{2}} \nu_L \pm \frac{1}{\sqrt{2}} N^c_R \\ m_{3,4} &\simeq \frac{m_u}{y^R_{\Psi_{22}} v_R} \left(\mu_{\Psi_{22}} \pm y^L_{\Psi_{22}} v_L\right) & \nu_{3,4} &\simeq \frac{1}{\sqrt{2}} N_L \pm \frac{1}{\sqrt{2}} \nu^c_R \end{aligned} \tag{D.37}$$

where the above results are insensitive to the relative size of $|m_u|$ to $|y^L_{\Psi_{22}} v_L|$ and $|\mu_{\Psi_{22}}|$. Sufficiently light neutrinos now implies the ratio

$$\frac{m_\nu}{m_u} \simeq \frac{\mu_{\Psi_{22}}}{y^R_{\Psi_{22}} v_R} \simeq 10^{-11} \tag{D.38}$$

where we have estimated $m_\nu \lesssim 10^{-9}$ GeV from known neutrino upper mass limits and $m_u \simeq 170$ GeV in the case of the top quark. This consequently implies that

$$m_\ell \simeq y^L_{\Psi_{22}} v_L \tag{D.39}$$

for the charged-lepton masses as the second term in Eq. (D.36) will be highly suppressed. Therefore in order to recover the correct charged-lepton masses we require $y^L_{\Psi_{22}} v_L \simeq 1$ GeV for the tau lepton and as we have assumed $|\mu_{\Psi_{22}}| > |y^L_{\Psi_{22}} v_L|$ this necessarily implies

$$|\mu_{\Psi_{22}}| > 1 \text{ GeV} \tag{D.40}$$

and therefore

$$|y^R_{\Psi_{22}} v_R| > 10^{11} \text{ GeV} \tag{D.41}$$

using Eq. (D.38). Therefore for $|\mu_{\Psi_{22}}| > |y^L_{\Psi_{22}} v_L|$, sufficiently light neutrino masses are only possible for very large $SU(2)_R$/PS breaking scales.

Alternatively the hierarchy $|y^R_{\Psi_{22}} v_R| \gg |y^L_{\Psi_{22}} v_L| > \frac{1}{2}|\mu_{\Psi_{22}}|$ leads to

$$\begin{aligned}
m_{1,2} &\simeq v_R\, y^R_{\Psi_{22}} & \nu_{1,2} &\simeq \frac{1}{\sqrt{2}}\nu_L \pm \frac{1}{\sqrt{2}} N^c_R \\
m_3 &\simeq \frac{v_L}{v_R}\frac{2y^L_{\Psi_{22}} m_u}{y^R_{\Psi_{22}}} & \nu_3 &\simeq \nu^c_R \\
m_4 &\simeq \frac{1}{v_L v_R}\frac{\mu^2_{\Psi_{22}} m_u}{2\, y^L_{\Psi_{22}} y^R_{\Psi_{22}}} & \nu_4 &\simeq N_L
\end{aligned} \tag{D.42}$$

where again the results are insensitive to the overall size of $m_u$ as long as it is smaller than $y^R_{\Psi_{22}} v_R$. This scenario therefore leads to the neutrino mass hierarchy

$$m_{\nu_4} \ll m_{\nu_3} \ll m_{\nu_{1,2}} \tag{D.43}$$

Sufficiently light neutrinos implies

$$\frac{m_\nu}{m_u} y^L_{\Psi_{22}} v_L \simeq 10^{-11} \text{ GeV} \simeq \frac{1}{2}\frac{\mu^2_{\Psi_{22}}}{y^R_{\Psi_{22}} v_R} \tag{D.44}$$

for the same estimates. Once again this implies that the second term in Eq. (D.36) will be subdominant and therefore the charged lepton masses are given by $m_\ell \simeq y^L_{\Psi_{22}} v_L$. Now light neutrinos are possible for low PS breaking scales for similar reasons to the usual inverse seesaw mechanism, for example for $y^R_{\Psi_{22}} v_R \simeq 10$ TeV we can estimate

$$\mu_{\Psi_{22}} \simeq 4.4 \times 10^{-3} \text{ GeV}. \tag{D.45}$$

Therefore we find for a mass matrix of the form in Eq. (D.32), only one hierarchy of parameters leads to a viable neutrino mass spectrum for low scales of PS breaking. As this requires the term $\mu_{\Psi_{22}}$ to be very small, this also conveniently leads to a helicity-suppression in the PS mediated rare meson decays, and therefore allows the limits for PS breaking to be significantly lowered as discussed in Section 4.5.1.

In the multi-generational scenario we find the block diagonalisation of Eq. (D.32), assuming the hierarchy $\|y^R_{\Psi_{22}} v_R\| \gg \|y^L_{\Psi_{22}} v_L\| > \|\mu_{\Psi_{22}}\|$[4], is given at first order by

$$\begin{aligned}
m_{1,2} &\simeq v_R \, Y^R_{\Psi_{22}} \\
m_3 &\simeq \frac{v_L}{v_R} \left( Y^L_{\Psi_{22}} (Y^R_{\Psi_{22}})^{-1} m_u + m_u^T \left[ Y^L_{\Psi_{22}} (Y^R_{\Psi_{22}})^{-1} \right]^T \right) \\
m_4 &\simeq \frac{1}{v_L v_R} \mu_{\Psi_{22}} \left[ (Y^R_{\Psi_{22}})^T (m_u^T)^{-1} Y^L_{\Psi} + (Y^L_{\Psi_{22}})^T m_u^{-1} Y^R_{\Psi_{22}} \right]^{-1} \mu^T_{\Psi_{22}}
\end{aligned} \tag{D.46}$$

for each mass block where $Y^{L/R}_{\Psi_{22}}$, $m_u$ and $\mu_{\Psi_{22}}$ are now matrices of appropriate dimension.

We estimate the relationship between the mass and interaction eigenstates for the relevant light neutrinos states to be

$$\begin{aligned}
\nu_4 \simeq\ & U_N^\dagger \left[ \mu_{\Psi_{22}} (y^R_{\Psi_{22}})^{-1} \right]^\dagger \nu_L^c - \frac{1}{2} U_N^\dagger \left[ Y^L_{\Psi_{22}} (y^R_{\Psi_{22}})^{-1} ([y^R_{\Psi_{22}}]^\dagger)^{-1} \mu^\dagger_{\Psi_{22}} \right]^\dagger \nu_R \\
& \qquad + U_N^\dagger \left[ \mathbb{1} - \frac{1}{2} \mu_{\Psi_{22}} (Y^R_{\Psi_{22}})^{-1} ([Y^R_{\Psi_{22}}]^\dagger)^{-1} \mu^\dagger_{\Psi_{22}} \right]^\dagger N_L^c \\
\nu_3 \simeq\ & O_3^\dagger \left[ Y^L_{\Psi_{22}} (Y^R_{\Psi_{22}})^{-1} \right]^\dagger \nu_L^c \\
& - \frac{1}{2} O_3^\dagger \left[ Y^L_{\Psi_{22}} (Y^R_{\Psi_{22}})^{-1} ([Y^R_{\Psi_{22}}]^\dagger)^{-1} \mu^\dagger_{\Psi_{22}} \right]^\dagger N_L^c + O_3^\dagger \left[ m_u^T (Y^R_{\Psi_{22}})^{T-1} \right]^\dagger N_R \\
& + O_3^\dagger \left[ \mathbb{1} - \frac{1}{2} \left( Y^L_{\Psi_{22}} (Y^R_{\Psi_{22}})^{-1} ([Y^R_{\Psi_{22}}]^\dagger)^{-1} (Y^L_{\Psi_{22}})^\dagger + m_u^T (Y^R_{\Psi_{22}})^{T-1} ([Y^R_{\Psi_{22}}]^*)^{-1} m_u^* \right) \right]^\dagger \nu_R
\end{aligned} \tag{D.47}$$

using a perturbative seesaw expansion where $U_N^\dagger$ and $O_3$ diagonalise the lightest and next-to-lightest mass blocks of the neutrino mass matrix after block diagonalisation. Therefore for the lightest neutrino states, $\nu_4$, the deviation from unitarity between its

[4] More accurately, the hierarchy between each matrix required for a low scale spectrum is given by $\|\mu_{\Psi_{22}} (y^R_{\Psi_{22}} v_R)^{-1} m_u\| < \|v_L v_R \left( Y^L_{\Psi_{22}} (y^R_{\Psi_{22}} v_R)^{-1} m_u + [Y^L_{\Psi_{22}} (y^R_{\Psi_{22}} v_R)^{-1} m_u]^T \right)\|$ for non-commuting matrices. This should in general imply the hierarchy $\|\mu_{\Psi_{22}}\| < \|Y^L_{\Psi_{22}} v_L\|$ however.

couplings to the SM charged leptons, which are predominately made up of $E_L$ which weakly couples to $N_L$, is given at lowest order by the matrix

$$\eta \simeq \frac{1}{2}\mu_{\Psi_{22}}(Y^R_{\Psi_{22}})^{-1}\left(\mu_{\Psi_{22}}(Y^R_{\Psi_{22}})^{-1}\right)^{\dagger}. \tag{D.48}$$

This determines the degree of non-unitarity in the physical PMNS matrix which stems from mixing effects within the neutral sector. As the fermion bi-doublet also introduced additional exotic charged-lepton states, there will additionally be mixing effects within the charged sector which leads to additional non-unitarity effects for the PMNS. Interestingly, as shown in Section 4.5.1.1 we find the deviation of non-unitarity within the charged lepton sector to be the same as in the neutral sector above implying

$$U_{\text{PMNS}} \simeq (\mathbb{1}-\eta)\, U_N^{\dagger}\, (\mathbb{1}-\eta)\, O_L^e. \tag{D.49}$$

Figure D.1 plots the norm of the required matrix $\mu_{\Psi_{22}}$ for a given choice of $v_R$ and $Y^R_{\Psi_{22}}$ which leads to a viable mass spectrum for the active neutrinos where we have fixed the lightest neutrino mass to

$$m_{\nu_1} = 10^{-10}\ \text{GeV} \tag{D.50}$$

and assumed a normal ordering for the remaining masses. The matrix $Y^R_{\Psi_{22}}$ was randomly scanned over where we assumed a degenerate spectrum such that the singular values of the matrix were within an order of magnitude to each other. The $SU(2)_R$ breaking scale $v_R$ was scanned between $1-10^4$ TeV and $\mu_{\Psi_{22}}$ was fixed by

$$\mu_{\Psi_{22}} = U_\nu^* m_\nu^{1/2} A \left[Y_L m_u^{-1} Y^R_{\Psi_{22}} + (Y^R_{\Psi_{22}})^T (m_u^T)^{-1} Y_L\right]^{1/2} \tag{D.51}$$

through a Casas-Ibarra parametrisation [131]. Here $U_\nu$ corresponds to the unitary matrix which diagonalises the lightest neutrino mass block, $m_\nu$ is a diagonal matrix composed of the assumed neutrino masses and $A$ is a random orthogonal matrix. The left plot of Fig. D.1 shows that as $v_R$ increases, the singular values of $\mu_{\Psi_{22}}$ must increase for a fixed neutrino mass scale. As a result at around $10^3$ TeV, the singular values of $\mu_{\Psi_{22}}$ become larger than $Y^L_{\Psi_{22}}$ spoiling the required hierarchy of scales for light neutrinos at low scales.

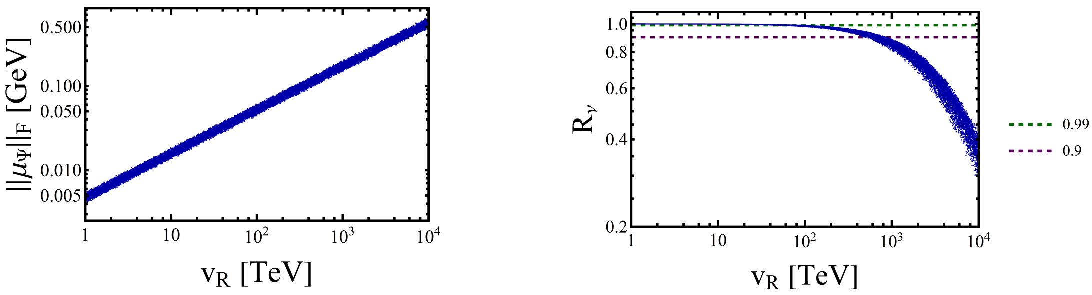


FIGURE D.1: The Frobenius norm of the matrix $\mu_{\Psi_{22}}$ generated through a Casas-Ibarra parametrisation as a function of $v_R$ **(left)** and $R_\nu$ as a function of the same scale **(right)**, where $R_\nu$ is defined in Eq. (D.52). Here we have randomly scanned over a degenerate spectrum for $Y^R_{\Psi_{22}}$ such that the heavy charged lepton partners have masses at around the scale $v_R$. For larger values of $v_R$ the generated $\mu_{\Psi_{22}}$ develops singular values larger than the required hierarchy $\|Y^L_{\Psi_{22}}\| > \|\mu_{\Psi_{22}}\|$ where $Y^L_{\Psi_{22}} v_L$ is fixed to give the correct SM charged-lepton masses and the resultant neutrino masses begin to disagree with experimental values.

The right plot of Fig. D.1 plots the same scale as a function of $R_\nu$ where

$$R_\nu = \prod_i \frac{m_i}{m_i^{\text{input}}} \tag{D.52}$$

where $m_i$ corresponds to the mass of the i-th generation of the three active neutrinos numerically calculated after diagonalising the mass matrix and $m_i^{\text{input}}$ to the masses inputed via the Casas-Ibarra parameterisation. Clearly larger scales for $v_R$ are unable to reproduce the correct neutrino masses. For all points considered the light states from the charged-lepton mass matrix reproduce the charged-lepton masses with $m_e \simeq Y^L_{\Psi_{22}}$ to a high degree of accuracy. Therefore the neutral- and charged-lepton mass matrices generated in the scenario with additional fermionic bi-doublets are viable candidates for a low-scale PS setup provided that

$$y^R_{\Psi_{22}} v_R \lesssim 10^3 \text{ TeV}. \tag{D.53}$$

### D.0.5 Lepton masses with additional triplets

The neutrino mass matrix which arises with the addition of $SU(2)_{L/R}$ triplets is given by the usual linear/inverse seesaw:

$$\mathcal{L}_{\nu N} = \frac{1}{2}\begin{pmatrix} \overline{\nu_L} & \overline{\nu_R^c} & \overline{N_R^c} \end{pmatrix} \begin{pmatrix} 0 & m_u & y^L_{\Psi_3} v_L \\ m_u & 0 & y^R_{\Psi_3} v_R^* \\ y^L_{\Psi_3} v_L & y^R_{\Psi_3} v_R^* & \mu_\Psi \end{pmatrix} \begin{pmatrix} \nu_L^c \\ \nu_R \\ N_R \end{pmatrix} \tag{D.54}$$

where we have labelled the fields as in Eq. (4.75) and the PS symmetry enforces that the singular values of $m_u$ are given by the up-quark masses. As discussed in Sections 4.4.1.1 and 4.5.1, both $y^L_{\Psi_3} v_L$ and $y^L_{\Psi_3} v_R$ are required in order to generate a phenomenologically valid charged lepton mass spectrum. Both terms will not be present if the usual scalars $\chi_{L/R}$ are assumed and therefore require a more exotic choice of scalars. For example if $\chi_L \sim (\mathbf{4}, \mathbf{2}, \mathbf{1})$ is replaced with $\chi' \sim (\mathbf{4}, \mathbf{2}, \mathbf{3})$ in the case of the $SU(2)_R$ triplet as was done in [213], the missing mass term in the Yukawa Lagrangian will now be generated. We will therefore assume in what follows that the scalar spectrum is such that all the terms appearing in Eq. (D.54) are present. Consequently the charged lepton mass matrix will be given by

$$\mathcal{L}_{eE} = \begin{pmatrix} \overline{e_L} & \overline{E_L} \end{pmatrix} \begin{pmatrix} m_d & \sqrt{2}\, y^L_{\Psi_3} v_L \\ \sqrt{2}\, y^R_{\Psi_3} v_R^* & \mu_{\Psi_3} \end{pmatrix} \begin{pmatrix} e_R \\ E_R \end{pmatrix} \tag{D.55}$$

where now the top-right entry is non-zero and therefore a valid spectrum of charged-lepton masses is possible, unlike before.

Unlike the usual low-scale PS setup, as described in Section 4.2.2, the neutral lepton mass mixing matrix is related to a charged lepton mass mixing matrix and a viable neutrino mass spectrum may not be possible whilst simultaneously generating a viable charged-lepton mass spectrum. As in Appendix D.0.4 we analyse all possible hierarchies of parameters in the two mass matrices in order to establish whether a viable charged-lepton and neutrino mass spectrum can be simultaneously generated for the SM-like states for low scales of PS breaking.

In the scenario where $\mu_{\Psi_3}$ is the dominant block in each mass matrix, there are multiple different possible neutrino mass regimes depending on the hierarchy between the non-dominant parameters.

Firstly if $|\mu_{\Psi_3}| > |m_u| > |\frac{(y^L_{\Psi_3} v_L)^2}{\mu_{\Psi_3}}, \frac{(y^R_{\Psi_3} v_R)^2}{\mu_{\Psi_3}}|$ is satisfied the mass states are given at first order by

$$\begin{aligned} m_1 &\simeq \mu_\Psi & \nu_{1,2} &\simeq N^c_R \\ m_{2,3} &\simeq m_u & \nu_{3,4} &\simeq \frac{1}{\sqrt{2}}\nu_L \pm \frac{1}{\sqrt{2}}\nu^c_R \end{aligned} \tag{D.56}$$

and therefore this hierarchy is ruled out as the light neutrinos would be pseudo-Dirac with masses comparable to the up-quark sector.

If instead $|\mu_{\Psi_3}| > |\frac{(y^R_{\Psi_3} v_R)^2}{\mu_{\Psi_3}}| > |m_u|$ is satisfied the mass spectrum is now given by

$$\begin{aligned} m_1 &\simeq \mu_{\Psi_3} & \nu_{1,2} &\simeq N^c_R \\ m_2 &\simeq \frac{(y^R_{\Psi_3})^2 v_R^2}{\mu_{\Psi_3}} & \nu_2 &\simeq \nu^c_R \\ m_3 &\simeq \left| \frac{1}{v_R^2}\left(\frac{m_u}{y^R_{\Psi_3}}\right)^2 \mu_{\Psi_3} - \frac{2v_L}{v_R}\frac{y^L_{\Psi_3} m_u}{y^R_{\Psi_3}} \right| & \nu_3 &\simeq \nu_L \end{aligned} \tag{D.57}$$

which is rather interesting as the lightest mass state contains a term linearly (rather than inversely) proportional to the dominant term in the seesaw but is still small due to the hierarchy in the non-dominant parameters. The SM charged lepton has a mass given by

$$m_\ell \simeq m_d - v_L v_R \frac{y^L_{\Psi_3} y^R_{\Psi_3}}{\mu_{\Psi_3}} \tag{D.58}$$

by diagonalising Eq. (D.55). These equations can be solved for $y^L_{\Psi_3} v_L$ and $y^R_{\Psi_3} v_R$ as a function of $\mu_{\Psi_3}$ for the required lepton masses. In the case of the third generation where $m_b \simeq 4.2$ GeV, $m_t \simeq 173$ GeV, $m_\tau \simeq 1.7$ GeV and setting $m_\nu \simeq 10^{-10}$ GeV leads to

$$\frac{(y^L_{\Psi_3} v_L)^2}{\mu_{\Psi_3}} \simeq 10^{-14}\text{ GeV} \qquad \text{and} \qquad \frac{(y^R_{\Psi_3} v_R)^2}{\mu_{\Psi_3}} \simeq 10^{14}\text{ GeV} \tag{D.59}$$

which implies that $\mu_{\Psi_3} > 10^{14}$ GeV by the initial seesaw assumption, therefore requiring both a viable charged-lepton and neutrino mass spectrum with $\mu_{\Psi_3}$ dominant is only possible for high scale PS breaking scenarios. The final possible hierarchy where $|\mu_{\Psi_3}| > |(y^L_{\Psi_3} v_L)^2/\mu_{\Psi_3}| > |m_u|$ is also unviable for similar arguments.

The alternative scenario where $|y^R_{\Psi_3} v_R|$ is the dominant term in the mass matrix recovers the usual inverse/linear seesaw

$$\begin{aligned} m_{1,2} &\simeq y^R_{\Psi_3} v_R & \nu_{1,2} &\simeq \frac{1}{\sqrt{2}} N^c_R \pm \frac{1}{\sqrt{2}} \nu^c_R \\ m_3 &\simeq \left| \frac{1}{v_R^2} \left( \frac{m_u}{y^R_{\Psi_3}} \right)^2 \mu_{\Psi_3} - \frac{2 v_L}{v_R} \frac{y^L_{\Psi_3} m_u}{y^R_{\Psi_3}} \right| & \nu_3 &\simeq \nu_L. \end{aligned} \tag{D.60}$$

and the lightest charged-lepton mass is given by

$$m_\ell \simeq v_L y^L_{\Psi_3} - \frac{1}{v_R} \frac{m_d \mu_{\Psi_3}}{y^R_{\Psi_3}}. \tag{D.61}$$

The lightest neutrino state is now suppressed by the scale $y^R_{\Psi_3} v_R$ as usual, it is quite interesting that the lightest neutrinos in Eqs. (D.57) and (D.60) have identical masses for completely different hierarchies of parameters.

For three generations of each fermion multiplet the light mass blocks are given by

$$m_\nu \simeq \frac{1}{v_R^2} m_u [(Y^R_{\Psi_3})^T]^{-1} \mu_{\Psi_3} (Y^R_{\Psi_3})^{-1} m_u^T - \frac{v_L}{v_R} m_u [(Y^R_{\Psi_3})^T]^{-1} (Y^L_{\Psi_3})^T - \frac{v_L}{v_R} Y^L_{\Psi_3} (Y^R_{\Psi_3})^{-1} m_u^T \tag{D.62}$$

for the neutrinos and

$$m_\ell \simeq Y^L_{\Psi_3} v_L - \frac{1}{v_R} m_d (Y^R_{\Psi_3})^{-1} \mu_{\Psi_3} \tag{D.63}$$

for the charged leptons.

For a given choice of $v_R Y^R_{\Psi_3}$, the unknown matrices $v_L Y^L_{\Psi_3}$ and $\mu_{\Psi_3}$ are fixed by solving the above equations. Due to the complexity of solving the above matrix equations we solve Eqs. (D.62) and (D.63) numerically where we assume a normal ordering for the light neutrino masses and fix the lightest neutrino mass to

$$m_{\nu_1} = 10^{-10} \text{ GeV}. \tag{D.64}$$

The left plot in Fig. D.2 plots the Frobenius norm of the required matrix $\mu_{\Psi_3}$ (in blue) required in order to solve the two above equations for different choices of $v_R Y^R_{\Psi_3}$. The orange line corresponds to $\|\mu_{\Psi_3}\|_F = \|v_R Y^R_{\Psi_3}\|_F$ and for any choice of $v_R Y^R_{\Psi_3}$ the required size of $\mu_{\Psi_3}$ in order to solve the above equations is larger, destroying the hierarchy

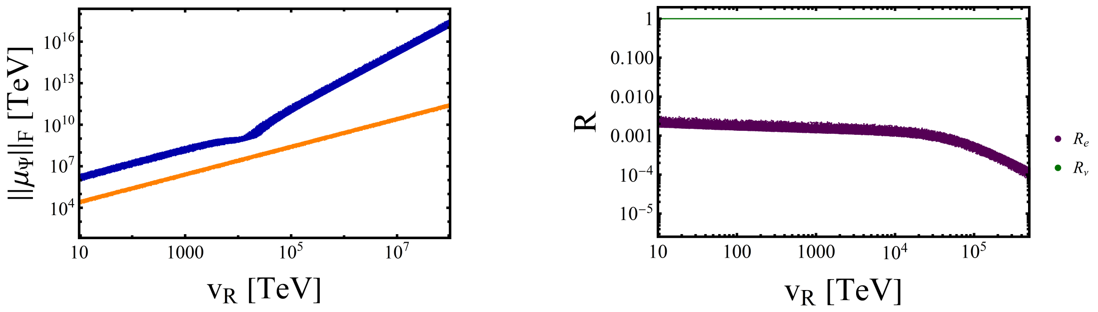


FIGURE D.2: Plot of the Frobenius norm of $\mu_{\Psi_3}$ generated by solving Eqs. (D.54) and (D.55) **(left)** as a function of the scale $v_R$ with a random scan over $Y^R_{\Psi_3}$ with degenerate singular values and a plot of $R_{\nu/e}$ **(right)**, defined in Eq. (D.65), as a function of the same scale. The orange line in the left plot corresponds to $\|\mu_{\Psi_3}\|_F = \|Y^R_{\Psi_3}\|_F v_R$ and therefore at all scales considered the required size of $\mu_{\Psi_3}$ spoils the assumed hierarchy of parameters in order to achieve an inverse/linear seesaw. Though $R_\nu \simeq 1$, the resultant charged-lepton masses after diagonalisation are signficantly differnet to their input values and therefore we find that additional triplets to the usual PS fermions alone are not sufficient to lead to a viable mass spectrum for all SM fermions (due to the quark-lepton symmetry assumed).

assumed in deriving Eqs. (D.62) and (D.63). The right plot of Fig. D.2 plots

$$R_{\nu/e} = \prod_i \frac{m_i}{m_i^{\text{input}}} \tag{D.65}$$

where $m_i$ corresponds to the numerically computed mass for the i-th generation of lepton and $m_i^{\text{input}}$ corresponds to the experimental values for the masses inputted (run up to the appropriate scale). The charged lepton masses which result are significantly departed from their SM values whilst the neutrino values are well predicted, this is a coincidence due to the light neutrino mass block having the same formula regardless of the hierarchy[5] between $\|\mu_{\Psi_3}\|$ and $\|Y^R_{\Psi_3} v_R\|$ as can be seen in Eqs. (D.57) and (D.60).

The light, charged-lepton mass block however is different depending on the hierarchy and we therefore find that due to the SM parameters $m_u$ and $m_d$ entering Eqs. (D.54) and (D.55) as well as requiring viable correct charged-lepton and neutrino masses upon diagonalisation is not possible for low seesaw scales (for the entries of $Y^R_{\Psi_3} v_R$ which we scanned over). Though unlikely, it may be possible that special textures within $Y^R_{\Psi_3} v_R$ could lead to valid charged-lepton and neutrino masses for the appropriate hierarchy of block matrices. Therefore the addition of triplets to the usual PS multiplets will in general require additional physics, in [213] for example an additional fermionic singlet $S_L$ was introduced and a viable mass spectrum for the leptons was recovered. The addition

[5] $\|Y^R_{\Psi_3} v_R\| > \|m_u\|$ is always satisfied in our scan.

of both an $SU(2)_L$ and $SU(2)_R$ triplet was found to lead to an unviable mass spectrum for the scalars $\chi_L$ and $\chi_R$, if more exotic scalars were introduced such that all mass terms in the Yukawa sector were generated, a viable mass spectrum would likely be generated for a specific hierarchy of parameters which may or may not lead to a chiral suppression of the $X_\mu$ mass limits as with the bi-doublet. In this case however the neutrino mass matrix would not be given by an inverse/linear seesaw and would be similar to Eq. (4.82) with additional entries.

# Appendix E

# Running of the Gauge and Yukawa couplings

In order to estimate the running of the relevant SM parameters up to the potential scale of PS breaking we solve the simultaneous differential equation

$$\mu \frac{dx}{d\mu} = \frac{1}{(4\pi)^2}\beta_x^{(1)} + \dots \tag{E.1}$$

where for simplicity we restrict ourselves to the one-loop renormalisation group equations. We make two reasonable assumptions on the running of each parameter: the exotic PS particle content does not significantly affect the running of the SM parameters below the scale of PS breaking we are interested in (due to their masses) and secondly as a simplifying assumption, we only include the contribution from the top-quark Yukawa coupling and gauge couplings in the evaluation of all relevant parameters due to its dominant role.

The beta functions $\beta_x^{(i)}$ have been extensively studied for the SM [245–248], at one-loop the beta functions which are non-zero when only the gauge and top-quark couplings are included[1] are

$$\begin{aligned}
\beta_{g_i}^{(1)} &= b_i \big[g_i(\mu)\big]^3 \\
\beta_{y_{d,i}}^{(1)} &= y_{d,i}(\mu)\left(a_i \big[y_{u,3}(\mu)\big]^2 - \left\{\frac{1}{4}\big[g_1(\mu)\big]^2 + \frac{9}{4}\big[g_2(\mu)\big]^2 + 8\big[g_3(\mu)\big]^2\right\}\right)
\end{aligned}$$

[1] Additionally as in [246], terms smaller than $\mathcal{O}(10^{-3})$ in $\beta_x/x$ were approximated to zero for simplicity.

| | $\mu = m_Z$ |
|---|---|
| $g_1$ | $0.461425^{+0.000044}_{-0.000043}$ |
| $g_2$ | $0.65184^{+0.00018}_{-0.00017}$ |
| $g_3$ | $1.2143^{+0.000044}_{-0.000043}$ |

| | $\mu = m_Z$ |
|---|---|
| $y_u$ | $7.4^{+1.5}_{-3.0} \times 10^{-6}$ |
| $y_c$ | $3.6^{+0.11}_{-0.11} \times 10^{-3}$ |
| $y_t$ | $0.9861^{+0.0086}_{-0.0087}$ |
| $y_d$ | $1.58^{+0.23}_{-0.10} \times 10^{-5}$ |
| $y_s$ | $3.12^{+0.17}_{-0.16} \times 10^{-4}$ |
| $y_b$ | $1.639^{+0.015}_{-0.015} \times 10^{-2}$ |
| $\theta^q_{12}$ | $0.22735^{+0.00072}_{-0.00071}$ |
| $\theta^q_{23}$ | $4.208^{+0.064}_{-0.064} \times 10^{-2}$ |
| $\theta^q_{13}$ | $3.64^{+0.13}_{-0.13} \times 10^{-3}$ |
| $\delta_{\text{CKM}}$ | $1.208^{+0.054}_{-0.054}$ |

| | $\mu = m_Z$ |
|---|---|
| $y_e$ | $2.79^{+0.000015}_{-0.000016} \times 10^{-6}$ |
| $y_\mu$ | $5.90^{+0.000019}_{-0.000018} \times 10^{-4}$ |
| $y_\tau$ | $1.00^{+0.00090}_{-0.00091} \times 10^{-2}$ |
| $\theta^\ell_{12}$ | $0.59^{+0.0136}_{-0.0133}$ |
| $\theta^\ell_{23}$ | $0.84^{+0.0192}_{-0.0332}$ |
| $\theta^\ell_{13}$ | $0.15^{+0.0023}_{-0.0023}$ |
| $\delta_{\text{PMNS}}$ | $3.87^{+0.6632}_{-0.4887}$ |
| $\Delta m^2_{21}/\text{eV}^2$ | $7.39^{+0.21}_{-0.20} \times 10^{-5}$ |
| $\Delta m^2_{31}/\text{eV}^2$ | $2.523^{+0.032}_{-0.030} \times 10^{-3}$ |

TABLE E.1: Values used for the SM parameters at $\mu = m_Z$ in the $\overline{\text{MS}}$ scheme taken from Table 1 of [243] for the gauge couplings, quark and charged-lepton parameters with their respective $1\sigma$ uncertainty. The neutrino parameters with their $1\sigma$ uncertainty are taken from [192], which are not measured at $\mu = m_Z$, however as the PMNS parameters do not significantly run at low energies [244] (in the SM) we take these values to be valid at this scale.

$$
\begin{aligned}
\beta^{(1)}_{y_{\ell,i}} &= y_{\ell,i}(\mu)\left(3\left[y_{u,3}(\mu)\right]^2 - \frac{9}{4}\left\{\left[g_1(\mu)\right]^2 + \left[g_2(\mu)\right]^2\right\}\right)\\
\beta^{(1)}_{y_{u,i}} &= y_{u,i}(\mu)\left((3a_i - 2c_i)\left[y_{u,3}(\mu)\right]^2 - \left\{\frac{17}{20}\left[g_1(\mu)\right]^2 + \frac{9}{4}\left[g_2(\mu)\right]^2 + 8\left[g_3(\mu)\right]^2\right\}\right)\\
\beta^{(1)}_{\theta_i} &= \theta_i(\mu)\left(c_i\left[y_{u,3}(\mu)\right]^2\right).
\end{aligned}
\tag{E.2}
$$

Here $y_{d,i} = (y_d, y_s, y_b)$ and similarly for the charged-lepton and up-type Yukawa couplings, $\theta_i = (\theta_{13}, \theta_{23}, \theta_{12})$ are the CKM mixing angles and

$$
a_i = \begin{cases} 3 & i = 1,2 \\ \frac{3}{2} & i = 3 \end{cases}, \qquad b_i = \begin{cases} \frac{41}{10} & i = 1 \\ -\frac{19}{6} & i = 2 \\ -7 & i = 3 \end{cases} \quad \text{and} \quad c_i = \begin{cases} 3 & i = 1,2 \\ 0 & i = 3 \end{cases}
\tag{E.3}
$$

where the gauge coupling $g_1$ is given as it usually is in $SU(5)$ normalisation: $g_1^2 = 5/3 g_Y^2$. The beta functions (at one-loop) for the CP-violating CKM parameter $\delta_{CKM}$ and all the parameters related to the neutrino sector are zero for our stated assumptions and therefore will not run. The parameters in Eq. (E.2) are run up from $\mu = m_Z$ with initial values taken from [243] which utilised the Mathematica package RunDec to evolve the QCD parameters up to $m_Z \simeq 91.19$ GeV in the $\overline{\text{MS}}$ scheme and are summarised in

Table E.1.

The results of Eqs. (E.1) and (E.2) are shown in Fig. E.1 for the Yukawa couplings, gauge couplings and relevant CKM parameters run from $\mu = m_Z$ up to $\mu = 1000$ TeV. The points on the left plots correspond to the results obtained using RunDec at two-loops [243] at 1, 3 and 10 TeV in the SM. The plots on the right correspond to the ratio of the running parameter to its initial value at $\mu = m_Z$. The quark Yukawa couplings all significantly decrease as the energy scale increases whereas the charged-lepton Yukawa modestly increase. Due to the approximations we assume in Eq. (E.2), the ratios $\beta_x^{(1)}/x$ are equal for the first and second generations of quark Yukawas, all three generations of charged-lepton Yukawas as well as between $\theta_{13}$ and $\theta_{23}$.

As is often chosen, we work in a basis where the Yukawa coupling matrix for the up-type quarks and charged leptons is diagonal. Therefore the running of each relevant Yukawa coupling matrix, for the SM fermions, at a given energy scale is given by

$$
\begin{aligned}
Y_u(\mu) &= \mathrm{diag}\big[y_u(\mu),\, y_c(\mu),\, y_t(\mu)\big] \\
Y_d(\mu) &= V_{\mathrm{CKM}}^{\dagger}\big[\theta_{12}^q(\mu),\, \theta_{23}^q(\mu),\, \theta_{13}^q(\mu), \delta_{\mathrm{CKM}}(\mu)\big]\, \mathrm{diag}\big[y_d(\mu),\, y_s(\mu),\, y_b(\mu)\big] \\
Y_\ell(\mu) &= \mathrm{diag}\big[y_e(\mu),\, y_\mu(\mu),\, y_\tau(\mu)\big]
\end{aligned}
\tag{E.4}
$$

where we use the numerical results from solving Eqs. (E.1) and (E.2) using Table E.1 as the initial values.

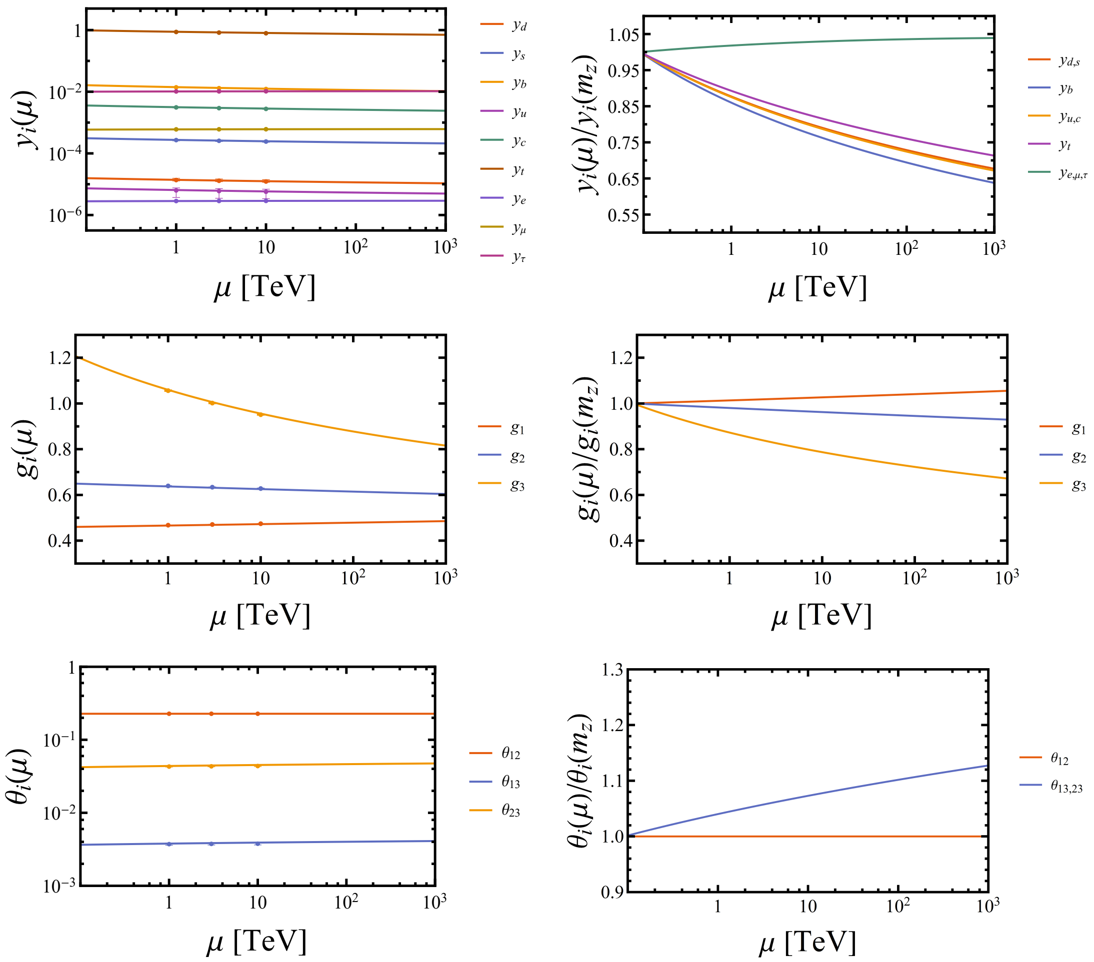


Figure E.1: Plot of the numerical running of various SM parameters **(left)** (run up from $\mu = m_Z$) at one-loop as a function of the energy scale $\mu$. The points correspond to values taken from [243] at 1, 3 and 10 TeV with their respective $1\sigma$ uncertainties, where the running was performed to two-loops to demonstrate the accuracy of our one-loop approximations. Also shown are the ratios **(right)** of the run parameter against its initial value at $\mu = m_Z$.

# Bibliography


[1] M. J. Dolan, T. P. Dutka and R. R. Volkas, *Dirac-Phase Thermal Leptogenesis in the extended Type-I Seesaw Model*, *JCAP* **1806** (2018) 012, [1802.08373].

[2] M. J. Dolan, T. P. Dutka and R. R. Volkas, *Low-scale leptogenesis with minimal lepton flavor violation*, *Phys. Rev. D* **99** (2019) 123508, [1812.11964].

[3] M. J. Dolan, T. P. Dutka and R. R. Volkas, *Lowering the scale of Pati-Salam breaking through seesaw mixing*, [2012.05976].

[4] A. Einstein, *The Foundation of the General Theory of Relativity*, *Annalen Phys.* **49** (1916) 769–822.

[5] S. Glashow, *Partial Symmetries of Weak Interactions*, *Nucl. Phys.* **22** (1961) 579–588.

[6] A. Salam and J. C. Ward, *Electromagnetic and weak interactions*, *Phys. Lett.* **13** (1964) 168–171.

[7] S. Weinberg, *A Model of Leptons*, *Phys. Rev. Lett.* **19** (1967) 1264–1266.

[8] A. Salam, *Weak and Electromagnetic Interactions*, *Conf. Proc. C* **680519** (1968) 367–377.

[9] S. Glashow, J. Iliopoulos and L. Maiani, *Weak Interactions with Lepton-Hadron Symmetry*, *Phys. Rev. D* **2** (1970) 1285–1292.

[10] G. 't Hooft, *Renormalizable Lagrangians for Massive Yang-Mills Fields*, *Nucl. Phys. B* **35** (1971) 167–188.

[11] D. J. Gross and F. Wilczek, *Ultraviolet Behavior of Nonabelian Gauge Theories*, *Phys. Rev. Lett.* **30** (1973) 1343–1346.

[12] H. Politzer, *Reliable Perturbative Results for Strong Interactions?*, *Phys. Rev. Lett.* **30** (1973) 1346–1349.

[13] M. W. Grünewald, *Experimental precision tests for the electroweak standard model.*, in *Physics and Methods. Theory and Experiments* (H. Schopper, ed.), Volume 21A of *Landolt-Boernstein - Group I Elementary Particles, Nuclei and Atoms*, Chapter 6. Springer-Verlag, 2008. [0710.2838].

[14] Particle Data Group collaboration, P. Zyla et al., *Review of Particle Physics*, *PTEP* **2020** (2020) 083C01.

[15] N. Cabibbo, *Unitary Symmetry and Leptonic Decays*, *Phys. Rev. Lett.* **10** (1963) 531–533.

[16] M. Kobayashi and T. Maskawa, *CP Violation in the Renormalizable Theory of Weak Interaction*, *Prog. Theor. Phys.* **49** (1973) 652–657.

[17] B. Pontecorvo, *Inverse beta processes and nonconservation of lepton charge*, *Sov. Phys. JETP* **7** (1957) 172-173 .

[18] Z. Maki, M. Nakagawa and S. Sakata, *Remarks on the unified model of elementary particles*, *Prog. Theor. Phys.* **28** (1962) 870–880.

[19] G. Bellini, L. Ludhova, G. Ranucci and F. Villante, *Neutrino oscillations*, *Adv. High Energy Phys.* **2014** (2014) 191960, [1310.7858].

[20] Kamiokande-II collaboration, K. Hirata et al., *Observation of a small atmospheric muon-neutrino / electron-neutrino ratio in Kamiokande*, *Phys. Lett. B* **280** (1992) 146–152.

[21] R. Becker-Szendy et al., *Neutrino measurements with the IMB detector*, *Nucl. Phys. B Proc. Suppl.* **38** (1995) 331–336.

[22] Super-Kamiokande collaboration, Y. Fukuda et al., *Evidence for oscillation of atmospheric neutrinos*, *Phys. Rev. Lett.* **81** (1998) 1562–1567, [hep-ex/9807003].

[23] J. Davis, Raymond, D. S. Harmer and K. C. Hoffman, *Search for neutrinos from the sun*, *Phys. Rev. Lett.* **20** (1968) 1205–1209.

[24] B. Cleveland, T. Daily, J. Davis, Raymond, J. R. Distel, K. Lande, C. Lee et al., *Measurement of the solar electron neutrino flux with the Homestake chlorine detector*, *Astrophys. J.* **496** (1998) 505–526.

[25] GALLEX collaboration, W. Hampel et al., *GALLEX solar neutrino observations: Results for GALLEX IV*, *Phys. Lett. B* **447** (1999) 127–133.

[26] SAGE collaboration, J. Abdurashitov et al., *Measurement of the solar neutrino capture rate with gallium metal*, *Phys. Rev. C* **60** (1999) 055801, [astro-ph/9907113].

[27] SNO collaboration, Q. Ahmad et al., *Measurement of the rate of $\nu_e + d \to p + p + e^-$ interactions produced by $^8B$ solar neutrinos at the Sudbury Neutrino Observatory*, *Phys. Rev. Lett.* **87** (2001) 071301, [nucl-ex/0106015].

[28] SNO collaboration, Q. Ahmad et al., *Direct evidence for neutrino flavor transformation from neutral current interactions in the Sudbury Neutrino Observatory*, *Phys. Rev. Lett.* **89** (2002) 011301, [nucl-ex/0204008].

[29] K2K collaboration, E. Aliu et al., *Evidence for muon neutrino oscillation in an accelerator-based experiment*, *Phys. Rev. Lett.* **94** (2005) 081802, [hep-ex/0411038].

[30] MINOS collaboration, D. Michael et al., *Observation of muon neutrino disappearance with the MINOS detectors and the NuMI neutrino beam*, *Phys. Rev. Lett.* **97** (2006) 191801, [hep-ex/0607088].

[31] Double Chooz collaboration, Y. Abe et al., *Indication of Reactor $\bar{\nu}_e$ Disappearance in the Double Chooz Experiment*, *Phys. Rev. Lett.* **108** (2012) 131801, [1112.6353].

[32] Daya Bay collaboration, F. An et al., *Observation of electron-antineutrino disappearance at Daya Bay*, *Phys. Rev. Lett.* **108** (2012) 171803, [1203.1669].

[33] RENO collaboration, J. Ahn et al., *Observation of Reactor Electron Antineutrino Disappearance in the RENO Experiment*, *Phys. Rev. Lett.* **108** (2012) 191802, [1204.0626].

[34] I. Esteban, M. Gonzalez-Garcia, M. Maltoni, T. Schwetz and A. Zhou, *The fate of hints: updated global analysis of three-flavor neutrino oscillations*, *JHEP* **09** (2020) 178, [2007.14792].

[35] J. Schechter and J. Valle, *Neutrinoless Double beta Decay in $SU(2) \times U(1)$ Theories*, *Phys. Rev. D* **25** (1982) 2951.

[36] PLANCK collaboration, N. Aghanim et al., *Planck 2018 results. VI. Cosmological parameters*, *Astron. Astrophys.* **641** (2020) A6, [1807.06209].

[37] S. Roy Choudhury and S. Choubey, *Updated Bounds on Sum of Neutrino Masses in Various Cosmological Scenarios*, *JCAP* **09** (2018) 017, [1806.10832].

[38] KATRIN collaboration, M. Aker et al., *Improved Upper Limit on the Neutrino Mass from a Direct Kinematic Method by KATRIN*, *Phys. Rev. Lett.* **123** (2019) 221802, [1909.06048].

[39] KATRIN collaboration, M. Aker et al., *First operation of the KATRIN experiment with tritium*, *Eur. Phys. J. C* **80** (2020) 264, [1909.06069].

[40] P. Minkowski, *$\mu \to e\gamma$ at a Rate of One Out of $10^9$ Muon Decays?*, *Phys. Lett.* **67B** (1977) 421–428.

[41] T. Yanagida, *Horizontal Symmetry and Masses of Neutrinos*, *Progress of Theoretical Physics* **64** (09, 1980) 1103–1105.

[42] M. Gell-Mann, P. Ramond and R. Slansky, *Complex Spinors and Unified Theories*, *Conf. Proc.* **C790927** (1979) 315–321, [1306.4669].

[43] R. N. Mohapatra and G. Senjanovic, *Neutrino Mass and Spontaneous Parity Violation*, *Phys. Rev. Lett.* **44** (1980) 912.

[44] S. L. Glashow, *The Future of Elementary Particle Physics*, *NATO Sci. Ser. B* **61** (1980) 687.

[45] G. 't Hooft, *Naturalness, chiral symmetry, and spontaneous chiral symmetry breaking*, *NATO Sci. Ser. B* **59** (1980) 135–157.

[46] M. Magg and C. Wetterich, *Neutrino Mass Problem and Gauge Hierarchy*, *Phys. Lett. B* **94** (1980) 61–64.

[47] J. Schechter and J. Valle, *Neutrino Masses in $SU(2) \times U(1)$ Theories*, *Phys. Rev. D* **22** (1980) 2227.

[48] T. Cheng and L.-F. Li, *Neutrino Masses, Mixings and Oscillations in $SU(2) \times U(1)$ Models of Electroweak Interactions*, *Phys. Rev. D* **22** (1980) 2860.

[49] G. Lazarides, Q. Shafi and C. Wetterich, *Proton Lifetime and Fermion Masses in an SO(10) Model*, *Nucl. Phys. B* **181** (1981) 287–300.

[50] R. N. Mohapatra and G. Senjanovic, *Neutrino Masses and Mixings in Gauge Models with Spontaneous Parity Violation*, *Phys. Rev.* **D23** (1981) 165.

[51] R. Foot, H. Lew, X. He and G. C. Joshi, *Seesaw Neutrino Masses Induced by a Triplet of Leptons*, *Z. Phys. C* **44** (1989) 441.

[52] P. A. Dirac, *The quantum theory of the electron*, *Proc. Roy. Soc. Lond. A* **117** (1928) 610–624.

[53] P. Dirac, *A Theory of Electrons and Protons*, *Proc. Roy. Soc. Lond. A* **126** (1930) 360–365.

[54] C. Anderson, *The Positive Electron*, *Phys. Rev.* **43** (1933) 491–494.

[55] Y. Y. Wong, *Analytical treatment of neutrino asymmetry equilibration from flavor oscillations in the early universe*, *Phys. Rev. D* **66** (2002) 025015, [hep-ph/0203180].

[56] K. N. Abazajian, J. F. Beacom and N. F. Bell, *Stringent Constraints on Cosmological Neutrino Antineutrino Asymmetries from Synchronized Flavor Transformation*, *Phys. Rev. D* **66** (2002) 013008, [astro-ph/0203442].

[57] Z. Zeng, S. Yeung and M.-C. Chu, *Effects of neutrino mass and asymmetry on cosmological structure formation*, *JCAP* **03** (2019) 015, [1808.00357].

[58] C. J. Copi, D. N. Schramm and M. S. Turner, *Big bang nucleosynthesis and the baryon density of the universe*, *Science* **267** (1995) 192–199, [astro-ph/9407006].

[59] E. W. Kolb and M. S. Turner, *The Early Universe*, Chapter 3, pp. 78–79. Frontiers in Physics. Westview Press, Boulder, CO, 1990. 10.1201/9780429492860.

[60] WMAP collaboration, G. Hinshaw et al., *Nine-Year Wilkinson Microwave Anisotropy Probe (WMAP) Observations: Cosmological Parameter Results*, *Astrophys. J. Suppl.* **208** (2013) 19, [1212.5226].

[61] A. H. Guth, *The Inflationary Universe: A Possible Solution to the Horizon and Flatness Problems*, *Adv. Ser. Astrophys. Cosmol.* **3** (1987) 139–148.

[62] A. D. Linde, *A New Inflationary Universe Scenario: A Possible Solution of the Horizon, Flatness, Homogeneity, Isotropy and Primordial Monopole Problems*, *Adv. Ser. Astrophys. Cosmol.* **3** (1987) 149–153.

[63] A. Sakharov, *Violation of CP Invariance, C asymmetry, and baryon asymmetry of the universe*, *Sov. Phys. Usp.* **34** (1991) 392–393.

[64] F. R. Klinkhamer and N. Manton, *A Saddle Point Solution in the Weinberg-Salam Theory*, *Phys. Rev. D* **30** (1984) 2212.

[65] G. 't Hooft, *Symmetry Breaking Through Bell-Jackiw Anomalies*, *Phys. Rev. Lett.* **37** (1976) 8–11.

[66] M. Dine and A. Kusenko, *The Origin of the matter - antimatter asymmetry*, *Rev. Mod. Phys.* **76** (2003) 1, [hep-ph/0303065].

[67] K. Kajantie, M. Laine, K. Rummukainen and M. E. Shaposhnikov, *Is there a hot electroweak phase transition at* $m_H \gtrsim m_W$*?*, *Phys. Rev. Lett.* **77** (1996) 2887–2890, [hep-ph/9605288].

[68] K. Kajantie, M. Laine, K. Rummukainen and M. E. Shaposhnikov, *A Nonperturbative analysis of the finite T phase transition in* $SU(2) \times U(1)$ *electroweak theory*, *Nucl. Phys. B* **493** (1997) 413–438, [hep-lat/9612006].

[69] F. Karsch, T. Neuhaus, A. Patkos and J. Rank, *Critical Higgs mass and temperature dependence of gauge boson masses in the* $SU(2)$ *gauge Higgs model*, *Nucl. Phys. B Proc. Suppl.* **53** (1997) 623–625, [hep-lat/9608087].

[70] M. Gurtler, E.-M. Ilgenfritz and A. Schiller, *Where the electroweak phase transition ends*, *Phys. Rev. D* **56** (1997) 3888–3895, [hep-lat/9704013].

[71] K. Kajantie, M. Laine, J. Peisa, K. Rummukainen and M. E. Shaposhnikov, *The Electroweak phase transition in a magnetic field*, *Nucl. Phys. B* **544** (1999) 357–373, [hep-lat/9809004].

[72] F. Csikor, Z. Fodor and J. Heitger, *Endpoint of the hot electroweak phase transition*, *Phys. Rev. Lett.* **82** (1999) 21–24, [hep-ph/9809291].

[73] M. Shaposhnikov, *Baryon Asymmetry of the Universe in Standard Electroweak Theory*, *Nucl. Phys. B* **287** (1987) 757–775.

[74] J. Bell and R. Jackiw, *A PCAC puzzle: $\pi^0 \to \gamma\gamma$ in the $\sigma$ model*, *Nuovo Cim. A* **60** (1969) 47–61.

[75] S. L. Adler, *Axial vector vertex in spinor electrodynamics*, *Phys. Rev.* **177** (1969) 2426–2438.

[76] S. Coleman, *Aspects of Symmetry: Selected Erice Lectures*, Chapter 5. Cambridge University Press, 1985. 10.1017/CBO9780511565045.

[77] P. B. Arnold and L. D. McLerran, *Sphalerons, Small Fluctuations and Baryon Number Violation in Electroweak Theory*, *Phys. Rev. D* **36** (1987) 581.

[78] A. Bochkarev and M. Shaposhnikov, *Electroweak Production of Baryon Asymmetry and Upper Bounds on the Higgs and Top Masses*, *Mod. Phys. Lett. A* **2** (1987) 417.

[79] P. B. Arnold and L. D. McLerran, *The Sphaleron Strikes Back*, *Phys. Rev. D* **37** (1988) 1020.

[80] S. Khlebnikov and M. Shaposhnikov, *The Statistical Theory of Anomalous Fermion Number Nonconservation*, *Nucl. Phys. B* **308** (1988) 885–912.

[81] E. Mottola and A. Wipf, *Unsuppressed fermion-number violation at high temperature: An $O(3)$ model*, *Phys. Rev. D* **39** (Jan, 1989) 588–602.

[82] J. A. Harvey and M. S. Turner, *Cosmological baryon and lepton number in the presence of electroweak fermion number violation*, *Phys. Rev.* **D42** (1990) 3344–3349.

[83] M. Fukugita and T. Yanagida, *Baryogenesis Without Grand Unification*, *Phys. Lett.* **B174** (1986) 45–47.

[84] A. Pilaftsis and T. E. J. Underwood, *Resonant leptogenesis*, *Nucl. Phys.* **B692** (2004) 303–345, [hep-ph/0309342].

[85] A. Pilaftsis and T. E. J. Underwood, *Electroweak-scale resonant leptogenesis*, *Phys. Rev.* **D72** (2005) 113001, [hep-ph/0506107].

[86] G. Engelhard, Y. Grossman, E. Nardi and Y. Nir, *The Importance of $N_2$ leptogenesis*, *Phys. Rev. Lett.* **99** (2007) 081802, [hep-ph/0612187].

[87] E. W. Kolb and S. Wolfram, *Baryon Number Generation in the Early Universe*, *Nucl. Phys. B* **172** (1980) 224.

[88] A. Abada, S. Davidson, A. Ibarra, F.-X. Josse-Michaux, M. Losada and A. Riotto, *Flavour Matters in Leptogenesis*, *JHEP* **09** (2006) 010, [hep-ph/0605281].

[89] S. Davidson and A. Ibarra, *A Lower bound on the right-handed neutrino mass from leptogenesis*, *Phys. Lett.* **B535** (2002) 25–32, [hep-ph/0202239].

[90] W. Buchmuller, P. Di Bari and M. Plumacher, *Cosmic microwave background, matter - antimatter asymmetry and neutrino masses*, *Nucl. Phys. B* **643** (2002) 367–390, [hep-ph/0205349].

[91] W. Buchmuller, P. Di Bari and M. Plumacher, *The Neutrino mass window for baryogenesis*, *Nucl. Phys. B* **665** (2003) 445–468, [hep-ph/0302092].

[92] F. Vissani, *Do experiments suggest a hierarchy problem?*, *Phys. Rev.* **D57** (1998) 7027–7030, [hep-ph/9709409].

[93] J. D. Clarke, R. Foot and R. R. Volkas, *Electroweak naturalness in the three-flavor type I seesaw model and implications for leptogenesis*, *Phys. Rev.* **D91** (2015) 073009, [1502.01352].

[94] M. Khlopov and A. D. Linde, *Is It Easy to Save the Gravitino?*, *Phys. Lett. B* **138** (1984) 265–268.

[95] J. R. Ellis, J. E. Kim and D. V. Nanopoulos, *Cosmological Gravitino Regeneration and Decay*, *Phys. Lett. B* **145** (1984) 181–186.

[96] M. Kawasaki, K. Kohri, T. Moroi and A. Yotsuyanagi, *Big-Bang Nucleosynthesis and Gravitino*, *Phys. Rev. D* **78** (2008) 065011, [0804.3745].

[97] D. Croon, N. Fernandez, D. McKeen and G. White, *Stability, reheating and leptogenesis*, *JHEP* **06** (2019) 098, [1903.08658].

[98] J. A. Dror, T. Hiramatsu, K. Kohri, H. Murayama and G. White, *Testing the Seesaw Mechanism and Leptogenesis with Gravitational Waves*, *Phys. Rev. Lett.* **124** (2020) 041804, [1908.03227].

[99] E. K. Akhmedov, V. A. Rubakov and A. Yu. Smirnov, *Baryogenesis via neutrino oscillations*, *Phys. Rev. Lett.* **81** (1998) 1359–1362, [hep-ph/9803255].

[100] L. Boubekeur, T. Hambye and G. Senjanovic, *Low scale leptogenesis and soft supersymmetry breaking*, *Phys. Rev. Lett.* **93** (2004) 111601, [hep-ph/0404038].

[101] M. Frigerio and C. E. Yaguna, *Sterile Neutrino Dark Matter and Low Scale Leptogenesis from a Charged Scalar*, *Eur. Phys. J.* **C75** (2015) 31, [1409.0659].

[102] M. Le Dall and A. Ritz, *Leptogenesis and the Higgs Portal*, *Phys. Rev. D* **90** (2014) 096002, [1408.2498].

[103] J. D. Clarke, R. Foot and R. R. Volkas, *Natural leptogenesis and neutrino masses with two Higgs doublets*, *Phys. Rev.* **D92** (2015) 033006, [1505.05744].

[104] T. Alanne, T. Hugle, M. Platscher and K. Schmitz, *Low-scale leptogenesis assisted by a real scalar singlet*, *JCAP* **03** (2019) 037, [1812.04421].

[105] G. B. Gelmini, *Prospect for relic neutrino searches*, *Phys. Scripta T* **121** (2005) 131–136, [hep-ph/0412305].

[106] A. Ringwald, *Prospects for the direct detection of the cosmic neutrino background*, *Nucl. Phys. A* **827** (2009) 501C–506C, [0901.1529].

[107] P. Vogel, *How difficult it would be to detect cosmic neutrino background?*, *AIP Conference Proceedings* **1666** (2015) 140003.

[108] E. Akhmedov, *Relic neutrino detection through angular correlations in inverse $\beta$-decay*, *JCAP* **09** (2019) 031, [1905.10207].

[109] A. Gamba, R. E. Marshak and S. Okubo, *On a symmetry in weak interactions*, *Proceedings of the National Academy of Sciences* **45** (1959) 881–885.

[110] G. Danby, J. Gaillard, K. A. Goulianos, L. Lederman, N. B. Mistry, M. Schwartz et al., *Observation of High-Energy Neutrino Reactions and the Existence of Two Kinds of Neutrinos*, *Phys. Rev. Lett.* **9** (1962) 36–44.

[111] J. Bjorken and S. Glashow, *Elementary Particles and* $SU(4)$, *Phys. Lett.* **11** (1964) 255–257.

[112] H. Georgi and S. Glashow, *Unity of All Elementary Particle Forces*, *Phys. Rev. Lett.* **32** (1974) 438–441.

[113] H. Georgi, *The State of the Art—Gauge Theories*, *AIP Conf. Proc.* **23** (1975) 575–582.

[114] H. Fritzsch and P. Minkowski, *Unified Interactions of Leptons and Hadrons*, *Annals Phys.* **93** (1975) 193–266.

[115] J. C. Pati and A. Salam, *Lepton Number as the Fourth Color*, *Phys. Rev.* **D10** (1974) 275–289.

[116] J. C. Pati, A. Salam and U. Sarkar, $\Delta B = -\Delta L$, *neutron* $\to e^- \pi^+$, $e^- K^+$, $\mu^- \pi^+$ *and* $\mu^- K^+$ *decay modes in* $SU(2)_L \times SU(2)_R \times SU(4)^{col}$ *or* $SO(10)$, *Physics Letters B* **133** (1983) 330–336.

[117] BaBar collaboration, J. Lees et al., *Measurement of an Excess of* $\bar{B} \to D^{(*)}\tau^-\bar{\nu}_\tau$ *Decays and Implications for Charged Higgs Bosons*, *Phys. Rev. D* **88** (2013) 072012, [1303.0571].

[118] Belle collaboration, S. Hirose et al., *Measurement of the* $\tau$ *lepton polarization and* $R(D^*)$ *in the decay* $\bar{B} \to D^*\tau^-\bar{\nu}_\tau$, *Phys. Rev. Lett.* **118** (2017) 211801, [1612.00529].

[119] LHCb collaboration, R. Aaij et al., *Test of Lepton Flavor Universality by the measurement of the* $B^0 \to D^{*-}\tau^+\nu_\tau$ *branching fraction using three-prong* $\tau$ *decays*, *Phys. Rev. D* **97** (2018) 072013, [1711.02505].

[120] LHCb collaboration, R. Aaij et al., *Differential branching fractions and isospin asymmetries of* $B \to K^{(*)}\mu^+\mu^-$ *decays*, *JHEP* **06** (2014) 133, [1403.8044].

[121] J. Aebischer, W. Altmannshofer, D. Guadagnoli, M. Reboud, P. Stangl and D. M. Straub, *B-decay discrepancies after Moriond 2019*, *Eur. Phys. J. C* **80** (2020) 252, [1903.10434].

[122] R. Foot and H. Lew, *Quark - Lepton Symmetric Model*, *Phys. Rev. D* **41** (1990) 3502.

[123] R. Foot, H. Lew and R. Volkas, *Quark - lepton symmetry*, in *7th Meeting of the APS Division of Particles Fields*, pp. 1253–1255, 11, 1992, [hep-ph/9211287].

[124] H. Lew and R. Volkas, *Discrete quark - lepton symmetry need not pose a cosmological domain wall problem*, *Phys. Rev. D* **47** (1993) 1356–1369, [hep-ph/9209288].

[125] I. Esteban, M. C. Gonzalez-Garcia, M. Maltoni, I. Martinez-Soler and T. Schwetz, *Updated fit to three neutrino mixing: exploring the accelerator-reactor complementarity*, *JHEP* **01** (2017) 087, [1611.01514].

[126] S. Pascoli, S. T. Petcov and A. Riotto, *Connecting low energy leptonic CP-violation to leptogenesis*, *Phys. Rev.* **D75** (2007) 083511, [hep-ph/0609125].

[127] S. Pascoli, S. T. Petcov and A. Riotto, *Leptogenesis and Low Energy CP Violation in Neutrino Physics*, *Nucl. Phys.* **B774** (2007) 1–52, [hep-ph/0611338].

[128] A. Anisimov, S. Blanchet and P. Di Bari, *Viability of Dirac phase leptogenesis*, *JCAP* **0804** (2008) 033, [0707.3024].

[129] K. Moffat, S. Pascoli, S. T. Petcov and J. Turner, *Leptogenesis from Low Energy $CP$ Violation*, *JHEP* **03** (2019) 034, [1809.08251].

[130] F. Deppisch and J. W. F. Valle, *Enhanced lepton flavor violation in the supersymmetric inverse seesaw model*, *Phys. Rev.* **D72** (2005) 036001, [hep-ph/0406040].

[131] J. A. Casas and A. Ibarra, *Oscillating neutrinos and $\mu \to e, \gamma$*, *Nucl. Phys.* **B618** (2001) 171–204, [hep-ph/0103065].

[132] M. Lindner, T. Ohlsson and G. Seidl, *Seesaw mechanisms for Dirac and Majorana neutrino masses*, *Phys. Rev.* **D65** (2002) 053014, [hep-ph/0109264].

[133] M. Aoki, N. Haba and R. Takahashi, *A model realizing inverse seesaw and resonant leptogenesis*, *PTEP* **2015** (2015) 113B03, [1506.06946].

[134] S. Blanchet, T. Hambye and F.-X. Josse-Michaux, *Reconciling leptogenesis with observable $\mu \to e\gamma$ rates*, *JHEP* **04** (2010) 023, [0912.3153].

[135] B. Adhikary, M. Chakraborty and A. Ghosal, *Flavored leptogenesis with quasidegenerate neutrinos in a broken cyclic symmetric model*, Phys. Rev. **D93** (2016) 113001, [1407.6173].

[136] P. S. Bhupal Dev, P. Millington, A. Pilaftsis and D. Teresi, *Flavour Covariant Transport Equations: an Application to Resonant Leptogenesis*, Nucl. Phys. **B886** (2014) 569–664, [1404.1003].

[137] P. S. Bhupal Dev, P. Millington, A. Pilaftsis and D. Teresi, *Kadanoff–Baym approach to flavour mixing and oscillations in resonant leptogenesis*, Nucl. Phys. **B891** (2015) 128–158, [1410.6434].

[138] J. M. Cline, K. Kainulainen and K. A. Olive, *Protecting the primordial baryon asymmetry from erasure by sphalerons*, Phys. Rev. **D49** (1994) 6394–6409, [hep-ph/9401208].

[139] F. F. Deppisch and A. Pilaftsis, *Lepton Flavour Violation and $\theta_{13}$ in Minimal Resonant Leptogenesis*, Phys. Rev. **D83** (2011) 076007, [1012.1834].

[140] D. Borah, M. K. Das and A. Mukherjee, *Common Origin of Non-zero $\theta_{13}$ and Baryon Asymmetry of the Universe in a TeV scale Seesaw Model with $A_4$ Flavour Symmetry*, [1711.02445].

[141] A. Abada and M. Lucente, *Looking for the minimal inverse seesaw realisation*, Nucl. Phys. **B885** (2014) 651–678, [1401.1507].

[142] J. G. Korner, A. Pilaftsis and K. Schilcher, *Leptonic CP asymmetries in flavor changing $H^0$ decays*, Phys. Rev. **D47** (1993) 1080–1086, [hep-ph/9301289].

[143] P. S. B. Dev and A. Pilaftsis, *Minimal Radiative Neutrino Mass Mechanism for Inverse Seesaw Models*, Phys. Rev. **D86** (2012) 113001, [1209.4051].

[144] A. Das, P. S. Bhupal Dev and N. Okada, *Direct bounds on electroweak scale pseudo-Dirac neutrinos from $\sqrt{s} = 8$ TeV LHC data*, Phys. Lett. **B735** (2014) 364–370, [1405.0177].

[145] P. S. B. Dev and R. N. Mohapatra, *TeV Scale Inverse Seesaw in $SO(10)$ and Leptonic Non-Unitarity Effects*, Phys. Rev. **D81** (2010) 013001, [0910.3924].

[146] W. Abdallah, A. Awad, S. Khalil and H. Okada, *Muon Anomalous Magnetic Moment and $\mu \to e\gamma$ in $B - L$ Model with Inverse Seesaw*, *Eur. Phys. J.* **C72** (2012) 2108, [1105.1047].

[147] E. Fernandez-Martinez, J. Hernandez-Garcia and J. Lopez-Pavon, *Global constraints on heavy neutrino mixing*, *JHEP* **08** (2016) 033, [1605.08774].

[148] MEG collaboration, A. M. Baldini et al., *Search for the lepton flavour violating decay $\mu^+ \to \mathrm{e}^+\gamma$ with the full dataset of the MEG experiment*, *Eur. Phys. J.* **C76** (2016) 434, [1605.05081].

[149] A. Ilakovac and A. Pilaftsis, *Flavor violating charged lepton decays in seesaw-type models*, *Nucl. Phys.* **B437** (1995) 491, [hep-ph/9403398].

[150] MEG II collaboration, P. W. Cattaneo, *The MEGII detector*, *JINST* **12** (2017) C06022, [1705.10224].

[151] Particle Data Group collaboration, C. Patrignani et al., *Review of Particle Physics*, *Chin. Phys. C* **40** (2016) 100001.

[152] COMET collaboration, B. E. Krikler, *An Overview of the COMET Experiment and its Recent Progress*, in *Proceedings, 17th International Workshop on Neutrino Factories and Future Neutrino Facilities (NuFact15)*, 2015, [1512.08564].

[153] F. Deppisch, T. S. Kosmas and J. W. F. Valle, *Enhanced $\mu^- - e^-$ conversion in nuclei in the inverse seesaw model*, *Nucl. Phys.* **B752** (2006) 80–92, [hep-ph/0512360].

[154] A. Abada, M. E. Krauss, W. Porod, F. Staub, A. Vicente and C. Weiland, *Lepton flavor violation in low-scale seesaw models: SUSY and non-SUSY contributions*, *JHEP* **11** (2014) 048, [1408.0138].

[155] Y. Kuno and Y. Okada, *Muon decay and physics beyond the standard model*, *Rev. Mod. Phys.* **73** (2001) 151–202, [hep-ph/9909265].

[156] M. Blennow, E. Fernandez-Martinez, J. Lopez-Pavon and J. Menendez, *Neutrinoless double beta decay in seesaw models*, *JHEP* **07** (2010) 096, [1005.3240].

[157] J. Lopez-Pavon, S. Pascoli and C.-f. Wong, *Can heavy neutrinos dominate neutrinoless double beta decay?*, *Phys. Rev.* **D87** (2013) 093007, [1209.5342].

[158] J. Lopez-Pavon, E. Molinaro and S. T. Petcov, *Radiative Corrections to Light Neutrino Masses in Low Scale Type I Seesaw Scenarios and Neutrinoless Double Beta Decay*, *JHEP* **11** (2015) 030, [1506.05296].

[159] A. Abada and T. Toma, *Electron electric dipole moment in Inverse Seesaw models*, *JHEP* **08** (2016) 079, [1605.07643].

[160] D. V. Forero, S. Morisi, M. Tortola and J. W. F. Valle, *Lepton flavor violation and non-unitary lepton mixing in low-scale type-I seesaw*, *JHEP* **09** (2011) 142, [1107.6009].

[161] A. Abada, G. Arcadi, V. Domcke and M. Lucente, *Lepton number violation as a key to low-scale leptogenesis*, *JCAP* **1511** (2015) 041, [1507.06215].

[162] K. Agashe, P. Du, M. Ekhterachian, C. S. Fong, S. Hong and L. Vecchi, *Natural Seesaw and Leptogenesis from Hybrid of High-Scale Type I and TeV-Scale Inverse*, *JHEP* **04** (2019) 029, [1812.08204].

[163] S. Antusch, E. Cazzato and O. Fischer, *Sterile neutrino searches at future $e^-e^+$, pp, and $e^-p$ colliders*, *Int. J. Mod. Phys.* **A32** (2017) 1750078, [1612.02728].

[164] A. Pilaftsis, *Heavy Majorana neutrinos and baryogenesis*, *Int. J. Mod. Phys.* **A14** (1999) 1811–1858, [hep-ph/9812256].

[165] P.-H. Gu and U. Sarkar, *Leptogenesis with Linear, Inverse or Double Seesaw*, *Phys. Lett.* **B694** (2011) 226–232, [1007.2323].

[166] S. Blanchet, P. S. B. Dev and R. N. Mohapatra, *Leptogenesis with TeV Scale Inverse Seesaw in $SO(10)$*, *Phys. Rev.* **D82** (2010) 115025, [1010.1471].

[167] K. Agashe, P. Du, M. Ekhterachian, C. S. Fong, S. Hong and L. Vecchi, *Hybrid seesaw leptogenesis and TeV singlets*, *Phys. Lett.* **B785** (2018) 489–497, [1804.06847].

[168] V. Cirigliano, B. Grinstein, G. Isidori and M. B. Wise, *Minimal flavor violation in the lepton sector*, *Nucl. Phys.* **B728** (2005) 121–134, [hep-ph/0507001].

[169] D. N. Dinh, L. Merlo, S. T. Petcov and R. Vega-Álvarez, *Revisiting Minimal Lepton Flavour Violation in the Light of Leptonic CP Violation*, *JHEP* **07** (2017) 089, [1705.09284].

[170] R. S. Chivukula and H. Georgi, *Composite Technicolor Standard Model*, *Phys. Lett.* **B188** (1987) 99–104.

[171] A. J. Buras, P. Gambino, M. Gorbahn, S. Jager and L. Silvestrini, *Universal unitarity triangle and physics beyond the standard model*, *Phys. Lett.* **B500** (2001) 161–167, [hep-ph/0007085].

[172] G. D'Ambrosio, G. F. Giudice, G. Isidori and A. Strumia, *Minimal flavor violation: An Effective field theory approach*, *Nucl. Phys.* **B645** (2002) 155–187, [hep-ph/0207036].

[173] L. Merlo and S. Rosauro-Alcaraz, *Predictive Leptogenesis from Minimal Lepton Flavour Violation*, *JHEP* **07** (2018) 036, [1801.03937].

[174] V. Cirigliano, G. Isidori and V. Porretti, *CP violation and Leptogenesis in models with Minimal Lepton Flavour Violation*, *Nucl. Phys.* **B763** (2007) 228–246, [hep-ph/0607068].

[175] G. C. Branco, A. J. Buras, S. Jager, S. Uhlig and A. Weiler, *Another look at minimal lepton flavour violation, $l_i \to l_j \gamma$, leptogenesis, and the ratio $M_\nu/\Lambda_{LFV}$*, *JHEP* **09** (2007) 004, [hep-ph/0609067].

[176] V. Cirigliano, A. De Simone, G. Isidori, I. Masina and A. Riotto, *Quantum Resonant Leptogenesis and Minimal Lepton Flavour Violation*, *JCAP* **0801** (2008) 004, [0711.0778].

[177] P. S. B. Dev, P. Millington, A. Pilaftsis and D. Teresi, *Corrigendum to "Flavour Covariant Transport Equations: an Application to Resonant Leptogenesis"*, *Nucl. Phys.* **B897** (2015) 749–756, [1504.07640].

[178] A. Pilaftsis and D. Teresi, *Mass bounds on light and heavy neutrinos from radiative minimal-flavor-violation leptogenesis*, *Phys. Rev.* **D92** (2015) 085016, [1506.08124].

[179] M. B. Gavela, T. Hambye, D. Hernandez and P. Hernandez, *Minimal Flavour Seesaw Models*, *JHEP* **09** (2009) 038, [0906.1461].

[180] R. Alonso de Pablo, *Dynamical Yukawa Couplings*, Ph.D. thesis, Madrid, Autonoma U., 2013. 1307.1904.

[181] G. Isidori, *Flavor physics and CP violation*, in *Proceedings, 2012 European School of High-Energy Physics (ESHEP 2012)*, pp. 69–105, 2014, [1302.0661].

[182] T. Hurth, G. Isidori, J. F. Kamenik and F. Mescia, *Constraints on New Physics in MFV models: A Model-independent analysis of* $\Delta\ F = 1$ *processes*, *Nucl. Phys.* **B808** (2009) 326–346, [0807.5039].

[183] G. Isidori, Y. Nir and G. Perez, *Flavor Physics Constraints for Physics Beyond the Standard Model*, *Ann. Rev. Nucl. Part. Sci.* **60** (2010) 355, [1002.0900].

[184] T. Hurth and F. Mahmoudi, *The Minimal Flavour Violation benchmark in view of the latest LHCb data*, *Nucl. Phys.* **B865** (2012) 461–485, [1207.0688].

[185] A. Crivellin and L. Mercolli, $B \to X_d\gamma$ *and constraints on new physics*, *Phys. Rev.* **D84** (2011) 114005, [1106.5499].

[186] LHCb, CMS collaboration, V. Khachatryan et al., *Observation of the rare* $B^0_s \to \mu^+\mu^-$ *decay from the combined analysis of CMS and LHCb data*, *Nature* **522** (2015) 68–72, [1411.4413].

[187] Particle Data Group collaboration, M. Tanabashi et al., *Review of Particle Physics*, *Phys. Rev.* **D98** (2018) 030001.

[188] S. Watanuki et al., *Measurements of isospin asymmetry and difference of direct* $CP$ *asymmetries in inclusive* $B \to X_s\gamma$ *decays*, in *39th International Conference on High Energy Physics (ICHEP 2018)*, 2018, [1807.04236].

[189] ATLAS collaboration, M. Aaboud et al., *Study of the rare decays of* $B^0_s$ *and* $B^0$ *mesons into muon pairs using data collected during 2015 and 2016 with the ATLAS detector*, *JHEP* **04** (2019) 098, [1812.03017].

[190] S. Davidson and F. Palorini, *Various definitions of Minimal Flavour Violation for Leptons*, *Phys. Lett.* **B642** (2006) 72–80, [hep-ph/0607329].

[191] R. Alonso, G. Isidori, L. Merlo, L. A. Munoz and E. Nardi, *Minimal flavour violation extensions of the seesaw*, *JHEP* **06** (2011) 037, [1103.5461].

[192] I. Esteban, M. Gonzalez-Garcia, A. Hernandez-Cabezudo, M. Maltoni and T. Schwetz, *Global analysis of three-flavour neutrino oscillations: synergies and tensions in the determination of $\theta_{23}$, $\delta_{CP}$, and the mass ordering*, *JHEP* **01** (2019) 106, [1811.05487].

[193] R. Alonso, M. B. Gavela, D. Hernandez and L. Merlo, *On the Potential of Leptonic Minimal Flavour Violation*, *Phys. Lett.* **B715** (2012) 194–198, [1206.3167].

[194] R. Alonso, M. B. Gavela, D. Hernández, L. Merlo and S. Rigolin, *Leptonic Dynamical Yukawa Couplings*, *JHEP* **08** (2013) 069, [1306.5922].

[195] R. Alonso, M. B. Gavela, G. Isidori and L. Maiani, *Neutrino Mixing and Masses from a Minimum Principle*, *JHEP* **11** (2013) 187, [1306.5927].

[196] S. Uhlig, *Minimal Lepton Flavour Violation and Leptogenesis with exclusively low-energy CP Violation*, *JHEP* **11** (2007) 066, [hep-ph/0612262].

[197] V. Cirigliano and B. Grinstein, *Phenomenology of minimal lepton flavor violation*, *Nucl. Phys.* **B752** (2006) 18–39, [hep-ph/0601111].

[198] T. Hambye, J. March-Russell and S. M. West, *TeV scale resonant leptogenesis from supersymmetry breaking*, *JHEP* **07** (2004) 070, [hep-ph/0403183].

[199] R. Coy and M. Frigerio, *Effective approach to lepton observables: the seesaw case*, *Phys. Rev. D* **99** (2019) 095040, [1812.03165].

[200] R. N. Mohapatra, *Unification and Supersymmetry. The Frontiers of Quark-Lepton Physics*, Chapter 6, pp. 145–146. Springer, Berlin, 1986. 10.1007/978-1-4757-1928-4.

[201] R. Foot, *An Alternative $SU(4) \times SU(2)_L \times SU(2)_R$ model*, *Phys. Lett.* **B420** (1998) 333–339, [hep-ph/9708205].

[202] R. Foot and G. Filewood, *Implications of TeV scale $SU(4) \times SU(2)_L \times SU(2)_R$ quark lepton-lepton unification*, *Phys. Rev.* **D60** (1999) 115002, [hep-ph/9903374].

[203] LHCb collaboration, R. Aaij et al., *Measurement of the ratio of branching fractions $\mathcal{B}(\bar{B}^0 \to D^{*+}\tau^-\bar{\nu}_\tau)/\mathcal{B}(\bar{B}^0 \to D^{*+}\mu^-\bar{\nu}_\mu)$*, *Phys. Rev. Lett.* **115** (2015) 111803, [1506.08614].

[204] LHCb collaboration, R. Aaij et al., *Test of lepton universality with $B^0 \to K^{*0}\ell^+\ell^-$ decays*, *JHEP* **08** (2017) 055, [1705.05802].

[205] LHCb collaboration, R. Aaij et al., *Test of lepton universality using $B^+ \to K^+\ell^+\ell^-$ decays*, *Phys. Rev. Lett.* **113** (2014) 151601, [1406.6482].

[206] LHCb collaboration, R. Aaij et al., *Search for lepton-universality violation in $B^+ \to K^+\ell^+\ell^-$ decays*, *Phys. Rev. Lett.* **122** (2019) 191801, [1903.09252].

[207] J. Heeck and D. Teresi, *Pati-Salam explanations of the B-meson anomalies*, *JHEP* **12** (2018) 103, [1808.07492].

[208] L. Di Luzio, A. Greljo and M. Nardecchia, *Gauge leptoquark as the origin of B-physics anomalies*, *Phys. Rev. D* **96** (2017) 115011, [1708.08450].

[209] L. Calibbi, A. Crivellin and T. Li, *Model of vector leptoquarks in view of the B-physics anomalies*, *Phys. Rev. D* **98** (2018) 115002, [1709.00692].

[210] M. Bordone, C. Cornella, J. Fuentes-Martin and G. Isidori, *A three-site gauge model for flavor hierarchies and flavor anomalies*, *Phys. Lett. B* **779** (2018) 317–323, [1712.01368].

[211] M. Blanke and A. Crivellin, *B Meson Anomalies in a Pati-Salam Model within the Randall-Sundrum Background*, *Phys. Rev. Lett.* **121** (2018) 011801, [1801.07256].

[212] S. Balaji, R. Foot and M. A. Schmidt, *Chiral $SU(4)$ explanation of the $b \to s$ anomalies*, *Phys. Rev.* **D99** (2019) 015029, [1809.07562].

[213] S. Balaji and M. A. Schmidt, *Unified $SU(4)$ theory for the $R_{D^{(*)}}$ and $R_{K^{(*)}}$ anomalies*, *Phys. Rev. D* **101** (2020) 015026, [1911.08873].

[214] G. Valencia and S. Willenbrock, *Quark - lepton unification and rare meson decays*, *Phys. Rev.* **D50** (1994) 6843–6848, [hep-ph/9409201].

[215] D. Chang, R. N. Mohapatra, J. Gipson, R. E. Marshak and M. K. Parida, *Experimental Tests of New $SO(10)$ Grand Unification*, *Phys. Rev.* **D31** (1985) 1718.

[216] D. Croon, T. E. Gonzalo and G. White, *Gravitational Waves from a Pati-Salam Phase Transition*, *JHEP* **02** (2019) 083, [1812.02747].

[217] F. J. Gilman and M. Reno, *Restrictions on Left-right Symmetric Gauge Theories From the Neutral Kaon System and B Decays*, *Phys. Lett. B* **127** (1983) 426–428.

[218] R. N. Mohapatra, G. Senjanovic and M. D. Tran, *Strangeness Changing Processes and the Limit on the Right-handed Gauge Boson Mass*, *Phys. Rev.* **D28** (1983) 546.

[219] F. J. Gilman and M. Reno, *Restrictions From the Neutral $K$ and $B$ Meson Systems on Left-right Symmetric Gauge Theories*, *Phys. Rev. D* **29** (1984) 937.

[220] G. Barenboim, M. Gorbahn, U. Nierste and M. Raidal, *Higgs Sector of the Minimal Left-Right Symmetric Model*, *Phys. Rev. D* **65** (2002) 095003, [hep-ph/0107121].

[221] M. Pospelov, *FCNC in left-right symmetric theories and constraints on the right-handed scale*, *Phys. Rev. D* **56** (1997) 259–264, [hep-ph/9611422].

[222] S. Bertolini, A. Maiezza and F. Nesti, *Present and Future K and B Meson Mixing Constraints on TeV Scale Left-Right Symmetry*, *Phys. Rev. D* **89** (2014) 095028, [1403.7112].

[223] A. D. Smirnov, *Contributions of gauge and scalar leptoquarks to $K_L^0 \to l_i^+ l_j^-$ and $B^0 \to l_i^+ l_j^-$ decay and constraints on leptoquark masses from the decays $K_L^0 \to e^\mp \mu^\pm$ and $B^0 \to e^\mp \tau^\pm$*, *Phys. Atom. Nucl.* **71** (2008) 1470–1480.

[224] M. D. Goodsell, S. Liebler and F. Staub, *Generic calculation of two-body partial decay widths at the full one-loop level*, *Eur. Phys. J. C* **77** (2017) 758, [1703.09237].

[225] A. V. Kuznetsov and N. V. Mikheev, *Vector leptoquarks could be rather light?*, *Phys. Lett.* **B329** (1994) 295–299, [hep-ph/9406347].

[226] Y. Cai, J. Gargalionis, M. A. Schmidt and R. R. Volkas, *Reconsidering the One Leptoquark solution: flavor anomalies and neutrino mass*, *JHEP* **10** (2017) 047, [1704.05849].

[227] A. D. Smirnov, *Mass limits for scalar and gauge leptoquarks from $K_L^0 \to e^\mp \mu^\pm$, $B^0 \to e^\mp \tau^\pm$ decays*, *Mod. Phys. Lett.* **A22** (2007) 2353–2363, [0705.0308].

[228] A. D. Smirnov, *Vector leptoquark mass limits and branching ratios of $K_L^0, B^0, B_s \to l_i^+ l_j^-$ decays with account of fermion mixing in leptoquark currents*, *Mod. Phys. Lett.* **A33** (2018) 1850019, [1801.02895].

[229] Particle Data Group collaboration, M. Tanabashi, K. Hagiwara, K. Hikasa, K. Nakamura, Y. Sumino, F. Takahashi et al., *Review of particle physics*, *Phys. Rev. D* **98** (Aug, 2018) 030001.

[230] R. R. Volkas, *Prospects for mass unification at low-energy scales*, *Phys. Rev.* **D53** (1996) 2681–2698, [hep-ph/9507215].

[231] H. Georgi and C. Jarlskog, *A New Lepton - Quark Mass Relation in a Unified Theory*, *Phys. Lett.* **86B** (1979) 297–300.

[232] J. Hisano, H. Murayama and T. Yanagida, *Nucleon decay in the minimal supersymmetric SU(5) grand unification*, *Nucl. Phys. B* **402** (1993) 46–84, [hep-ph/9207279].

[233] CMS collaboration, A. M. Sirunyan et al., *Search for Evidence of the Type-III Seesaw Mechanism in Multilepton Final States in Proton-Proton Collisions at* $\sqrt{s} = 13$ TeV, *Phys. Rev. Lett.* **119** (2017) 221802, [1708.07962].

[234] N. Kumar and S. P. Martin, *Vectorlike Leptons at the Large Hadron Collider*, *Phys. Rev. D* **92** (2015) 115018, [1510.03456].

[235] ATLAS collaboration, G. Aad et al., *Search for the production of single vector-like and excited quarks in the $Wt$ final state in pp collisions at $\sqrt{s}$ = 8 TeV with the ATLAS detector*, *JHEP* **02** (2016) 110, [1510.02664].

[236] J. C. Helo, M. Hirsch and T. Ota, *Proton decay at one loop*, *Phys. Rev. D* **99** (2019) 095021, [1904.00036].

[237] T. Han, I. Lewis and Z. Liu, *Colored Resonant Signals at the LHC: Largest Rate and Simplest Topology*, *JHEP* **12** (2010) 085, [1010.4309].

[238] CMS collaboration, A. M. Sirunyan et al., *Search for high mass dijet resonances with a new background prediction method in proton-proton collisions at $\sqrt{s}$ = 13 TeV*, *JHEP* **05** (2020) 033, [1911.03947].

[239] F. Hahn-Woernle, M. Plumacher and Y. Y. Y. Wong, *Full Boltzmann equations for leptogenesis including scattering*, *JCAP* **0908** (2009) 028, [0907.0205].

[240] M. A. Luty, *Baryogenesis via leptogenesis*, *Phys. Rev.* **D45** (1992) 455–465.

[241] W. Grimus and L. Lavoura, *The Seesaw mechanism at arbitrary order: Disentangling the small scale from the large scale*, *JHEP* **11** (2000) 042, [hep-ph/0008179].

[242] F. Besnard, *A remark on the mathematics of the seesaw mechanism*, *J. Phys. Comm.* **1** (2018) 015005, [1611.08591].

[243] S. Antusch and V. Maurer, *Running quark and lepton parameters at various scales*, *JHEP* **11** (2013) 115, [1306.6879].

[244] S. Antusch, J. Kersten, M. Lindner, M. Ratz and M. A. Schmidt, *Running neutrino mass parameters in see-saw scenarios*, *JHEP* **03** (2005) 024, [hep-ph/0501272].

[245] M. E. Machacek and M. T. Vaughn, *Two Loop Renormalization Group Equations in a General Quantum Field Theory. 2. Yukawa Couplings*, *Nucl. Phys. B* **236** (1984) 221–232.

[246] C. Balzereit, T. Mannel and B. Plumper, *The Renormalization group evolution of the CKM matrix*, *Eur. Phys. J. C* **9** (1999) 197–211, [hep-ph/9810350].

[247] M.-x. Luo and Y. Xiao, *Two loop renormalization group equations in the standard model*, *Phys. Rev. Lett.* **90** (2003) 011601, [hep-ph/0207271].

[248] S. R. Juarez Wysozka, S. Herrera H., P. Kielanowski and G. Mora, *Scale dependence of the quark masses and mixings: Leading order*, *Phys. Rev. D* **66** (2002) 116007, [hep-ph/0206243].